Targeting Tumour-Associated Macrophages with Locally-Expressed T Cell Engagers

Eleanor Scott

Balliol College

A thesis submitted for the degree of Doctor of Philosophy to the

Department of Oncology, University of Oxford

Trinity Term 2019

“A learning experience is one of those things that says,

'You know that thing you just did? Don't do that.’”

- Douglas Adams

Abstract

Tumour associated macrophages (TAMs) are implicated in cancer progression but can also exert anti-tumour activities. In this thesis, a strategy to redirect endogenous T cell cytotoxicity towards cancer supporting (M2-like) TAMs is explored. A panel of novel bi- and tri-valent T cell engagers (BiTEs/TriTEs) was generated, recognising CD3ε on T cells and M2-like macrophage markers CD206 or folate receptor β (FRβ). Primary human T cells activated by the BiTEs/TriTEs preferentially killed M2- over M1-polarised autologous macrophages, with EC_{50} values in the nanomolar range. This work represents the first to demonstrate the feasibility of redirecting T cells to kill macrophages.

To avoid on-target off-tumour toxicities, we propose localising BiTE/TriTE expression to the tumour with an engineered oncolytic virus. We confirmed the feasibility of this approach by modifying an oncolytic adenovirus in early-phase clinical trials for solid cancers, enadenotucirev (EnAd), to express the BiTEs. Critically, T cell engager-armed EnAd retained its oncolytic and replicative capacities, whilst mediating BiTE expression from infected cancer cells.

In immunosuppressive human malignant ascites samples, free and EnAd-encoded FRβ-targeting BiTEs (but not CD206-targeting T cell engagers) triggered endogenous T cell activation and IFN-γ production, leading to increased T cell numbers and a reduction in the number of $CD11b^{+}CD64^{+}$ ascites macrophages. Strikingly, surviving macrophages exhibited a general increase in M1-like marker expression, suggestive of a repolarisation of the microenvironment towards a more immune-responsive state. Taken together, this approach to deplete cancer-promoting TAMs in the context of the immune-stimulatory effects of BiTEs and oncolytic viruses offers a powerful new strategy for removing barriers to anti-tumour immunity in patients with cancer.

Declaration of Authentication

The material presented in this thesis was performed under the supervision of Professor Leonard Seymour, Department of Oncology, Division of Medical Sciences, University of Oxford. This work is entirely my own, and any contribution to the thesis made by others has been acknowledged. The work submitted here does not form part of another thesis in this or any other university.

Eleanor Scott
October 2019

Publication note

The work presented in Chapters 3-7 of this thesis is in revision at *Journal for Immunotherapy of Cancer*:

- **Scott EM,** Jacobus E, Lyons B, Frost S, Freedman JD, Dyer A, Khalique H, Taverner WK, Carr A, Champion B, Fisher KD, Seymour LW, Duffy MR. "Bi- and Tri-valent T cell Engagers Deplete TAMs in Cancer Patient Samples." In revision at *JITC*, October 2019.

Material from the following review article in *Macromolecular Bioscience* is used in the Introduction (Chapter 1):

- **Scott EM,** Duffy MR, Freedman JD, Fisher KD, Seymour LW. (2017) "Solid Tumor Immunotherapy with T Cell Engager-Armed Oncolytic Viruses." *Macromol Biosci.* 18:1.

Material from the following chapter in *Methods in Molecular Biology* is used in the introductory section of Chapter 6:

- **Scott EM,** Frost S, Khalique H, Freedman JD, Seymour LW, Lei-Rossman J. (2019) "Use of liquid patient ascites fluids as a pre-clinical model for oncolytic virus activity." *Methods Mol Biol.* 2058:261-270.

Other contributions to published work made over the course of this DPhil:

- Dyer A, Schoeps B, Frost S, Jakeman P, **Scott EM,** Freedman J, Jacobus EJ, Seymour LW. (2019) "Antagonism of Glycolysis and Reductive Carboxylation of Glutamine Potentiates Activity of Oncolytic Adenoviruses in Cancer Cells." *Cancer Res.* 15;79(2):331-345.
- Freedman JD, Duffy MR, Lei-Rossmann J, Muntzer A, **Scott EM,** Hagel J, Campo L, Bryant RJ, Verrill C, Lambert A, Miller P, Champion BR, Seymour LW, Fisher KD. "An Oncolytic Virus Expressing a T-cell Engager Simultaneously Targets Cancer and Immunosuppressive Stromal Cells." *Cancer Res.* 2018 Dec 15;78(24):6852-6865
- Dyer A, Baugh R, Chia SL, Frost S, Iris, Jacobus EJ, Khalique H, Pokrovska TD, **Scott EM,** Taverner WK, Seymour LW, Lei J. "Turning cold tumours hot: oncolytic virotherapy gets up close and personal with other therapeutics at the 11th Oncolytic Virus Conference." *Cancer Gene Ther.* 2018 Sep 4.
- Freedman JD, Hagel J, **Scott EM**, Psallidas I, Gupta A, Spiers L, Miller P, Kanellakis N, Ashfield R, Fisher KD, Duffy MR, Seymour LW. (2017) "Oncolytic adenovirus expressing bispecific antibody targets T-cell cytotoxicity in cancer biopsies." *EMBO Mol Med.* 9(8).

Acknowledgements

I would firstly like to acknowledge Prof. Len Seymour for his invaluable scientific input, good humour and mentorship. I am also exceptionally grateful to Dr. Margaret Duffy for her unwavering guidance and encouragement throughout this PhD – Margaret, I feel so lucky to have had your support from the beginning. I would also like to thank Dr. Kerry Fisher for his fantastic insight, and for always being keen to chat about our latest adventures.

I offer my sincere and heartfelt gratitude for each and every member of the Seymour group (aka Len's Angels), who made every day of this PhD (especially Thursdays) a pleasure. In particular, I would like to thank the lovely Sally Frost, Arthur Dyer, Richard Baugh, and Flurin Caviezel, whose support and enthusiasm - especially in recent months - has been invaluable in lifting my spirits. I also extend my gratitude to my fellow final year students, Will Taverner and Dr. Tzveta Pokrovska, for their camaraderie and good humour in times of (let's face it) utmost despair. I am grateful also for the inspirational Dr. Janet Lei and Dr. Hena Khalique, who gracefully juggle post-doctoral research and motherhood, and somehow still find the time to help and look out for us all. I would also like to acknowledge Dr. Brian Lyons and Dr. Viviana Cobos Jiminez for their endless patience and expert advice in HPLC and macrophage culture. Finally, I thank the very talented Dr. Joshua Freedman and Dr. Egon Jacobus, for their invaluable scientific advice and creativity (in the use of clamp-stands and cable ties, for instance).

Much of the work in this thesis would not have been possible without the expertise and generosity of Alison Carr and her colleagues at the Churchill Hospital, Oxford. For their amazing patience and flexibility, I am also very grateful to Ruth Webb and Aubrina Ashton at the NHSBT Oxford Blood Donor Centre.

Looking back, I would like to thank Dr. Antonio Marchini and Dr. Serena Bonifati from DKFZ, Heidelberg, for welcoming me so warmly into their lab in the days before I knew how to hold a pipette, and for introducing me to the wonderful world of oncolytic viruses (and scientific research in general). I also thank my old friends from Bristol, "AI", for their support throughout my undergraduate studies – fortunately, thesis-writing wasn't fuelled this time by frozen pasta bakes.

It is with great pleasure that I extend my gratitude to my friends in Oxford, who have made this such a happy time. In particular, thank you to Angharad Jones, Tom Lowenthal, Jamie Beacom, Greg Farquhar and Rosanna Sheehan; I'm glad this thesis didn't end up in the garden. Lastly, but of course not least, I would like to thank the lovely Paul Rademeyer for his incredible support through all of the ups and the downs, and for being the reason that, probably very unusually, the final year of this PhD was also my favourite.

Finally, I would like to thank my wonderful mum, Carolyn Willis, and brother, Ali Scott, for their love and encouragement throughout all of my studies. This thesis is dedicated to my dad, Mike Scott, who would have been very proud of us.

Table of Contents

List of abbreviations

ACT	Adoptive cell therapies
ADCC	Antibody-dependent cellular cytotoxicity
ADCP	Antibody-dependent cellular phagocytosis
APC	Antigen-presenting cell
BCMA	B cell maturation antigen
BiTE	Bispecific T cell engager
BSA	Bovine serum albumin
BTLA	B- and T-lymphocyte attenuator
CAF	Cancer-associated fibroblast
CAR	Chimeric antigen receptor
CCL	Chemokine ligand
CCR	C-C chemokine receptor
CD	Cluster of differentiation
CDC	Complement-dependent cytotoxicity
CEA	Carcinoembryonic antigen
CFSE	Carboxyfluorescein succinimidyl ester
CMV	Cytomegalovirus immediate-early promoter
CSF-1	Colony stimulating factor-1
CSF-1R	Colony stimulating factor-1 receptor
CTLA-4	Cytotoxic T-lymphocyte-associated protein 4
CXCL	C-X-C motif chemokine ligand
DAMPs	Danger-associated molecular patterns
DARTs	Dual-affinity-retargeting formats

DC	Dendritic cell
DMEM	Dulbecco's modified Eagle's medium
DMSO	Dimethyl sulfoxide
E.coli	*Escherichia coli*
E:T ratio	Effector:target ratio
ECM	Extracellular matrix
EDTA	Ethylenediaminetetraacetic acid
EGFR	Epidermal growth factor receptor
EGFRvIII	EGFR variant 3
EnAd	Enadenotucirev
EpCAM	Epithelial cell adhesion molecule
EphA2	Ephrin type-A receptor 2
FAP	Fibroblast activation protein
FBS	Foetal bovine serum
Fc	Fragment crystallisable
FDA	Food and Drug Administration
FRb	Folate receptor ß
GFP	Green fluorescent protein
GM-CSF	Granulocyte-macrophage colony-stimulating factor
HER2	Human epidermal growth factor receptor 2
HLA	Human leukocyte antigen
HMGB1	High mobility group box 1 protein
HSV	Herpes simplex virus
HS	Human serum
ICAM-1	Intercellular adhesion molecule 1

ICI	Immune checkpoint inhibitor
IDO	Indoleamine 2,3-dioxygenase
IFN	Interferon
Ig	Immunoglobulin
IGF-1	Insulin-like growth factor 1
IL	Interleukin
LAG-3	Lymphocyte-activation gene 3
LAT	Linker for activation of T cells
LB	Lysogeny broth
LPS	Lipopolysaccharide
mAb	Monoclonal antibody
MAPK	Mitogen-activated protein kinase
M-CSF	Macrophage colony-stimulating factor
MDM	Monocyte-derived macrophage
MDSC	Myeloid-derived suppressor cell
MHC	Major histocompatibility complex
MLP	Adenovirus major late promoter
NK cell	Natural killer cell
NOS2	Nitric oxide synthase 2, inducible
ORR	Objective response rate
OV	Oncolytic virus
PAMPs	Pathogen-associated molecular patterns
PBMCs	Peripheral blood mononuclear cells
PBST	PBS-Tween
PBST	Phosphate-buffered saline

PCR	Polymerase chain reaction
PD-1	Programmed cell death protein 1
PD-L1	Programmed death-ligand 1
Ph	Philadelphia chromosome
PI	Propidium iodide
PI3K	Phosphoinositide 3-kinase
PSA	Prostate-specific antigen
SA	Splice-acceptor
sCD206	Soluble CD206
scFv	Single-chain variable fragment
TAAs	Tumour-associated antigens
TAMs	Tumour-associated macrophages
TandAbs	Tandem diabodies
TCR	T cell receptor
TGF-β	Transforming growth factor beta
Th	T helper
TIGIT	T cell immunoreceptor with Ig and ITIM domains
TILs	Tumour-infiltrating lymphocytes
TIM-3	T cell immunoglobulin and mucin-domain containing-3
TMB	3,3',5,5'-Tetramethylbenzidine
TME	Tumour microenvironment
TNF-α	Tumour necrosis factor-alpha
Treg	Regulatory T cell
Tris	Trisaminomethane
TriTEs	Tri-valent T cell engagers

T-VEC	Talimogene laherparepvec
v/v	volume/volume
VEGF	Vascular endothelial growth factor
VH domain	Heavy chain variable domain
VL domain	Light chain variable domain
VV	Vaccinia virus
ZAP-70	Zeta-chain-associated protein kinase 70

1 Introduction

Despite advances in chemotherapy, radiotherapy and surgery, metastatic cancer remains an incurable disease for the majority of patients. With an increased understanding of the interplay between cancer and the immune system, however, a new chapter in the war against cancer has opened. Immunotherapy is a form of treatment in which the body's natural immune responses to cancer are boosted. Recent decades have witnessed remarkable breakthroughs in the field of cancer immunotherapy, achieving durable remissions in patients with previously incurable disease. Nevertheless, most patients do not respond to immunotherapy, and there is an urgent need to elucidate and address the mechanisms underlying such resistance. This thesis explores an approach to target one barrier to effective immunotherapy: tumour-associated macrophages (TAMs)

1.1 General Introduction

1.1.1 Traditional approaches to cancer therapy

Cancer is a group of diseases characterised by an uncontrolled multiplication and spread of cells (Hanahan and Weinberg, 2000). The resultant masses of abnormal tissue – tumours - may be removed or debulked surgically, although this approach is only feasible in the treatment of accessible (usually primary) tumours (Arruebo et al., 2011). Radiotherapy is an effective option for many surgically-inaccessible tumours, but is similarly limited in its utility against distant micro-metastases, and is associated with significant damage to surrounding healthy tissues (Barnett et al., 2009).

Surgery and radiotherapy dominated the field of cancer therapy until around the 1960s, when chemotherapy first demonstrated its clinical utility (Brunner and Young, 1965; Li et al., 1958). Chemotherapeutic agents are generally administered via the bloodstream, and

therefore have the potential to target all cancer cells throughout the body. These treatments are not selective for cancer cells, however, rather exerting their toxicity towards all rapidly-dividing cells. Chemotherapy is therefore associated with serious side effects which significantly impact upon the quality of life of patients (Coates et al., 1983).

The deeper understanding of the molecular basis of cancer gained from the 1990s onwards enabled the development of targeted therapies exploiting cancer cell-specific abnormalities (e.g. aberrant kinase activity). These are generally well-tolerated and have achieved significant clinical successes, for instance in the treatment of chronic myeloid leukaemia with Imatinib, a tyrosine kinase inhibitor (Druker et al., 2001). However, the intrinsic genomic instability of cancer cells facilitates their escape from such therapies, and relapses are common (Lahaye et al., 2005).

1.1.2 Cancer and the immune system

Awareness of a possible link between cancer and the immune system dates back over a century ago, with observations of transient remissions in cancer patients coinciding with their incidental contractions of bacterial or viral infections (Decker et al., 2017). Since then, dual roles for the immune system in both the control and progression of cancer have been uncovered. The dynamic relationship between cancer and the immune system may be divided into three phases: elimination, equilibrium and escape (Dunn et al., 2002).

Elimination

Neoplastic transformation is an inherently stressful process for cells, triggering their up-regulation of stress-related surface markers (e.g. NKG2D ligands). These are usually detected by components of the innate immune system, leading to eradication of the transformed cell (Muralidharan and Mandrekar, 2013). Cancer cells are also eliminated via adaptive immune responses; tumour-associated antigens (TAAs), acquired during

neoplastic transformation, are captured by antigen-presenting cells (APCs) and presented on major histocompatibility complex (MHC) molecules to naïve T cells in lymphoid tissues, leading to their differentiation and expansion. Activated tumour-reactive effector T cells traffic back to tumours where they kill their target cells via T cell receptor (TCR) recognition of their cognate MHC/peptide complex (Chen and Mellman, 2013). Additional TAAs, released by dying cancer cells, enter subsequent revolutions of the cycle, increasing the breadth of the anti-tumour response in a process termed the "cancer-immunity cycle" (Chen and Mellman, 2013).

Equilibrium

In the "equilibrium" phase of cancer immuno-editing, the immune system is able to control tumour growth but not eradicate it entirely. Owing to a lack of appropriate animal models and a paucity of human data (discussed in (Mittal et al., 2014)), this phase is poorly understood. However, it is hypothesised that tumours go through a period of dormancy in which cancer cells are subjected to constant selection pressure by the immune system, driving the emergence of variants that "escape" immune detection, as described below.

Escape

Eventually, the capacity of cancer cells to evade immune detection outstrips that of the immune system to destroy them. This phase – "escape" – involves the outgrowth of a tumour into one that is clinically apparent and potentially metastatic (Dunn et al., 2002). Mechanisms of immune evasion by cancer cells include disruption of antigen presentation pathways (e.g. through loss of MHC expression), up-regulation of immune-inhibitory surface molecules (e.g. programmed death-ligand 1 (PD-L1)), secretion of immunomodulatory cytokines (e.g. interleukin (IL)-10, transforming growth factor (TGF)-β) and resistance to cell death pathways (Mittal et al., 2014). Furthermore, tumour-

resident immune cells (which may have been recruited originally in an attempt to eradicate cancer cells) can be hijacked by the tumour to facilitate escape from immune detection. The role of the tumour microenvironment (TME) in tumour immune evasion is discussed in greater detail in 1.3.2.

1.2 Cancer Immunotherapy

Cancer immunotherapy encompasses a range of approaches designed to supplement or invigorate existing anti-tumour immune responses (summarised in Table 1). In contrast to targeted therapies, which are associated with high response rates but transient disease control, cancer immunotherapies are effective in only minority of patients, but achieve long-lasting remissions (Figure 1.1). The potentially curative nature of these treatments in previously terminal cancer patients has sparked a paradigm shift in cancer therapy. In the following sections, several key strategies for cancer immunotherapy are discussed, with the advantages and limitations of each approach highlighted.

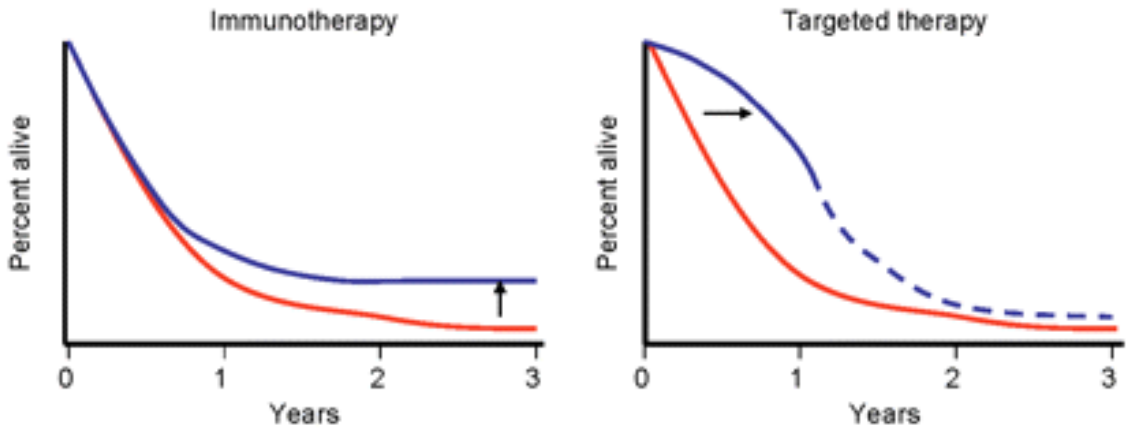

Figure 1.1. Survival curves for melanoma patients after treatment with targeted therapy and immunotherapy. Adapted from (Ribas et al., 2012).

Table 1: Overview of cancer immunotherapy strategies.

Approach	Mechanism(s) of action	Limitations	Clinical development	Refs
mAbs targeting TAAs	Fc-dependent (ADCP, ADCC, CDC) and – independent effects towards target cells	- Poor penetration of solid tumours - Vulnerable to antigen escape - Lack of durable responses	>30 FDA-approved for various solid and blood cancers	(Kimiz-Gebologlu et al., 2018; Zhang et al., 2019)
Therapeutic cancer vaccines	Boost the host cancer immunity cycle by stimulating uptake/presentation of TAAs by APCs	- Lack of efficacy - Vulnerable to MHC loss	One FDA-approved for prostate cancer >1000 Phase I-III clinical trials	(Hollingsworth and Jansen, 2019; Song et al., 2018)
TIL-based ACT	*Ex vivo* expansion of tumour-reactive T cells, followed by reinfusion	- Costly and labour-intensive procedure - Challenging for less immunogenic tumours - Vulnerable to MHC loss	One phase III clinical trial for melanoma >20 Phase I-II clinical trials	(Rohaan et al., 2018; Rosenberg et al., 2011)
CAR-based ACT	*Ex vivo* engineering of T cells to express an artificial receptor recognising TAAs, followed by reinfusion	- Costly and labour-intensive procedure - "On-target off-tumour" toxicities - Vulnerable to antigen escape	Two FDA-approved for blood cancers >400 Phase I-III clinical trials	(June and Sadelain, 2018)
Checkpoint inhibitors	Stimulate the host immune system by release of "brakes" on T cell responses	- Serious immune-related toxicities - Vulnerable to MHC loss	7 FDA-approved for various solid and blood cancers >2000 Phase I-III clinical trials	(Darvin et al., 2018)
Bispecific T cell-engager antibodies	Redirect endogenous T cells to target cells expressing chosen TAAs	- Short serum half-life - "On-target off-tumour" toxicities - Vulnerable to antigen escape	One FDA-approved for acute lymphoblastic leukaemia >20 Phase I-III clinical trials	(Ellerman, 2019)

ACT, adoptive cell therapy; ADCC, antibody-dependent cellular cytotoxicity; ADCP, antibody-dependent cellular phagocytosis; APC, antigen-presenting cell; CAR, chimeric antigen receptor; CDC, complement-dependent cytotoxicity; FDA, Food and Drug Administration; mAbs, monoclonal antibodies; MHC, major histocompatibility complex; TAA, tumour-associated antigen; TIL, tumour-infiltrating lymphocyte.

1.2.1 Monoclonal antibodies targeting TAAs

Since the advent of hybridoma technology in 1975, monoclonal antibodies (mAbs) have become invaluable tools in biomedical research and the treatment of disease. One of the first mAbs to enter the clinic was rituximab, a cluster of differentiation (CD)20-targeting chimeric human/murine antibody which gained Food and Drug Administration (FDA) approval in 1997 for the treatment of non-Hodgkin lymphoma (Leget and Czuczman, 1998). Since then, more than 30 mAbs have received regulatory approval for the treatment of solid and haematological malignancies (Zhang et al., 2019). The anti-cancer activities of mAbs may be fragment crystallisable (Fc)-dependent (i.e. involving engagement of immune cells or complement via the Fc tail), Fc-independent or a combination of both. Fc-dependent mechanisms are antibody-dependent cellular cytotoxicity (ADCC), mediated by natural killer cells, macrophages and granulocytes, antibody-dependent cellular phagocytosis (ADCP), mediated by macrophages, and complement-dependent cytotoxicity (CDC) (Kimiz-Gebologlu et al., 2018). Fc-independent effects, meanwhile, include direct receptor antagonism and induction of apoptosis (Kimiz-Gebologlu et al., 2018).

mAbs have proven to be effective treatment options for cancer, prolonging survival in several malignancies, including breast (Lv et al., 2018), colorectal (Jonker et al., 2007) and blood cancers (Fraser et al., 2007). Responses are seldom durable, however, with the selection pressures exerted by mAbs leading to acquired antigen loss and drug resistance (Friedberg, 2005). Moreover, as large molecules, mAbs are limited in their ability to penetrate solid tumours (Thurber et al., 2007).

1.2.2 Therapeutic cancer vaccines

Vaccinations for infectious disease rank among the greatest triumphs in the history of medicine. In recent decades, the possibility of extending their utility to the treatment of cancer has been explored. Unlike prophylactic vaccines, which are administered to healthy individuals, therapeutic cancer vaccines are designed to boost the pre-existing anti-tumour immune responses of patients with cancer. Strategies include: i) autologous tumour cell vaccines, prepared from patient-derived tumour cells or cancer cell lines; ii) autologous dendritic cell (DC) vaccines, loaded with TAAs; iii) protein/peptide-based vaccines, derived from TAAs, and iv) DNA/RNA-based vaccines encoding TAAs (reviewed in (Hollingsworth and Jansen, 2019)).

In general, clinical trials of therapeutic cancer vaccines have yielded disappointing results (Guo et al., 2013). Given that most TAAs (with the exception of viral and neo-antigens) are self-antigens, T cells recognising TAAs with high affinity are deleted during thymic selection. Therapeutic cancer vaccination strategies are therefore faced with the considerable challenge of activating T cells with low affinity for TAAs. In many clinical trials of therapeutic cancer vaccines, the activation and expansion of tumour-reactive T cells has been weak, and insufficient to achieve anti-tumour efficacy. For instance, in a phase II trial of PROSTVAC-VF, a vector-based vaccine targeting prostate-specific antigen (PSA) in prostate cancer, only 0.03% of circulating $CD8^+$ T cells were PSA-specific after treatment (as compared to an average of >5% for anti-viral vaccines) (Hollingsworth and Jansen, 2019). Moreover, the activity of tumour-reactive T cells is hindered by the highly immunosuppressed nature of the TME (discussed in section 1.3.2).

Despite these hurdles, in a phase III trial involving patients with castration-resistant prostate cancer, a DC-based vaccine, PROVENGE, improved the 3-year survival rate by

over 20% (compared to the placebo group), with a 4.1-month increase in median survival (Kantoff et al., 2010). In 2010, PROVENGE became the first cancer vaccine to receive FDA approval, providing proof-of-concept for the potential of this approach (Cheever and Higano, 2011).

1.2.3 Adoptive cell therapies

In contrast to cancer vaccines, which aim to boost a pre-existing population of tumour-reactive T cells, adoptive cell therapies (ACTs) involve *ex vivo* manipulation of patient T cells. There are two strategies for ACT: i) isolation and expansion of tumour-infiltrating lymphocytes (TILs), and ii) genetic modification of peripheral T cells to endow them with anti-tumour activity (most notably with chimeric antigen receptor (CAR) technology).

Expansion of TILs

Increasing evidence indicates that tumours contain T cells capable of recognising TAAs, but that they are insufficient in numbers (or too dysfunctional/suppressed) to mediate tumour regression (Topalian et al., 1987). In an approach pioneered by Rosenberg and colleagues at the National Cancer Institute, TILs isolated from resected tumours can be expanded *ex vivo,* before re-infusion into lympho-depleted patients, who subsequently receive IL-2 treatment (Rosenberg et al., 2011). TIL-based ACT has achieved impressive results in clinical trials involving advanced melanoma patients, with objective response rates (ORRs) of around 40-50% and complete remissions in 10-30% of patients (Besser et al., 2010; Dudley et al., 2010; Dudley et al., 2005; Dudley et al., 2008; Rosenberg et al., 2011). TIL-based ACT is mostly well-tolerated, with toxicities relating mainly to the pre-conditioning regimen and IL-2 treatment (Rosenberg et al., 2011).

Whilst very promising, TIL-based ACT is a labour-intensive and costly process which does not provide benefit to all patients. Mutational burden is a strong predictive biomarker of

response to TIL-based ACT (Lauss et al., 2017). Whether the efficacy of TIL-based ACT against melanoma, which is characterised by a high mutational burden, may extend to other solid tumour indications remains to be seen. Indeed, whilst TILs have recently been isolated and expanded from breast (Lee et al., 2017b), renal cell (Baldan et al., 2015), pancreatic (Hall et al., 2016) and non-small cell lung tumours (Ben-Avi et al., 2018), their tumour-reactivity was variable.

CAR T cells

In an alternative approach, peripheral T cells may be isolated and engineered to express CARs before expansion and re-infusion into lympho-depleted patients (Eshhar et al., 1993; Kochenderfer et al., 2010). CARs comprise an extracellular binding domain (usually a single-chain variable fragment (scFv), derived from the variable regions of a TAA-targeting mAb) fused to an intracellular CD3ζ chain, together with one or more co-stimulatory domains (e.g. CD28 or 4-1-BB) (June and Sadelain, 2018). CAR binding to the relevant TAA triggers CD3ζ phosphorylation and the initiation of downstream signalling cascades, leading to T cell activation and cytotoxic activity. CAR-transduced T cells thus recognise and kill tumour cells in a polyclonal fashion, with no requirement for MHC presentation (June and Sadelain, 2018).

CAR T cells have enjoyed unprecedented success in the treatment of haematological malignancies, with CD19-targeting CAR T cells demonstrating efficacy against B cell non-Hodgkin lymphoma (Turtle et al., 2016), acute lymphoblastic leukaemia (Brentjens et al., 2013) and chronic lymphocytic leukaemia (Kalos et al., 2011). Thus far, CD19-targeting CAR T cell therapies have received regulatory approval for relapsed/refractory B-cell precursor acute lymphoblastic leukaemia and diffuse large B-cell lymphoma (June and Sadelain, 2018), providing proof-of-concept for the potential of this approach. Also under

clinical evaluation are CAR T cells recognising CD30 (Hodgkin lymphoma), CD33 and CD123 (acute myeloid leukaemia) and B Cell Maturation Antigen (BCMA) (multiple myeloma) (Leick and Maus, 2019).

Results in solid tumours have been less encouraging. While the non-specific effects of CAR T cells are generally manageable when targeting haematological cancers (B cell aplasia for CD19 CAR T cells, for instance), they can be dose-limiting and even lethal in the context of solid tumours. In a widely cited case report by Morgan et al., infusion of anti-human epidermal growth factor receptor 2 (HER2) CAR T cells in a patient with metastatic colorectal cancer triggered severe respiratory distress, leading to death of the patient five days later (Morgan et al., 2010). This was attributed to on-target off-tumour activity against healthy lung tissue with low-level HER2 expression (Morgan et al., 2010). Solid tumours also present challenges in terms of efficacy, with a hostile, immunosuppressive microenvironment and aberrant chemokine profiles which disfavour T cell trafficking to the tumour (see section 1.4).

1.2.4 Soluble T cell-activating therapies

Other T cell-based therapies aim to stimulate tumour-resident T cells *in vivo*. These are mostly antibody-based, and, as a result, more practical from a clinical perspective than ACT. T cell-activating antibodies can be divided into two main classes: immune checkpoint inhibitors (ICIs) and bispecific antibodies.

Immune checkpoint inhibitors

The development of ICIs has been hailed as a revolution in the treatment of cancer. ICIs promote anti-tumour T cell responses by disrupting inhibitory signalling pathways - "checkpoints"- that are exploited by cancer cells to evade immune elimination. The first ICI to receive regulatory approval was ipilimumab, an anti-cytotoxic T-lymphocyte-

associated protein 4 (CTLA-4) antibody which blocks the negative interaction between CTLA-4 on activated T cells and CD80/CD86 on APCs (Lipson and Drake, 2011). In a randomised phase III trial, ipilimumab became the first agent to be associated with an improvement in overall survival in patients with advanced metastatic melanoma (Hodi et al., 2010), with 20% of patients achieving long-term survival (Schadendorf et al., 2015). Other clinically-approved ICIs target programmed cell death protein 1 (PD-1), an inhibitory receptor on T cells, or its ligand PD-L1, over-expressed on tumour as well as stromal cells. Inhibitors of PD-1 (nivolumab, cemiplimab and pembrolizumab) and PD-L1 (atezolizumab, avelumab and durvalumab), have received regulatory approval for the treatment of multiple solid tumours, as well as Hodgkin lymphoma (Lee et al., 2019b). Head-to-head comparisons of pembrolizumab and ipilimumab in the treatment of advanced melanoma revealed progression-free survival rates of 47.3 and 26.5%, respectively, with fewer severe adverse events in the pembrolizumab group (13.3% versus 19.9%) (Robert et al., 2015), possibly indicating superiority of PD-1-targeting approaches.

ICIs undoubtedly represent a breakthrough in the field of cancer immunotherapy. Nevertheless, only a fraction of patients currently benefit from immune checkpoint inhibition, and severe immune-related adverse events are common. As with TIL-based ACT, tumour mutational burden is predictive of response to ICIs (Goodman et al., 2017). Other determinants of ICI efficacy include the "inflammatory status" of tumours, with immunologically "hot" tumours (i.e. highly infiltrated with T cells) benefiting more from immune checkpoint inhibition than "cold" tumours (i.e. devoid of T cell infiltration) (Tumeh et al., 2014).

Bispecific antibodies

T cells may also be redirected towards tumour cells in a direct manner with bispecific antibodies. By simultaneously engaging T cells (most often via CD3ε) and tumour cells (via TAAs), bispecific antibodies polyclonally activate T cells to kill chosen cells (Frankel and Baeuerle, 2013). A key advantage of this strategy is the possibility to target cells which have lost expression of MHC – a common mechanism of resistance to therapies such as ICI and TIL-based ACT, which rely on TCR recognition of cognate peptide/MHC complexes.

Over 100 different platforms of bispecific antibody have been developed; these include "immunoglobulin (Ig)G-like" formats, which contain an Fc-tail and thus exert Fc-dependent effector functions (see 1.3.1), and "non-IgG-like" formats, lacking Fc-tails (Brinkmann and Kontermann, 2017). Examples of IgG-like bispecific antibodies are dual-variable-domain immunoglobulin and CrossmAb technologies. T cell-redirecting CrossmAbs include RG7802, which binds CD3ε on T cells and carcinoembryonic antigen (CEA) on tumour cells. Following promising pre-clinical studies in PBMC-engrafted xenograft tumour models (Bacac et al., 2016), RG7802 is currently the subject of a phase I/Ib clinical trial involving patients with CEA-positive solid cancers (NCT02324257).

Although IgG-like bispecific antibodies exhibit favourable pharmacokinetics (e.g. a long serum half-life), the large size of Fc-tail-containing antibodies may preclude their efficient penetration of tumours, as is the case for mAbs (Thurber et al., 2007). Advances in molecular cloning technology have enabled the creation of a variety of non-IgG-like bispecific antibody formats, comprising fragments of the variable regions of mAbs. Non-IgG-like bispecific antibody platforms include tandem diabodies (TandAbs), dual-affinity-retargeting formats (DARTs) and bispecific T cell engagers (BiTEs) (Brinkmann and Kontermann, 2017).

Though promising, as with all approaches targeting a single TAA, bispecific antibody-based therapies are vulnerable to both acquired and innate antigen loss. Moreover, their success relies critically upon the presence of sufficient numbers of intratumoural T cells, and their continued functionality in immunosuppressed tumours. Among the most clinically-advanced bispecific antibodies are BiTEs, which will be discussed in detail in section 1.5.

1.3 Resistance to Cancer Immunotherapy

The unprecedented durability of responses to cancer immunotherapy has sparked a revolution in the treatment of cancer. Nevertheless, even for the most immunogenic cancer types (i.e. those with a high mutational burden and a heavy infiltration with immune cells), the majority of patients do not benefit from these therapies (e.g. 80% of patients treated with ipilimumab (Hodi et al., 2010)), and some responders relapse over time (e.g. 1/4 to 1/3 of responders to CTLA-4 or PD-1 blockade (Schachter et al., 2017)). The following sections will discuss several key mechanisms of resistance to cancer immunotherapy, with a focus on those limiting T cell-based therapies.

1.3.1 Tumour cell-intrinsic mechanisms

Cancer immunotherapy strategies may be divided broadly into those which rely on T cells' recognition of cancer cells via TCR-peptide/MHC interactions (e.g. ICIs, TIL-based ACT, therapeutic cancer vaccines), and those which polyclonally activate T cells through redirection towards a specific TAA (e.g. CAR T cells, bispecific antibodies). Perhaps the most simplistic explanation for resistance to T cell-based therapies is an absence of the necessary target proteins on the tumour cell surface. Cancer cells are frequently defective in antigen presentation, most notably due to downregulation of MHC-I expression. Indeed, analysis of tumour biopsies from patients with advanced melanoma revealed that,

in 43% of cases, more than half of tumour cells were devoid of MHC-1 expression (Rodig et al., 2018), with these patients exhibiting resistance to CTLA-4 blockade. Approaches relying on the targeting of a single TAA, meanwhile, are limited by the inherent heterogeneity of tumours in antigen expression, as well as antigen loss under therapy pressure. In clinical trials of CD19-targeting CAR T cells, for instance, 7-33% of initially-responding patients were found to relapse due to loss of cell surface CD19 (Shah et al., 2019). Antigen loss is predicted to represent an even greater challenge in the treatment of solid tumours, which exhibit greater heterogeneity in TAA expression.

Other tumour cell-intrinsic mechanisms of resistance to immunotherapy involve disruption of T cell activity. Tumour cells frequently over-express the ligands for inhibitory receptors on T cells, including not only PD-1 (discussed above, 1.2.4), but also additional checkpoints such as lymphocyte-activation gene 3 (LAG-3), T cell immunoglobulin and mucin-domain containing-3 (TIM-3), T cell immunoreceptor with Ig and ITIM domains (TIGIT), B- and T-lymphocyte attenuator (BTLA) and CD160 (Zarour, 2016). Tumour cells have also been found to trigger T cell apoptosis directly via expression of death ligands such as Fas ligand (Hahne et al., 1996). Signalling through certain oncogenic pathways such as mitogen-activated protein kinase (MAPK), meanwhile, leads to tumour cell production of immunomodulatory cytokines such as IL-8 and vascular endothelial growth factor (VEGF) (Bancroft et al., 2001), which disrupt T cell trafficking and function.

1.3.2 Tumour cell-extrinsic mechanisms: the tumour microenvironment in resistance to cancer immunotherapy

Tumours comprise not only cancer cells but also extracellular matrix (ECM), vasculature, immunomodulatory cytokines, chemokines, and a variety of non-malignant immune and stromal cells. Together, these form a complex, organ-like ecosystem – the TME – which is

continuously shaped by cancer cells to support their proliferation and metastasis (Figure 1.2). As discussed below, the TME is also central in facilitating tumour immune evasion and resistance to immunotherapy.

Most advanced solid tumours are immunologically "cold", i.e. largely devoid of effector immune cell infiltration and, as a consequence, unresponsive to immunotherapy. In these tumours, aberrant chemokine profiles disfavour the trafficking of cytotoxic T cells (Harlin et al., 2009), whilst tumour endothelial cells downregulate key adhesion molecules required for T cell extravasation (Griffioen et al., 1996). An additional (yet often overlooked) barrier to tumour T cell penetration is posed by the tumour stroma; cancer-associated fibroblasts (CAFs) frequently form a thick layer surrounding the tumour vasculature, where they produce abundant ECM and C-X-C motif chemokine ligand 12 (CXCL12) to limit T cell migration deeper into the tumour (Feig et al., 2013; Salmon et al., 2012)

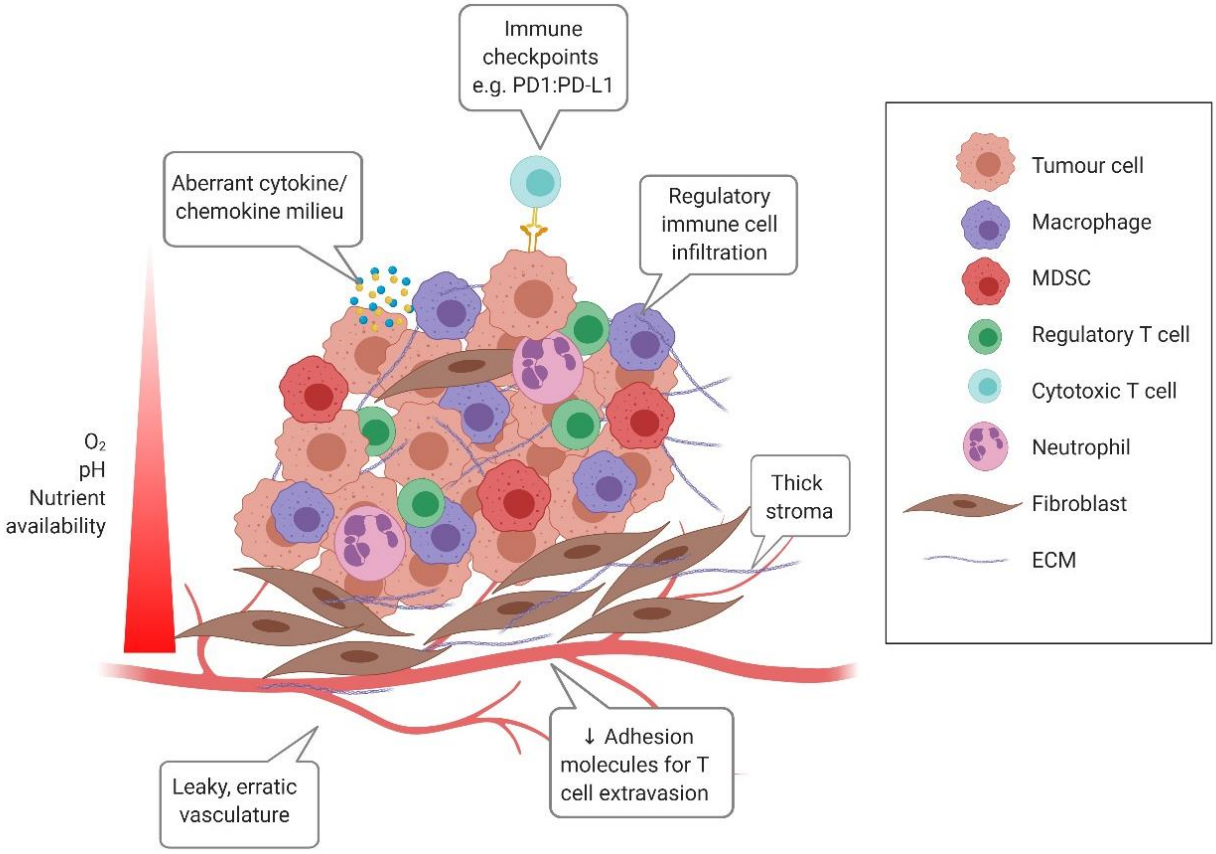

Figure 1.2. The immunosuppressive TME. Tumours comprise not only cancer cells but also a variety of non-cancerous immune and stromal cells which together promote tumour immune evasion and cancer progression. Acellular factors such as immunoregulatory cytokines/chemokines, low pH, hypoxia and dense ECM also contribute towards the creation of an environment which disfavours the activity of anti-tumour immune effector cells. Image created with BioRender.

For cytotoxic T cells that do reach the vicinity of cancer cells, their proliferation and anti-tumour activity may be impeded by immunomodulatory cytokines such as TGF-β (Massagué, 2008). Aberrant vasculature, meanwhile, creates regions of hypoxia in which the expansion and survival of cytotoxic T cells is disfavoured. Due to a heavy reliance of cancer cells on glycolysis and glutaminolysis, the TME is also characterised by low pH, an accumulation of lactate, and a paucity of glutamine, which together promote the activity of regulatory- over cytotoxic T cells (Renner et al., 2017).

The aberrant cytokine/chemokine and metabolic makeup of tumours is both cause and consequence of another feature of the TME: heavy infiltration with non-cancerous immunoregulatory cells. These include regulatory T cells (Tregs), myeloid-derived suppressor cells (MDSCs) and neutrophils, which contribute towards tumour immune suppression through secretion of soluble immunomodulatory factors (e.g. IL-10, TGF-β (Binnewies et al., 2018)), contact-dependent inhibition of immune effector cells (e.g. via membrane-bound TGF-β1 (Li et al., 2009)) and depletion of amino acids which are vital for T cell activity (e.g. cysteine (Srivastava et al., 2010))

The most abundant non-cancerous immune cells in the TME, however, are tumour-associated macrophages (TAMs). Comprising up to 50% of the tumour mass, TAMs are a heterogeneous population of cells which exert a profound influence over the immune landscape of tumours (Poh and Ernst, 2018). In the following section, we explain the case for therapeutic targeting of TAMs to improve cancer immunotherapy.

1.4 Tumour-Associated Macrophages

1.4.1 Macrophages in health and disease

Macrophages are innate immune cells with central roles in development, tissue homeostasis and host defence. Macrophages can be found in even primitive multicellular organisms and, in humans, are abundant in virtually all tissues throughout the body.

A key feature of macrophages is their ability to adopt distinct functional phenotypes in response to different environmental cues (Shapouri-Moghaddam et al., 2018). Upon encountering pathogens, for instance, these cells assume an anti-microbial role, characterised by secretion of pro-inflammatory cytokines such as IL-12 and production of nitric oxide via arginine metabolism by nitric oxide synthase 2, inducible (NOS2).

Following tissue injury, macrophages promote repair and immunoregulation, producing IL-4 and IL-13 and metabolising arginine (via arginase-1) instead to ornithine, which promotes cell proliferation. Inspired by the T helper (Th) 1 versus Th2 nomenclature, the two extremes of macrophage polarisation were termed "M1-polarised" or "M2-polarised", respectively (Mills et al., 2000). In experimental systems, M1-polarised macrophages are induced by Th1 cytokines (e.g. interferon gamma (IFN-γ)) and microbial products (e.g. lipopolysaccharide (LPS)), whilst M2-polarised macrophages are induced by Th2 cytokines (e.g. IL-4 and IL-13) (Mantovani et al., 2004).

Whilst providing a useful system for the *in vitro* study of macrophages, the M1/M2 dichotomy is now regarded as an over-simplification. Macrophage phenotype is determined not only by soluble stress signals (which are unlikely to be binary, as suggested by the M1/M2 framework), but also by their local tissue microenvironment and ontogeny (Ginhoux et al., 2016) (Figure 1.3). Indeed, at least three sources of tissue macrophage (adult monocyte-derived, foetal liver monocyte-derived and yolk sac-derived) have been identified, each yielding cells which respond in a distinct fashion to the same stimulatory signals (e.g. LPS) (Ginhoux et al., 2016).

Despite their importance in health, macrophages are also implicated in the pathogenesis of many diseases, including auto-immunity, sepsis, arthritis, metabolic syndromes and, as discussed in the following sections, cancer (Schultze et al., 2015).

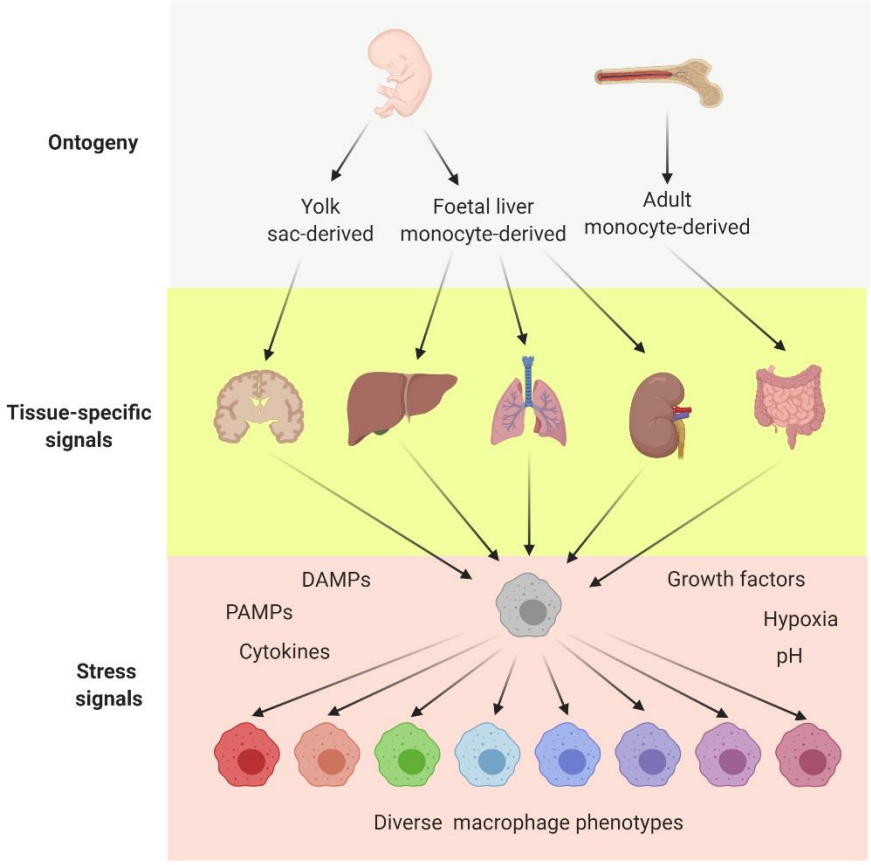

Figure 1.3. Factors determining macrophage phenotype. Ontogeny, tissue-specific signals and stress signals interplay to determine the phenotype of a given macrophage. DAMPs, danger associated molecular patterns; PAMPs, pathogen-associated molecular patterns. Image created with BioRender.

1.4.2 Origins of TAMs

TAMs are among the most abundant non-cancerous cell types in solid tumours, constituting up to 80% of tumour-infiltrating immune cells (Göttlinger et al., 1985). Although most resident macrophages in steady-state tissues derive from embryonic precursors that self-renew locally, macrophages in disease states, including cancer, appear to originate predominantly from circulating bone marrow-derived monocytes (Cassetta and Pollard, 2018). In most murine models of cancer, TAMs derive from circulating monocytes that are recruited (e.g. by tumour-derived chemokine ligand (CCL)2) to progressing tumours, where they differentiate into TAMs under the influence of colony stimulating factor-1 (CSF-1)-colony stimulating factor-1 receptor (CSF-1R) pro-survival

signalling (Arwert et al., 2018; Franklin et al., 2014; Qian et al., 2011; Tymoszuk et al., 2014). Notable exceptions include pancreatic cancer and glioma mouse models, in which mixtures of bone marrow- and foetal liver-derived TAMs have been observed (Bowman et al., 2016; Chen et al., 2017; Zhu et al., 2017). Data on the origins of human TAMs is limited; however, a recent study of secondary tumours in the recipients of sex-mismatched bone marrow transplants revealed that, consistent with pre-clinical studies in mice, most TAMs were bone-marrow derived (Kurashige et al., 2018). A monocytic origin for human TAMs is also suggested by a positive correlation between serum CCL2 levels and TAM numbers in patients with breast cancer (Ueno et al., 2000).

1.4.3 TAMs: roles in cancer initiation and progression

TAMs have been implicated in every stage of tumour progression, from neoplastic transformation to metastasis (Figure 1.4). During early tumourigenesis, the activation of oncogenes and release of danger-associated molecular patterns (DAMPs) is thought to activate macrophages in an M1-like fashion, triggering their production of tumour necrosis factor-alpha (TNF-α), reactive oxygen species and nitric oxide (Cassetta and Pollard, 2018). Although these factors are potentially tumouricidal, they also serve to establish a mutagenic environment which may accelerate neoplastic transformation (Canli et al., 2017; Moore et al., 1999).

As tumours progress, TAMs are educated by tumour-derived Th2 cytokines (IL-4, IL-10 and/or IL-13), CSF-1 and lactic acid towards a more M2-like immunoregulatory/trophic phenotype (Colegio et al., 2014; Noy and Pollard, 2014). Tumour-educated TAMs secrete IL-10 and TGF-β, as well as Treg-attracting chemokines (e.g. CCL22) (Biswas et al., 2006), thereby promoting the infiltration and expansion of regulatory- over cytotoxic T lymphocytes. TAMs also inhibit immune effector cells directly, expressing T- and natural

killer (NK) cell inhibitory ligands (PD-L1, PD-L2, human leukocyte antigen (HLA)-E, HLA-G) and depriving T cells of essential nutrients (e.g. L-arginine and tryptophan) (Noy and Pollard, 2014).

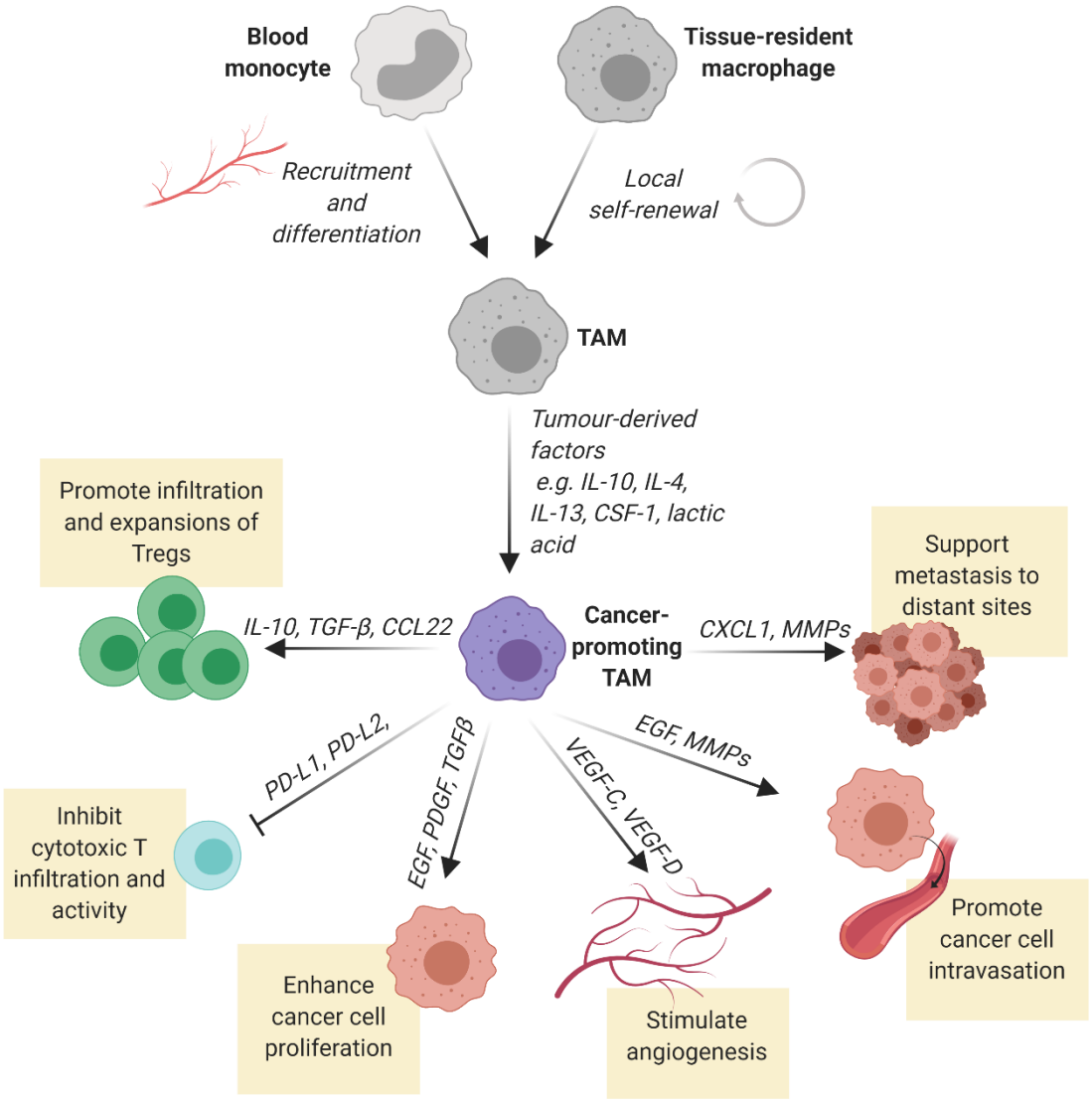

Figure 1.4. Origins and functions of TAMs. Depending on the tumour type, TAMs derive either from the recruitment and differentiation of blood monocytes or the *in situ* proliferation of tissue-resident macrophages, or both. In advanced solid tumours, TAMs are polarised into cancer-promoting phenotypes which promote cancer progression in a variety of ways. Examples of TAM-derived factors mediating each function are provided. Image created with BioRender.

Tumour-educated TAMs are pivotal in the benign-to-malignant transition, having been shown to enhance neovascularisation (through secretion of angiogenic factors e.g. VEGF), cancer cell motility (through production of ECM-degrading proteases and pro-migratory factors e.g. EGF) and extravasation (Aras and Zaidi, 2017). TAMs also promote dissemination from the primary tumour by helping to establish "pre-metastatic niches" – distant tissue sites which support the seeding of circulating cancer cells - through secretion of cancer cell-attracting chemokines, growth factors and adhesion molecules (Doak et al., 2018).

TAMs play important roles in resistance to cancer therapy, with several pre-clinical studies demonstrating a reversal in chemoresistance following macrophage depletion (e.g. with anti-CSF-1 antibodies, see below) (DeNardo et al., 2011; Paulus et al., 2006; Shree et al., 2011). By shaping the immune microenvironment of tumours, TAMs are also predicted to influence the success of cancer immunotherapy. Indeed, macrophage depletion was found to enhance the efficacy of immune checkpoint blockade in murine models of breast cancer (Peranzoni et al., 2018) and melanoma (Neubert et al., 2018), and of adoptive T cell transfer in a murine model of melanoma (Mok et al., 2014).

Perhaps unsurprisingly given the myriad roles of TAMs in disease progression, a high density of intratumoural macrophages has been identified as a poor prognostic factor for most tumour types. Indeed, a meta-analysis of 55 studies evaluating the prognostic significance of TAMs revealed a negative correlation between high TAM density and overall survival for gastric, breast, ovarian, oral and thyroid cancers, with the only exception to this trend being colorectal cancer (Zhang et al., 2012), for which a more pro-inflammatory TAM phenotype has been observed (Ong et al., 2012).

1.4.4 Therapeutic approaches to target TAMs

The genetic stability of TAMs, coupled with their importance in disease progression and association with poor prognosis, render these cells attractive targets for therapeutic intervention. Strategies to target TAMs (summarised in Table 2) are under intensive investigation, and include: i) systemic macrophage depletion, ii) inhibition of monocyte/macrophage recruitment, differentiation and survival, and iii) repolarisation of macrophages towards a more M1-like phenotype.

1.4.4.1 Systemic macrophage depletion

One example of this strategy is the use of bisphosphonates. Typically used in the treatment of osteoporosis, bisphosphonates inhibit osteoclast-mediated bone resorption, but also display anti-tumour effects, possibly due to their ability to trigger apoptosis of macrophages (Rogers and Holen, 2011). To direct this therapy towards macrophages, bisphosphonates such as clodronate have been encapsulated within liposomes, encouraging their preferential uptake by phagocytic cells. As a single agent, clodronate-loaded liposomes have been shown to deplete monocytes/macrophages and reduce tumour growth in murine models of teratocarcinoma (Zeisberger et al., 2006), rhabdomyosarcoma (Zeisberger et al., 2006), melanoma (Gazzaniga et al., 2007) and metastatic lung cancer (Hiraoka et al., 2008). Moreover, clodronate-loaded liposomes enhanced the anti-tumour efficacy of sorafenib, a tyrosine kinase inhibitor, in mouse models of metastatic hepatocellular carcinoma (Zhang et al., 2010).

Systemic macrophage depletion may also be achieved with trabectedin, a clinically-approved DNA-damaging agent which also triggers apoptosis of monocytes and macrophages. Compelling evidence for a role of macrophage depletion in the anti-tumour activity of trabectedin arose from the finding that mice bearing drug-resistant tumours

still received benefit from trabectedin therapy, an effect that was associated with depletion of TAMs (Germano et al., 2013). Depletion of monocytes and TAMs has been confirmed in soft tissue sarcoma patients treated with trabectedin (Germano et al., 2013), although in this case a contribution to efficacy was not determined.

1.4.4.2 Inhibition of monocyte/macrophage recruitment and survival

As discussed above (section 1.4.2), TAM pools are maintained mostly through the recruitment of circulating monocytes, notably via the CCL2-C-C chemokine receptor type 2(CCR2) axis. Disruption of CCL2-CCR2 signalling has therefore been proposed as a means to prevent further TAM expansion. Anti-CCL2 antibodies reduced tumour burden in mouse models of hepatocellular carcinoma (Teng et al., 2017) and renal cell carcinoma (Arakaki et al., 2016), as well inhibiting metastasis in a murine breast cancer model (Qian et al., 2011). However, cessation of anti-CCL2 therapy was found to accelerate breast cancer metastasis in mice due to a rebound in monocyte recruitment (Bonapace et al., 2014), warranting caution over its clinical use. Carlumab, a recombinant human IgG1κ anti-CCL2 antibody, was well-tolerated in a phase I clinical trial in patients with various solid cancers, as well as showing signs of anti-tumour activity (Sandhu et al., 2013). Suppression of free serum CCL2 by carlumab was transient, however, and a lack of clinical activity in a phase II trial in patients with prostate cancer led to its discontinuation (Pienta et al., 2013). A number of CCR2-targeting drugs have also been developed, including a small molecule inhibitor PF-04136309, which improved the anti-tumour efficacy of gemcitabine in pre-clinical models of pancreatic cancer (Mitchem et al., 2013). Although a combination of PF-04136309 and FOLFIRINOX was well-tolerated and improved ORRs in a phase Ib trial in patients with locally-advanced pancreatic cancer (Nywening et al.,

2016), unacceptable levels of pulmonary toxicity were observed in a subsequent phase Ib trial of PF-04136309, gemcitabine and paclitaxel (Noel et al., 2019).

Table 2: Overview of macrophage-targeting therapies in clinical trials for solid cancers. Adapted from (Lin et al., 2019).

Drug	Target	Treatment	Cancer type	Phase	Results	Refs
Systemic macrophage depletion						
Trabectedin	Pan-macrophages	Monotherapy	Mesothelioma	I	Recruiting	NCT02194231
Inhibition of monocyte/macrophage recruitment and survival						
PLX3397	CSF-1R	Monotherapy	TGCT	III	ORR, 39%	(Tap et al., 2019)
		Monotherapy	Melanoma	I/II	Active, not recruiting	NCT02975700
		Monotherapy	Glioblastoma	II	No anti-tumour activity	(Butowski et al., 2016)
		Paclitaxel	Solid tumours	I	Completed, not yet reported	NCT01525602
		Durvalumab	Colorectal, pancreatic	I	Active, not recruiting	NCT02777710
RG7155	CSF-1R	Monotherapy	Solid tumours	Ia/b	No anti-tumour activity	(Gomez-Roca et al., 2019)
		Paclitaxel	Solid tumours	Ia/b	No anti-tumour activity	(Gomez-Roca et al., 2019)

		Monotherapy	Dt-GCT	I	CR + PR, 86% SD, 11%	(Ries et al., 2014)
		Atezolizumab	Solid tumours	I	Active, not recruiting	NCT02323191
		Paclitaxel + bevacizumab	Ovarian	II	Active, not recruiting	NCT02923739
Carlumab	CCL2	Monotherapy	Solid tumours	Ib	Signs of anti-tumour activity	(Sandhu et al., 2013)
		Monotherapy	Prostate	II	No anti-tumour activity	(Pienta et al., 2013)
PF-04136309	CCR2	FOLFIRINOX	Pancreatic	Ib	ORR, 49%	(Nywening et al., 2016)
		Gemcitabine, paclitaxel	Pancreatic	Ib	Pulmonary toxicities	(Noel et al., 2019)
Macrophage re-polarisation						
CP-870, 893	CD40	Monotherapy	Solid tumours	I	OPR, 14%	(Vonderheide et al., 2007)
		Gemcitabine	Pancreatic	I	ORR, 19% PFS, 5.6% OS, 7.4%	(Beatty et al., 2013)
		Paclitaxel + carboplatin	Solid tumours	I	PR, 20% SD, 40% CR, 0%	(Vonderheide et al., 2013)

ORR, objective response rate; PR, partial response; CR, complete response; SD, stable disease, PFS, progression-free survival; OS, overall survival; OPR, objective partial response; CSF-1R, colony stimulating factor 1 receptor; GCT, giant cell tumour. CCL2, chemokine ligand 2.

The most clinically-advanced TAM-targeting strategy relies on inhibition of CSF-1/CSF-1R signalling, the major axis for differentiation, survival and proliferation of cells of the mononuclear phagocyte system and in particular macrophages. Blockade of CSF-1R, either with small molecules (e.g. PLX3397 and BLZ945) or antibodies (e.g. RG7155), has proven efficacious at the pre-clinical level, reducing TAM numbers and tumour growth in various animal models of cancer (Paulus et al., 2006; Ries et al., 2014; Yan et al., 2017). For the treatment of tenosynovial giant cell tumours (TGCT), a rare neoplasm characterised by overexpression of CSF-1, clinical development of CSF-1R inhibitors is at an advanced stage; a phase III clinical trial of PLX3397 in patients with TGCT was recently completed, with an ORR of 39% versus 0% for the placebo (Tap et al., 2019). Although generally well-tolerated, hepatotoxicity emerged as a severe side effect of PLX3397. Early-phase clinical trials of CSF-1R inhibitors for other solid tumour indications are ongoing or have been completed, though results so far have been less promising. In a phase II clinical trial in patients with glioblastoma, monotherapy with PLX3397 was well-tolerated but ineffective, with no improvement in progression-free survival relative to radiotherapy and temozolomide (Butowski et al., 2016). Several mechanisms of resistance to CSF-1R inhibition have been proposed, including macrophage-mediated secretion of insulin-like growth factor 1 (IGF-1), a phenomenon observed in glioma-bearing mice in response to treatment with BLZ945, which lead to elevated phosphoinositide 3-kinase (PI3K) activity in tumours (Quail et al., 2016). Moreover, in mouse models of various solid tumours, CSF-1R inhibition was unexpectedly found to induce an accumulation of pro-tumourigenic MDSCs, abrogating the benefits of TAM depletion (Kumar et al., 2017). Improved anti-tumour efficacy of CSF-1R inhibitors has been observed at the pre-clinical level upon combination with other agents, such as ICIs (Zhu et al., 2014), suggesting that the

therapeutic potential of this approach may be maximised as part of a combinatorial regimen.

Nevertheless, given their critical functions in homeostasis and immune defence, concerns remain regarding the safety of long-term macrophage depletion in tissues throughout the body (Cannarile et al., 2017),

1.4.4.3 Macrophage re-polarisation

A third strategy exploits the inherent plasticity of TAMs to restore their tumouricidal functions. Several agents are under investigation for their ability to re-polarise TAMs towards a more M1-like phenotype, including agonists of toll-like receptors, anti-CD40 antibodies, certain histone deacetylase inhibitors and IFN-α (Kowal et al., 2019). The most extensively-tested macrophage-repolarising agents are agonistic anti-CD40 antibodies, which reduce tumour growth and stimulate anti-tumour immunity in various mouse models (Beatty et al., 2011; Rakhmilevich et al., 2012). Several anti-CD40 antibodies, such as CP870,893, a fully human IgG2 antibody, are under early clinical assessment either as a monotherapy or in combination with chemotherapy or immunotherapy. In a phase I clinical trial in patients with advanced solid tumours, systemic administration of CP870,893 monotherapy achieved an ORR of 14% (Vonderheide et al., 2007), with one melanoma patient exhibiting a complete response which has persisted for at least a decade (Bajor et al., 2014). Furthermore, phase I clinical trials of CP870,893 in combination with chemotherapeutic agents (paclitaxel+carboplatin or gemcitabine) in patients with advanced solid tumours have suggested enhanced anti-tumour activity of the combinatorial regimens relative to chemotherapy alone (Beatty et al., 2013; Vonderheide et al., 2013). Following promising results in pre-clinical models (Ito et al., 2000), a combination of CP-870,893 and anti-CTLA-4 antibody is also under clinical evaluation in

melanoma patients (NCT01103635). CD40 agonism is associated with notable immune-related adverse effects, however, with dose-limiting toxicities observed in some patients (Vonderheide et al., 2007)

1.4.5 TAMs exist as sub-populations exerting distinct pro-tumour functions

Whilst promising, many of the approaches described above fail to address the heterogeneity of TAMs, which appear to exist as sub-populations exerting distinct functions (Yang et al., 2018). Indeed, TAMs residing in different tumour compartments are exposed to widely varying stimulatory signals and, as such, can be predicted to adopt a variety of phenotypes.

At least in animal models, TAMs in hypoxic regions are polarised by lactic acid, low pH and cancer cell-derived high mobility group box 1 protein (HMGB1) towards a pro-angiogenic and immunosuppressive phenotype, characterised by expression of VEGFA, IL-10 and PD-L1 (Colegio et al., 2014; Huber et al., 2016; Lewis et al., 2000). In the stroma, meanwhile, TAMs receive signals from ECM components (e.g. collagen) and non-malignant cells like fibroblasts, pericytes and endothelial cells. Stromal TAMs are often $Tie2^{+}$ and angiogenic, as well as enhancing cancer cell migration and intravasation (Pinto et al., 2017; Varol and Sagi, 2018). TAMs lying close to tumour blood vessels - perivascular TAMs - are similarly associated with high levels of Tie2 expression and stimulation of angiogenesis, and, in addition, play key roles in chemo- and radiotherapy resistance (Lewis et al., 2016). High numbers of hypoxic, stromal and perivascular TAMs correlate with poor prognosis in many solid tumour types (Yang et al., 2018). On the other hand, TAMs in close proximity to tumour cells (i.e. within cancer nests) have been found to express NOS2 (Shimura et al., 2000), suggestive of an M1-like phenotype with anti-tumour potential.

Indeed, high numbers of nest TAMs correlated with favourable prognosis for endometrial (Ohno et al., 2004) and gastric cancers (Ohno et al., 2003).

The existence of sub-populations of TAMs with distinct functions is also supported by the finding that, for many cancers, expression levels of subset-specific (mostly M2-like) macrophage markers are of greater prognostic significance than those of pan-macrophage markers (Cui et al., 2013; Herwig et al., 2013; Lan et al., 2013; Le Page et al., 2012; Ma et al., 2010; Zhang et al., 2011; Zhang et al., 2014). Two M2-like macrophage markers associated with poor patient outcomes are CD206 and folate receptor β (FRβ).

CD206$^+$ TAMs

The mannose receptor, CD206, is a C-type lectin receptor expressed at high levels by IL-4-activated M2-like macrophages and TAMs. In a mouse mammary tumour model, CD206$^+$ TAMs were found to be MHC-II^{low} and more angiogenic than their CD206$^-$ counterparts (Movahedi et al., 2010). For ovarian and hepatocellular carcinomas, the density of CD206$^+$ TAMs, and not overall CD68$^+$ TAM density, was identified as a poor prognostic factor (Le Page et al., 2012; Shu et al., 2016).

FRβ$^+$ TAMs

Another M2-like macrophage marker associated with cancer-supporting TAMs is FRβ. A high number of FRβ$^+$ TAMs correlated with increased metastasis and poor prognosis in pancreatic cancer patients, with FRβ$^+$ TAMs being VEGF$^+$ and most prominent in the perivascular regions of the invasive fronts of the tumours (Kurahara et al., 2012). In *ex vivo* samples isolated from melanoma and breast adenocarcinoma patients, FRβ$^+$ TAMs were found to be CD163$^+$ and IL-10-producing, suggesting that they represent an immunosuppressive TAM population (Puig-Kröger et al., 2009).

1.4.6 Strategies to achieve targeted depletion of specific TAM subsets

In light of the heterogeneity of TAMs and their anti-tumour potential, selective targeting of the most cancer-promoting TAM subsets is a highly desirable approach. However, relative to pan-macrophage-targeting treatments, there are currently very few therapeutic options for the depletion of specific M2-like TAM subsets.

One strategy involves conjugation of drug-loaded liposomes to molecules preferentially recognised by M2-like macrophages. For instance, liposomes containing zoledronic acid were coated with folate to encourage their phagocytosis by FRβ-expressing macrophage (Hattori et al., 2015). Although selective cytotoxicity towards $FR\beta^+$ cells was observed *in vitro*, this formulation triggered lethal toxicities in murine tumour models, with no appreciable anti-tumour activity (Hattori et al., 2015). The mechanisms underlying these adverse effects - which were also observed with non-folate-linked liposomal zoledronic acid - were not determined (Hattori et al., 2015).

Liposomes coated with mannose have also been engineered and shown to be phagocytosed specifically by M2-like macrophages (Zhu et al., 2013), although their anti-tumour activity is yet to be explored. Very recently, doxorubicin-loaded liposomes coated with anti-CD163 antibodies were reported to selectively deplete $CD163^+$ TAMs in a mouse model of melanoma, leading to tumour regression due to an infiltration of cytotoxic T cells and inflammatory monocytes (Etzerodt et al., 2019). Interestingly, non-targeted doxorubicin-loaded liposomes, which indiscriminately reduced the total TAM population, were less effective than their CD163-targeted counterparts in reducing tumour growth (Etzerodt et al., 2019), suggesting a role for $CD163^-$ TAMs in mediating tumour regression.

In an alternative approach, *Pseudomonas* exotoxin A was fused to a disulphide-stabilised fragment of variable regions from an anti-FRβ antibody (Nagai et al., 2009). In a mouse

model of glioma, the FRβ-targeting immunotoxin depleted TAMs whilst being well-tolerated, leading to reduced tumour growth (Nagai et al., 2009). Other M2 macrophage-targeting fusion proteins are based on dKLA, a pro-apoptotic peptide which disrupts mitochondrial membranes. Using a phage library screening approach, researchers identified a peptide ("M2pep") which preferentially bound M2- over M1-polarised murine macrophages (Cieslewicz et al., 2013). M2pep fused to dKLA selectively reduced the M2-like TAM population in syngeneic tumour-bearing mice, slowing tumour growth and prolonging animal survival (Cieslewicz et al., 2013). More recently, dKLA was fused to melittin, a peptide component of bee venom which preferentially binds M2-over M1-polarised murine macrophages (Lee et al., 2017a). Melittin-dKLA induced apoptosis in M2-like TAMs, reducing angiogenesis and tumour growth in a syngeneic mouse model of lung cancer (Lee et al., 2019a).

Although they serve to illustrate the benefits of depleting M2-like TAMs, the strategies described above are limited in their clinical applicability; large-scale production and delivery of liposome-based therapies, for instance, presents significant technical challenges (reviewed in (Sercombe et al., 2015)), whilst immunotoxins have been associated with high levels of toxicity and immunogenicity (Mazor et al., 2016). Regarding the dKLA-based fusion proteins, preferential recognition of M2-like macrophages was demonstrated in murine and not human immune cells (Cieslewicz et al., 2013; Lee et al., 2019a). Given that the binding sites of melittin and M2pep are yet to be elucidated (Cieslewicz et al., 2013; Lee et al., 2019a), it is unknown whether their specificity for M2-like murine macrophages will extend to human systems. Thus, there is an unmet need for safe and feasible therapeutic options to target M2-like TAM subsets, and for their validation in relevant human models.

In the following sections, an argument for targeting M2-like TAMs with BiTE technology will be put forward. The mode of action and clinical development of BiTEs is first described, followed by discussion of a strategy to localise their expression to tumours with engineered oncolytic viruses (OVs).

1.5 Bispecific T Cell Engagers

1.5.1 Structure and mode of action of BiTEs

BiTEs ordinarily comprise two scFvs joined by a flexible glycine-serine linker, with one scFv recognising CD3ε on T cells and the other recognising a selected targeted antigen (Figure 1.5A). Binding of multiple BiTEs to their respective target antigen triggers CD3 cross-linking, T cell activation and the formation of a pseudo-immunological synapse with the target cell (Offner et al., 2006). Secretion of perforin and granzyme B, as well as surface expression of Fas ligand, by BiTE-activated T cells triggers target cell killing by apoptosis (Osada et al., 2010) (Figure 1.5B). Depending on the level of T cell activation, cytotoxicity may be accompanied by the release of cytokines (e.g. IL-2) and proliferation (Osada et al., 2010; Wong et al., 2013).

T cell activation by BiTEs occurs independently of TCR recognition, and without a requirement for co-stimulation (e.g. with CD28 agonism or IL-12) (Dreier et al., 2002). BiTEs are extremely potent agents, with EC_{50} values in the picomolar range, and mediate target cell killing even at low effector:target (E:T) ratios (<1:5), indicative of serial killing by BiTE-activated T cells (Hoffmann et al., 2005). Indeed, video-associated microscopy revealed sequential killing of multiple target cells by T cells activated with a CD19-targeting BiTE (Hoffmann et al., 2005). Given that T cell activation by BiTEs occurs independently of peptide/HLA recognition by their TCR, all T cells can, in theory, be targeted with this approach. Interestingly, not only cytotoxic $CD8^+$ but also helper $CD4^+$

T cells are capable of mediating BiTE-directed target cell lysis, albeit with delayed kinetics (Mack et al., 1997). Whether or not the cytolytic potential of BiTE-activated $CD4^+$ T cells extends to Tregs is yet to be resolved, with pre-clinical studies yielding conflicting results (Choi et al., 2013a; Koristka et al., 2014), possibly due to differing methods of Treg isolation used by researchers. Unlike CAR-based therapies, for which naïve T cells exert superior efficacy *in vivo*, only antigen-experienced T cells were reported to carry out BiTE-mediated target cell killing (Dreier et al., 2002), although clear evidence supporting this assertion is still lacking.

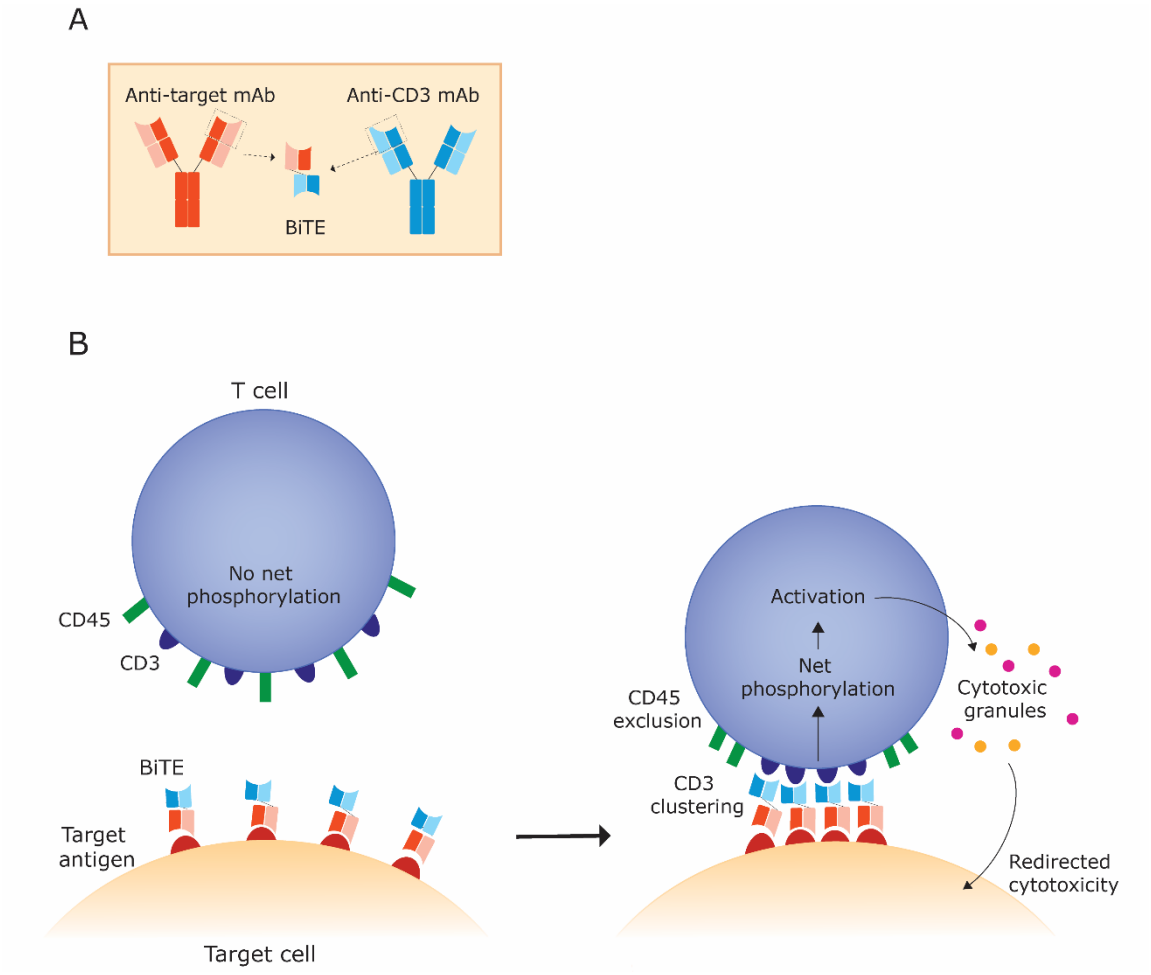

Figure 1.5. Structure and postulated mode of action of BiTEs. (**A**) Schematic representation of BiTE structure. (**B**) Simultaneous binding of multiple BiTEs to their respective target antigens triggers the formation of a pseudo-immunological synapse, with CD3 clustering and CD45 exclusion from the synapse, leading to net TCR phosphorylation, T cell activation and redirected cytotoxicity towards the target cell. Adapted from (Scott et al., 2018).

In addition to mediating direct toxicity towards target cells, BiTE-activated T cells have been reported to induce bystander killing of neighbouring cells devoid of target antigen expression (Ross et al., 2017). In the case of an epidermal growth factor receptor (EGFR)-targeting BiTE, this was attributed to T cell-mediated secretion of cytokines and the up-regulation of intercellular adhesion molecule (ICAM)-1 and FAS receptor on bystander cells, which may have caused their sensitisation to killing by activated T cells (Ross et al., 2017). BiTEs are also predicted to act on target antigen-negative cells via "epitope spreading" - a phenomenon in which immune responses broaden from the initially-targeted epitope(s) to others. Pre-clinical evidence for epitope spreading due to BiTE treatment comes from studies with a bispecific antibody targeting WT1, an intracellular oncoprotein presented on HLA-A*02:01. Patient-derived PBMCs treated *ex vivo* with the WT1-targeting BiTE (in the presence of autologous tumour cells) were found to gain responsiveness to antigens other than WT1 peptide, such as HER2, suggestive of epitope spreading (Dao et al., 2015).

1.5.2 Clinical progress in BiTE therapy of haematological malignancies

The most clinically-advanced BiTE is blinatumomab, a CD19-targeting BiTE which received accelerated FDA approval in 2014 for the treatment of Philadelphia chromosome (Ph)–negative relapsed/refractory (R/R) B cell precursor acute lymphoblastic leukaemia (ALL) (Przepiorka et al., 2015). Approval was granted based on the results of a single-arm trial involving 185 R/R ALL patients, 32% of whom experienced a complete remission (Przepiorka et al., 2015). A subsequent randomised phase III trial (TOWER) demonstrated superiority of blinatumomab over standard-of-care chemotherapy (complete remission rate of 34% versus 16%; 3.7-month improvement in median survival), leading to its full approval in 2017 (Pulte et al., 2018). Since then, regulatory approval of blinatumomab has

been extended to the treatment of Ph-positive R/R ALL (Pulte et al., 2018), and B cell ALL with minimal residual disease (Jen et al., 2019). Clinical trials of blinatumomab for the treatment of other CD19-positive malignancies are ongoing (Velasquez et al., 2018). Other BiTEs targeting haematological cancers include CD33-targeting AMG 330 and BCMA-targeting AMG 420, which are in early-phase clinical trials for the treatment of R/R acute myeloid leukaemia and multiple myeloma, respectively (NCT02520427, NCT03836053).

Clinical experience with blinatumomab has highlighted a number of advantages and disadvantages of BiTEs. First, in line with their remarkable potency *in vitro* and in animal studies, low doses of BiTE are sufficient to elicit a clinical response; in a phase II trial involving patients with ALL, a dose of 15 μg m^{-2} per day eliminated minimal residual disease in 80% of patients (Topp et al., 2011). At 55 kDa, BiTEs are below the threshold to avoid renal clearance (~60 kDa) and thus exhibit a short serum half-life (1.25 h in humans for blinatumomab (Klinger et al., 2012)). This necessitates their continuous intravenous infusion (28 days per cycle for blinatumomab), which poses significant clinical challenges; indeed, medication errors (overdose), were reported for 4% of patients in the blinatumomab arm of the phase III TOWER trial (Kantarjian et al., 2017). On the other hand, the short half-life of BiTEs may be viewed as an advantage as it permits fine-tuning of serum BiTE concentration, possibly avoiding adverse effects. Frequent side effects of blinatumomab treatment include fever and neutropenia, observed in up to 75% (Topp et al., 2014) and 37% (Kantarjian et al., 2017) of patients, respectively. Whilst less common, dose-limiting side effects (cytokine release syndrome and neurotoxicity) have also been reported (Kantarjian et al., 2017), particularly in patients with a high disease burden.

1.5.3 BiTE therapies for solid tumours

BiTEs targeting a range of solid tumour antigens (epithelial cell adhesion molecule (EpCAM), EGFR, ephrin type-A receptor 2 (EphA2), prostate stem cell antigen, prostate-specific membrane antigen (PSMA), CEA, EGFR variant 3 (EGFRvIII)) have also been developed, and shown to exert anti-tumour effects in various murine xenograft tumour models (Brischwein et al., 2006; Choi et al., 2013b; Friedrich et al., 2012; Herrmann et al., 2010; Osada et al., 2010). Unlike BiTE therapies for haematological cancers, however, their efficacy in the clinic is yet to be proven. The first BiTE to undergo clinical evaluation for the treatment of solid tumour indications was solitomab (MT110, AMG 110), an EpCAM-targeting BiTE which was evaluated in a phase I trial for the treatment of patients with refractory, EpCAM-positive solid cancers (Fiedler et al., 2012). Dose-limiting adverse events (liver toxicity and diarrhoea) were observed, and attributed to "on-target off-tumour" effects of solitomab on EpCAM-expressing healthy tissue (Kebenko et al., 2018). Subsequently, a CEA-targeting BiTE, AMG 211 was assessed in early-phase clinical trials involving patients with advanced gastric adenocarcinoma. In a phase I study in which AMG 211 was administered intermittently, no objective responses were observed (Pishvaian et al., 2016), prompting the launch of a second phase I clinical trial to assess continuous infusion of AMG 211 (Moek et al., 2018). Though well-tolerated, the treatment triggered the production of anti-AMG 211 antibodies in all patients and no therapeutic effects were observed, leading to discontinuation of the trial (Moek et al., 2018). More recently, a phase I clinical trial of a BiTE recognising PSMA (AMG 212) in patients with metastatic castration-resistant prostate cancer was completed (Hummel et al., 2019). AMG 212 was well-tolerated and triggered a dose-dependent decline in serum PSA levels (Hummel et al., 2019), making it the first BiTE to demonstrate signs of clinical activity against solid tumours.

Taken together, despite the promising activity demonstrated by AMG 212, the clinical development of BiTEs for solid tumours lags far behind that of BiTEs targeting haematological malignancies. Solid tumours pose a number of challenges for BiTEs in terms of safety and efficacy, which will be discussed in the following section.

1.5.4 Challenges for effective BiTE therapy of solid tumours

Selection of an appropriate TAA for BiTE-based targeting is particularly problematic in the case of solid cancers. TAAs generally fall into two categories: i) those that are not unique to tumour cells, but are rather overexpressed on tumour versus benign tissues (e.g. EGFR), and ii) truly tumour-specific "neoantigens" (e.g. EGFRvIII). Given that as few as 1,000 target antigens are reportedly necessary for BiTE-mediated T cell killing of target cells (Stone et al., 2012), it seems unlikely that BiTE therapies will discriminate effectively between elevated (tumour) and benign levels of TAA expression. In the treatment of haematological malignancies, such "on-target, off-tumour" side effects are often manageable; B cell aplasia associated with CD19-targeting BiTEs, for instance, is generally well-tolerated and can be treated with antibody infusion. For BiTEs targeting solid tumours, however, toxicity towards benign tissues with low levels of antigen expression can be severe and dose-limiting, as demonstrated by the phase I trial of EpCAM-targeting solitomab (discussed above) (Kebenko et al., 2018). Similarly, serious liver and kidney toxicities were observed in non-human primates treated with high doses of an EGFR-targeting BiTE, which was attributed to EGFR expression in these tissues (Lutterbuese et al., 2010).

Solid tumours also pose unique challenges for BiTEs in terms of efficacy. Although BiTEs overcome several immune escape mechanisms, their success in the treatment of solid tumours still hinges, critically, upon: (i) the presence of sufficient numbers of T cells

within tumours and (ii) continued T cell functionality in the often hostile TME. As discussed in section 1.3, advanced solid tumours evolve a myriad of mechanisms to inhibit the infiltration and activity of cytotoxic T cells, altogether resulting in a great diversity in the magnitude and nature of tumour T cell infiltrates between patients. This diversity is expected to cause heterogeneity between patients in their responsiveness to BiTEs.

1.6 Oncolytic Virotherapy

1.6.1 Introduction to oncolytic virotherapy

Oncolytic viruses (OVs) are those which preferentially replicate in and lyse cancer cells. The concept of using viruses to treat cancer first arose in the late 1800s, with anecdotal reports of temporary remissions in cancer patients coinciding with their contraction of viral infections (Dock, 1904). Clinical trials using a range of wild-type human viruses were conducted during the mid-20th century and showed encouraging signs of therapeutic activity (Hoster et al., 1949; Smith et al., 1956; Southam and Moore, 1952; Webb et al., 1966), although at that time there were no means to ensure cancer-selectivity of virus infection. Interest in the field increased in the 1990s with the advent of genetic engineering, which enabled the development of next-generation OVs with improved safety and anti-tumour activity. Since then, over 100 clinical trials involving OVs have been initiated or completed. The most clinically-advanced OV is Talimogene laherparepvec (T-VEC), an attenuated herpes simplex virus (HSV)-1 encoding granulocyte-macrophage colony-stimulating factor (GM-CSF). Following a pivotal phase III clinical trial in which T-VEC outperformed GM-CSF alone (durable response rate of 16% versus 2%), T-VEC gained FDA approval in 2015 for the treatment of advanced metastatic melanoma (Rehman et al., 2016).

1.6.2 Basis of OVs' cancer cell selectivity

Many wild-type viruses, including Newcastle disease virus, reovirus, rodent protoparvoviruses, myxoma virus, and Seneca Valley virus, display an intrinsic preference for multiplication in tumour cells. Their oncotropism is thought to reflect the fact that many of the hallmarks of cancer, as described by Hanahan and Weinberg (Hanahan and Weinberg, 2011), are also facilitators of virus propagation. For instance, sustained proliferation, resistance to death and immune dysregulation are all factors that potentiate the completion of virus life cycles (Seymour and Fisher, 2016).

Cancer-selectivity of viruses may also be achieved (or enhanced) through genetic modification. For example, viral genes that are essential for replication in normal cells but dispensable in cancer cells may be deleted, thus restricting productive infection to tumour tissues. Notable examples include variants of adenovirus (e.g., 24bp deletion in E1A), HSV (e.g., deletion of ICP34.5), and vaccinia virus (VV) (e.g. thymidine kinase deletions).

A promising alternative approach to generate OVs is bioselection, wherein diverse libraries of viruses are serially passaged in cancer cells under conditions that favour recombination. Each successive passage selects for viruses with the greatest replicative and/or lytic capabilities, and the most potent OVs will eventually predominate. The power of bioselection resides particularly in its ability to select for viruses that target the cancer cell "phenotype," as opposed to specific oncogenic pathways. Enadenotucirev (EnAd), a chimera of group B adenoviruses type 3 and type 11p, is one example of a bioselected OV (Kuhn et al., 2008) and is currently the subject of early-phase clinical trials (NCT02028442, NCT02028117). EnAd is utilised in Chapter 6 of this thesis and will be discussed in greater detail in subsequent sections.

1.6.3 Route of OV delivery

The route of OV delivery is an important consideration. While most OV trials employ intratumoural administration, systemic delivery arguably represents the most attractive option, affording the opportunity to target disseminated disease. Viruses delivered via the bloodstream are vulnerable, however, to a range of serum factors like complement, natural immunoglobulin M, antiviral cytokines, and - in the case of pre-existing or acquired immunity to the virus – neutralising antibodies. In addition, a significant portion of the initial OV dose will likely be sequestered by macrophages in the lung, liver, and spleen (the mononuclear phagocyte system), reducing the number of virus particles that reach tumours. Non-immune factors may also hinder systemic OV delivery; binding to erythrocytes and to blood coagulation factors has been observed in the case of adenovirus (Carlisle et al., 2009) and the characteristically high interstitial fluid pressure of tumours, dense ECM and stroma may disfavour extravasation of OVs into tumours (McKee et al., 2006). Despite these challenges, several OVs, including EnAd, have demonstrated convincing intratumoural replication following systemic delivery (Gil-Martin et al., 2014). Approaches to facilitate delivery of other viruses, such as cell carriers (Iankov et al., 2007; Muthana et al., 2013), or physical methods using ultrasound-induced cavitation to improve tumour penetration (Bazan-Peregrino et al., 2012), have also yielded promising results.

1.6.4 Mechanisms of action of oncolytic viruses

A key advantage of OVs is their ability to induce cancer cell death by multiple mechanisms, and in a manner distinct from those elicited by chemotherapies, radiotherapy and other immunotherapies. The first is direct OV-mediated killing; following cell entry, OVs hijack the cellular machinery to aid their own replication, actively inducing lysis after production

of progeny virions. In the "oncolytic paradigm," lysis then leads to the release of new virus particles and spread of the virus throughout the tumour (Figure 1.6). OVs may also exert their anti-cancer effects indirectly. At least *in vivo,* OV-induced cell death is often accompanied by the release of DAMPs and pathogen-associated molecular patterns (PAMPs) into the TME, promoting the maturation of APCs and, subsequently, an induction of tumour- and virus-specific $CD4^+$ and $CD8^+$ T cell responses (Guo et al., 2014) (Figure 1.6). Indeed, the clinical candidate EnAd was found to kill independently of p53 and caspase; instead, infected cells were characterised by high surface exposure of calreticulin and release of the immunomodulatory molecules heat shock protein 70, ATP, and HMGB1 in a death mechanism reminiscent of oncosis (Dyer et al., 2017). *In vitro*, EnAd infection led to stimulation of DCs and $CD4^+$ T cells in mixed tumour-leukocyte cell reactions (Dyer et al., 2017). Early clinical trial data complements these findings, with $CD8^+$ T cells recruited to sites of viral activity in tumour biopsies extracted from patients treated systemically with EnAd (Boni et al., 2014).

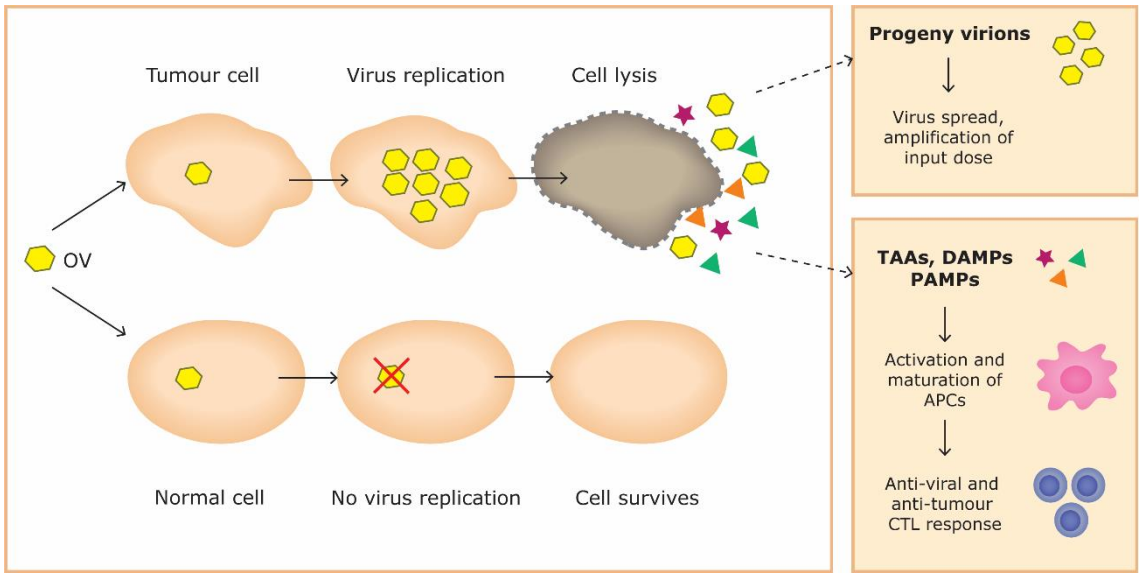

Figure 1.6. Mechanisms of action of OVs. OVs replicate selectively in cancer cells, leading to oncolysis and spread of progeny virions. OVs also exert anti-tumour effects indirectly, through stimulation of anti-tumour immune responses due to the induction of immunogenic cell death. (Scott et al., 2018).

1.6.5 "Arming" oncolytic viruses

In addition to directly inducing lysis and stimulating antitumor immunity, OVs can be engineered to encode biological therapeutics that are expressed locally as the virus replicates (Bauzon and Hermiston, 2014). Incorporation of a signal peptide enables secretion of biologics by infected cancer cells directly into the TME, leading to high-level accumulation selectively within the tumour. Importantly, the expression of therapeutic transgenes can be placed under the control of late viral promoters, restricting their production to cancer cells harbouring a productive virus infection. In this manner, therapeutic efficacy may be maximised while minimising systemic toxicities.

This approach also provides an exciting opportunity to facilitate delivery of alternative therapeutic formats, such as BiTEs, that are less amenable to systemic administration due to poor pharmacokinetics and/or off-tumour effects. Furthermore, increasing evidence suggests that OV treatment is associated with increased intratumoural T cell infiltration (see below), possibly providing a greater availability of effector cells for redirection with BiTEs. In the following sections, we will put forward a case for coupling OVs with BiTEs.

1.6.6 Oncolytic viruses and T cells

The induction of antiviral T cell responses is a well-documented consequence of viral infection of normal tissues. At least in animal models, OV-triggered inflammation in the tumour bed has been shown to alter the chemokine and cytokine milieu in such a way as to increase tumour infiltration with T cells (Benencia et al., 2005; John et al., 2012; Li et al., 2017b; Patel et al., 2015; Zamarin et al., 2014). Though more limited at present, clinical data also supports this phenomenon. Analysis of tissue specimens from melanoma patients treated in a Phase II trial with T-VEC revealed extensive infiltration of injected lesions with tumour-specific T cells (Kaufman et al., 2010). Similarly, increased

intratumoural T cells were observed in a Phase I trial of oncolytic measles virus involving patients with cutaneous T cell lymphoma, although it was not determined in this case whether these were virus or tumour-specific (Heinzerling et al., 2005). In patients with recurrent metastatic breast cancer, injection of a spontaneously mutated HSV-1 variant, HF10, triggered intratumoural $CD8^+$ T cell infiltration (Sahin et al., 2012). In a Phase I trial of a GM-CSF-encoding VV in patients with refractory melanoma, there was evidence of $CD4^+$ and $CD8^+$ T cell infiltration in injected lesions (Mastrangelo et al., 1999). Finally, preliminary data from a Phase I trial of EnAd against colorectal cancer has demonstrated $CD8^+$ T cell infiltration in virus-infected regions of tumours (Boni et al., 2014).

Such observations support the rational combination of OVs with T cell-based immunotherapies. Several clinical trials investigating OVs in combination with ICIs are underway or completed. In a phase II clinical trial of T-VEC in combination with ipilimumab in patients with advanced melanoma, the combination therapy achieved a higher ORR than ipilimumab monotherapy (39% vs 18%) (Chesney et al., 2018). Promising results were also reported in a phase Ib trial of T-VEC with pembrolizumab, which increased $CD8^+$ T cell infiltration (Ribas et al., 2017), and a phase II trial of this combination is underway.

1.6.7 Arming oncolytic viruses with BiTEs

The possibility of tumour-localised expression, combined with a virus-mediated influx of T lymphocytes into the TME, render OVs very appealing platforms for the delivery of BiTEs. This approach harnesses the advantages of BiTEs - namely, redirecting T cell cytotoxicity to any cell surface target, independent of the TCR specificity of the T cell and without MHC presentation—while bypassing the need for continuous intravenous infusion and avoiding associated toxicities. From another perspective, BiTEs may improve

OV efficacy by acting as immune "decoys," redirecting anti-viral TILs toward tumour cells and reducing premature, immune-mediated viral clearance. Such rationale have inspired the generation of several OV-armed BiTEs, combining the strengths of both approaches.

The first BiTE-armed OV to undergo preclinical evaluation was a double TK deleted Western reverse strain VV, engineered by Yu et al. to encode a BiTE targeting ephrin type-A receptor 2 (EphA2) (Yu et al., 2014). Expression of the EphA2-BiTE was placed under the control of a late viral promoter, F17R, restricting its expression to cells in which virus was replicating. *In vitro,* EphA2-BiTE-VV retained the replicative and oncolytic properties of its parental virus while mediating secretion of EphA2-BiTE from infected cancer cells, leading to T cell activation. Importantly, EphA2-BiTE-VV achieved bystander T cell-mediated killing of uninfected A549 cells, resulting in an overall increase in cytotoxicity relative to a control, green fluorescent protein (GFP)-expressing VV (GFP-VV). Improved efficacy was also demonstrated *in vivo*; systemic administration of EphA2-BiTE-VV, but not GFP-VV, together with human peripheral blood mononuclear cells (PBMCs) significantly improved survival in an A549 lung cancer xenograft model.

Taking a similar approach, Fajardo et al. have armed an oncolytic adenovirus, ICOVIR-15K, with an EGFR-targeting BiTE (Fajardo et al., 2017). EGFR-BiTE-ICOVIR-15K was able to replicate in and lyse tumour cells in vitro, resulting in expression and secretion of EGFR-BiTE, which was placed under the transcriptional control of the major late viral promoter. In co-culture experiments with adenovirus-permissive and refractory cancer cells, EGFR-BiTE-ICOVIR-15K, but not its unarmed counterpart, triggered T cell activation and bystander killing of resistant cells. Using two tumour xenograft models, the authors reported improved efficacy of both intratumourally and intravenously administered

EGFR-BiTE-ICOVIR- 15K, relative to the parental virus (Fajardo et al., 2017). This effect was dependent upon the subsequent delivery of human PBMCs or T cells.

While very encouraging, these studies describe efficient killing of target tumour cells using exogenous T cells, which may not be representative of the clinical situation in which patient T cells are subject to immunosuppression. In our laboratory, EnAd encoding a BiTE targeted to EpCAM was found to overcome immune-suppressive effects associated with the TME (Freedman et al., 2017). Virally-encoded EpCAM-BiTE was capable of activating endogenous T cells to target and kill tumour cells in primary human samples of malignant peritoneal ascites and pleural exudates isolated from cancer patients with various indications (Freedman et al., 2017)

Arming OVs with BiTEs targeting the TME

More recently, OVs have also been engineered to express BiTEs targeting non-cancerous cells of the TME. In one approach, EnAd was engineered to express a BiTE recognising CAFs (via fibroblast activation protein (FAP)). FAP BiTE-armed EnAd retained its oncolytic and replicative properties, as well as mediating T cell activation and cytotoxicity towards CAFs (Freedman et al., 2018). In solid cancer biopsies and malignant ascites samples, FAP BiTE-armed EnAd triggered T cell activation and CAF depletion. Excitingly, a pro-inflammatory repolarisation of malignant ascites was also observed upon treatment with FAP BiTE-armed EnAd, with a decrease in CAF-associated immunosuppressive factors (Freedman et al., 2018). Using a similar strategy, de Sostoa et al. reported the generation of another oncolytic adenovirus, ICOVIR-15K, armed with a FAP-targeting BiTE (de Sostoa et al., 2019). In murine xenograft models of lung and pancreatic cancer, treatment with FAP BiTE-armed ICOVIR-15K, together with pre-activated human T cells,

achieved superior anti-tumour efficacy relative to the parental or control BiTE-armed viruses (de Sostoa et al., 2019).

OVs armed with TME-targeting BiTEs thus offer a unique possibility to simultaneously target cancer and stromal cells in a tumour-localised manner. The potential of this multi-pronged therapeutic approach has been demonstrated at the pre-clinical level for OVs armed with BiTEs recognising CAFs. However, a similar strategy to target TAMs is yet to be explored.

1.7 Thesis Overview

1.7.1 Our proposed strategy

Effective immunotherapy of advanced solid tumours is hampered by the presence of a heavily immunosuppressed TME. Key among cancer-supporting cells of the TME are TAMs, a population of immune cells with central roles in tumour progression, immunosuppression, metastasis and therapy resistance. TAMs are highly heterogeneous, however, and can also exert anti-tumour effects. Selectively eradicating the most cancer-promoting subsets of TAMs, whist leaving those with anti-tumour potential unharmed, is a desirable but challenging goal.

One potentially-exploitable variation between TAM subsets is their differential expression of certain surface markers. These include M2-like macrophage markers FRβ and CD206, overexpression of which is associated with poor patient prognosis. Whilst a number of FRβ- and CD206-targeting strategies have been attempted (e.g. liposomes, immunotoxins), they are limited in their clinical applicability (as described in section 1.4.6). This thesis explores the possibility of harnessing BiTE technology to target cancer-promoting TAMs. BiTEs represent valuable tools with which to achieve surface marker-based killing of chosen target cells. By redirecting endogenous T cells to kill target cells of choice, BiTEs achieve targeted cell lysis with remarkable levels potency and specificity. BiTEs will be engineered to direct T cell cytotoxicity towards cells with high levels of FRβ and CD206 (i.e. M2-like, cancer-promoting TAMs), whilst leaving those with very low levels of these antigens, which may have anti-tumour properties (i.e. M1-like TAMs), unharmed.

The presence of FRβ and CD206 on healthy tissues makes safe targeting of these antigens with BiTEs challenging. A promising strategy to achieve tumour-localised BiTE expression

involves the use of "armed" OVs, encoding therapeutic transgenes that are expressed intratumourally as the virus replicates. A second part of this thesis involves the generation of oncolytic adenoviruses (EnAd) encoding the TAM-targeting T cell engagers.

Successful translation of cancer therapies is hindered by the use of murine models which do not fully recapitulate the immunosuppressed nature of advanced tumours. Throughout the thesis, clinically-relevant *ex vivo* models of human cancer (malignant ascites samples) will therefore be employed to assess the efficacy of the free- and virally-encoded TAM-targeting T cell engagers.

1.7.2 Thesis hypotheses

1. BiTEs engineered to recognise FRβ or CD206 (i.e. TAM-targeting BiTEs) will direct T cell cytotoxicity towards cells expressing FRβ or CD206, respectively
2. TAM-targeting BiTEs will exhibit selectivity for M2- over M1-polarised macrophages
3. Endogenous T cells in human malignant ascites samples will be activated by TAM-targeting BiTEs to deplete autologous M2-like ascites macrophages
4. Engineering EnAd to encode the TAM-targeting BiTEs will facilitate BiTE secretion from virus-infected cells without compromising its oncolytic activities
5. TAM-targeting BiTE-armed EnAd will mediate simultaneous killing of cancer cells and M2-like macrophages
6. Depletion of M2-like macrophages (either with free- or virally-encoded EnAd) will repolarise *ex vivo* models of cancer towards a more pro-inflammatory, immune-responsive state

1.7.3 Thesis structure

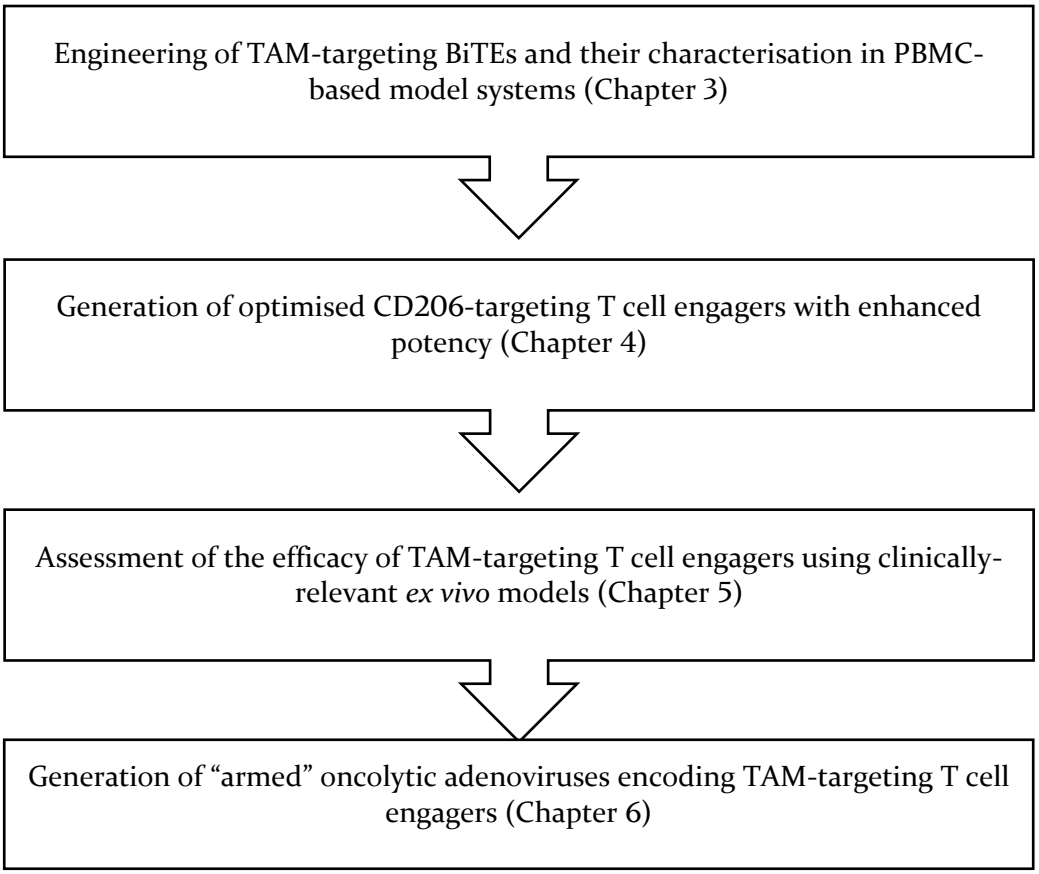

2 Materials and Methods

2.1 Cell Culture

2.1.1 Cells and maintenance

Immortalised cell lines (characteristics summarised in Table 2.1) were maintained in Dulbecco's modified Eagle's medium (DMEM, Sigma-Aldrich, UK) supplemented with 10% volume/volume (v/v) heat-inactivated foetal bovine serum (FBS, Gibco, UK, #10500064). Primary cells were cultured in X-VIVO medium (Lonza #04-380Q) supplemented with 1% heat-inactivated human AB serum (HS; Sigma-Aldrich #H4522), unless otherwise stated.

Table 2.1. Immortalised cell lines used in this study.

Cell line	Description	Source	Doubling time
HEK293A	• Originally derived from human embryonic kidney cells • Contains a stably integrated copy of the adenovirus E1 gene • Adherent	ATCC	~20 h
DLD-1	• Human colorectal adenocarcinoma cell line • Adherent	ATCC	~20 h
SKOV3	• Human ovarian adenocarcinoma cell line • Adherent	ATCC	~48 h

ATCC, American Type Culture Collection

To avoid high confluency, immortalised cells were sub-cultured every 2-4 days by enzymatic dissociation with Trypsin/Ethylenediaminetetraacetic acid (EDTA) (0.25% Trypsin, 0.02% EDTA; Sigma-Aldrich #T4049). Following medium aspiration, cells were

washed in Dulbecco's phosphate-buffered saline (PBS; Sigma-Aldrich #14190250) and trypsined for 2-5 min at 37°C. Cells were resuspended in complete medium and, according to their growth rates, split at a ratio of 1:3 to 1:10.

2.1.2 Cryopreservation and recovery

Cells to be cryopreserved were resuspended in FBS containing 10% (v/v) dimethyl sulfoxide (DMSO), aliquoted and cooled slowly in freezing containers (Cryo 1°C Mr. Frosty, Nalgene) at -80°C. For long-term storage, cells were transferred to a liquid nitrogen tank (-196°C). Cryopreserved cells were recovered by thawing at 37°C, resuspending drop-wise into pre-warmed complete medium, followed by centrifugation (400 x g, 5 min) and final resuspension in fresh complete medium.

2.1.3 DNA transfection to generate BiTEs/TriTEs

HEK293A cells were seeded in 6-well plates (small-scale transfections) or T175 flasks (large-scale transfections) and, at 80-90% confluency, transfected with plasmid DNA using Lipofectamine 2000 (#11668019, ThermoFisher, UK). Plasmid DNA and Lipofectamine 2000 (quantities displayed in Table 2.2) were diluted in Opti-MEM (#11058021, ThermoFisher, UK) and incubated for 5 min at room temperature (RT). The two solutions were then mixed and incubated together for 20 min at RT. The resultant DNA:lipofectamine complexes were further diluted in Opti-MEM (volumes in Table 2.2), and added drop-wise to the cells. For every transfection performed, an empty parental vector (pSF-CMV-Amp or pSF-CMV-Kan, as appropriate) was transfected in parallel and served as a negative control, whilst a GFP-containing plasmid (pSF-CMV-eGFP) was used to assess transfection efficiency.

Four hours later, transfection medium was replaced with fresh Opti-MEM. BiTE-containing supernatants were harvested 48 h later and processed, as described in section 2.3.1.

Table 2.2. Reaction mixtures for Lipofectamine 2000 transfections.

Scale	Plasmid DNA (μg)	Lipofectamine 2000 (μL)	Opti-MEM (dilution volumes)	Opti-MEM (final volume)
6-well plate	2.5	7.5	2 * 250 μL	1 mL
T175 flask	40	120	2 * 4 mL	18 mL

2.2 Molecular Cloning Techniques

2.2.1 Restriction digests

Enzymatic restriction digests were performed for i) diagnostic purposes, ii) to prepare vector backbones for HiFi DNA assembly, and iii) to linearise the EnAd viral backbone prior to transfection. Digests were performed in accordance with manufacturers' instructions (NEB, UK) (see Table 2.3 for reaction mixtures), incubating for a total of 2 hours at 37°C. For the preparation of vector backbones, alkaline phosphatase (1 μL, #M0290S, NEB, UK) was added to the reaction mixture for the final 1 hour of incubation to minimise re-ligation.

Table 2.3. Reaction mixtures for restriction digests.

Purpose	Plasmid DNA (µg)	Restriction enzyme (µL)	CutSmart buffer (µL)	Total volume (made up with H_2O, µL)
Diagnostic digest	**0.5**	**0.25**	**1**	**10**
Vector preparation	**2**	**1**	**4**	**40**
EnAd backbone linearisation	**25**	**5**	**11**	**1100**

2.2.2 Polymerase chain reaction (PCR)

PCR amplifications were performed with Phusion polymerase in 20 µL reactions comprising 1 ng template DNA, 10 µL Phusion Mastermix (2X; NEB, UK, #M0531L) and 0.5 µM forward and reverse primers (for primer list see Appendix III: Primers) . The following thermocycling conditions were used:

1. **Initial denaturation:** 98°C for 30 s
2. **Denaturation:** 98°C for 10 s
3. **Annealing:** Primer-specific annealing temperature for 30 s
4. **Extension:** 72°C for 1 min/kb
5. **Repeated cycles:** Return to 2, x 34
6. **Final extension:** 72°C for 10 min
7. 4°C forever

PCR reactions were performed using a PTC-225 Peltier Thermal Cycler DNA Engine Tetrad (MJ Research, US).

2.2.3 Agarose gel electrophoresis

Restriction digest and PCR products were resolved and visualised by agarose gel electrophoreses. Briefly, 1% (w/v) agarose gels were prepared using 1x TAE (50x TAE Buffer: 242 g trisaminomethane (Tris), 100 mL 0.5 M EDTA and 57.1 mL Glacial Acetic

Acid in 1L H_2O) and contained GelRed nucleic acid gel stain (Biotium, UK, #BT41003) for DNA visualisation. Samples were mixed with 6x loading dye (NEB, UK, #B7025S) and ran alongside a DNA ladder (Quick-load 1 kb DNA ladder, NEB, UK, #N0468S, unless otherwise specified) in TAE buffer at 120V for 30-60 minutes. Gels were subsequently visualised under UV light using an Alpha Imager (Alpha Innotech, USA).

Where necessary (i.e. for all DNA fragments intended for Gibson assembly), bands were excised by visualising under blue light using a Dark Reader trans-illuminator (GRI, UK). DNA was then extracted and purified with a Monarch DNA gel extraction kit (NEB, UK, #T1020L), eluting in 10 µL H_2O.

2.2.4 Gibson assembly

Gibson assembly is a cloning method which enables the joining of multiple DNA fragments in a single reaction. This technique relies upon the presence of overlapping regions of DNA (20-40 bp) between adjacent fragments, which anneal following the generation of complementary overhangs by a 5' exonuclease (Gibson et al., 2009). Overlapping fragments were generated through PCR amplification of insert DNA (see Appendix III: Primers) and restriction digest of plasmid backbones.

Gibson assembly was performed using HiFi DNA Assembly Master Mix with HF buffer (NEB, UK, #E2621L). According to manufacturer's recommendations for 2-3 fragment assemblies, for most reactions 50 ng vector and a vector:insert molar ratio of 1:2 were utilised. As an exception, all reactions involving the EnAd viral backbone were performed at a vector:insert ratio of 1:15 owing to the large size of this vector. Following incubation for 1 hour at 50°C, the reaction products were used immediately for bacterial transformation or stored at 4°C until further use.

2.2.5 Bacterial transformation

After being thawed on ice, competent XL10 *Escherichia coli* (*E. coli*) cells were mixed with 2 µL HiFi DNA assembly reaction product and incubated on ice for 30 min. Cells were then heat-shocked at 42°C for 45 seconds, before returning to ice for a further 2 minutes. 500 µL SOC outgrowth medium (#15544-034, Thermo Fisher, UK) were added and the culture incubated for 1 hour at 37°C on a shaker. Finally, cells were spread onto agar plates containing 50 ng/mL of the appropriate antibiotic and incubated at 37°C overnight.

2.2.6 Plasmid preparation and purification

Bacterial colonies were selected and grown in Lysogeny broth (LB) medium (3 mL or 150 mL for mini and maxi-preparations, respectively; #L3022, Sigma-Aldrich, UK) under ampicillin or kanamycin selection, where appropriate. Cultures were incubated overnight at 37°C in an orbital shaker at 200 rpm. Plasmid purification was then performed using the QIAprep Spin Miniprep Kit (#27106, Qiagen, UK) or Qiagen Plasmid-Plus Maxiprep Kit (#12945, Qiagen, UK) as appropriate, following manufacturer's instructions.

For purification of linearised recombinant EnAd constructs (prior to transfection), an isopropanol precipitation method was used. In brief, DNA was mixed with 0.6 volumes of isopropanol and centrifuged at 12,000 g for 30 min at 4°C. After removing the isopropanol, the pellet (containing precipitated DNA) was washed with 70% ethanol, then centrifuged again at 12,000 g for 2 min at RT. Residual ethanol was removed by pipetting and subsequent air-drying. Finally, the DNA pellet was resuspended in a small volume (<10 µL) of dH_2O.

2.2.7 Sequencing

Plasmid clones with the correct restriction digest patterns were sequenced by Sanger sequencing at Eurofins genomics (Germany), and aligned with the predicted sequences using Geneious software (US).

2.3 Protein Production and Analysis

2.3.1 BiTE/TriTE preparation

Supernatants from HEK293A cells transfected with BiTE/TriTE-encoding plasmids were collected 48 h post-transfection and clarified by centrifugation (400 g, 5-10 min, depending on volume). Supernatants were then concentrated 10- to 20-fold with Amicon Ultra-15 Centrifugal Filter Units (#UFC901024, Merck, UK), aliquoted and stored at -80°C until required.

2.3.2 Immunoblotting

BiTE/TriTE expression was assessed and quantified by western or dot blotting with anti C-terminal His antibody (3D5, Invitrogen, UK, #R930-25, Table 2.4).

For western blotting analysis, BiTE/TriTE-containing supernatants were mixed with Laemmli buffer, denatured at 95°C for 10 min, then loaded alongside a Protein ladder (PageRuler Plus, ThermoFisher, UK, #26619, unless otherwise specified) in 12-well 4-20% pre-cast polyacrylamide gels (Mini-PROTEAN TGX Precast Gels, BioRad, UK, #4561095) and run at 120 V for 1 hour in sodium dodecyl sulfate (SDS) running buffer (for recipe see Appendix I: Materials). Resolved proteins were transferred to a nitrocellulose membrane (BioRad, UK, #1620213) at 300 A for 90 min at 4°C, using transfer buffer containing 10% methanol (see Appendix I: Materials). Efficiency of transfer was assessed by Ponceau staining (Biotium, UK, #22001). For dot blotting, serially-diluted samples (1 µL) were

dotted directly onto membranes. To generate a standard curve, a deca-His tagged standard protein of known concentration was serially diluted and applied in parallel. Membranes were dried and subjected to the same procedure as western blots (see below).

Membranes were blocked in 5% milk (Sigma-Aldrich, UK, #70166) (diluted in PBS-Tween (PBST), 0.1 % Tween) for 1 hour at RT, then incubated with anti C-terminal His tag (1:5,000 dilution in 5% milk, clone 3D5, Invitrogen, UK, #46-069) primary antibody overnight at 4°C. After washing 3 times in PBST, membranes were further incubated with horseradish peroxidase (HRP)-conjugated secondary antibody (1:3,000, Cell Signalling Technology, UK, #7076, Table 2.4) for 1 hour at RT. Following more washing with PBST, SuperSignal West Dura Extended Duration Substrate (Thermo Fisher, UK, #34075) was applied and the membrane exposed to X-ray film, which was subsequently developed in an automatic film processor (Agfa CP1000).

Table 2.4. Antibodies used in immunoblotting and ELISA assays.

Target	Clone	Dilution	Isotype	Conjugate	Company	Cat. number(s)
6xHis	3D5	1:5,000	Ms IgG2b	-	Invitrogen, UK	#46-069
Mouse IgG	Polyclonal	1:3,000	Horse IgG	HRP	Cell Signalling Technology, UK	#7076

2.3.3 Enzyme-linked immunosorbent assay (ELISA) to assess BiTE/TriTE binding

BiTE binding to CD206 was assessed by ELISA. In brief, Nunc-Immuno 96-well plates (Sigma-Aldrich, UK, #M9410) were coated overnight at 4°C with 50 ng/well recombinant CD206 (R&D Systems, UK, #2534-MR), diluted in PBS. Wells were washed 6 times with PBST (0.05% Tween) and blocked with 5 % bovine serum albumin (BSA) diluted in PBST

for 1 hour at RT. BiTE/TriTE samples were diluted in PBST and applied to the plate for 2 hours at RT, after which time wells were washed 6 times with PBST. Plates were subsequently incubated with anti C-terminal His tag primary antibody (Invitrogen, UK, #46-069) diluted 1:5,000 in 1% BSA in PBST for 1 hour at RT, then washed 6 times with PBST. Plates were further incubated with an HRP-conjugated secondary antibody (Table 2.4) for 45 min at RT and washed 6 times with PBST. For chemiluminescent detection, 3,3',5,5'-Tetramethylbenzidine (TMB) substrate (ThermoFisher, UK, #34028) was applied to test wells and incubated for 2–30 minutes, before the addition of a stop solution (0.16 M H_2SO_4). Absorbance at 450 nm was measured with a Wallac 1420 Victor2 plate reader (Perkin Elmer, USA).

2.3.4 ELISA to quantify soluble factors in ascites supernatants

ELISAs to quantify cytokines and soluble CD206 were performed with commercially-available kits measuring IL-6 (Biolegend, UK, #30504), IL-10 (Biolegend, UK, #430604), IFN-γ (Biolegend, UK, #430104), TGF-beta 1 Human/Mouse ELISA Kit (Invitrogen, UK, #88 8350 88) and CD206 (RayBiotech, USA, #ELH MMR 1), following manufacturers' instructions. Prior to analysis, samples were centrifuged (400 g, 10 min) to remove cellular components and diluted two-fold (IL-6 and IL-10), five-fold (TGF-β), ten-fold (IFN γ) or thirty-fold (CD206) in PBS.

2.4 Human PBMC-Based Models

2.4.1 Isolation of lymphocytes and monocytes from peripheral blood by double-density gradient centrifugation

Human blood from anonymised healthy donors was obtained from the NHS Blood and Transplant Service (Oxford, UK) in the form of leukocyte cones, which comprise a small

volume (~ 10 mL) of packed leukocytes from a platelet donation by apheresis. To isolate PBMCs, the initial volume of blood was first diluted to 140 mL with PBS. Fifteen mL of diluted blood were then overlaid onto 35 mL Ficoll-Paque Plus (GE Healthcare, UK, #17-1440-02) and centrifuged at 950 g for 30 min with half-maximal acceleration and no braking. Following centrifugation, five layers could be observed: an upper layer of plasma, a PBMC interphase, Ficoll, and a pellet of red blood cells (RBCs) (Figure 2.1). The PBMC interphase was collected and washed three times with PBS at room temperature, using the centrifugation settings described in Table 2.5.

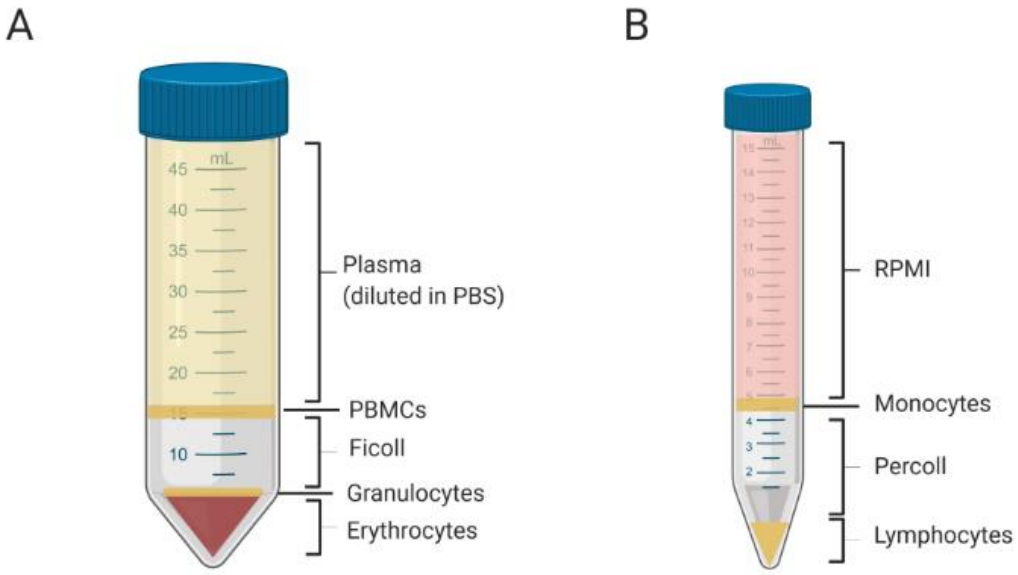

Figure 2.1. Double density gradient centrifugation to isolate lymphocytes and monocytes from human peripheral blood. Schematic representations of the layers observed after centrifugation of whole blood layered on Ficoll (**A**), and of PBMCs layered on 46% Percoll (**B**). Image created with BioRender.

Table 2.5. Wash steps for density gradient centrifugation.

Step	Speed	Time	Acceleration	Braking
1	950 g	10 min	Maximal	Half-maximal
2	450 g	10 min	Maximal	Maximal
3	200 g	10 min	Maximal	Maximal

After washing, PBMCs were resuspended in 20 mL complete RPMI. Five mL of the resultant cell suspension were overlaid onto 5 mL Percoll PLUS (46%, 285 mOsm; GE Healthcare, #17-5445-01) and centrifuged as before at 950 g for 10 min with half-maximal acceleration and no braking. From top to bottom, four layers were formed: an upper layer containing RPMI, a monocyte interphase, Percoll and a lymphocyte pellet (Figure 2.1). The monocyte and lymphocyte fractions were collected separately and washed three times with PBS, as above (Table 2.5). Monocytes were used to generate macrophages (see below, 2.4.2), whilst lymphocytes were frozen at -80°C until needed (at 20 million cells/1 mL freezing medium).

2.4.2 Monocyte-derived macrophage (MDM) generation

Human peripheral blood monocytes were differentiated into macrophages through 6 days' total culture in medium containing 1% HS. Cells were seeded at a density of 3.5-4 million/mL and cultured in T175 flasks with a hydrophobic surface (Sarstedt, UK, #83.3912.500) to ease their subsequent dissociation. Where specified, day-4 MDMs were polarised for 48 h using IL 4 (25 ng/mL, Miltenyi Biotec, UK, #130 095 373), IL-6 (25 ng/mL, Miltenyi Biotec, UK, #130 095 365) or IFN-γ (25 ng/mL, Miltenyi Biotec, UK, #130 096 873) and LPS (10 ng/mL, Sigma Aldrich, UK). For generation of FRβ^{high} MDMs, HS was omitted from the culture medium and monocytes were instead differentiated with

recombinant macrophage colony-stimulating factor (M-CSF) (50 ng/mL, Miltenyi Biotec, UK, #130 096 491). Where specified, monocytes were differentiated in the presence of ascites supernatant, diluted 1:2 in medium containing 1% HS.

2.4.3 Celigo-based cytotoxicity assay

Cytotoxicity of MDMs in healthy PBMC-based models was assessed using Celigo-based image cytometry (Nexcelom Bioscience, USA). Day-6 MDMs (polarised as indicated) were harvested by dissociation with 20 mM EDTA, stained with 5 µM carboxyfluorescein succinimidyl ester (CFSE, Invitrogen, UK, #C34554), then washed with PBS and seeded at a density of 25,000 cells/well into flat-bottom 96-well plates (Corning, UK, #CLS3585). On the same day, autologous lymphocytes were thawed and rested overnight at 37°C in X-VIVO medium (1% HS) at a density of 2-4 million cells/mL. The next day, MDMs were treated with the indicated dilutions of BiTE/TriTEs, in the presence or absence of autologous lymphocytes (E:T ratio of 10:1, unless otherwise specified). In some experiments, cells were cultured in the presence of 50% ascites supernatants. Co-cultures were incubated for 96 h, at which point supernatants (containing lymphocytes) were removed. Lymphocytes were processed for flow cytometry, as outlined below (section 2.6). MDMs were washed with PBS then stained with propidium iodide (PI; diluted to 1 µg/mL in PBS, Sigma Aldrich, UK, #P4864) to identify dead cells. Cells were then imaged on a Celigo image cytometer (Figure 2.2). Live MDMs were identified as being both CFSE positive and PI negative. % Live cells was calculated as follows:

$$\%\ Live\ cells = \frac{CFSE^{+}PI^{-}\ count\ (test)}{CFSE^{+}PI^{-}\ count\ (mock)} \times 100\%$$

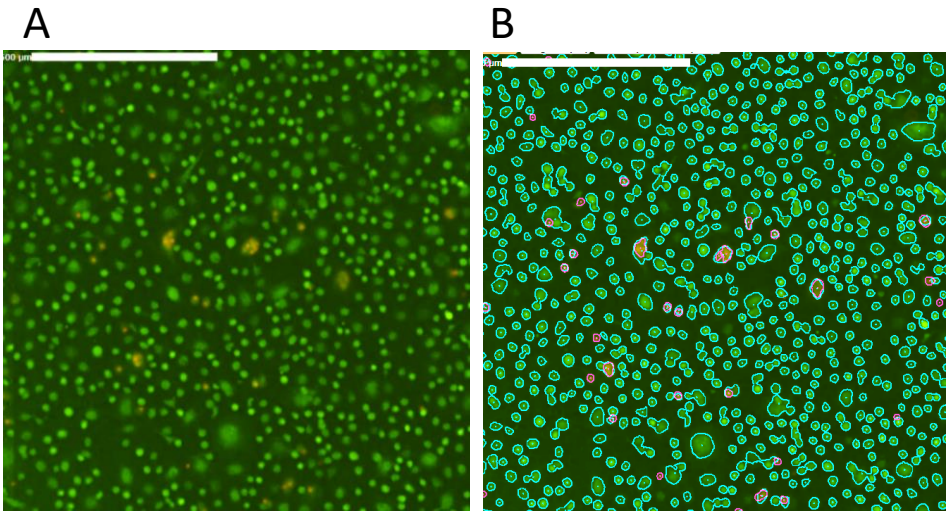

Figure 2.2. Live cell analysis by Celigo image cytometry. MDMs were labelled with CFSE (green), then co-cultured with autologous lymphocytes and BiTEs. 96 h later, lymphocytes were removed and MDMs stained with PI (red) to identify dead cells. An exemplary fluorescence image is shown in (**A**), with the corresponding segmentation outlines shown in (**B**). Cells identified as being $CFSE^+$ or PI^+ are outlined in cyan and pink, respectively.

2.5 Malignant Ascites Models

2.5.1 General statement

Ascites samples were acquired with informed consent from routine paracentesis of cancer patients at the Churchill Hospital, Oxford, UK. Ethical approval for the study was gained from the institutional review board and research ethics committee of the Oxford Centre for Histopathology Research (Reference 09/H0606/5+5) in accordance with the UK Human Tissue Act 2004 and the Declaration of Helsinki.

2.5.2 Malignant ascites processing and characterisation

Ascites were collected aseptically and centrifuged (400 g for 10 min at RT) to separate the cellular and fluid components. The fluid fraction was stored in aliquots at 20°C until required. The cellular fraction was treated with red blood cell lysis buffer (Qiagen, UK, #158904) and cryopreserved (at 20 million cells/1 mL freezing medium) until further use.

For characterisation, cells were stained (as described in section 2.6) with Live/Dead Fixable Near IR stain (Invitrogen, UK, #L10119) and antibodies targeting CD4, CD8, EpCAM, FAP, PD-L1, CD11b, CD206, and FRβ (see Table 2.6 for list of antibodies), then analysed by flow cytometry using an Attune™ NxT Flow Cytometer (Thermo Fisher, UK). Data were processed with FlowJo v10.0.7r2 software (TreeStar Inc., USA).

2.5.3 Ascites-based cytotoxicity and activation assays

Unpurified ascites cells were seeded at 250,000 cells/well in 100 µL medium into flat-bottom ultra-low attachment 96-well plates (Corning, UK, #CLS3474). After resting overnight, cells were treated with BiTEs/TriTEs or viruses, diluted in 100 µL medium or autologous ascites supernatant. Five days later, suspension and adherent cells were harvested (the latter by dissociation with 20 mM EDTA) and combined, then processed for flow cytometry (detailed in section 2.6), using Live/Dead Fixable Near IR stain (Invitrogen, UK, #L10119) and antibodies targeting CD11b (ICRF44, Biolegend, UK, #301310), CD64 (10.4, Biolegend, UK, # 305006), CD80 (2D10, Biolegend, UK, #305208), CD86 (BU63, Biolegend, UK, #374210), CD4 (OKT4, Biolegend, UK, #317408), CD8 (HIT8a, Biolegend, UK, #300912) and CD25 (BC96, Biolegend, UK, #302606).

2.6 Flow Cytometry

2.6.1 Overview of flow cytometry method

Where necessary, cells were first detached from the culture surface using non-enzymatic dissociation with 20 mM EDTA (diluted in PBS). Cells were distributed in V-bottom 96-well plates (Corning, UK, CLS3896) at a density of at least 100,000 cells/well. Cells were washed twice with cold PBS, centrifuging between washes for 5 min at 400 g, then incubated for 10 min at 4°C with Fc receptor blocking reagent (Miltenyi, UK, #130-059-

901), diluted 1 in 100 in MACS buffer (see Appendix I: Materials). After a further PBS wash, cells were incubated with fluorophore-conjugated antibodies (see Table 2.6) (or the appropriate isotype control antibodies, Table 2.7), diluted in MACS buffer for 30 min at 4°C, protected from light. Following two more PBS washes, cells were fixed using 4 % paraformaldehyde. After incubating for 15 min at RT, fixed cells were washed twice in PBS and resuspended in MACS buffer, then stored at 4°C until required.

Table 2.6. List of antibodies used in flow cytometry.

Target	Clone	Dilution	Isotype	Fluorophore(s)	Company	Cat. number(s)
CD4	OKT4	1:200	Ms IgG2b, κ	FITC, APC	Biolegend, UK	#317408, #317416
CD8	HIT8a	1:200	Ms IgG1, κ	APC	Biolegend, UK	#300912
CD11b	ICRF44	1:100	Ms IgG1, κ	APC	Biolegend, UK	#301310
CD25	BC96	1:200, 1:100	Ms IgG1, κ	PE, FITC	Biolegend, UK	#302606
CD69	FN50	1:200	Ms IgG1, κ	FITC	Biolegend, UK	#310904
CD64	10.1	1:100	Ms IgG1, κ	FITC	Biolegend, UK	#305006
CD80	2D10	1:100	Ms IgG1, κ	PE	Biolegend, UK	#305208
CD86	IT2.2	1:100	Ms IgG2b, κ	PE-Cy7	Biolegend, UK	#'305422
CD107a	H4A3	1:200	Ms IgG1, κ	PE	Biolegend, UK	#328608
CD206	15-2	1:100	Ms IgG1, κ	PE, PE-Cy7	Biolegend, UK	#321106
EpCAM	9C4	1:100	Ms IgG2b, κ	PE	Biolegend, UK	#324206
EGFR	AY13	1:100	Ms IgG1, κ	PE	Biolegend, UK	#352904
FAP	427819	1:50	Polyclonal sheep IgG	PE	R&D Systems UK	#MAB3715
FRβ	94b/FOLR2	1:100	Ms IgG1, κ	PE	Biolegend, UK	#391704

HLA-DR	L243	1:200	Ms IgG2a, κ	FITC	Biolegend, UK	#307632
LAG-3	11C3C65	1:100	Ms IgG1, κ	FITC	Biolegend, UK	#369308
PD-1	EH12.2H7	1:100	Ms IgG1, κ	PE	Biolegend, UK	#329906
PD-L1	MIH3	1:100	Ms IgG1, κ	PE	Biolegend, UK	#374512
Tim-3	F38-2E2	1:100	Ms IgG1, κ	PE	Biolegend, UK	#345006

Ms, mouse

Table 2.7. List of isotype control antibodies used in flow cytometry.

Species	Isotype	Clone	Fluorophore (s)	Company	Cat. number(s)
Mouse	IgG1, κ	MOPC-21	FITC, PE, PE-Cy7 APC	Biolegend, UK	#400108, #981804, #400126, #400120
Mouse	IgG2a, κ	MOPC-173	FITC	Biolegend, UK	#400208
Mouse	IgG2b, κ	MPC-11	FITC, PE, PE-Cy7, APC	Biolegend, UK	#400310, #400314, #400326, #400322

2.6.2 Data acquisition and analysis

Flourescence was detected using a Attune™ NxT Flow Cytometer (Thermo Fisher, UK), with at least 10,000 events acquired per sample. Data were processed with FlowJo v10.0.7r2 software (TreeStar Inc., USA) (Figure 2.3).

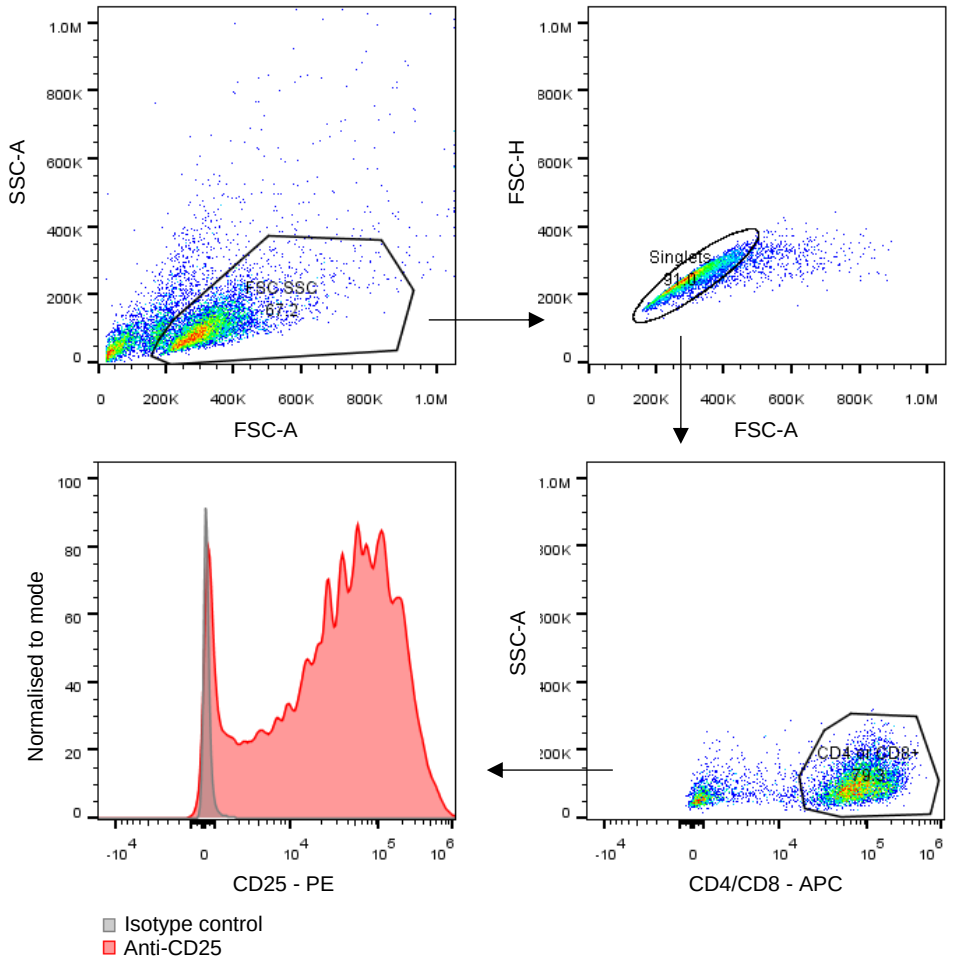

Figure 2.3. Exemplary gating strategy for flow cytometric analysis of T cell activation. Lymphocyes were co-cultured with MDMs and BiTEs for 96 h, then harvested and stained with anti-CD4 (APC) anti-CD8 (APC) and anti-CD25 (PE) antibodies. Data were acquired with an Attune NxT flow cytometer then processed with FlowJo software. Cell debris were first excluded by FSC/SSC gating (top left panel), followed by doublet discrimination by plotting FSC-area(A) against FSC-height(H) (top right panel). Within this gate, CD4- or CD8-positive cells were selected (bottom right panel) and analysed for expression of CD25 (bottom left panel).

2.7 Generation of Recombinant Adenoviruses

2.7.1 Cloning to generate transgene-armed EnAd viruses

Transgene cassettes encoding the BiTEs/TriTEs were inserted into SbfI-linearised parental EnAd plasmid (EnAd2.4) with Gibson assembly technology, as described in section 2.2.4. Transgene cassettes contained either an exogenous CMV promoter or an inserted splice acceptor (SA, mediating expression from the adenovirus major late promoter (MLP)), as well as a 3′ polyadenylation sequence. Successful transgene insertion was confirmed by restriction digest and Sanger sequencing (Eurofins Genomics, Germany).

2.7.2 Virus transfection

Prior to transfection, EnAd-BiTE/TriTE constructs were linearised through digestion with AscI (see section 2.2.1) and purified by isopropanol precipitation (see section 2.26). HEK293A cells were seeded in T25 flasks (1 million cells/flask) and transfected 24 h later with linearised EnAd-BiTE/TriTE constructs. In brief, 5 µg EnAd-BiTE/TriTE DNA were diluted in 50 µL Opti-MEM, whilst 20 µL Lipofectamine 2000 were diluted in 30 uL Opti-MEM. The two solutions were incubated separately for 5 min at RT, then mixed and incubated for a further 20 min. After topping up to 4 mL with Opti-MEM, the transfection mixture was added to cells. Four hours later, transfection medium was replaced with DMEM containing 2% FBS. Cells and supernatant were harvested upon observation of extensive cytopathic effect (CPE).

2.7.3 Plaque purification

HEK93A cells were seeded in complete medium in 6-well plates at a density of 800,000 cells/well to generate a monolayer. Plaque purification was performed by applying 10-fold serial dilutions of virus, which were removed after 4 h and replaced with an overlay of 1%

agarose-DMEM (supplemented with 2% FBS). Single virus plaques were picked by careful scraping with a pipette tip, then amplified through re-infection of HEK293A cells (seeded in 6-well plates in DMEM 2% FBS). Amplified viruses were harvested upon observation of extensive CPE, then assessed for BiTE/TriTE secretion, as detailed in section 6.3.2, before proceeding to large-scale virus preparation.

2.7.4 Large-scale virus preparation and purification

To generate large-scale viral stocks, HEK293A cells were seeded in 10-layer Hyperflasks (Corning, UK, #CLS10034) and, at 80-90% confluency, infected with the selected virus clones (diluted in DMEM containing 2% FBS). Upon the first signs of CPE (24-48 h later), cells were harvested and intracellular virus particles released by performing three freeze/thaw cycles with liquid nitrogen and a 37°C water bath. After 1 h incubation at 4°C with water-saturated n-butanol (diluted 1:100), cellular debris was pelleted through centrifugation (500 g, 10 min, 4°C). The supernatant containing free virus particles was subsequently collected and applied to a discontinuous caesium chloride gradient, prepared in Beckman Coulter Ultra-Clear centrifuge tubes (Fischer Scientific, UK, #12706558). This procedure (outlined below) was performed in collaboration with Sally Frost (DPhil student, Seymour group, Department of Oncology, University of Oxford).

In brief, the caesium chloride gradient consisted of 3 mL of 1:32ρ caesium chloride carefully underlaid with 2 mL of 1:45ρ caesium chloride. Two mL of 40% Glycerol were then carefully added on top (for recipe see Appendix I: Materials) then finally overlaid with virion-containing supernatant. Tubes were centrifuged at 25,000 rpm at 10°C for 1 hr 30 min in a Beckman L8-70M Ultracentrifuge with SW40TI rotor. After centrifugation, two discrete bands were visible: a lower band containing intact virus particles, and an upper band containing incomplete virus particles (Figure 2.4). The lower band was collected by

carefully puncturing the tube with a 21g needle and aspirating into a 10 mL syringe. Caesium chloride was removed through three rounds of dialysis in PBS using a 3-12 mL Slide-A-Lyzer dialysis cassette (ThermoFisher, UK, #66810). The resultant virus-PBS solution was extracted with a 21g needle and a syringe, and treated for 1 h at RT with magnesium chloride (2 mM) and benzonase (1 µL/mL) to degrade unpackaged DNA.

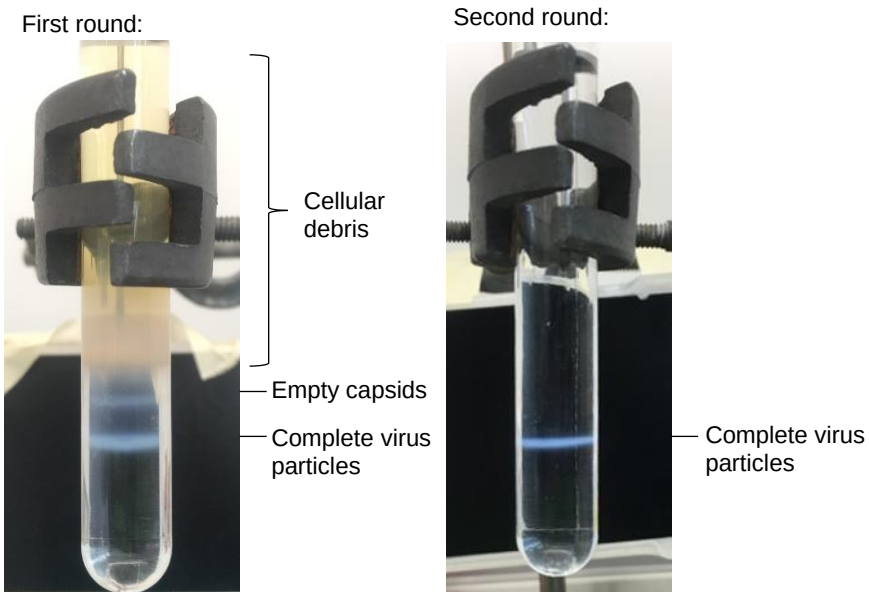

Figure 2.4. Adenovirus purification by double caesium chloride density gradient centrifugation. Representative images of the bands observed after each round of caesium chloride banding. Empty adenovirus capsids are observed at the interface between glycerol and 1.32p CsCl (upper blue band), whilst intact virus particles are observed at the interface between 1:32p and 1:45p CsCl (lower blue band).

A second round of caesium chloride banding was performed as above, with dialysis carried out using a smaller, 0.5-3 mL Slide-A-Lyzer dialysis cassette (ThermoFisher, UK, #66380). The final round of dialysis was performed with PBS containing 5 mM HEPES. The virus solution was removed and glycerol – acting as a cryoprotectant – added to a final concentration of 20%. Viruses were aliquoted and snap-frozen in liquid nitrogen, then stored at -80°C until further use.

2.7.5 Picogreen assay for adenovirus quantification

Estimates of viral genomes/mL were obtained using the Picogreen assay (ThermoFisher, UK, #P7589), which quantifies dsDNA by exploiting a nucleic acid probe that fluoresces upon binding to dsDNA. Purified virus stocks were diluted 1:10 in TE buffer (for recipe see Appendix I: Materials) before addition of SDS (0.05%) and heat treatment (56°C, 30 min) to remove non-encapsidated DNA. Further dilutions of virus stocks (up to 1:50) were performed with TE to ensure their concentrations fell within the range of the standard curve. Quantities of dsDNA were determined according to the manufacturer's instructions, using a standard curve of bacteriophage lambda DNA. Estimates of viral genomes/mL were calculated by assuming a ratio of 1 µg DNA per 2.7×10^{10} adenovirus particles.

2.7.6 HPLC

As a further layer of quality control, all viruses were analysed by anion-exchange HPLC using GMP grade EnAd (provided by PsiOxus Therapeutics, UK) of known concentration to generate a standard curve. In addition, each adenovirus serotype has a distinctive retention time so this provided an extra layer of quality control. Sample dilutions (typically 1/10) and standards were pipetted into HPLC vials and spun to eliminate bubbles. The vials were run using a robotic autosampler on a Shimadzu Prominence pre-fitted with a Resource Q (anion exchange) column. To elute the virus from the column the NaCl gradient shown below was run, with UV detection at 260nm, 280nm and fluorescent detection Ex 275, Em 303nm. 260nm provided an estimation of viral DNA content, 280nm an estimate of protein content and due to its greater sensitivity fluorescence (Ex 275nm, Em 303nm) was used when sample concentration was low. HPLC was performed in

collaboration with Dr. Brian Lyons (post-doctoral researcher, Seymour group, Department of Oncology, University of Oxford).

2.7.7 Quantitative PCR to assess adenoviral genome replication

To assess adenovirus replication, viral genomes were quantified at 24 and 72 h after infection of DLD-1 cells. Cells were seeded in 24-well plates at a density of 150,000 cells/well and, the next day, infected at 100 vg/cell. At the specified time-points, cells and supernatant were harvested and combined, and total DNA extracted using PureLink genomic DNA mini kit (ThermoFisher, UK, #K182002). Samples were diluted in water (final dilution 1:100) and mixed with a hexon-specific primer/probe set (primers: TACATGCACATCGCCGGA/CGGGCGAACTGCACCA,
probe: CCGGACTCAGGTACTCCGAAGCATCCT), as well as a QPCRBIO probe mix Hi-Rox (PCR Biosystems) master mix. The qPCR was run on an ABI PRISM 7000 (Applied Biosystems) with the following set-up:

1. **Polymerase activation:** 95°C for 2 min
2. **Denaturation:** 98°C for 5 s
3. **Annealing/extension:** 60°C for 20 s
4. **Extension:** 72°C for 1 min/kb
5. **Repeated cycles:** Return to 2, x 39

3 Engineering of TAM-Targeting BiTEs and their Characterisation in PBMC-Based Model Systems

3.1 Introduction

TAMs play central roles in cancer progression and resistance to therapy (Cassetta and Pollard, 2018). Several macrophage-targeting treatments are under clinical evaluation, though most do not discriminate between potentially pro- and anti-tumour macrophage subsets. One feature of pro-tumoural TAMs, which may facilitate their specific targeting, is high expression of certain M2-like macrophage markers.

CD206, the mannose receptor, is a transmembrane C-type lectin present on the surfaces of tissue macrophages, as well as subsets of DCs (Collin and Bigley, 2018) and endothelial cells (Martinez-Pomares et al., 2005). The functions of CD206 are wide-ranging, and include serum glycoprotein homeostasis (Martinez-Pomares et al., 2005) and immune recognition of pathogens via binding to high-mannose structures on their surfaces (Ezekowitz et al., 1990). CD206 is a prototypic marker of M2-polarised macrophages, being up-regulated by IL-4 signalling through the STAT6 pathway (Murray et al., 2014). Up-regulation of CD206 is also observed on TAMs, and a high density of $CD206^+$ TAMs has been identified as an independent poor prognostic factor for colorectal (Feng et al., 2019), pancreatic (Wang et al., 2016) and kidney (Shu et al., 2016; Xu et al., 2014) cancers. For ovarian and hepatocellular carcinomas, the ratio of $CD206^+/CD68^+$ cells, and not overall $CD68^+$ density, was associated with poor prognosis, suggesting the existence of a cancer-promoting, $CD206^+$ TAM subset. Indeed, studies on a mouse mammary tumour model revealed that $CD206^+$ TAMs were MHC-II^{low}, better able to penetrate hypoxic areas and more angiogenic than their $CD206^-$ counterparts, which were MHC-^{II} high and more

M1-oriented (Movahedi et al., 2010). For *in vivo* imaging of the CD206$^+$ TAM population, a radiolabelled nanobody targeting CD206 has been developed and validated in pre-clinical studies (Movahedi et al., 2012). However, therapeutic targeting of CD206$^+$ TAMs remains to be explored.

Another TAM marker associated with poor patient outcome is FRβ. FRβ is a GPI-anchored cell surface receptor which binds folic acid with high affinity, leading to its internalisation by receptor-mediated endocytosis (Matherly and Goldman, 2003). FRβ is present on CD34$^+$ bone marrow cells and certain activated cells of the myeloid lineage; however, it is only expressed in a functional state (i.e. able to bind folate) by activated macrophages and a subset of classical monocytes (Shen et al., 2014). FRβ was found to be highly expressed on macrophages activated with M-CSF, IL-6 and/or IL-10, but not GM-CSF-polarised or resting macrophages, leading to its classification as a marker of M2-like macrophages (Puig-Kröger et al., 2009). FRβ$^+$ TAMs have been observed across many solid tumour indications (Kurahara et al., 2012; O'Shannessy et al., 2015; Puig-Kröger et al., 2009; Shen et al., 2015; Yang et al., 2015), with a high number of FRβ$^+$ TAMs correlating with poor prognosis in pancreatic (Kurahara et al., 2012) and colorectal (Human Tissue Atlas) cancers, and increased metastasis in pancreatic (Kurahara et al., 2012) and breast (Yang et al., 2015) cancers. Moreover, FRβ$^+$ TAMs isolated from melanoma and breast adenocarcinoma samples were found to be CD163$^+$ and IL-10-producing, suggesting that they represent an immunosuppressive TAM population (Puig-Kröger et al., 2009). As discussed in section 1.4.6, FRβ$^+$ TAM depletion has been achieved with folate-conjugated cargo or recombinant immunotoxins, although these approaches carry limitations in terms of practicality and efficacy.

In this chapter, we first confirmed the expression of CD206 and FRβ by macrophages in clinically-relevant *ex vivo* models of human cancer. We then engineered novel BiTEs targeting these receptors, producing free BiTE protein for subsequent experiments using a mammalian expression system. To assess the functionality of the TAM-targeting BiTEs, we co-cultured healthy human T cells with autologous monocyte-derived macrophages, which were polarised with cytokines to generate cells with high or low levels of CD206 or FRβ. The specificity of the novel BiTEs for cells with high levels of CD206/FRβ was assessed using a combination of flow cytometry and Celigo-based image cytometry. We finally explored the activity of the TAM-targeting BiTEs in the presence of malignant ascites fluid, which is characterised by high levels of soluble immunoregulatory factors.

3.2 Chapter Aims

1. Assess CD206 and FRβ expression on *ex vivo* models of human TAMs.
2. Design CD206- and FRβ-targeting BiTEs and engineer plasmid vectors for their mammalian expression.
3. Measure BiTE-directed activation of primary T cells and their killing of autologous MDMs.
4. Determine the activity of TAM-targeting BiTEs in immunosuppressive malignant ascites fluid.

3.3 Results

3.3.1 M2-like macrophage markers CD206 and FRβ are up-regulated on *ex vivo* models of human TAMs

We first sought to determine the expression of two M2-like macrophage markers, CD206 and FRβ, by macrophages in clinically-relevant *ex vivo* models of human TAMs. Malignant ascites typically contains a large number of macrophages with cancer-supporting properties (Reinartz et al., 2014). Ascites-associated macrophages (identified as being double positive for CD11b and CD64) were found to express CD206 (4/5 patients) and FRβ (5/5 patients) at higher levels than M1-polarised monocyte-derived macrophages (MDMs; derived from healthy PBMCs (Figure 3.1). In an alternative approach, we cultured PBMC-derived human monocytes with cell-free malignant ascites fluid, which has been reported to generate MDMs that functionally and phenotypically resemble human TAMs (Duluc et al., 2007). Using ascites fluid from 11 cancer patients, we observed significant up regulation of CD206 (11/11 patients) and FRβ (6/11 patients) on human PBMC-derived MDMs, as compared to M1-polarised MDMs (Figure 3.2).

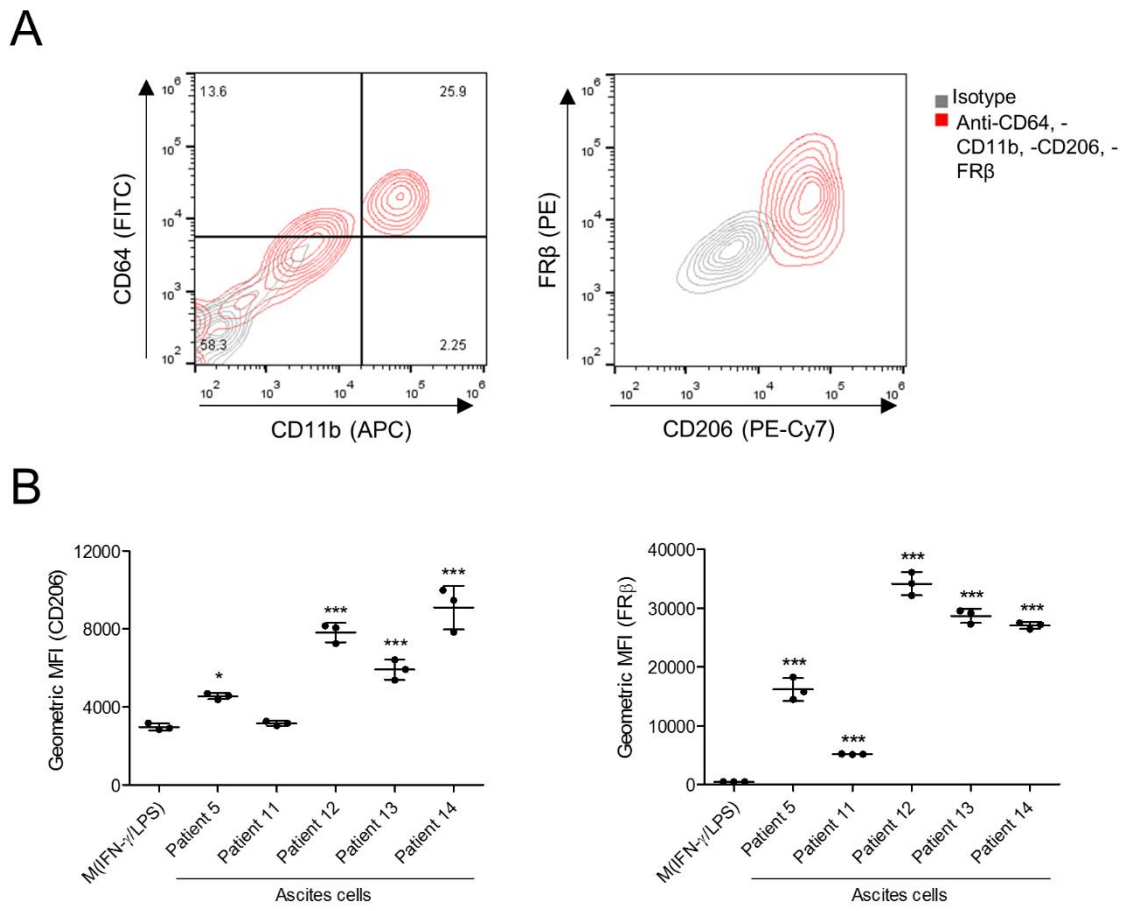

Figure 3.1. CD206 and FRβ are markers of human malignant ascites-associated macrophages. (**A**) Representative flow cytometry plots showing CD206 and FRβ expression on primary ascites cells after gating for CD11b+/CD64+ double positivity. (**B**) Expression levels of CD206 and FRβ on primary CD11b^{+}/CD64+ ascites cells from 5 different cancer patients, and on monocyte-derived macrophages (from healthy donors) polarised with 10 ng/mL LPS and 25 ng/mL IFN-γ ("M(IFN-γ/LPS)"), as determined by flow cytometric analysis. Data show mean ± SD of biological triplicates. **(B)** Statistical analysis was performed by one-way ANOVA with Dunnett's post-hoc analysis compared with "M(IFN-γ/LPS)" (*, $P < 0.05$; **, $P < 0.01$; ***, $P < 0.001$).

3.3.2 Generation and production of BiTEs targeting CD206 and FRβ

Having confirmed CD206 and FRβ expression in *ex vivo* models of human TAMs, we proceeded to engineer BiTEs targeting these molecules. Human TAM-targeting BiTEs were engineered by joining, with a flexible glycine-serine (GGGGS) linker, a single chain variable fragment (scFv) specific for CD3ε (clone L2K) to bind domains specific for human CD206 and FRβ. The CD206-binding domain was a single domain antibody fragment (nanobody, clone NbhMMRm3.1), whilst the FRβ-binding domain was a scFv (clone m923). Antibody fragments were selected based on their similarly high affinities (K_D of 3.4 nM and 2.48 nM for CD206-binding (Lynn et al., 2016) and FRβ-binding (patent #WO2014/140376A1) fragments, respectively.

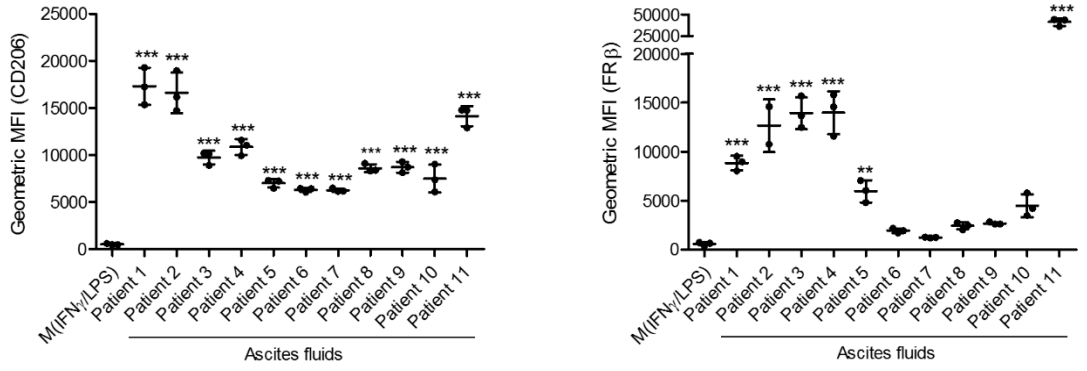

Figure 3.2. CD206 and FRβ are upregulated on malignant ascites-differentiated MDMs. Primary human monocytes from healthy donors were differentiated into macrophages through 6 days' culture in medium containing 1% human serum. Where indicated, culture medium contained 10 ng/mL LPS and 25 ng/mL IFN-γ ("M(IFN-γ/LPS)", added on Day 4), or 50% acellular ascitic fluid from 11 different cancer patients ("Patient 1"-"Patient 11", added on Day 0). Expression levels of CD206 and FRβ were determined by flow cytometry. Data show mean ± SD of biological triplicates. Statistical analysis was performed by one-way ANOVA with Dunnett's post-hoc analysis compared with "M(IFN-γ/LPS)" (*, $P < 0.05$; **, $P < 0.01$; ***, $P < 0.001$).

For FRβ targeting, two orientations of BiTE were engineered. In the first, the αFRβ scFv was placed at the N-terminus, with the αCD3 scFv joined to its C-terminus ("FR3 BiTE"). In an alternative arrangement, the αFRβ scFv was C-terminal whilst the αCD3 scFv was N-terminal ("3FR BiTE"). Given that the complementarity determining regions (CDRs) cluster at the N-termini of most nanobodies (Beghein and Gettemans, 2017), a single orientation of CD206-targeting BiTE was selected, in which the CD206 nanobody was placed at the N-terminus, with the αCD3 scFv fused to its C-terminus ("CD206 BiTE").

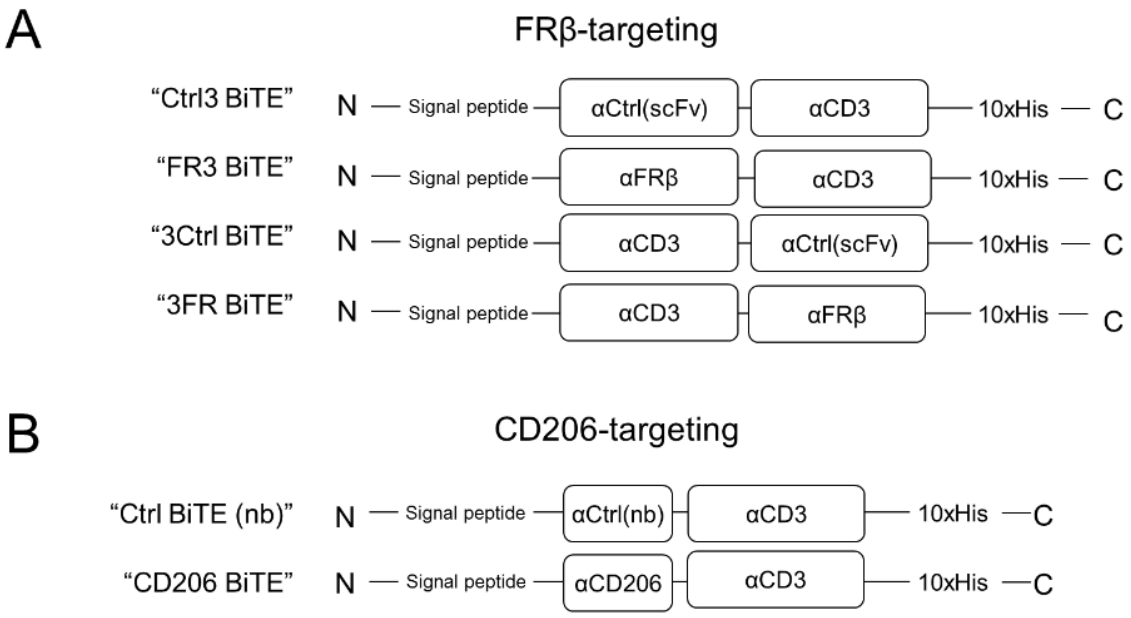

Figure 3.3. Schematic representations of the FRβ- and CD206-targeting BiTEs and their relevant controls. (A) The FRβ-targeting BiTEs and their matched controls are composed of scFvs recognising FRβ (αFRβ) or an irrelevant antigen (filamentous haemaglutinin adhesion (αCtrl(scFv)) joined by a glycine-serine linker to an anti-CD3 scFv (αCD3) The two binding domain orientations are depicted. **(B)** The CD206-targeting BiTE and its matched control BiTE comprise nanobodies targeting CD206 (αCD206) or an irrelevant antigen (rabies virus protein; αCtrl(nb)) joined by a glycine-serine linker to an anti-CD3 single chain variable fragment (scFv; αCD3). **(A, B)** All BiTEs contain an immunoglobulin signal peptide at the N-terminus for mammalian secretion and a deca-histidine (10xHis) tag at the C-terminus for detection and quantification.

Matched control (Ctrl) BiTEs, with the same CD3ε binding domain and either a nanobody or scFv recognising an irrelevant antigen (rabies virus protein for the CD206 BiTE and filamentous hemagglutinin adhesin (FHA) of Bordetella pertussis for the FRβ BiTE, respectively), were also generated (Figure 3.3). All BiTEs contained a signal peptide at the N-terminus for secretion and a deca-histidine (10xHis) tag at the C-terminus to facilitate BiTE detection and quantification. BiTE constructs were cloned into mammalian expression vectors under the control of the cytomegalovirus immediate-early (CMV) promoter (Figure 3.4), to be transfected into adherent HEK293A cells for production. Successful expression and secretion of all six BiTEs into the transfected cell supernatants was confirmed by immunoblotting with an anti-His primary antibody (Figure 3.5A). BiTE concentrations were determined by dot blot, using a 10xHis tagged protein of known concentration to generate a standard curve (Figures 3.5B-D).

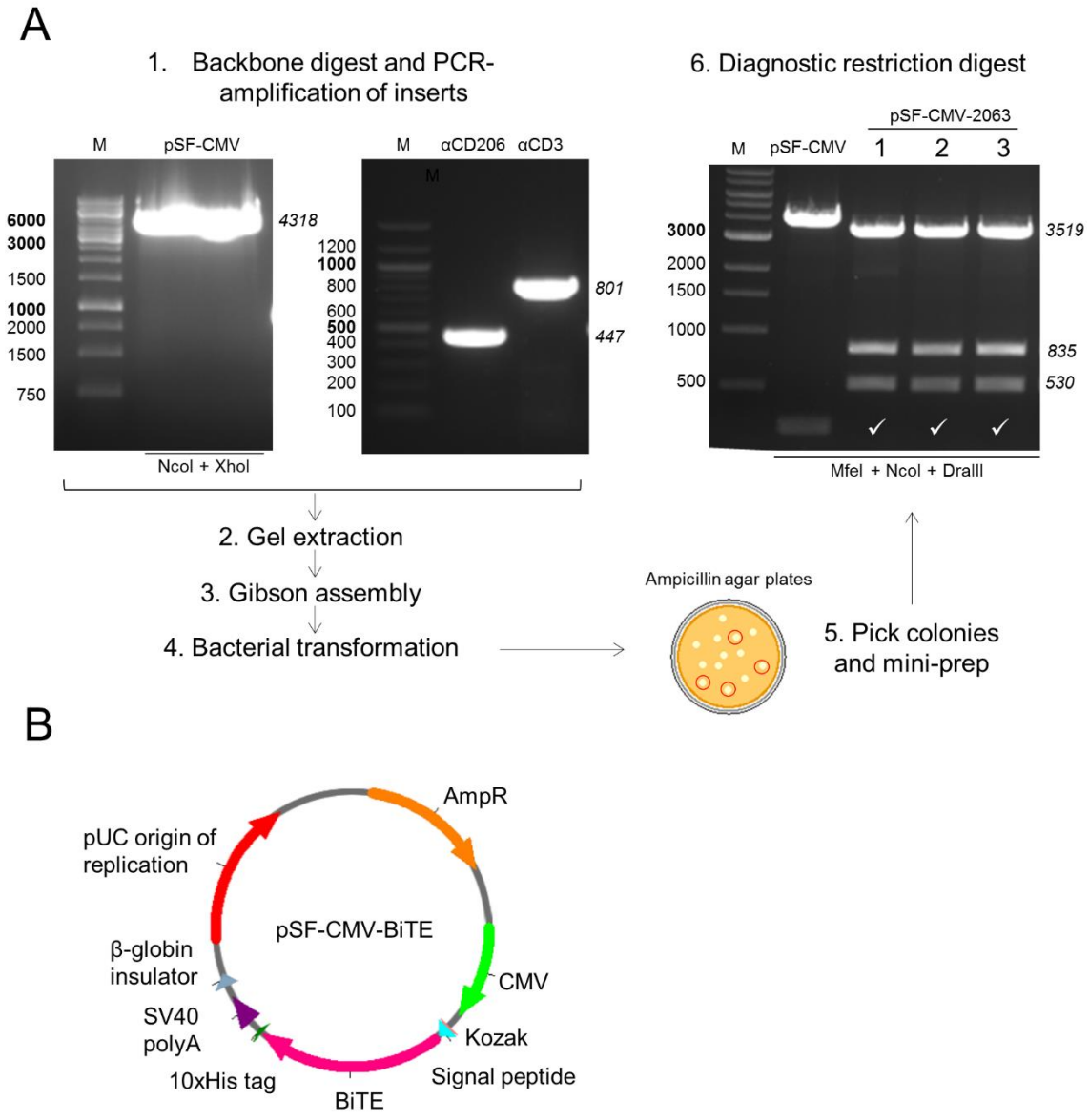

Figure 3.4. Generation of mammalian BiTE expression plasmids. (A) An exemplary cloning strategy to generate a BiTE expression plasmid (pSF-CMV-2063) is outlined. In brief, BiTE components were amplified by polymerase chain reaction (PCR) and inserted into a linearised expression vector (pSF-CMV) by Gibson assembly technology, before transformation into *E.coli*. Single antibiotic-resistant colonies were amplified and screened for transgene insertion by digestion with MfeI, NcoI and DraIII. DNA fragments were resolved on 1% agarose gel. Predicted band sizes are noted in italics. Colonies with the correct digestion pattern are indicated with a tick. CMV, Cytomegalovirus. **(B)** Schematic representation of a plasmid engineered for mammalian expression of a BiTE under the transcriptional control of a CMV promoter. AmpR, ampicillin resistance casette; SV40, Simian vacuolating virus 40.

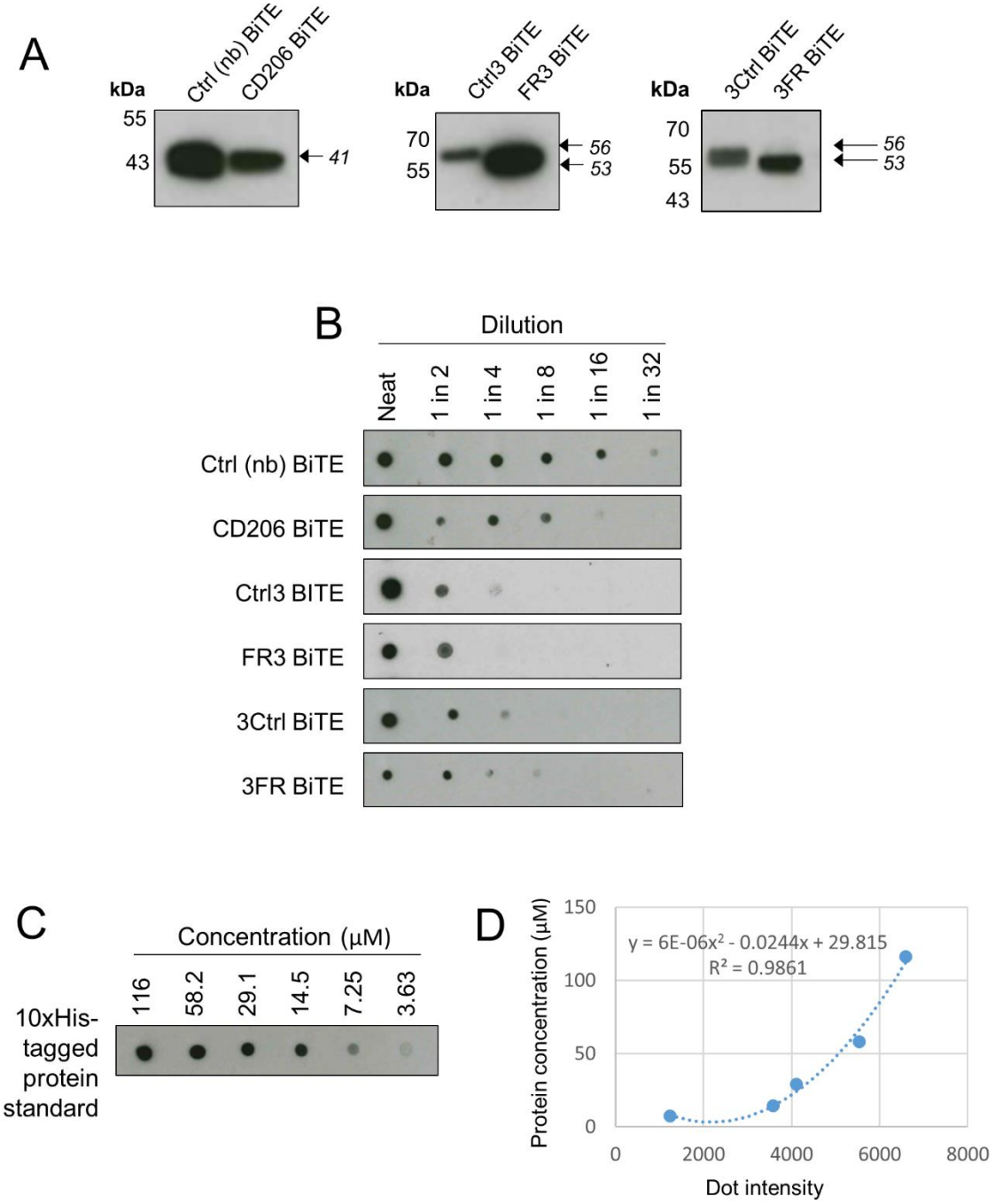

Figure 3.5. Expression and quantification of BiTEs. **(A)** Western blot analysis of supernatants from HEK293A cells 48 h after transfection with BiTE expression plasmids. Blots were probed with a mouse anti-His primary antibody, followed by an HRP-conjugated anti-mouse secondary antibody. Expected protein sizes are indicated in italics. kDa, kilodaltons. **(B)** Serially-diluted supernatants from HEK293A cells transfected with BiTE expression plasmids were applied to a nitrocellulose membrane, which was then air-dried and probed with anti-His primary antibody and HRP-conjugated secondary antibody. **(C,D)** A 10xHis-tagged protein of known concentration was serially-diluted and analysed by dot blot as above. **(D)** ImageJ software was employed to generate a standard curve of dot intensity vs. protein concentration.

3.3.3 Protocol optimisation to generate M1- and M2-polarised MDMs

Selective depletion of the most cancer-promoting TAMs will require discrimination between macrophages with high (M2-like) and low (M1-like) expression levels of target antigen. To determine the selectivity of the TAM-targeting BiTEs for M2- over M1-polarised macrophages, we first explored methods for the *in vitro* generation of MDMs with high or low levels of CD206 and FRβ. Healthy human peripheral blood monocytes were differentiated to macrophages through 6 days' total culture in medium (X-VIVO or RPMI) containing HS (1% v/v) or recombinant M-CSF (10 or 50 ng/mL). MDMs were polarised for 48 h with a variety of cytokines (IL-4, IL-6, IL-10 or IFNγ+LPS), added on the fourth day of differentiation (protocol outlined in Figure 3.6A). Flow cytometric analysis of CD206 and FRβ expression revealed a strong up-regulation of CD206 by IL-4-polarised, HS-differentiated MDMs, whilst FRβ levels were highest on IL-6-polarised, M-CSF-differentiated MDMs (with HS omitted) (Figure 3.6B). Interestingly, FRβ levels were greatest on MDMs cultured in RPMI medium; however, given the very low cell yield from this method (Figure 3.6C), a compromise was selected in which X-VIVO medium was utilised instead for generation of $FR\beta^{high}$ MDMs. M1-like MDMs with low levels of both CD206 and FRβ were generated through differentiation with HS and polarisation with IFNγ+LPS (Figure 3.6B). Representative flow cytometric histograms of CD206 and FRβ expression by MDMs generated by the three selected methods (outlined in Figure 3.7A) are displayed in Figure 3.7B.

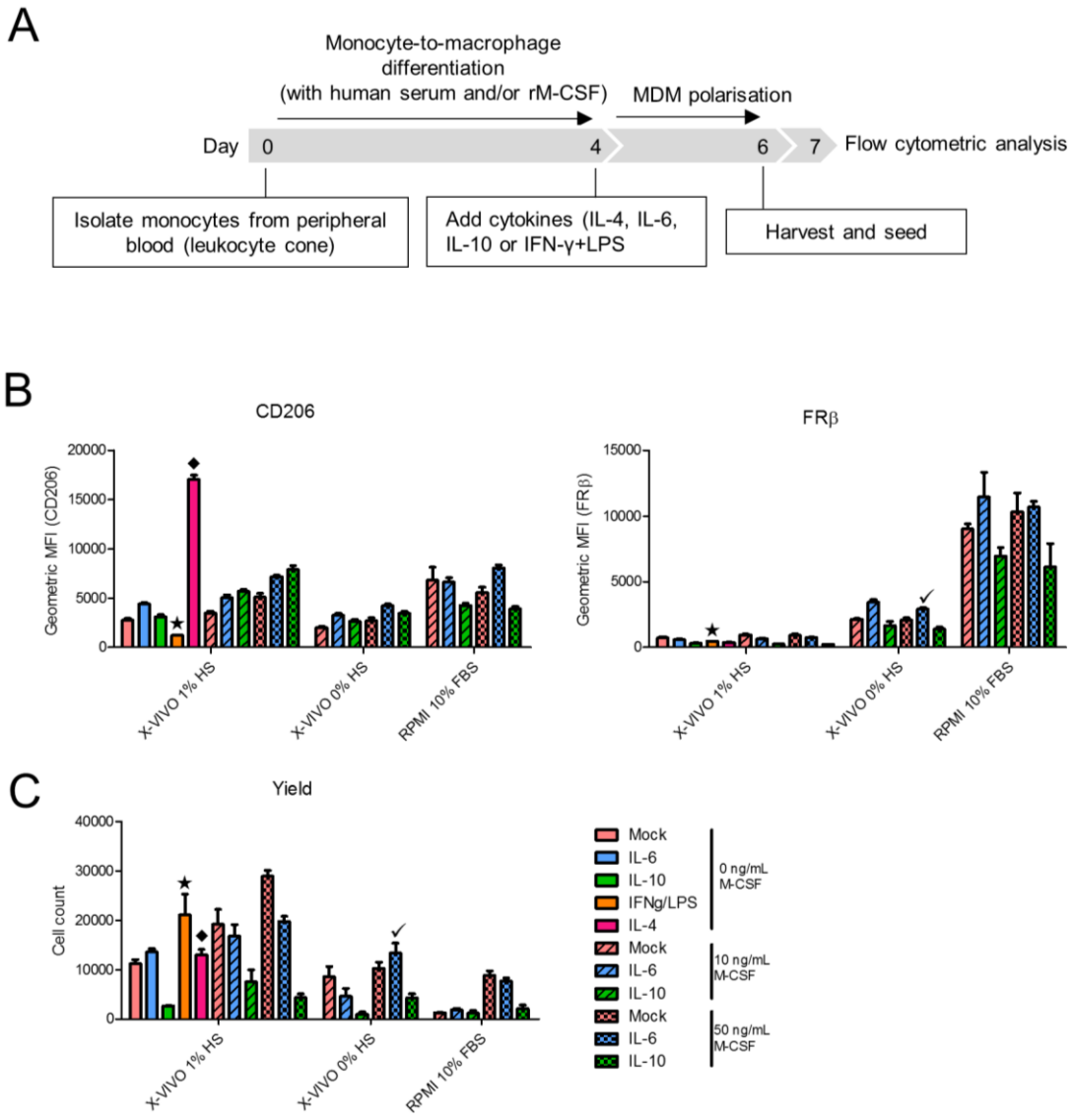

Figure 3.6. Optimisation of a protocol to generate human monocyte-derived macrophages (MDMs) with high or low levels of CD206 and FRβ. Monocytes were isolated from healthy human peripheral blood and differentiated into macrophages through 6 days' total culture in medium (X-VIVO or RPMI, as indicated) containing human serum (1% v/v) and/or recombinant M-CSF (10 or 50 ng/mL). Day-4 MDMs were polarised through addition of the indicated cytokines (all at 25 ng/mL, other than LPS (10 ng/mL)). Two days later, polarised MDMs were harvested and seeded in 24-well plates, for flow cytometric analysis the following day. **(A)** Experimental timeline. **(B)** CD206 and FRβ expression on polarised MDMs, as assessed by flow cytometry. **(C)** Cell counts for each condition, as determined by flow cytometry. HS, human serum; M-CSF, macrophage colony-stimulating factor. **(B,C)** Differentation/polarisation conditions selected for further experiments are indicated with a star ($CD206^{low}FR\beta^{low}$), a diamond ($CD206^{high}$) or a tick ($FR\beta^{high}$). Data show mean ± SD of biological triplicates.

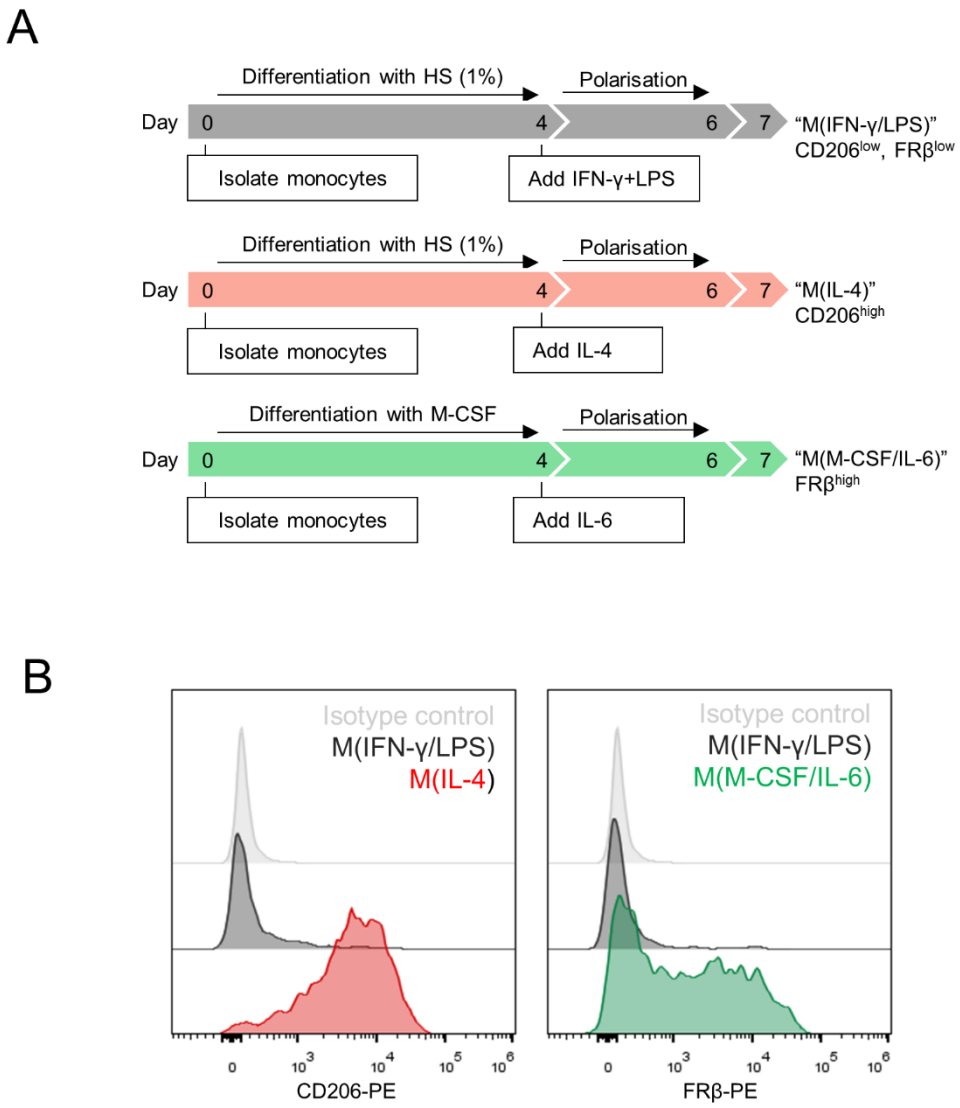

Figure 3.7. Expression of CD206 and FRβ by polarised human MDMs (A) Experimental timelines of the three methods used in the remainder of this thesis to generate polarised MDMs with low CD206 and FRβ (M(IFN-γ+LPS)), high CD206 (M(IL-4)) or high FRβ (M(M-CSF/IL-6)). **(B)** Representative flow cytometric histograms of CD206 and FRβ expression by polarised human MDMs.

3.3.4 CD206- and FRβ-targeting BiTEs trigger T cell-mediated cytotoxicity of M2- but not M1-polarised macrophages

Dose-responses of the BiTEs against polarised MDMs were then performed with autologous lymphocytes at an E:T ratio of 10:1 (Figure 3.8). All three BiTEs triggered T cell-mediated toxicity selectively towards the relevant M2-polarised (M(IL-4) or M(M-CSF/IL-6)) MDMs, with EC_{50} values in the nanomolar range (CD206 BiTE at 3.4 nM; FR3 BiTE at 61.22 nM; 3FR BiTE at 10.63 nM) (Figure 3.8C). At the highest doses tested, the % live MDMs were reduced to 26.8%, 12.9% and 6.69% for the CD206, FR3 and 3FR BiTEs, respectively (Figure 3.8B). There was no killing of M1-polarised (M(IFN-γ/LPS)) MDMs at any concentration of FRβ-targeting BiTE tested, and only minor cytotoxicity at the highest dose of the CD206 BiTE (reduction in % live MDMs to 89.4%, Figure 3.8B). Importantly, no killing of M1- or M2-polarised MDMs was induced by the control BiTEs at any concentration tested, confirming the target antigen-specificity of the TAM-targeting BiTEs (Figure 3.8B). In addition, exposure of M2-polarised MDMs to the relevant BiTEs in the absence of lymphocytes yielded no significant cell death (Figure 3.9), demonstrating that BiTE cytotoxic activity was dependent on these effector cells.

Together, these data demonstrate that the CD206 and FRβ-targeting BiTEs trigger selective killing of M2- over M1-polarised MDMs in a T cell- and target antigen-dependent manner.

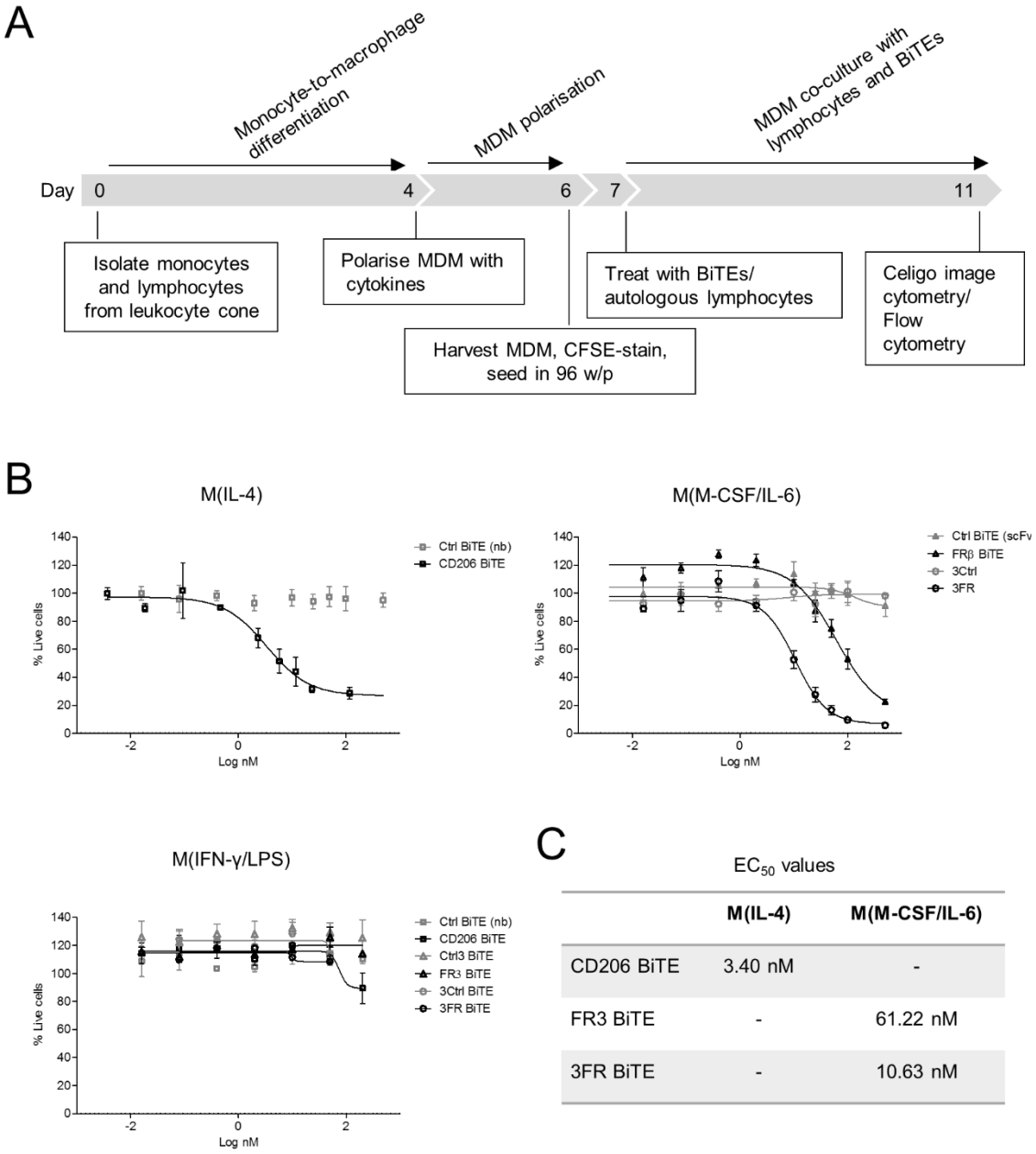

Figure 3.8. Dose responses of BiTEs against polarised MDMs (A) Overview of the protocol utilised to assess BiTE-mediated killing of polarised MDMs by autologous lymphocytes. **(B)** Day-4 human MDMs were polarised as indicated, stained with CFSE, and treated with T cells (10:1 effector:target ratio) and increasing concentrations of BiTEs. Macrophage killing was assessed 96 h later by propidium iodide staining and Celigo image cytometry. Data show mean ± SD of biological triplicates. EC_{50} values are displayed in **(C).**

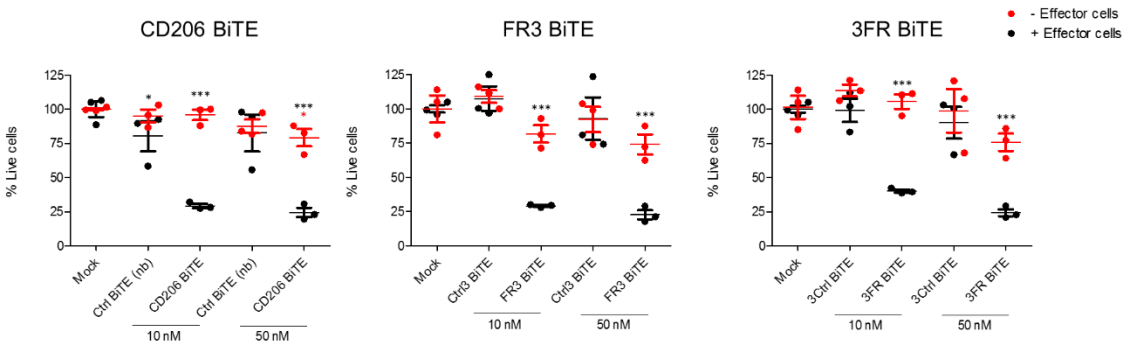

Figure 3.9. BiTE-mediate cytotoxicity is strictly dependent on the presence of effector cells. Polarised MDMs (M(IL-4) or M(M-CSF/IL-6), where relevant) were stained with CFSE and treated with the indicated concentrations of BiTE in the presence or absence of T cells (10:1 effector:target ratio). 96 h later, cytotoxicity was assessed by propidium iodide staining and analysis with a Celigo image cytometer. Data show mean ± SD of biological triplicates. Statistical analysis was performed by two-way ANOVA with Bonferroni post-hoc tests comparing with the relevant "Mock" condition (*, $P < 0.05$; **, $P < 0.01$; ***, $P < 0.001$).

3.3.5 Polyclonal CD4⁺ and CD8⁺ T cells are activated by the CD206- and FRβ-targeting BiTEs in a target cell-dependent manner

The ability of the TAM-targeting BiTEs to activate T cells was assessed by flow cytometric measurement of CD25 expression. Healthy human peripheral blood lymphocytes were co-cultured with the BiTEs for five days in the presence or absence of autologous target cells (M(IL-4) or M(M-CSF/IL-6) MDMs for CD206- and FRβ-targeting, respectively), then harvested and processed for flow cytometric analysis. All three BiTEs triggered activation of both CD4⁺ and CD8⁺ T cell subsets when co-cultured with the relevant target cells, with slightly higher CD25 expression by the CD4⁺ T cell subsets (Figure 3.10). No significant T cell activation was observed in the absence of target cells, or when matched control BiTEs were employed (Figure 3.10). T cell activation was strongest by the CD206 and 3FR BiTEs, which triggered 9.7- and 6.6-fold increases, respectively, in the CD25 geometric MFI values of CD4⁺ T cells, and 5.8- and 5.7- fold increases, respectively, in the CD25 geometric MFI values of CD8⁺ T cells (Figures 3.10A and B).

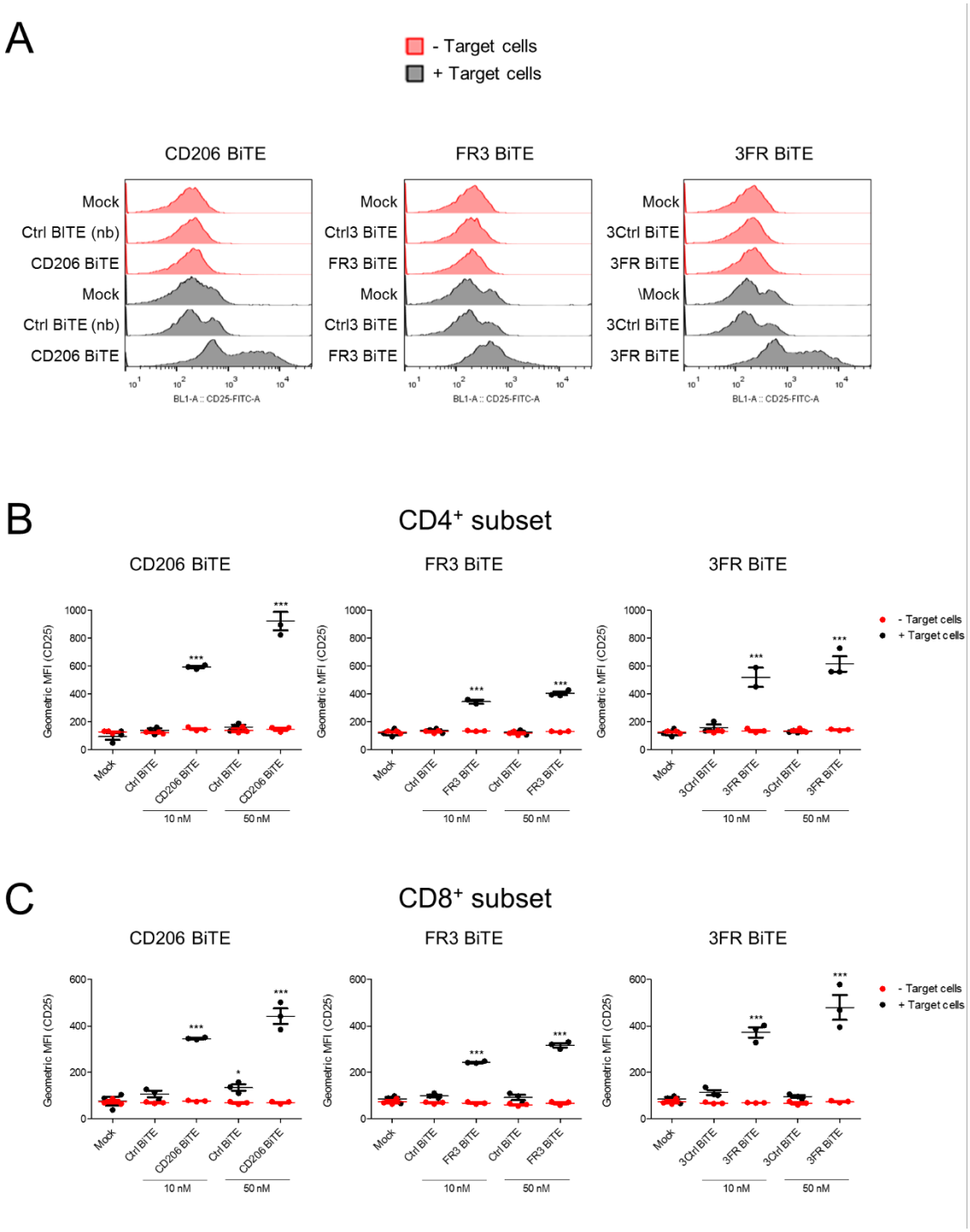

Figure 3.10. CD206 and FRβ-targeting BiTEs polyclonally activate CD4⁺ and CD8⁺ T cells. **(A-C)** T cell activation in the presence or absence of relevant target cells (M(IL-4) for CD206-targeting BiTE, M(M-CSF/IL-6) for FRβ-targeting BiTEs) was assessed by flow cytometric measurement of CD25 expression 96 h after BiTE addition. **(A)** Representative histograms of CD25 expression on total T cell population (BiTEs at 50 nM). **(B-C)** Geometric mean fluorescence intensity (MFI) values of CD25 expression on CD4⁺ and CD8⁺ T cell subsets. **(B, C)** Data show mean ± SD of biological triplicates. Statistical analysis was performed by two-way ANOVA with Bonferroni post-hoc tests comparing with the relevant "Mock" condition (*, $P < 0.05$; **, $P < 0.01$; ***, $P < 0.001$).

These data indicate that T cell activation by the TAM-targeting BiTEs is dependent on the presence of the relevant target antigen to initiate CD3 clustering.

3.3.6 Malignant ascites-induced MDMs are efficiently targeted by CD206 and FRβ BiTE treatments

As discussed above, acellular malignant ascites fluid has been shown to skew the differentiation of monocytes towards MDMs with TAM-like properties (Duluc et al., 2007). Indeed, ascites-induced MDMs were found to suppress T cell proliferation and induce T cell apoptosis in an indoleamine 2,3-dioxygenase (IDO)-dependent manner, as well as expressing T cell-inhibitory membrane protein B7-H4 (Duluc et al., 2007). Importantly, many of the immunoregulatory features of ascites-induced MDMs and TAMs were not shared by M2-polarised macrophages generated in a traditional manner (with IL-4, IL-1β or IL-10) (Duluc et al., 2007), highlighting the greater clinical relevance of these MDMs over other models.

We therefore asked whether the CD206 and FRβ-targeting BiTEs would retain their activity against ascites-induced MDMs. Three patient fluids were selected based on their ability to generate MDMs with elevated expression levels of both CD206 and FRβ (relative to unpolarised and M1-polarised MDMs; Figures 3.2 and 3.11D). After 6 days of incubation, ascites fluids were removed and the resultant ascites-induced MDMs harvested and co-cultured with autologous lymphocytes (E:T ratio of 10:1). Dose-response experiments (performed in the absence of ascites fluid) revealed robust killing of all three ascites-induced MDMs by CD206 BiTE treatment (Figure 3.11B), with EC_{50} values of 15.23 and 15.26 nM against M(Asc3) and M(Asc5), respectively (Figure 3.11C). The EC_{50} value of CD206 BiTE against M(Asc1) could not be calculated owing to a lack of bottom plateau. Both FRβ-targeting BiTEs also induced T cell-mediated cytotoxicity of all three ascites-

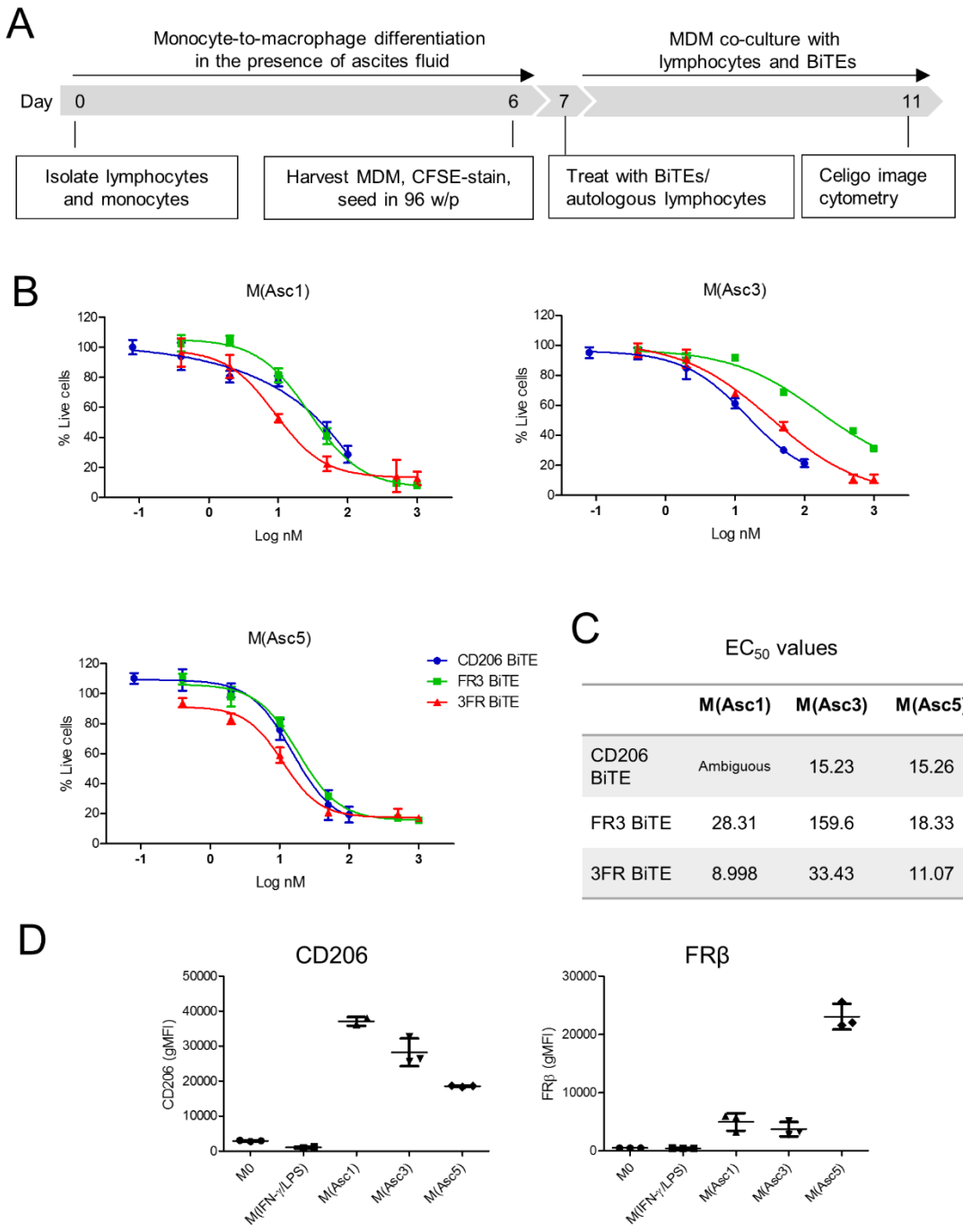

Figure 3.11. Dose responses of BiTEs against ascites-differentiated MDMs. **(A)** Outline of the protocol utilised to assess BiTE-mediated killing of ascites-differentiated MDMs by autologous lymphocytes. **(B)** Monocytes were differentiated to macrophages in the presence of ascites fluid (50% v/v) from three different patients, giving ascites-differentiated MDMs (M(Asc1), M(Asc3), M(Asc5)). Day-6 MDMs were stained with CFSE, seeded in 96-well plates and, 24 h later, treated with autologous lymphocytes (10:1 effector:target ratio) and the indicated concentrations of BiTEs. MDM killing was assessed 96 h later by propidium iodide staining and Celigo image cytometry. EC_{50} values are displayed in **(C).** **(D)** Expression levels of CD206 and folate receptor (FR) β by ascites-differentiated MDMs, as compared to unpolarised and IFN-γ/LPS-polarised MDMs. **(B, D)** Data show mean ± SD of biological triplicates.

induced MDMs (Figure 3.11B), with the greatest activity exhibited by the 3FR BiTE (EC_{50} values of 8.998, 33.43 and 11.07 nM against M(Asc1), M(Asc3) and M(Asc5), respectively) (Figure 3.11C).

Together, these data demonstrate that CD206 and FRβ-targeting BiTEs are active against clinically-relevant, ascites-induced MDMs, despite the immunosuppressive nature of these models.

3.3.7 The activity of the CD206 BiTE, but not the FRβ BiTEs, is markedly decreased in the presence of malignant ascites fluid

Acellular malignant ascites fluid is rich in soluble immunomodulatory factors (Matte et al., 2012) and, as such, represents a valuable tool for studying T cell activation in a tumour-like microenvironment (Simpson-Abelson et al., 2013). We therefore asked whether the TAM-targeting BiTEs would retain their activity in the presence of ascites fluid. Using human MDMs (polarised with cytokines) and autologous lymphocytes from healthy peripheral blood, we performed BiTE cytotoxicity assays in the presence of ascites supernatant (50% v/v) from three different cancer patients (Figure 3.12). The activities of both FRβ-targeting BiTEs were largely unaffected, triggering robust T cell activation (Figure 3.12A) and target cell cytotoxicity (Figure 3.12B) in the presence of ascites fluid. The efficacy of the CD206 BiTE, however, was greatly diminished, with little or no T cell cytotoxicity or activation observed in ascites fluid (Figures 3.12A and B).

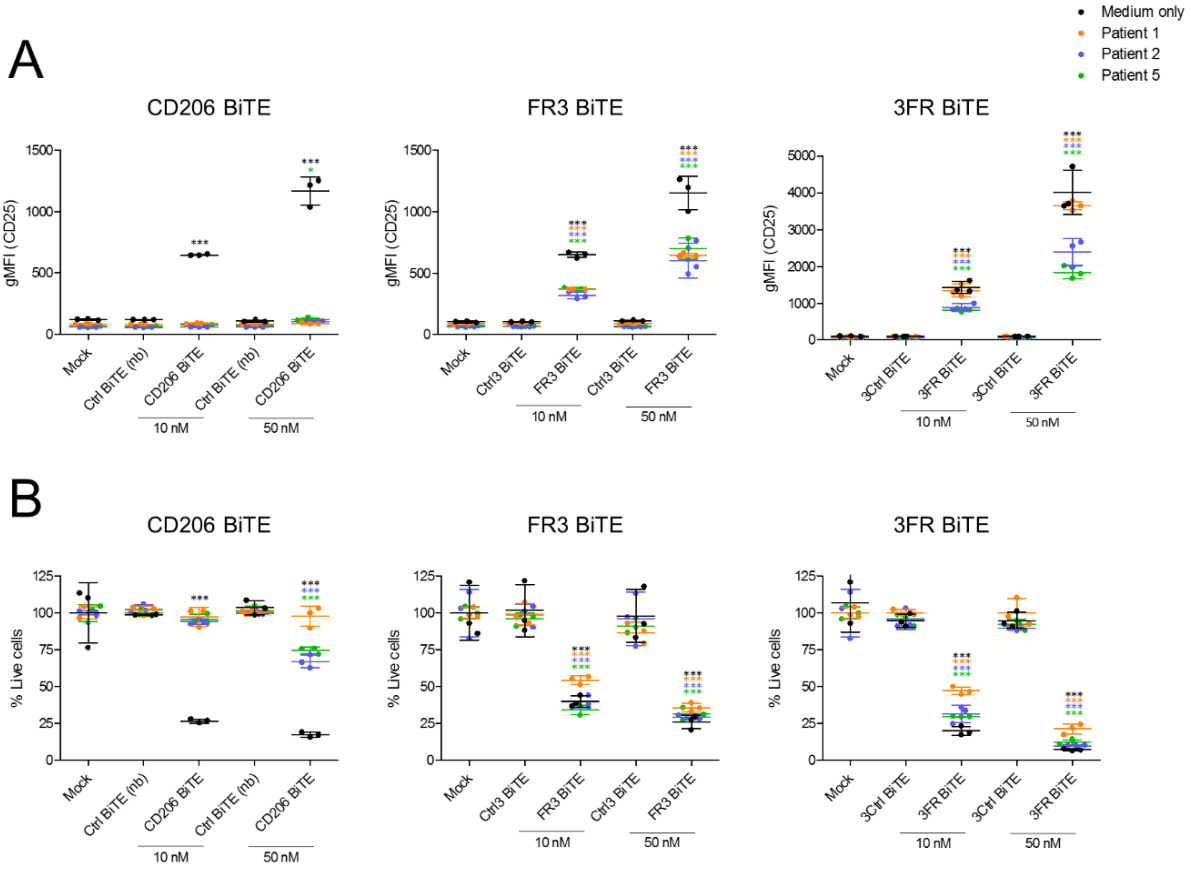

Figure 3.12. Human malignant ascites fluid suppresses CD206 BiTE activity but not FRβ BiTE activity. Human MDMs were polarised with IL-4 or M-CSF/IL-6 to generate CD206 and FRβ-high MDMs, respectively, then CFSE-stained and co-cultured with T cells (10:1 effector:target ratio) and the relevant BiTEs. Co-cultures were performed in the presence or absence of 50% ascites fluid (v/v) from three different cancer patients (Patients 1, 2 and 5). Four days later, T cell activation was assessed by flow cytometric measurement of CD25 expression **(A)**, while percentage live MDMs was determined with propidium iodide staining and a Celigo image cytometer **(B)**. **(A, B)** Each condition was measured in biological triplicate and represented as mean ± SD. Statistical significance was assessed by two-way ANOVA followed by Bonferroni post-hoc analysis, with each treatment being compared to the "Mock" condition within the relevant group (A and B). (*, $P < 0.05$; **, $P < 0.01$; ***, $P < 0.001$; ns, non-significant).

Given the dramatic inhibitory effect of ascites supernatant on CD206-, but not FRβ-targeting BiTE activity, we asked whether the fluids may contain any soluble inhibitory factors pertinent to this receptor. Activated DCs and macrophages are known to shed a soluble version of CD206 (sCD206), comprising the entire extracellular domain of the protein. Elevated serum sCD206 has been described in cases of sepsis and liver disease, as well as myeloma and gastric cancer (Rødgaard-Hansen et al., 2014). Given that sCD206

may block BiTE binding to membrane-bound CD206, we sought to determine whether sCD206 may be present in the malignant ascites fluids used in our study. Elevated levels of sCD206 (relative to healthy human serum pooled from three donors) were observed in 7/9 fluids tested (Figure 3.13A). Interestingly, the ascites sample with the greatest inhibitory effect on CD206 BiTE-mediated MDM cytotoxicity ("Patient 1") also contained the highest levels of sCD206 (Figure 3.14B). Nevertheless, there was no significant correlation between sCD206 levels and the magnitude of T cell activation (either % positivity for CD25, or CD25 geometric MFI) by the CD206 BiTE (Figure 3.13B), suggesting the influence of additional factors.

Prominent immunomodulatory factors reported in malignant ascites are IL-6, IL-10 and TGF-β (Kampan et al., 2017). Elevated levels of all three factors were observed in all ascites samples tested, relative to pooled human serum from healthy donors (Figure 3.14A). High quantities of IL-6 and TGF-β were detected in the ascites fluid from "Patient 1", perhaps indicating particularly important roles for these cytokines in suppressing BiTE activity (Figure 3.14B). Indeed, Pearson's correlation analysis revealed a significant negative correlation between soluble IL-6 levels and T cell activation (when considering CD25 geometric MFI) by the CD206 BiTE ($P < 0.0001$, R squared = 0.9864), and between soluble TGF-β and T cell activation, when considering % positivity for CD25 ($P = 0.0178$, R squared = 0.7903) (Figure 3.14B).

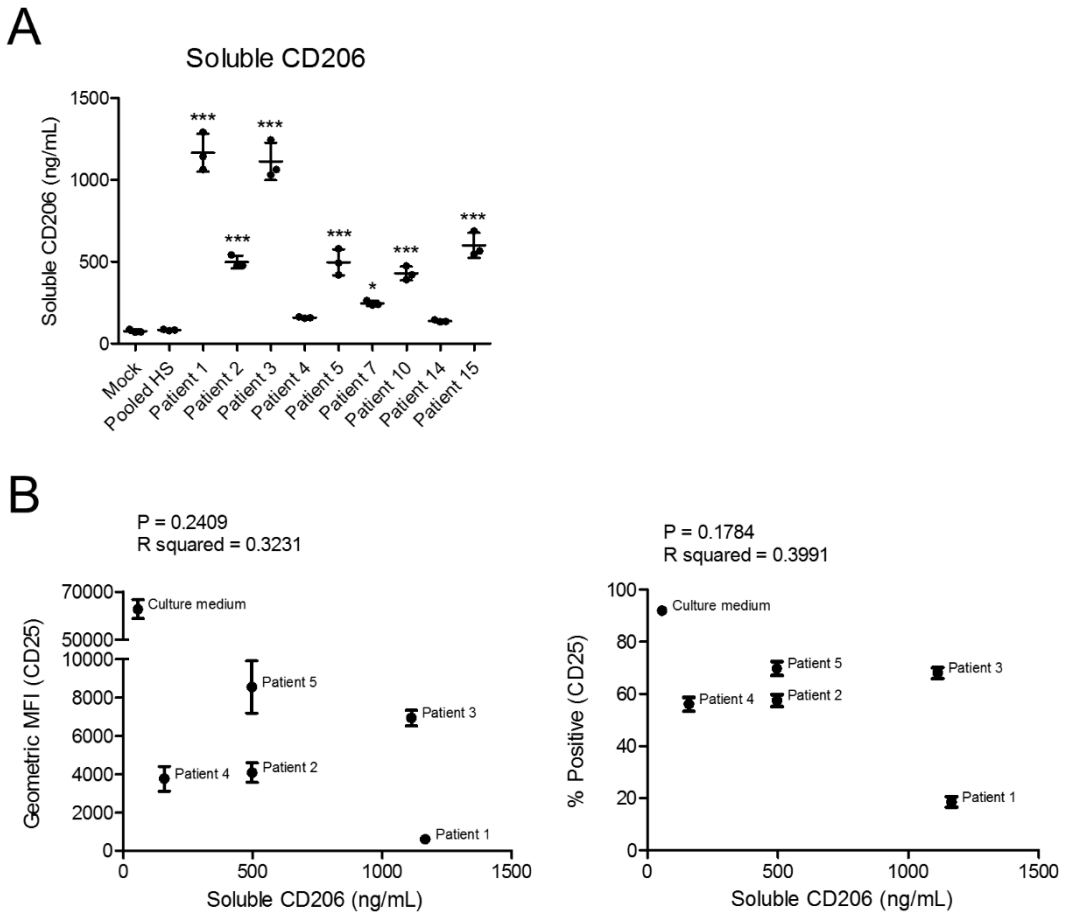

Figure 3.13. Soluble CD206 in detected at high levels in acellular ascites fluid. (**A**) Quantities of soluble CD206 in malignant ascites fluid from nine different patients were determined by ELISA. Pooled human serum (HS) from three healthy donors was included as a control. (**B**) T cell activation by the CD206 BiTEs after 96 h co-culture with IL-4-polarised (CD206high) MDMs in the presence or absence of the indicated patient ascites fluids (50% v/v) was assessed by flow cytometric measurement of CD25 expression. Plots of soluble CD206 (as determined by ELISA) versus T cell activation (CD25 geometric MFI or percentage positive) are displayed. Statistical analysis was performed by one-way ANOVA with Dunnett's post-hoc analysis compared with "Pooled HS" (*, $P < 0.05$; **, $P < 0.01$; ***, $P < 0.001$) (**A**), or by Pearson's correlation test (**B**).

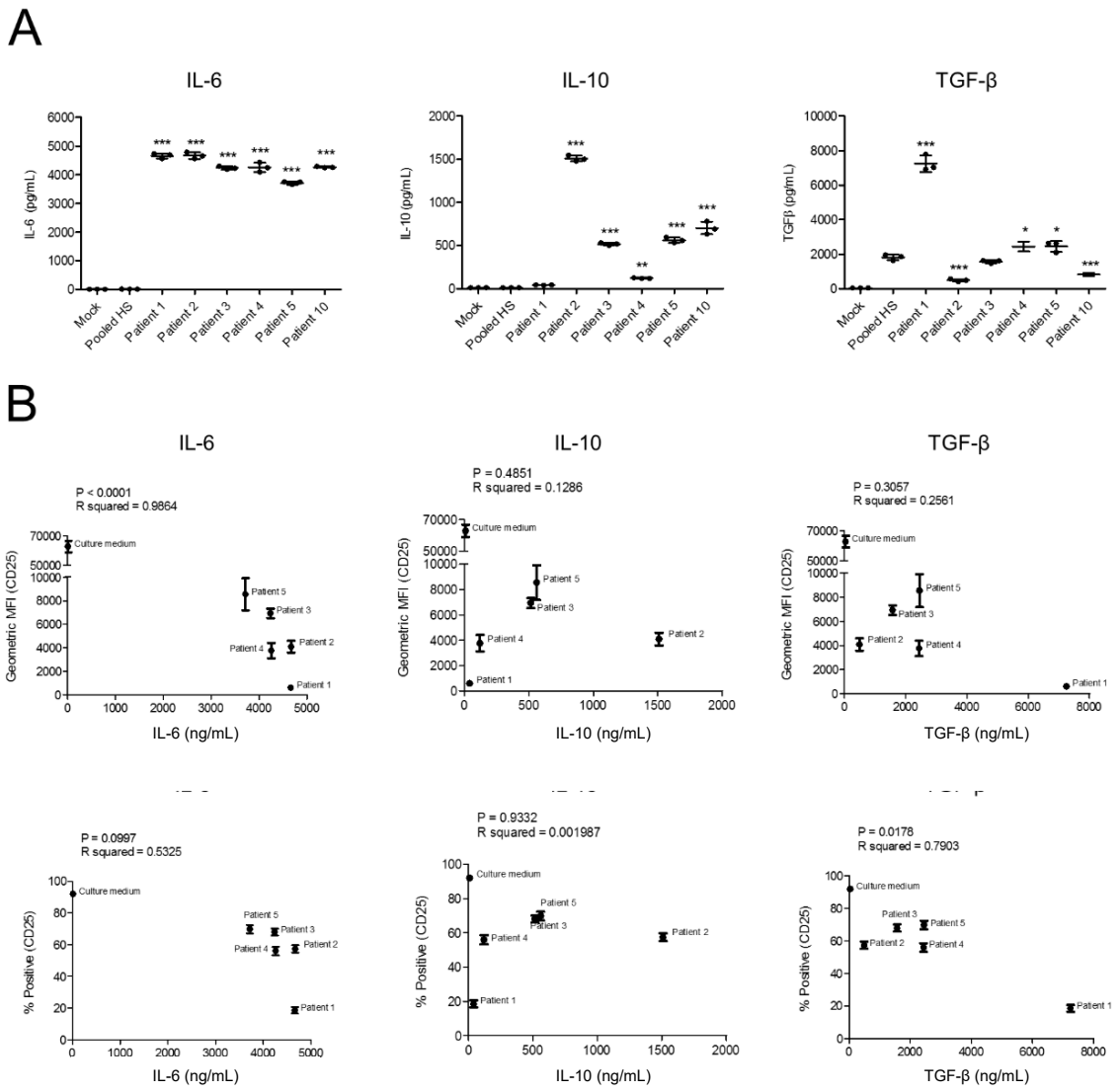

Figure 3.14. High levels of immunoregulatory cytokines are detected in malignant ascites fluid. **(A)** Quantities of IL-6, IL-10 and total (active and latent) TGF-β in malignant ascites fluid from six different patients, as determined by ELISA. Human serum (HS) pooled from three healthy donors was included as a control. **(B)** T cell activation by the CD206 BiTEs after 96 h co-culture with IL-4-polarised ($CD206^{high}$) MDMs in the presence or absence of the indicated patient ascites fluids (50% v/v) was assessed by flow cytometric measurement of CD25 expression. Plots of soluble IL-6, IL-10 and TGF-β (as determined by ELISA) versus T cell activation (CD25 geometric MFI or percentage positive) are displayed. Statistical analysis was performed by one-way ANOVA with Dunnett's post-hoc analysis compared with "Pooled HS" (*, $P < 0.05$; **, $P < 0.01$; ***, $P < 0.001$) **(A)**, or by Pearson's correlation test **(B)**.

3.4 Chapter conclusions

1. CD206 and FRβ are present on relevant models of human TAMs.
2. BiTEs engineered to recognise CD206 or FRβ trigger T cell-mediated cytotoxicity of autologous MDMs expressing high, but not low, levels of these receptors.
3. BiTE-mediated T cell activation is dependent on the presence of the relevant target antigen.
4. The activity of the CD206-targeting BiTE, but not the FRβ-targeting BiTEs, is compromised by acellular malignant ascites fluid.

3.5 Chapter discussion

CD206 and FRβ are markers of M2-like macrophages and human TAMs. Burgeoning clinical evidence suggests a correlation between $CD206^+$ and $FR\beta^+$ TAM density and poor patient prognosis, indicating that these markers may denote cancer-promoting TAM subsets. Here, we have successfully engineered the first BiTEs to target CD206 and FRβ. The novel BiTEs were functional in activating primary human T cells to kill autologous, M2-polarised MDMs, with little or no cytotoxicity towards M1-polarised MDMs (Figure 3.8). Consistent with previous studies on BiTEs (Haas et al., 2009; Mack et al., 1997), both $CD4^+$ and $CD8^+$ T cell subsets were activated by the TAM-targeting BiTEs, as shown by significant increases in their surface expression of CD25 (Figure 3.10). Importantly, T cell activation by the BiTEs was strictly target antigen-dependent, with no appreciable activation in the absence of target cells, or by control BiTEs recognising CD3ε and an irrelevant antigen (Figure 3.10). Moreover, BiTE-induced cytotoxicity of MDMs was observed only in the presence of effector cells, with no significant MDM killing by BiTEs alone (Figure 3.9).

To the best of our knowledge, the CD206- and FRβ-targeting BiTEs generated in this study represent the first biologics to redirect T cells towards autologous macrophages. Given the necessary interactions between macrophages and T cells during antigen presentation, it was possible that macrophages would display a degree of resistance to T cell-mediated killing. Indeed, reduced sensitivity to the cytotoxic effects of T cells is a well-characterised phenomenon for DCs, which persist during antigen presentation through expression of serine protease inhibitor-6, which inactivates granzyme B (Lovo et al., 2012). Whether or not macrophages utilise similar protective mechanisms is poorly understood; however, human immunodeficiency virus-infected macrophages were recently found to be more resistant to killing by cytotoxic T cells than their $CD4^+$ counterparts (Clayton et al., 2018), suggesting a degree of privilege from T cell-mediated cytotoxicity. Despite this, the TAM-targeting BiTEs were capable of inducing robust, T cell killing of macrophages, highlighting the potency of BiTE-mediated T cell activation.

In dose-response experiments with healthy T cells and autologous MDMs, the TAM-targeting BiTEs exhibited EC_{50} values in the nanomolar range (Figure 3.8). Interestingly, the 3FR BiTE outperformed the FR3 BiTE, with EC_{50} values of 10.6 and 61.2 nM, respectively. This is perhaps surprising given that EpCAM-targeting BiTEs containing the same anti-CD3 scFv (derived from mAb clone L2K) were reported to exhibit superior binding and cytotoxic capabilities when the CD3-binding domain was placed at the C-terminus (patent #WO2004106383A1). Indeed, most (if not all) bispecific antibodies containing an L2K-derived anti-CD3 domain have been developed in the latter orientation (Wu and Cheung, 2018). We hypothesise that the preferred arrangement of scFv domains is context-dependent, and likely influenced by the particular binding affinity and 3D structure of the second scFv.

Despite its similar performance against cells cultured in medium only, the CD206 BiTE was inferior to the FRβ BiTEs in the presence of acellular malignant ascites fluid. Indeed, T cell activation by the CD206 BiTE in the presence of these samples was extremely low or undetectable, leading to little or no killing of MDMs (Figure 3.12). By contrast, FRβ BiTE activity was largely unaffected (Figure 3.12). Several factors may underlie this finding. Soluble CD206 was detected at high quantities (up to ~1 mg/mL) in most malignant ascites fluids tested (Figure 3.13). The CD206-binding site of the BiTE may therefore have become saturated in the presence of ascites fluid, reducing its capacity to bind membrane-bound CD206. However, no correlation was observed between soluble CD206 levels and T cell activation by the BiTE (Figure 3.13), suggesting a role of additional factors. High levels of immunoregulatory cytokines (IL-6, IL-10 and TGF-β) were observed in the malignant ascites fluids, with a significant negative correlation between IL-6 and TGF-β levels and CD206 BiTE-mediated T cell activation (Figure 3.14). It is possible that T cell activation by the FRβ-targeting BiTEs was more powerful than that induced by the CD206 BiTE, enabling them to overcome the immunosuppressive effects of these cytokines.

One explanation for a more powerful activation of T cells by BiTEs targeting FRβ over CD206 may be the smaller size of the former antigen. According to the kinetic segregation model of TCR triggering (Davis and van der Merwe, 2006), T cell activation requires exclusion of the large, inhibitory phosphatase CD45 from the immunological synapse – a phenomenon which occurs when the two membranes are brought into close apposition (Davis and van der Merwe, 2006). The presence of a bulky extracellular domain in the immunological synapse would therefore be predicted to decrease the magnitude of T cell activation. In line with this, smaller antigens were found to facilitate superior BiTE-mediated T cell activation and target cell killing (Bluemel et al., 2010). At 170-180 kDa,

CD206 may represent a more challenging target for T cell based therapies than FRβ, which has a molecular weight of 30-40 kDa.

To summarise, the BiTEs generated in this chapter successfully induce T cell-mediated cytotoxicity towards autologous MDMs expressing high, but not low, levels of the relevant target antigen. These results provide a proof-of-concept for selective depletion of M2-like macrophages with BiTEs. Nevertheless, the activity of the CD206 BiTE is markedly reduced in the presence of malignant ascites fluid. In the next chapter, we seek to overcome this suppressive effect through the engineering of novel tri-valent CD206-targeting T cell engagers.

4 Generation of Novel CD206-Targeting Trivalent T Cell Engagers with Enhanced Potency

4.1 Introduction

In the previous chapter, we found that the activity of the CD206-targeting BiTE was markedly reduced in the presence of acellular malignant ascites fluids. One possible explanation for this inhibitory effect resides in the high levels of immunoregulatory cytokines (IL-6, IL-10 and TGF-β) detected in these samples. T cell activation is governed by the balance between positive and negative stimulatory signals received by a given cell (Chen and Flies, 2013). We therefore chose to explore whether adding a second T cell-activating domain to the parental CD206 BiTE would push the balance towards T cell activation and facilitate cytotoxicity in suppressive ascites fluid.

Alongside bispecific antibodies, a variety of multi-specific antibody formats are now available. Notable among these are "triplebodies": single-chain constructs comprising three scFvs joined in tandem (Kellner et al., 2008). Most triplebodies designed thus far aim to improve tumour cell targeting, containing two TAA-targeting scFvs (with the same or different specificities) fused to a single scFv specific for an effector cell receptor. For instance, a CD19-CD3-CD33 triplebody was found to preferentially kill CD19/CD33 dual-positive leukaemia cells over CD19 single-positive cells, possibly offering enhanced cancer cell-selectivity (Roskopf et al., 2016). Other dual TAA-targeting triplebodies include CD19-CD16-CD19 (Kellner et al., 2008) and CD19-CD16-HLA-DR (Schubert et al., 2012), both of which activate NK cells.

By contrast, there is only a single report of a single-chain antibody fragment co-targeting two effector cell receptors. In this study, an anti-CEA scFv was fused to an anti-CD3 scFv,

as well as an anti-CD28 heavy chain variable (VH) domain, providing co-stimulation (Wang et al., 2004) (Figure 4.1A). Although BiTE activity is not dependent on co-stimulation, agonistic anti-CD28 antibodies have been found to improve BiTE-induced T cell-mediated killing of primary human leukaemic cells (Laszlo et al., 2015), supporting the use of co-stimulatory agents to enhance these therapies. The CEA-CD3-CD28 tri-specific antibody mediated effective killing of CEA^+ target cells in the presence of PBMCs (Wang et al., 2004). However, the T cell-activating capacities of this antibody were not compared to a relevant bispecific antibody, and further development of this construct has not been reported.

Alternatively, T cell activation may be enhanced by increasing the valence of CD3 binding. Although this has yet to be attempted in a single-chain antibody format, the possible benefits of such an approach are illustrated by studies with TandAbs. TandAbs are bispecific tetra-valent antibodies which form from the association of complementary VH and light chain variable (VL) domains located on different polypeptides (Kipriyanov et al., 1999) (Figure 4.1B). Interestingly, a TandAb with dual binding sites for both CD3 and CD19 was found to trigger more potent lysis of $CD19^+$ cancer cells than the equivalent BiTE, with markedly improved activity at lower E:T ratios (Reusch et al., 2015). A TandAb recognising CD3 and CD33 has also been developed and validated pre-clinically (Reusch et al., 2016), although in this case direct comparisons to a CD33-targeting BiTE were not made.

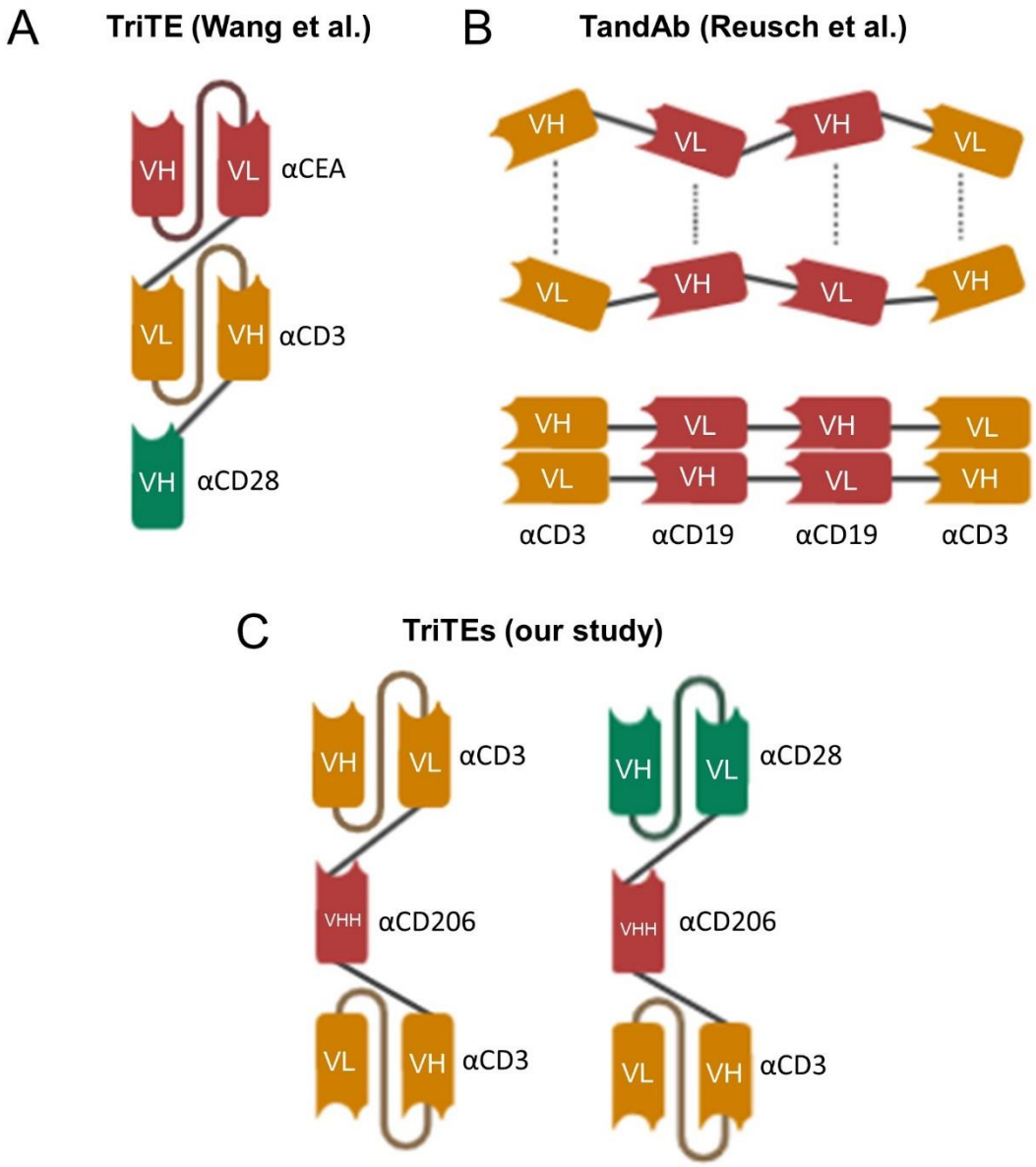

Figure 4.1. An overview of the different multi-valent T cell engager formats discussed in this chapter. (A) The trispecific antibody generated by Wang et al. comprised, from N- to C-termini, an anti-CEA scFv, an anti-CD3 scFv and an anti-CD28 VH domain. **(B)** TandAbs are homodimers formed from the head-to-tail association of cognate VH/VL pairs across two single chains. **(C)** The TriTEs generated in this study comprise the parental BiTE (an anti-CD206 VHH domain linked to an anti-CD3 scFv) with an additional anti-CD3 scFv or anti-CD28 at its N-terminus. VH, variable heavy; VL, variable light; VHH, nanobody; TriTE, trispecific T cell engager; TandAb, tandem diabody.

In this chapter, we attempted to improve the activity of the CD206-targeting T cell engager through addition of a second T cell-binding domain. Two different types of single-chain tri-valent T cell engagers (TriTEs) were engineered: one contained an anti-CD28 domain, providing T cell co-stimulation, whilst the other contained a second anti-CD3 binding domain, establishing bi-valent CD3 binding (Figure 4.1C). The activity of the TriTEs was compared to the parental BiTE in PBMC-based model systems, and their ability to overcome suppression by malignant ascites assessed.

4.2 Chapter Aims

1. Engineer CD206-targeting TriTEs containing anti-CD28 or –CD3 domains, as well as the relevant control TriTEs
2. Compare T cell activation by the CD206-targeting BiTE and TriTEs in co-culture with autologous MDMs
3. Assess the specificity for the novel TriTEs for M2- over M1-polarised MDMs
4. Determine the activity of the CD206-targeting BiTE and TriTEs in suppressive malignant ascites

4.3 Results

4.3.1 Engineering and production of CD206-targeting TriTEs using transfected HEK293A cells

We first sought to establish the optimal domain orientations for the novel TriTEs. The additional T cell-activating domains (anti-CD3 or anti-CD28) were added either to the N- or the C-terminus of the parental CD206 BiTE, thereby creating a total of four novel TriTEs ("206-3-3", 3-206-3", "206-3-28" and "28-206-3"; schematic representations in Figure 4.2A). CD206 TriTE sequences were inserted into a mammalian expression vector under the control of a CMV promoter (Fig 4.2B) by standard DNA cloning techniques (see Figure 3.4), for transfection into adherent HEK293A cells.

Western blotting analysis of the transfected cell supernatants revealed robust expression of the CD206 TriTEs when their additional T cell-binding domains were located at the N-terminus of the parental BiTE ("3-206-3" and "28-206-3") (Figure 4.2C). By contrast, placement of the anti-CD3 and anti-CD28 domains at the C-terminus of the parental CD206 BiTE yielded TriTEs ("206-3-3" and "206-3-28") with very low or undetectable expression levels (Figure 4.2C). Thus, despite the fact that fusion to the N-termini of nanobodies is generally to be avoided (due to clustering of the CDRs around their N-termini, see section 3.3.2), we proceeded only with development of the "3-206-3" and "28-206-3" TriTE variants.

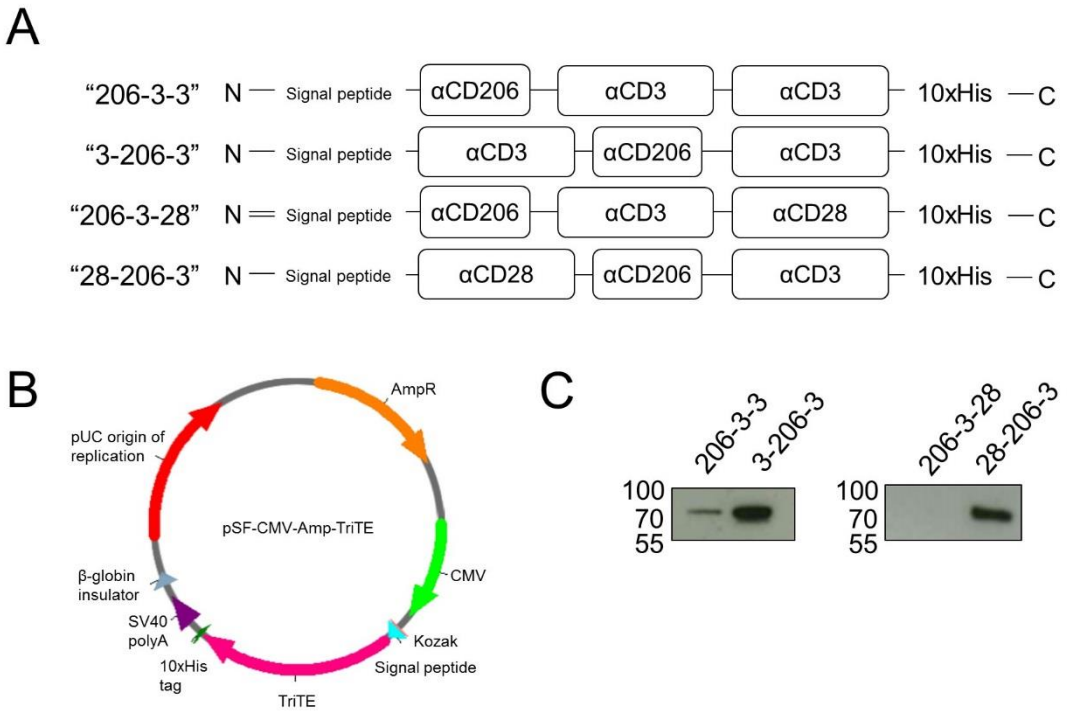

Figure 4.2. Optimisation of binding domain orientation to generate CD206-targeting TriTEs. TriTEs were generated by joining anti-CD3 (αCD3) or anti-CD28 (αCD28) single chain variable fragments (scFv) with a glycine-serine linker to the N- or C-termini of the parental CD206 BiTE. All TriTEs contained a signal peptide at the N-terminus and a deca-histidine (10xHis) tag at the C-terminus. **(A)** Schematic representations of the CD206-targeting TriTEs. **(B)** A representative vector for mammalian expression of TriTEs is depicted. CMV, cytomegalovirus. AmpR, ampicillin resistance casette; SV40, Simian vacuolating virus 40. **(C)** Supernatants from HEK293A cells transfected for 48 h with the TriTE expression vectors were subjected to western blotting analysis, using an anti-His primary antibody and horseradish peroxidase-conjugated anti-mouse secondary antibody.

Matched Ctrl TriTEs ("3-Ctrl-3", "28-Ctrl-3"; Figure 4.3A) were engineered and inserted into mammalian expression vectors as above. Supernatants from HEK293A cells transfected with expression vectors encoding the CD206 TriTEs ("3-206-3 and "28-206-3" and their matched controls ("3-Ctrl-3" and "28-Ctrl-3" were concentrated and analysed by western and dot blotting (Figures 4.3B and 4.3C).

Crucially, binding to recombinant CD206, as determined by ELISA, was not compromised by the addition of a second T cell binding domain (Figure 4.4).

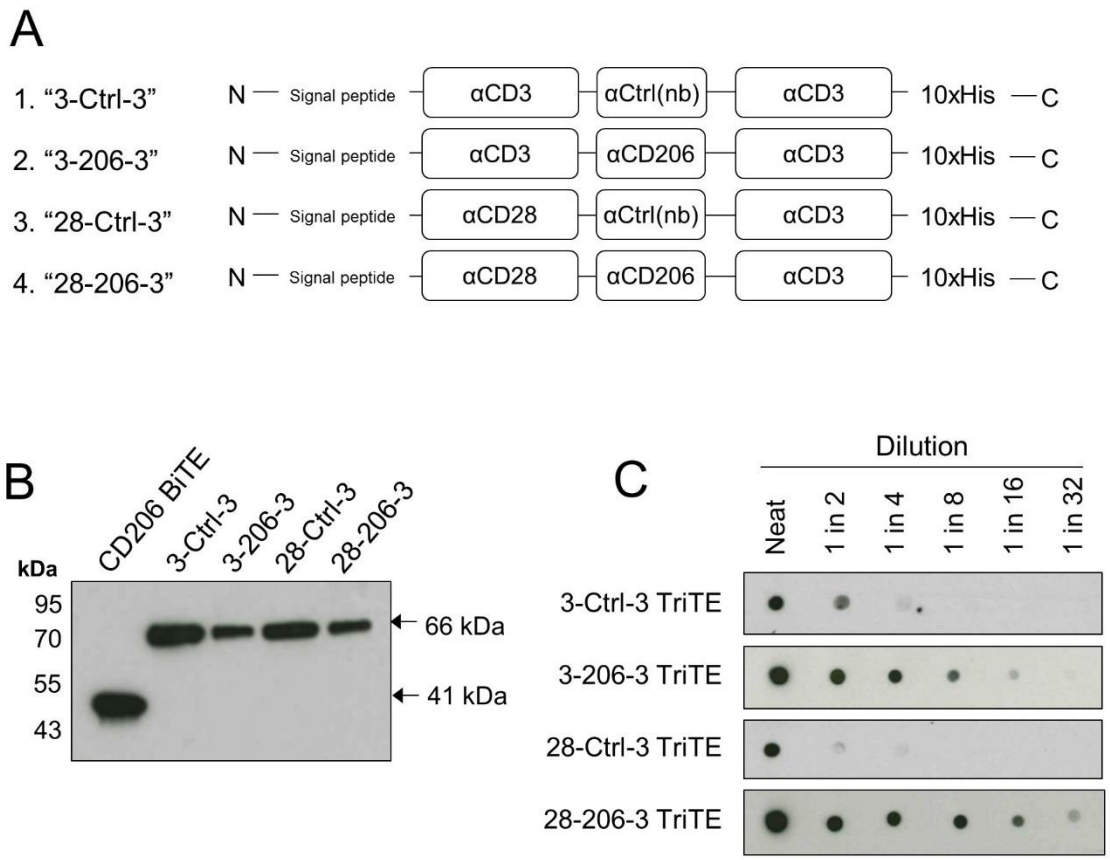

Figure 4.3. **Generation of CD206-targeting TriTEs and their matched controls.** TriTEs were generated by joining anti-CD3 (αCD3) or anti-CD28 (αCD28) scFvs with a glycine-serine linker to the N-termini of the parental CD206 or control (Ctrl) BiTEs. All TriTEs contained a signal peptide at the N-terminus and a deca-histidine (10xHis) tag at the C-terminus. **(A)** Schematic representations of the CD206-targeting TriTEs and their matched controls. **(B)** Supernatants from HEK293A cells transfected for 48 h with the TriTE expression vectors were subjected to western blotting analysis, using an anti-His primary antibody and horseradish peroxidase-conjugated anti-mouse secondary antibody. CD206 BiTE-containing supernatants were blotted alongside the TriTEs for comparison. **(C)** Exemplary dot blot analyses of serially-diluted TriTE-containing HEK293A cell supernatants.

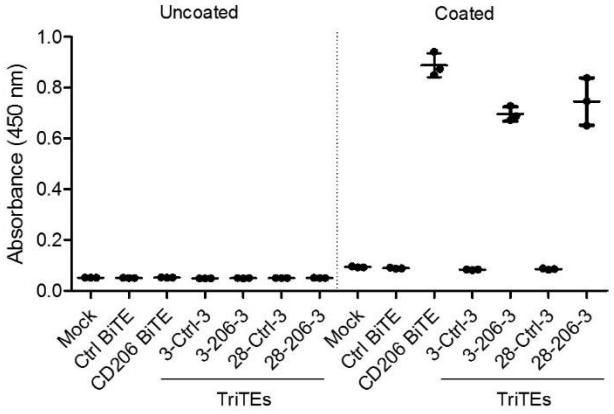

Figure 4.4. CD206-targeting TriTEs retain their ability to bind CD206. BiTE and TriTE binding to CD206 was determined by ELISA using a mouse anti-His primary antibody and an horseradish peroxidase-conjugated anti-mouse secondary antibody. Wells were coated with 50 ng recombinant CD206 protein or left uncoated, as indicated, then incubated with BiTE/TriTE containing supernatants prior to antibody addition. "Mock" wells were treated with phosphate-buffered saline in place of BiTE/TriTE-containing supernatants.

4.3.2 TriTEs containing an anti-CD28 domain, but not a second anti-CD3 domain, trigger non-specific activation of T cells

The T cell-activating capacities of the novel TriTEs were then assessed alongside the parental BiTE. Healthy human peripheral blood lymphocytes were incubated for four days with the BiTEs and TriTEs (or their matched controls) in the presence or absence of autologous IL-4-polarised MDMs (M(IL-4), $CD206^{high}$). Four days later, CD25 expression on T cells was assessed by flow cytometry. Addition of an anti-CD28 domain to the parental BiTE resulted in non-specific T cell activation, with similarly high levels of CD25 expression induced by the CD28 binding TriTE ("28-206-3") and its matched control ("28-Ctrl-3") in both the presence and absence of target cells (M(IL-4) MDMs) (Figures 4.5A and B). These findings were confirmed by the observation of IFN-γ secretion by T cells treated with both 28-206-3 and 28-Ctrl-3 TriTEs, in the presence and absence of target cells (Figure 4.5C).

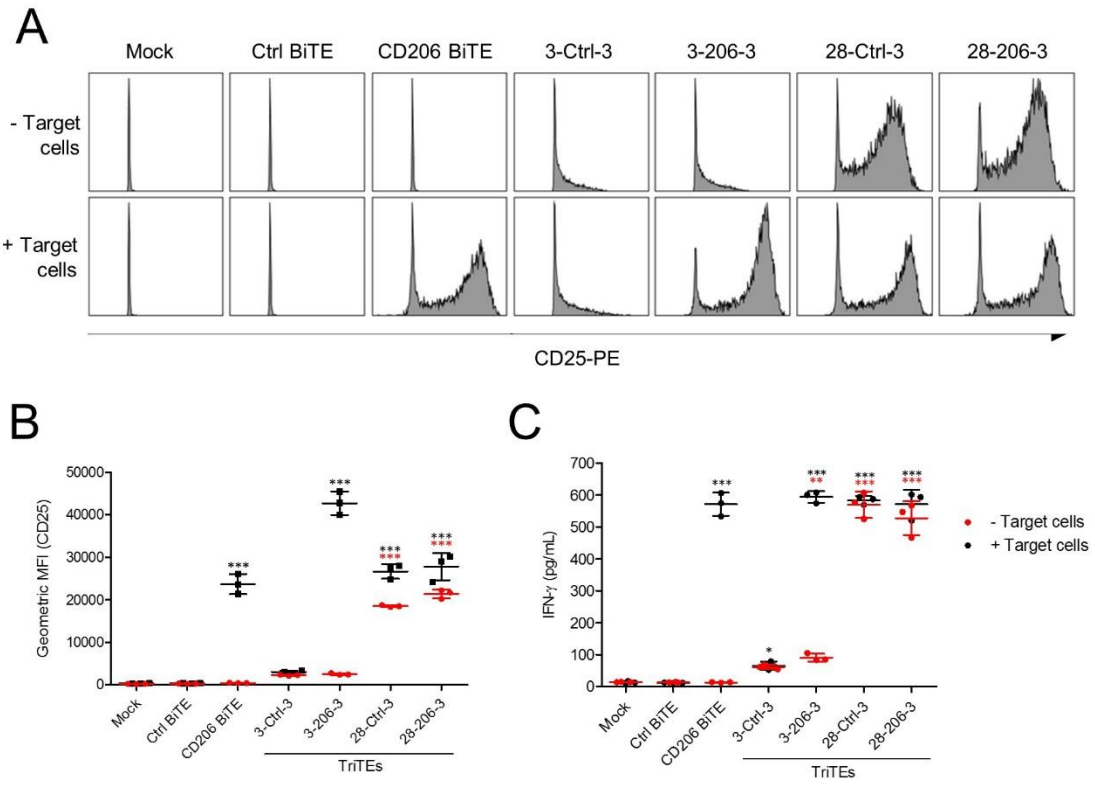

Figure 4.5. T cell activation by the CD206-targeting TriTEs. (A-C) Healthy human peripheral lymphocytes were incubated with the indicated BiTEs/TriTEs (at 50 nM), in the presence or absence of autologous IL-4-polarised ($CD206^{high}$) MDMs (effector:target ratio of 10:1). Four days later, T cell activation was assessed through flow cytometric measurement of CD25 expression (representative histograms in **(A)**, quantification in **(B)**), and enzyme-linked immunosorbent assay for IFN-γ secretion **(C)**. **(B, C)** Data show mean ± SD of biological triplicates. Statistical analysis was performed by two-way ANOVA with Bonferroni post-hoc tests comparing with the relevant "Mock" condition (*, $P < 0.05$; **, $P < 0.01$; ***, $P < 0.001$).

Conversely, the CD206 TriTE with bi-valent CD3 binding ("3-206-3") exhibited a requirement for its target antigen, triggering a significant (125-fold, relative to mock, Figure 4.5B) rise in CD25 expression by T cells only upon co-culture with target cells (Figures 4.5A and B). T cell activation by the CD206 TriTE was stronger than the parental BiTE, which elicited a 68.9-fold increase in CD25 expression (relative to mock, Figure 4.5B), around half that of the TriTE. The relevant control TriTE ("3-Ctrl-3") induced minor, albeit non-significant, T cell activation in the presence or absence of target cells (Figures 4.5A and B). The 3-206-3 TriTE resulted in an induction (43.5-fold, relative to mock) of

IFN-γ secretion in the presence of target cells, although a small rise (4.8-fold, relative to mock) was also observed when T cells were treated with the 3-Ctrl-3 TriTE (Figure 4.5C). These results suggest that the presence of two anti-CD3 domains within a single T cell engager may trigger minor non-specific T cell activity, but that potent T cell activation by the 3-206-3 TriTE nevertheless requires presence of its target antigen.

4.3.3 Dose responses of CD206 TriTEs against MDMs using autologous T cells as effector cells

We next explored the selectivity of the novel CD206 TriTEs for macrophages with high versus low expression levels of CD206 (M(IL-4) and M(IFN-γ/LPS) MDMs, respectively). Healthy human peripheral blood lymphocytes were co-cultured with autologous polarised MDMs (E:T ratio of 10:1) for four days in the presence of increasing concentrations of TriTEs or the parental BiTE. Percentage live cells were calculated by Celigo image cytometry. As shown in Figure 4.6A, bi-valent CD3 binding enhanced the potency of the parental BiTE against M(IL-4) MDMs, with EC_{50} values of 0.2145 nM and 2.894 nM for the 3-206-3 TriTE and CD206 BiTE, respectively (Figures 4.6A and C). Unlike the CD206 BiTE, which triggered only minor T cell-mediated cytotoxicity of $CD206^{low}$ cells (bottom best-fit value of 82.8%; EC_{50} value of 9.591 nM), the 3-206-3 TriTE elicited a strong T cell-mediated depletion of M(IFN-γ/LPS) MDMs (bottom best-fit value of 39.4%; EC_{50} value of 1.884 nM) (Figures 4.6A and C). In line with the observation that TriTEs containing an anti-CD28 domain trigger non-specific T cell activation, the 28-206-3 TriTE elicited similar levels of T cell-mediated cytotoxicity towards both M(IFN-γ/LPS) and M(IL-4) MDMs, with EC_{50} values of 6.370 and 7.916 nM, respectively (Figures 4.6A and C).

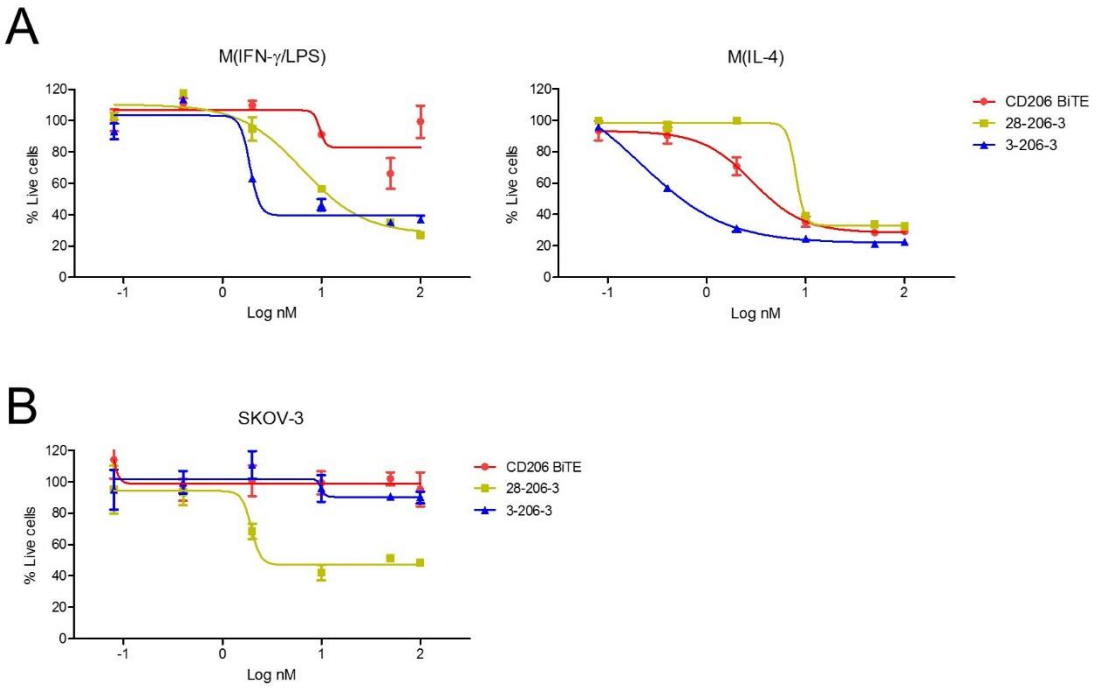

C

EC_{50} values

	M(IFN-γ/LPS)	M(IL-4)	SKOV-3
CD206 BiTE	9.591	2.894	-
28-206-3 TriTE	6.370	7.916	1.960
3-206-3 TriTE	1.884	0.2145	-

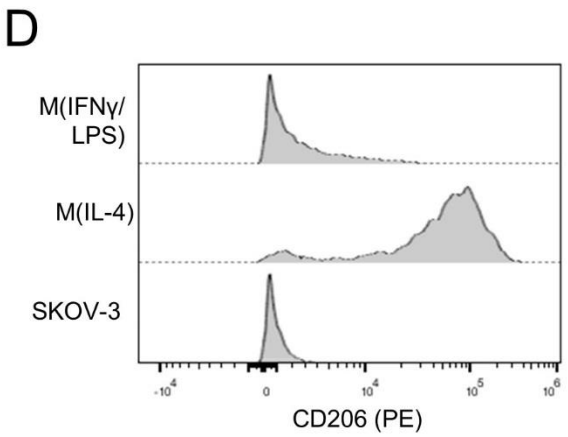

Figure 4.6. A bivalent CD3-binding TriTE, but not a CD28-containing TriTE, retains selectivity for target antigen-bearing cells. (A-D) Polarised human MDMs and SKOV-3 ovarian cancer cells were CFSE-stained and treated with the indicated dilutions of BiTE/TriTE and lymphocytes (effector:target ratio of 10:1). Four days later, % live cells was calculated with propidium iodide staining and Celigo image cytometry. EC_{50} values are displayed in **(C)**. Representative flow cytometric histograms of CD206 expression are depicted in **(D).** Data show mean ± SD of biological triplicates **(A)**.

Given that M(IFN-γ/LPS) MDMs are not CD206-negative, but rather express low levels of CD206 (Figure 4.6D), we asked whether a truly CD206-negative cell line, SKOV-3 ovarian cancer cells (Figure 4.6D), would also exhibit sensitivity to TriTE-mediated cytotoxicity.

SKOV-3 cells were selected based on their relatively long doubling time (35 hours), which minimised changes in E:T ratio over the course of the experiment. No significant cytotoxicity of SKOV-3 cells was elicited by the 3-206-3 TriTE after four days' co-culture with lymphocytes (E:T ratio of 10:1) (Figure 4.6B). By contrast, the 28-206-3 TriTE induced robust T cell-mediated killing of SKOV-3 cells, with an EC_{50} value of 1.960 nM (Figures 4.6B and C).

Together, these data show that addition of an anti-CD28 domain to the parental CD206 BiTE causes non-specific T activation, leading to cytotoxicity of surrounding cells in a target antigen-independent manner. Addition of a second CD3-binding domain, meanwhile, increases the potency of the parental CD206 BiTE whilst still maintaining a requirement for the relevant target antigen to initiate CD3 clustering. Nevertheless, the threshold of antigen density required to trigger T cell-mediated cytotoxicity by the 3-206-3 TriTE appears to be lower than that of the parental CD206 BiTE, with $CD206^{low}$ MDMs exhibiting sensitivity to the TriTE.

4.3.4 Selectivity of a CD206 TriTE for M2- over M1-polarised macrophages is retained at low effector:target ratios

Given the complete lack of target cell specificity of the 28-206-3 TriTE, we chose to proceed only with the 3-206-3 TriTE (hereafter referred to as "CD206 TriTE"). At an E:T ratio of 10:1, the CD206 TriTE appeared unable to discriminate effectively between cells with high and low levels of CD206 (Figure 4.6). We therefore asked whether TriTE selectivity for $CD206^{high}$ cells may be retained at lower, more physiologically-relevant E:T ratios (Thorsson et al., 2018). A checkerboard titration approach was employed, with M(IFN-γ/LPS) and M(IL-4) MDMs subjected to increasing BiTE/TriTE concentrations in the presence of increasing numbers of T cells (i.e. giving greater E:T ratios) (Figure 4.7).

Robust cytotoxicity towards M(IL-4) MDMs was observed even when low E:T ratios (<2:1) and BiTE/TriTE concentrations (<10 nM) were used (Figure 4.7A). Conversely, M(IFN-γ/LPS) MDMs were killed only when E:T ratio and TriTE concentration were simultaneously high (E:T ratio of 10:1 and TriTE concentration of 50 nM, % live cells reduced to 58.9%, Figure 4.7A). Similarly, the Ctrl TriTE only elicited MDM cytotoxicity at high E:T and TriTE concentrations (Figure 4.7A). M(IFN-γ/LPS) MDMs were unharmed by CD206 BiTE treatment at all concentrations and E:T ratios tested (Figure 4.7A).

Notably, the CD206 TriTE was capable of inducing cytotoxicity of M(IL-4) MDMs at lower concentrations and more physiologically-relevant E:T ratios than the CD206 BiTE (Fig 4.7A). For instance, at a BiTE/TriTE concentration of 2 nM and an E:T ratio of 2:1, the CD206 TriTE triggered a marked decrease in % live macrophages to 10.6%, whilst the CD206 BiTE was completely ineffective (Figures 4.7A and B).

Thus, whilst the selectivity of the CD206 TriTE for $CD206^{high}$ MDMs is minimal at high E:T ratios, its ability to discriminate between different target antigen densities is restored with decreasing effector cell availability. Critically, at low E:T ratios, the CD206 TriTE outperforms the CD206 BiTE against M(IL-4) MDMs, indicating that the TriTE platform will be necessary to achieve cytotoxicity of $CD206^{+}$ TAMs at more physiologically-relevant E:T ratios.

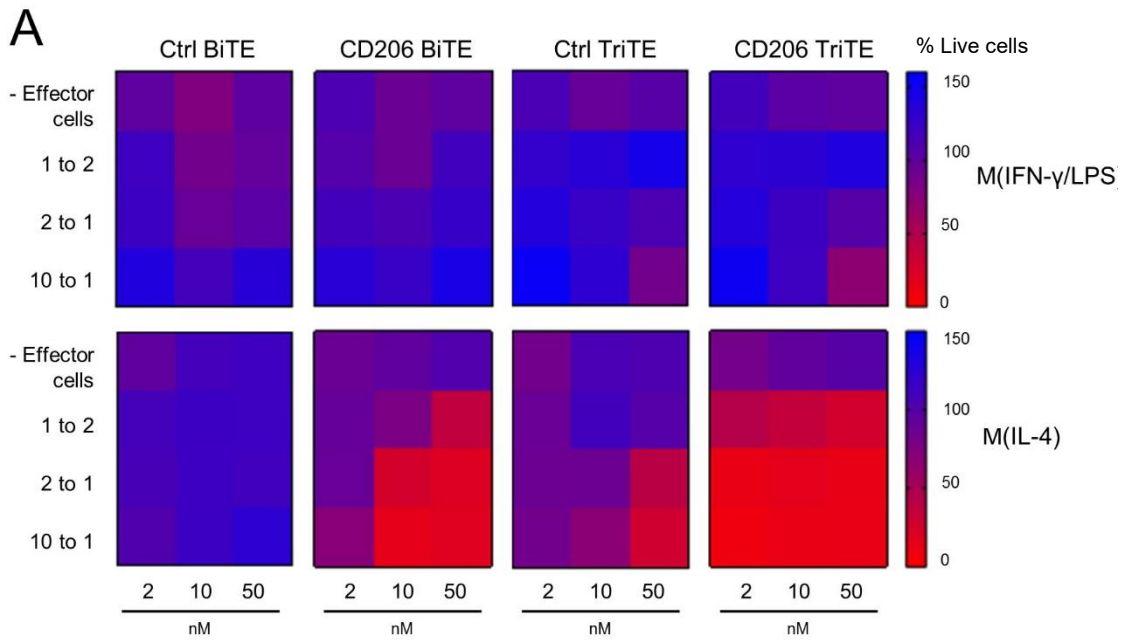
A
Ctrl BiTE
CD206 BiTE
Ctrl TriTE
CD206 TriTE
% Live cells
- Effector cells
1 to 2
2 to 1
10 to 1
150
100
50
0
M(IFN-γ/LPS)
M(IL-4)
2
10
50
nM

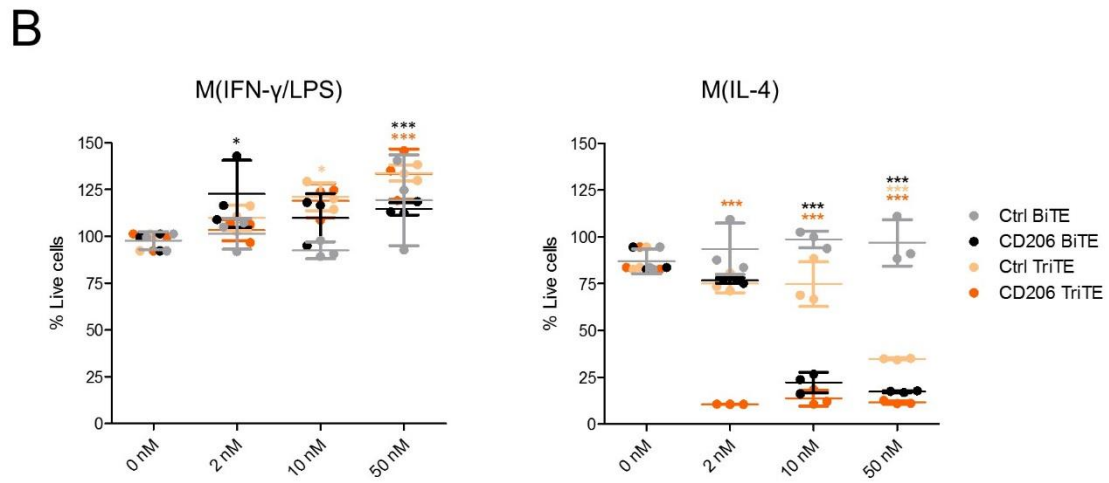
B
M(IFN-γ/LPS)
M(IL-4)
% Live cells
0 nM
2 nM
10 nM
50 nM
Ctrl BiTE
CD206 BiTE
Ctrl TriTE
CD206 TriTE

4.3.5 Rearrangement of the two anti-CD3 domains within the CD206 TriTE does not further increase potency

Although expression of the CD206 TriTE with two C-terminal anti-CD3 domains ("206-3-3" TriTE") was very weak (Figure 4.2C), we were interested in comparing its activity to the 3-206-3 TriTE. Dose responses of the two bi-valent CD3-binding TriTEs (quantified by dot blot) were performed with co-cultures of M(IL-4) MDMs and autologous peripheral blood lymphocytes from healthy donors. Four days later, MDM killing was assessed by Celigo image cytometry. As shown in Figure 4.8, the 3-206-3 TriTE outperformed the 206-3-3 TriTE, with EC_{50} values of 0.319 nM and 2.096 nM, respectively. Therefore, despite recommendations to build upon the C-terminus of nanobodies, the CD206-targeting BiTE appeared able to tolerate insertion at its N-terminus - in fact outperforming the other orientation.

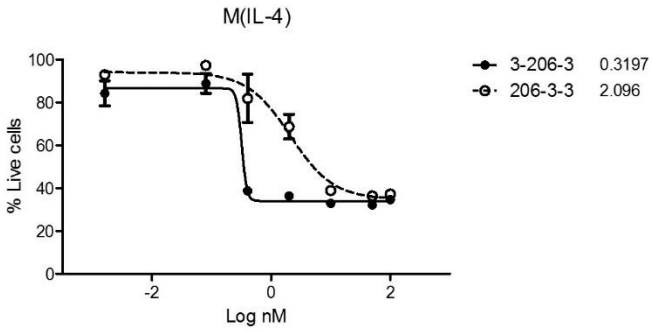

Figure 4.8. Rearrangement of the two CD3-binding domains within the single chain of the CD206 TriTE decreases its efficacy. IL-4 polarised human MDMs were CFSE-stained and co-cultured with autologous lymphocytes (effector:target ratio of 10:1) and the indicated concentration of TriTEs. % Live cells was calculated 96 h later with propidium iodide staining and Celigo image cytometry. Data show mean ± SD of biological triplicates.

4.3.6 The CD206 TriTE with bi-valent CD3 binding does not trigger T cell-mediated cytotoxicity of other T cells

Given the presence of two anti-CD3 binding domains within the single chain of the CD206 TriTE, one possible (and unfavourable) consequence of CD206 TriTE treatment may be the crosslinking of adjacent T cells, leading to T cell-T cell cytotoxicity. Before proceeding further with the CD206 TriTE, we therefore performed dose response experiments on healthy peripheral blood lymphocytes in the absence of target MDMs. Percentage live T cells were calculated with flow cytometry. As shown in Figure 4.9, no appreciable killing of T cells was observed at any concentration of 3-206-3 TriTE tested, perhaps suggesting that the bridging of two CD3 molecules on the surface of a single T cell is a statistically more likely event than bridging neighbouring cells.

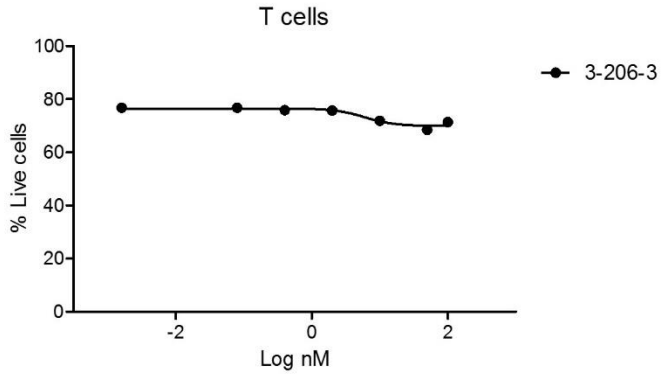

Figure 4.9. A bivalent CD3-binding TriTE does not trigger T cell-mediated cytotoxicity of other T cells. Healthy human peripheral lymphocytes were incubated with the CD206 TriTE with bivalent CD3 binding ("3-206-3") for 96 h. Percentage live cells were calculated with flow cytometric analysis after staining with anti-CD4 and –CD8 antibodies, and a live/dead stain. Data show mean ± SD of biological triplicates.

4.3.7 CD206 TriTE activity in the presence of malignant ascites fluid is superior to the parental CD206 BiTE

Next, CD206 TriTE activity in the presence of malignant ascites fluids was assessed. As before (section 3.3.8), healthy peripheral blood lymphocytes were co-cultured with autologous M(IL-4) MDMs (10:1 E:T ratio) in the presence or absence of malignant ascites fluid from three different patients (50% v/v). T cell activation and MDM killing by the BiTEs/TriTEs were assessed four days later. As shown in Figure 4.10, the CD206 TriTE exhibited markedly improved activity relative to the parental CD206 BiTE in all three patient fluids tested. At a low dose of 10 nM, the CD206 TriTE triggered significant T cell activation (as assessed by flow cytometric measurement of CD25 expression) in two of three patient samples, whilst, at 50 nM, T cell activation by the CD206 TriTE was significant in all three ascites fluids (Figure 4.10A). By contrast, the CD206 BiTE was unable to elicit significant T cell activation in any of the ascites fluids at either BiTE concentration tested (Figure 4.10A). Neither the Ctrl BiTE nor the Ctrl TriTE elicited appreciable T cell activation in medium only or the ascites fluids (Figure 4.10A). The Ctrl TriTE triggered a trend towards T cell activation, although this did not reach significance.

T cell activation by the CD206 TriTE in the presence of the ascites fluids was considerably lower than in medium only (Figure 4.10A). Nevertheless, in two of three patient fluids ("Patient 2" and "Patient 4"), the magnitude of T cell activation by the CD206 TriTE was comparable to that induced by the CD206 BiTE in medium only (Figure 4.10A). Thus, whilst ascites fluids do exert an inhibitory effect on CD206 TriTE-mediated T cell activity, the levels of activation should be sufficient to mediate efficient macrophage killing.

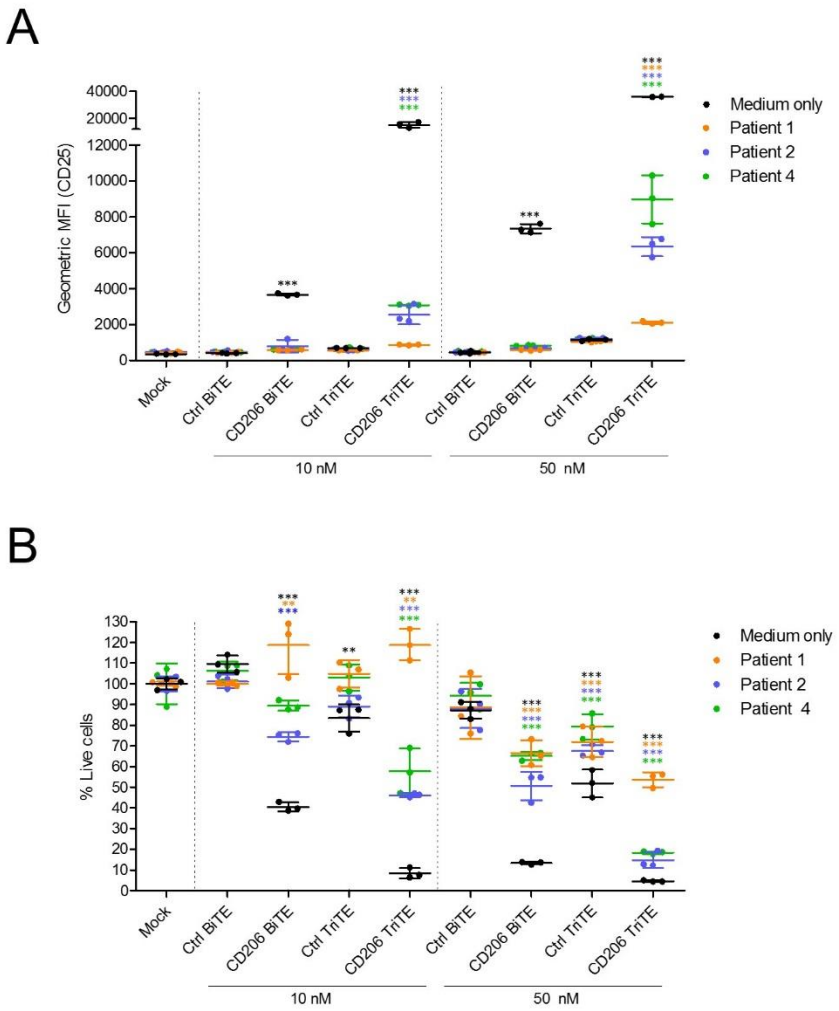

Figure 4.10. A CD206-targeting TriTE with bivalent CD3 binding outperforms the parental BiTE in suppressive malignant ascites fluids. (A, B) IL-4-polarised ($CD206^{high}$) MDMs were treated for 96 h with T cells (10:1 E:T ratio) and BiTEs/TriTEs in medium alone or 50 % ascites fluid (v/v) from three different patients (Patients 1, 2 and 4). **(A)** T cells were analysed for CD25 expression by flow cytometry. **(B)** MDMs were stained with propidium iodide and analysed with a Celigo image cytometer to calculate % live cells. **(A, B)** Data show mean ± SD of biological triplicates. Statistical significance was assessed by two-way ANOVA followed by Bonferroni post-hoc analysis, with each treatment being compared to the relevant "Mock" condition (B,C) (*, $P < 0.05$; **, $P < 0.01$; ***, $P < 0.001$).

Indeed, improved T cell mediated-cytotoxicity towards MDMs by the CD206 TriTE was observed; in the presence of fluids from "Patient 2" and "Patient 4", the CD206 TriTE (at 10 nM) induced a T cell-mediated decline in live MDMs to 46.1% and 57.8%, respectively, compared with 74.4% and 89.4% following treatment with the CD206 BiTE (Figure

4.10B). At 50 nM, the CD206 TriTE outperformed its parental BiTE in all three patient samples tested, reducing the percentage of live MDMs to 53.6%, 14.8% and 18.3% in ascites fluids from "Patient 1", "Patient 2" and "Patient 4", respectively, as compared to 66.4%, 50.6% and 65.1%, respectively, for the CD206 BiTE (Figure 4.10B).

At a dose of 10 nM, the non-specific effects of the Ctrl TriTE were observed only when cells were cultured in the absence of ascites fluid (Figure 4.10B). A significant (albeit modest) decline in percentage live MDMs was observed at 50 nM in all three ascites fluids, however, with a reduction in the percentage of live MDMs by Ctrl TriTE treatment to 72%, 67.6% and 79.3% in fluids from patients 1, 2 and 4 respectively.

Together, these data demonstrate that a CD206 TriTE with bi-valent CD3 binding can overcome the suppressive effects of ascites fluids to a sufficient degree to enable T cell-mediated cytotoxicity of MDMs. Although the presence of two anti-CD3 domains causes a degree of antigen-independent activity, these non-specific effects are reduced in more clinically-relevant settings.

4.4 Chapter conclusions

1. Addition of a third T cell-activating domain to the parental BiTE does not compromise its ability to bind CD206
2. TriTEs containing an anti-CD28 domain trigger target antigen-independent T cell activation and cytotoxicity
3. A CD206-targeting TriTE with bi-valent CD3 binding is selective for $CD206^{high}$ cells at physiologically-relevant effector:target cell ratios
4. The CD206-targeting TriTE outperforms its parental BiTE in malignant ascites fluid

4.5 Chapter discussion

Here, we have developed novel CD206-targeting TriTEs containing two T cell-activating domains. The CD206-targeting TriTEs were successfully expressed and secreted by transfected producer cells (Figure 4.3), and retained their ability to bind CD206 (Figure 4.4). Interestingly, an anti-CD28-containing CD206 TriTE, as well as its matched control TriTE, triggered potent non-specific T cell activation, leading to killing of even target antigen-negative cells (Figures 4.5 and 4.6). By contrast, a CD206 TriTE with two anti-CD3 domains (3-206-3) displayed a degree of target antigen-specificity (Figure 4.6), which was most pronounced at low TriTE concentrations and/or effector:target ratios (Figures 4.7). As hypothesised, the 3-206-3 TriTE outperformed the parental CD206 BiTE in the presence of malignant ascites fluid, providing a useful strategy to improve T cell activation in the face of immunosuppression (Figure 4.10).

To the best of our knowledge, we are the first to engineer a single-chain tri-valent antibody fragment with bi-valent CD3 binding. From an engineering perspective, our approach may be more flexible and straightforward than the TandAb platform, which requires considerable optimisation to prevent pairing of adjacent VH/VL domains (Le Gall et al., 2004a). Indeed, a number of scFvs, such as those derived from OKT3 (anti-CD3) and HD37 (anti-CD19), are not amenable to TandAb generation, preferentially forming monomers or tetramers over dimers (Le Gall et al., 1999; Le Gall et al., 2004b).

The bi-valent CD3-binding CD206 TriTE generated in this study was very potent, with an EC_{50} value almost ten times lower than that of the parental CD206 BiTE (Figure 4.6). Furthermore, the activity of the TriTE was retained even when a low, physiologically-relevant E:T ratio (1:2) was employed (Figure 4.7). The enhanced T cell activation achieved by our bi-valent CD3-binding antibody, and others' (Reusch et al., 2015), may be

advantageous for the treatment of heavily-immunosuppressed solid tumours. Nevertheless, there are concerns regarding possible non-specific T cell activation by these constructs, which may lead to off-target toxicities. In this study, we observed minor T cell activation by the control TriTE, and by the CD206 TriTE in the absence of target cells (Figure 4.5). Although it mostly failed to reach statistical significance, this low-level T cell activation impacted upon the viability of neighbouring MDMs, with a modest decrease in % live MDMs treated with T cells and the control TriTE (Figures 4.6 and 4.9). These non-specific effects were reduced, however, in more clinically-relevant settings (i.e. lower E:T ratios (Figure 4.7) and in the presence of malignant ascites fluid (Figure 4.10)). Other considerations include the possibility of T cell depletion by bi-valent CD3-binding antibodies due to homotypic T cell-T cell interactions (Hoffmann et al., 2005). However, no reduction in % live T cells was observed in dose-response experiments of the CD206 TriTE cultured with T cells alone (Figure 4.9), perhaps due to the relative unlikelihood of a TriTE bridging CD3 molecules on adjacent cells, as opposed to the surface of a single cell.

Unlike super-agonistic anti-CD28 antibodies, such as the now infamous TGN1412 (Suntharalingam et al., 2006), which activate T cells in the absence of TCR occupancy (Beyersdorf et al., 2005), the anti-CD28 scFv selected for our study was derived from an agonistic mAb (clone 9.3) which does not trigger T cell activation alone (Suchard et al., 2013). Furthermore, this mAb (as well as a monomeric fragment from its Fab region) failed to enhance the activation of T cells treated with soluble anti-CD3 antibody, only providing a helper signal to those cultured with immobilised anti-CD3 antibody (Baroja et al., 1989; Suchard et al., 2013). The potent T cell activation induced by our anti-CD28-containing TriTEs in the absence of a target antigen to induce CD3 clustering was therefore unexpected. It is possible that the presence of anti-CD3 and anti-CD28 domains within a

single chain brought these receptors into unusually close proximity, triggering an unknown stimulatory response. Whether or not the aforementioned CEA-CD3-CD28 antibody induced similar non-specific T cell activation was not reported (Wang et al., 2004).

In summary, the bi-valent CD3-binding CD206 TriTE outperformed the parental BiTE in suppressive malignant ascites fluid and, unlike the CD28-containing TriTEs, retained a degree of target antigen-selectivity. In the remaining chapters, the bi-valent CD3-binding CD206 TriTE (hereafter referred to as simply "CD206 TriTE") is evaluated alongside the CD206 and FRβ-targeting BiTEs.

5 Assessing the Activity of TAM-Targeting T cell Engagers in *Ex Vivo* Tumour Models

5.1 Introduction

The translational success of cancer therapies is expedited by the use of clinically-relevant *ex vivo* models. Malignant ascites recapitulates many features of the TME, making it an informative model for the pre-clinical evaluation of novel therapeutics. In this chapter, we assessed the activity of the TAM-targeting T cell engagers against whole human malignant ascites samples.

An accumulation of fluid in the peritoneum due to cancer, malignant ascites comprises a mixture of tumour cells, non-cancerous cells and soluble factors. Together, these form a complex microenvironment that fosters tumour growth, spread and immune evasion, as well as promoting resistance to chemotherapy (reviewed in (Ahmed and Stenvers, 2013)). The most common malignancies associated with the development of ascites are ovarian, breast, gastrointestinal and lung cancers. The presence of malignant ascites is associated with grave prognosis and significant morbidity, causing abdominal pain, anorexia, nausea, vomiting and respiratory issues (Sangisetty and Miner, 2012).

To alleviate symptoms, patients are regularly drained of excessive fluid by paracentesis. Ascites collected in this manner can be up to several litres in volume and would otherwise be discarded, making it a readily-available source of valuable material for study. Primary neoplastic cells isolated from ascites, which may exist as single cells or aggregates, can be propagated *in vitro*, acting as a model system that more faithfully resembles the patient situation than immortalised cell lines (Dunfield et al., 2002; Golan et al., 2014). Ascites also contains a range of non-cancerous cells such as CAFs, mesenchymal stem cells,

MDSCs, macrophages and T cells, which together influence tumour cell behaviour and response to therapy (Ahmed and Stenvers, 2013). Meanwhile, the acellular fraction of malignant ascites is rich in immunomodulatory chemokines and cytokines such as IL-6, IL-8 and IL-10 (Matte et al., 2012), as well as pro-survival factors, pro-angiogenic factors and ECM fragments.

Mounting evidence suggests that malignant ascites represents a site of substantial immune suppression. For example, acellular ascites fluid from ovarian cancer patients was found to inhibit the activation of T cells stimulated via TCR signalling, decreasing their proliferation and production of IFN-γ (Simpson-Abelson et al., 2013). Among ascites-associated lymphocytes (which may originate from the circulation or directly from the tumour), Tregs are found at increased frequencies, relative to healthy donor- and patient-derived PBMCs (Idorn et al., 2018; Landskron et al., 2015). Tregs in these samples also expressed higher levels of FoxP3 than those isolated from PBMCs, suggestive of an immune-suppressive T cell phenotype akin to those observed in solid tumours (Idorn et al., 2018). Meanwhile, although they do not necessarily derive from tumours, ascites-associated macrophages display a TAM-like phenotype, characterised by high expression of CD163 and immunomodulatory cytokines (e.g. IL-6, IL-10, leukaemia inhibitory factor) (Reinartz et al., 2014).

Together, these properties make malignant ascites a particularly valuable model for the evaluation of our TAM-targeting T cell engagers, containing all the relevant cell types in the context of an immunosuppressed microenvironment. In this chapter, we evaluated the ability of the TAM-targeting T cell engagers to activate endogenous ascites T cells to kill ascites-associated macrophages, as well as assessing the phenotypes of the remaining macrophages.

5.2 Chapter Aims

1. Characterise the cell sub-populations present within selected human malignant ascites samples.
2. Assess the activation and proliferation of endogenous ascites T cells in response to TAM-targeting T cell engagers.
3. Evaluate cytotoxicity of ascites-associated macrophages after treatment with the TAM-targeting T cell engagers.
4. Determine the phenotypes of ascites-associated macrophages remaining after BiTE/TriTE treatment.

5.3 Results

5.3.1 Processing and characterisation of human malignant ascites

Malignant ascites samples were acquired from the Churchill Hospital, Oxford, UK, following routine drainage of patients with advanced metastatic cancer (patient details summarised in Table 5.1), and after informed consent and ethical approval. Ascites cells were separated from the fluid fraction by centrifugation, then subjected to red blood cell lysis. Characterisation of the cell types present within each sample was performed by flow cytometry, staining with antibodies recognising T cells (via CD4 and CD8), tumour cells (via EpCAM), fibroblasts (via FAP) and myeloid cells (via CD11b) (gating strategy in Figure 5.1). The compositions of the samples used in this study are summarised in Table 5.2.

Table 5.1. Patient details for the malignant ascites samples used in this study. A list of patient indications and date of receipt of malignant ascites samples is displayed.

Sample ID	Cancer type	Date received
Patient 1	Ovarian	27/11/2015
Patient 2	Ovarian	24/01/2017
Patient 3	Ovarian	24/01/2017
Patient 4	Ovarian	30/03/2017
Patient 5	Melanoma	30/11/2017
Patient 6	Oesophageal	20/04/2018
Patient 7	Ovarian	14/05/2018
Patient 8	Pancreatic	12/07/2018
Patient 9	Pancreatic	30/08/2018
Patient 10	Breast	13/09/2018
Patient 11	Peritoneal	20/09/2018
Patient 12	Breast	01/11/2018
Patient 13	Serous tubal	05/11/2018
Patient 14	Unknown	28/11/2018
Patient 15	Ovarian	07/02/2019

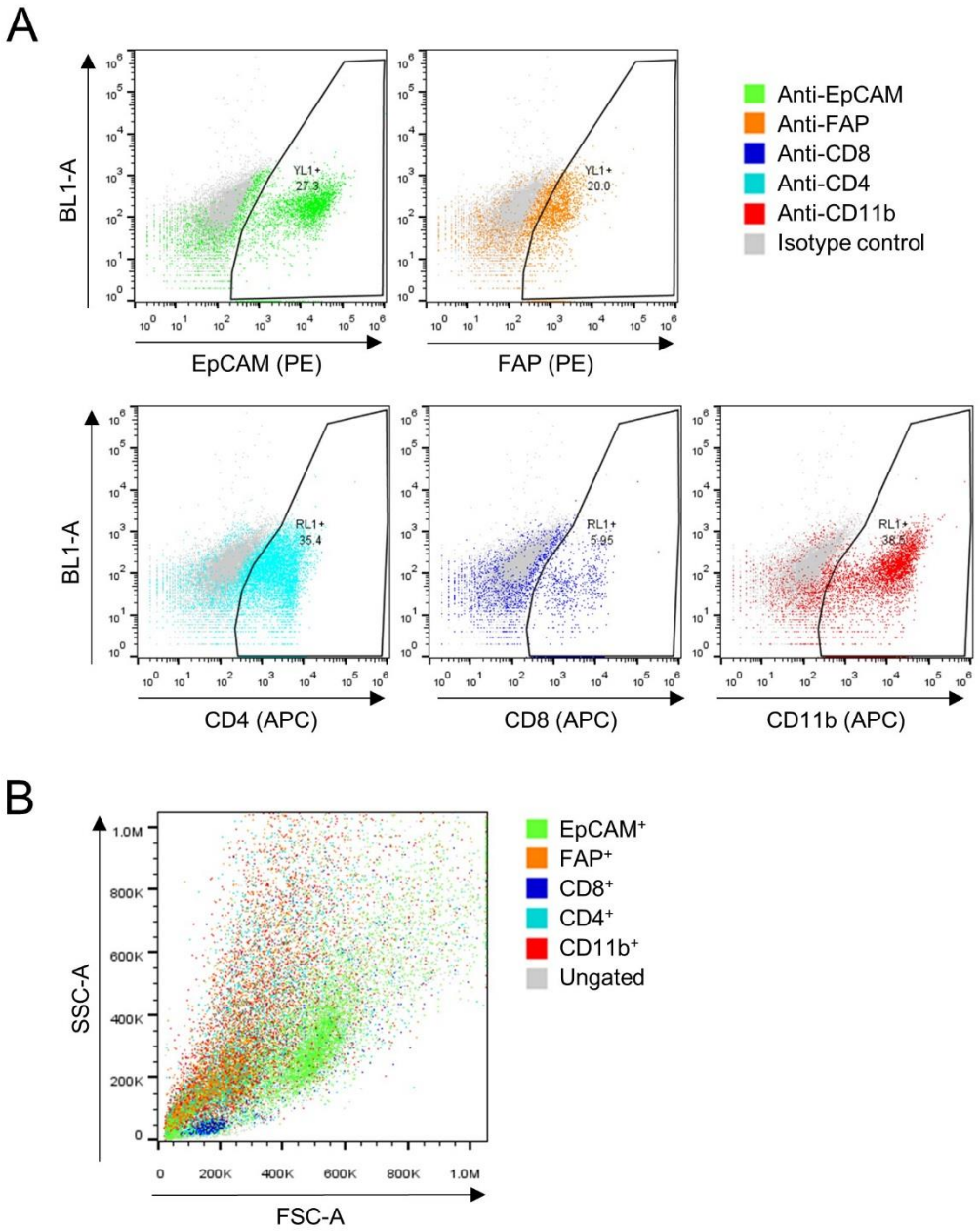

Figure 5.1. Representative gating strategies to determine the cellular composition of malignant ascites samples. Malignant ascites cells were processed for flow cytometry, staining with anti-CD4, anti-CD8, anti-EpCAM, anti-FAP, anti-PD-L1 and anti-CD11b antibodies, or relevant isotype controls. **(A)** Representative gating to determine positivity for the indicated markers is displayed. Background was excluded by plotting fluorescence against an unused channel (BL1). **(B)** Representative FSC/SSC dot plot after gating for the indicated cell populations.

Ascites samples contained variable proportions of tumour cells, ranging from undetectable levels ("Patient 2") to nearly half of the cellular fraction of the sample (48.8%, "Patient 11") (Table 5.2). Cells positive for FAP, representing CAFs, were also detected, albeit at lower levels (mostly < 10% of the total cellular population). T cells were present in all samples tested, with an elevated ratio of $CD4^+$ to $CD8^+$ cells (> 2.2, identified as a poor prognostic indicator in ovarian cancer) observed in six patient samples (CD4:CD8 ratios ranging from 2.94 to 5.95). Ascites samples also contained significant numbers of $CD11b^+$ cells, denoting cells of the myeloid lineage (monocytes, macrophages, MDSCs, granulocytes or DCs) or subsets of NK cells and T lymphocytes. Lastly, expression of the T cell-inhibitory molecule PD-L1 was detected in all malignant ascites samples tested, with $PD\text{-}L1^+$ cells representing up to 39.2 % of the total ascites cell numbers ("Patient 10").

Table 5.2. Cellular composition of the malignant ascites samples used in this study. Whole ascites cells were characterised by flow cytometry. The three ascites samples used in Chapters 5 and 6 are indicated with asterisks. N/D, not determined.

Sample ID	Proportion of total cells in biopsy (%)							CD4:CD8 ratio
	CD3	CD4	CD8	EpCAM	FAP	PD-L1	CD11b	
Patient 2	27.3	14.9	11.0	0	0	N/D	33.0	1.35
Patient 3	53.2	18.4	37.4	2.9	0	N/D	33.2	0.49
Patient 4	N/D	8.12	1.77	16.2	0.31	7.19	7.09	4.59
Patient 5	14.5	N/D	N/D	1.73	19	N/D	5.77	N/D
Patient 6	N/D	11.8	15.9	38.6	3.12	N/D	14.0	0.74
Patient 7	38.7	N/D	N/D	29.3	3.03	32.3	18.8	N/D
Patient 8	N/D	25.3	50.2	3.47	5.51	N/D	18.7	0.50
Patient 9	N/D	44.7	10.2	3.2	0.69	12.6	12.4	4.38
* Patient 10	N/D	35.4	5.95	32.1	29.1	39.2	38.5	5.95
Patient 11	N/D	14.1	12.0	48.8	14.8	29.7	21.0	1.18
Patient 12	N/D	30.1	7.90	4.80	0.77	N/D	36.4	3.81
Patient 13	N/D	24.5	31.7	1.10	6.00	N/D	26.9	0.77
* Patient 14	N/D	30.9	10.5	11.5	1.80	N/D	38.6	2.94
* Patient 15	N/D	30.2	9.04	22.6	2.41	24.6	43.2	3.34

The malignant ascites samples collected in this study thus represent rich sources of tumour-like material, containing several of the key cell types observed in solid tumours. Malignant ascites samples will be utilised throughout the next two chapters as *ex vivo* models with which to assess BiTE activity.

5.3.2 Further characterisation of three selected malignant ascites samples

Three malignant ascites samples (from "Patient 10", "Patient 14" and "Patient 15") were selected for more detailed characterisation and study. Samples were chosen based on their high levels of $CD11b^+$ cells (38.5%, 38.6% and 43.2% for Patients 10, 14 and 15, respectively), indicating that they contained a significant population of ascites-associated macrophages.

The $CD11b^+$ fraction of the three malignant ascites samples was first assessed by co-staining cells with anti-CD11b, -CD64, -CD206 and –FRβ antibodies, followed by flow cytometric analysis. Ascites macrophages, identified as being CD11b/CD64 dual-positive, were mostly positive for FRβ (94.2%, 98.1% and 65.1 % for patient samples 10, 14 and 15, respectively), whilst a smaller fraction were CD206-positive (58.6%, 64.6% and 56.5% for patient samples 10, 14 and 15, respectively, Figure 5.2). Absolute expression levels (represented as geometric MFI values) of CD206 and FRβ on ascites macrophages were elevated relative to IFN-γ/LPS-polarised MDMs from healthy donors, indicating that they may resemble a population of M2-like macrophages. Although a direct comparison between expression levels with flow cytometry is challenging due to possible differences in antibody affinities, levels of FRβ appeared significantly higher on the ascites macrophages than CD206; indeed, whilst FRβ expression was greater than unpolarised MDMs for all ascites samples, CD206 expression was only elevated above unpolarised MDMs in 2/3 ascites samples.

A

Sample ID	Proportion of total cells (%)				Proportion of $CD11b^+CD64^+$ cells (%)	
	$CD11b^+$	$CD11b^+CD64^+$	$CD206^+$	$FR\beta^+$	$CD206^+$	$FR\beta^+$
Patient 10	38.5	35.0	22.0	39.9	58.6	94.2
Patient 14	38.6	26.5	26.8	46.6	64.6	98.1
Patient 15	43.2	16.9	18.2	19.2	56.5	65.1

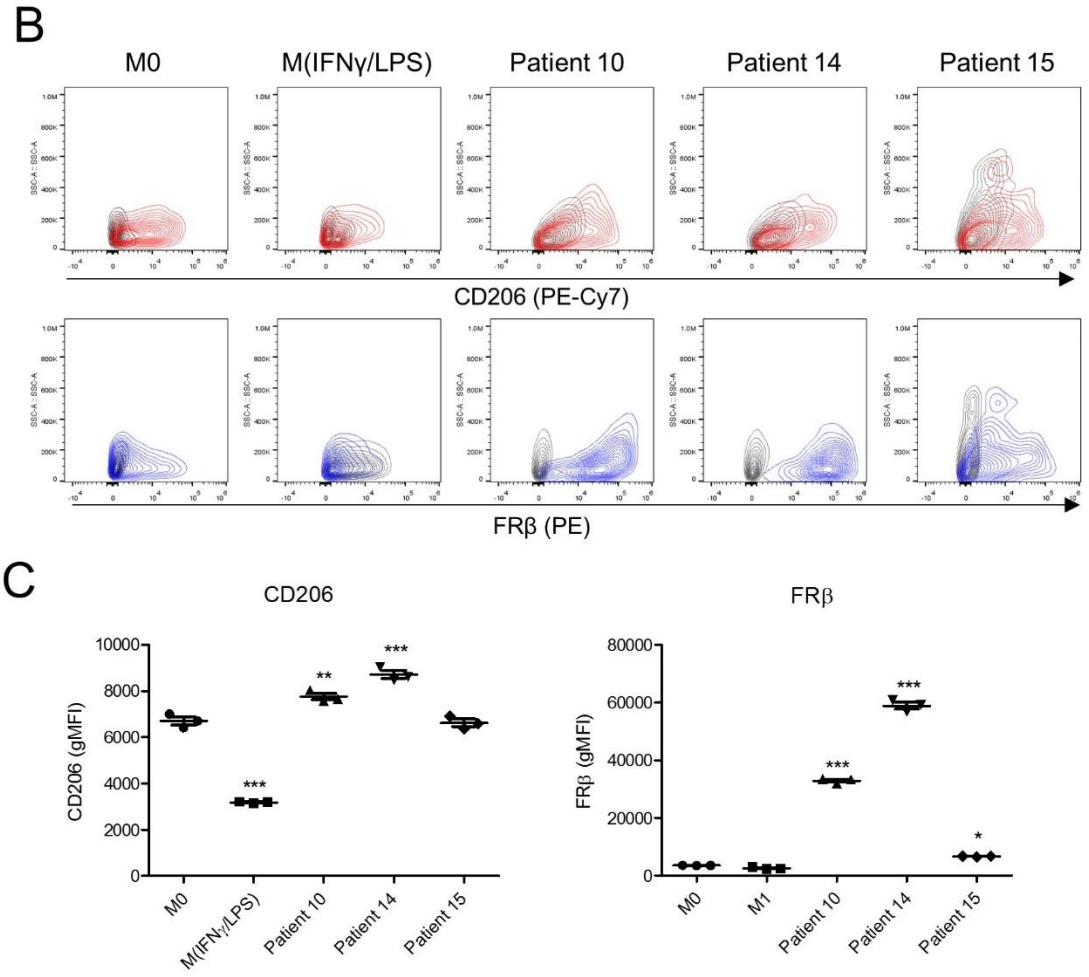

Figure 5.2. Cellular composition of the malignant ascites samples used in Chapters 5 and 6. Malignant ascites cells from the three patient samples were co-stained with anti-CD11b, anti-CD64, anti-CD206 and anti-FRβ antibodies. Unpolarised (M0) and IFN-γ/LPS-polarised (M1) MDMs from healthy peripheral blood were antibody-stained in parallel. Representative histograms of CD206 and FRβ expression on macrophages (identified as being $CD11b^+CD64^+$) are shown in **(B)**, with geometric mean fluorescence values (gMFI) values displayed in **(C)**. **(C)** Data show mean ± SD of biological triplicates. Statistical analysis was performed by one-way ANOVA with Dunnett's post-hoc analysis compared with "M(IFN-γ/LPS)" (*, $P < 0.05$; **, $P < 0.01$; ***, $P < 0.001$).

T cells within the three malignant ascites samples were then analysed for expression of co-inhibitory molecules PD-1, LAG-3 and TIM-3, all of which represent markers of T cell exhaustion. As shown in Figure 5.3, the proportion of PD-1$^+$ and TIM-3$^+$ cells within CD4$^+$ and CD8$^+$ ascites cell populations mostly exceeded that of healthy peripheral blood lymphocytes (PBLs). An enriched population of LAG-3$^+$ T cells was also observed within CD4$^+$ cells in two of three, and within CD8$^+$ cells in one of three ascites samples (Figure 5.3).

Together, these data support the use of the selected malignant ascites samples for assessment of TAM-targeting BiTE/TriTE activity.

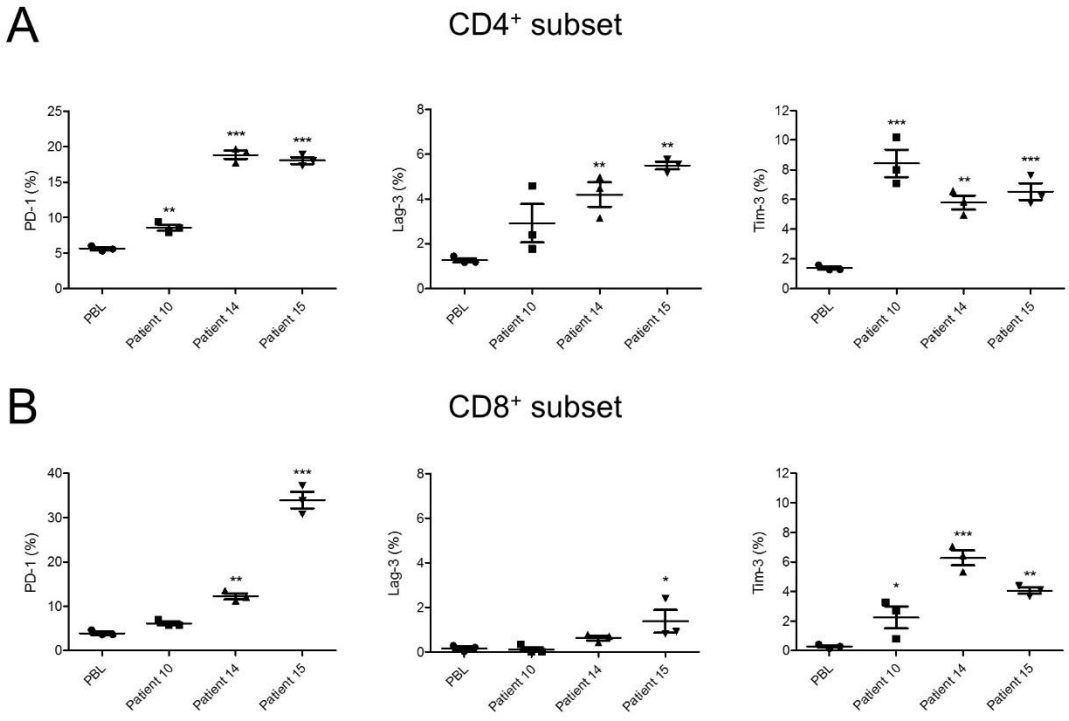

Figure 5.3. Characterisation of T cells present within the malignant ascites samples used in Chapters 5 and 6. (A, B) Ascites cells from three cancer patients (Patients 10, 14 and 15) were processed for flow cytometric analysis, staining with anti-CD4, anti-CD8, anti-PD-1, anti-Lag-3 and anti-Tim-3 antibodies. Healthy human peripheral blood lymphocytes (PBL) were antibody-stained and analysed in parallel. Data concerning the CD4$^+$ and CD8$^+$ cell subsets is depicted in **(A)** and **(B)**, respectively. Data show mean ± SD of biological triplicates. Statistical analysis was performed by one-way ANOVA with Dunnett's post-hoc analysis compared with "PBL" (*, $P < 0.05$; **, $P < 0.01$; ***, $P < 0.001$).

5.3.3 Activation of endogenous T cells in human malignant ascites by the FRβ BiTEs and CD206 BiTE/TriTE

To assess the T cell-activating capabilities of the BiTEs/TriTEs, unpurified ascites cells from the three selected patient samples were seeded in 96-well plates and treated with the BiTEs/TriTEs in the presence or absence of ascites fluid (50% v/v). Five days later, cells were harvested and processed for flow cytometry, staining with antibodies recognising CD4, CD8 and CD25. Due to variation in the levels of CD25 expression by activated T cells between different patient samples, percentage positivity for CD25 (as opposed to CD25 geometric MFI) was used when considering all three patients collectively. Individual patient data is displayed as geometric MFI values for CD25 expression.

Robust activation of endogenous $CD4^+$ and $CD8^+$ T cells was observed for all three patient samples upon treatment with the FRβ-targeting BiTEs (Figure 5.4). In the presence of ascites fluid, an average of 76.7% and 91.0% of $CD4^+$ cells were CD25-positive after treatment with the FR3 and 3FR BiTEs, respectively, whilst 52.2% and 75.7% of $CD8^+$ cells were CD25-positive. As shown in Figure 5.5, the magnitude of T cell activation by the FRβ-targeting BiTEs varied between patient samples and T cell subsets, with the greatest CD25 geometric MFI values observed in the $CD4^+$ population from "Patient 10" (up to 48.8-fold increase relative to mock-treated cells (3FR BiTE treatment in the absence of ascites fluid)). T cell activation was also influenced by FRβ BiTE orientation; consistent with its superior potency in healthy PBMC-based models, the 3FR BiTE outperformed the FR3 BiTE across all patient samples, triggering 23.5- and 107-fold average increases in the CD25 geometric MFI values of $CD4^+$ cells and $CD8^+$ cells, respectively, in the presence of autologous ascites fluid, versus 11.6- and 56.3-fold increases after FR3 BiTE treatment. Ascites fluid exerted an inhibitory effect upon FRβ-targeting BiTE-mediated T cell

activation. This was most pronounced for the $CD4^+$ subset, for which the fold-increase in CD25 expression after FR3 and 3FR BiTE treatment was reduced by 67.1% and 59.6%, respectively, when cells were cultured in ascites fluid, as compared to medium only. For the $CD8^+$ subset, the inclusion of ascites fluid caused 32% and 14% decrease in T cell activation by the FR3 and 3FR BiTEs, respectively. No significant activation of T cells was observed after treatment with the control BiTEs in any patient sample tested (Figures 5.4 and 5.5).

T cell activation by the CD206-targeting T cell engagers was more variable. Significant activation of $CD4^+$ and $CD8^+$ T cell subsets by the CD206 BiTE was observed in only one of three patient samples ("Patient 10", Figure 5.5). When considering all three patient samples collectively, no significant increases in the percentages of CD25-positive $CD4^+$ or $CD8^+$ T cells were observed following treatment with the CD206 BiTE (Figure 5.4). The CD206 TriTE elicited significant increases in $CD4^+$ and $CD8^+$ T cell activation, both when considering overall % CD25 positivity across all three samples (Figure 5.4), and individual patient sample geometric MFI values (Figure 5.5). T cell activation by the Ctrl TriTE was also observed, albeit at levels that were mostly significantly lower than that induced by the CD206 TriTE (for Patients 10 and 14, $p<0.001$ when comparing Ctrl and CD206 TriTE activation of both $CD4^+$ and $CD8^+$ T cells in the presence or absence of ascites fluids; for Patient 15, there was a significant increase in activation by the CD206 TriTE of $CD8^+$ but not $CD4^+$ T cells in the presence and absence of ascites fluid).

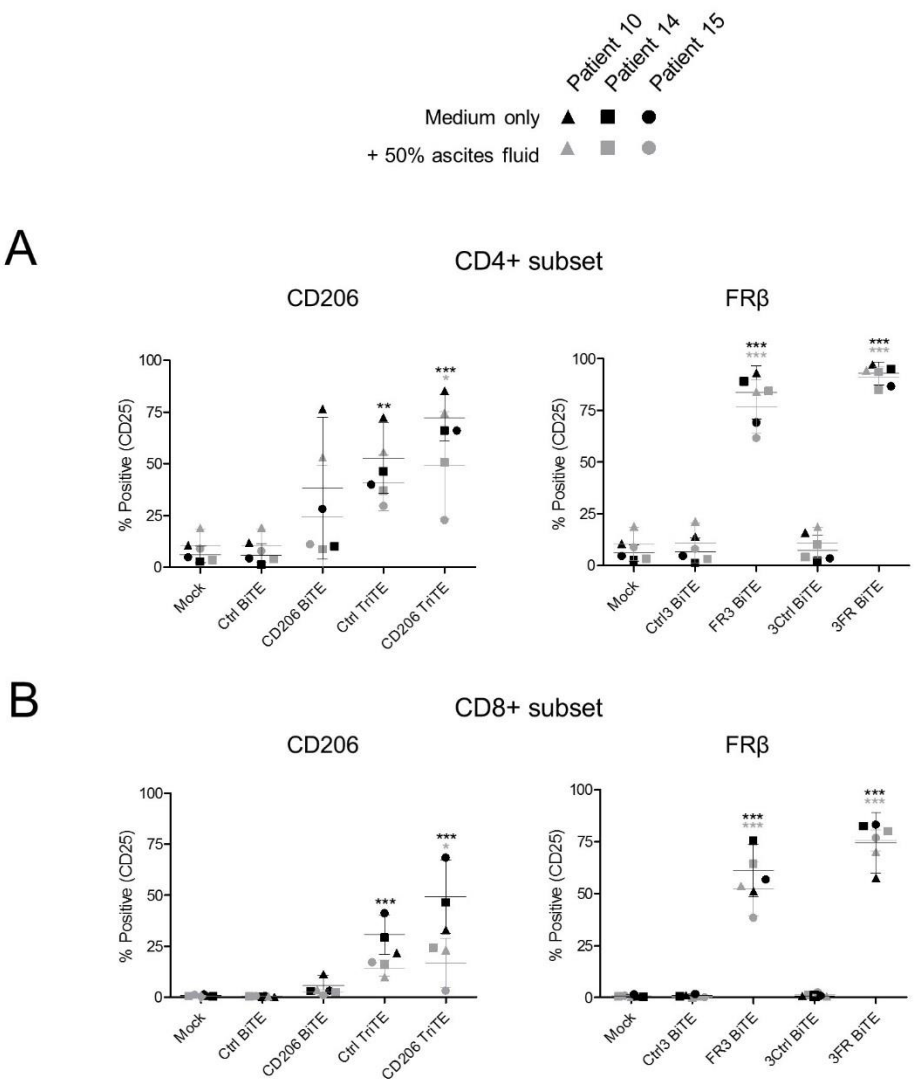

Figure 5.4. Macrophage-targeting T cell engagers activate CD4$^+$ and CD8$^+$ endogenous human ascites T cells. Total unpurified ascites cells from three different cancer patients (Patients 10, 14 and 15) were cultured for five days with 50 nM BiTEs/TriTEs in medium only or 50 % ascites fluid (v/v) from the same patient sample. Activation of endogenous CD4$^+$ and CD8$^+$ ascites T cells was assessed by flow cytometric measurement of CD25 expression after gating for CD4 **(A)** or CD8 **(B)** positivity. Data show the grand mean ± SD of three individual patient means (each calculated from biological triplicate). **(A, B)** Statistical significance was assessed by two-way ANOVA followed by Bonferroni post-hoc analysis, with each treatment being compared to the relevant "Mock" condition (*, $P < 0.05$; **, $P < 0.01$; ***, $P < 0.001$).

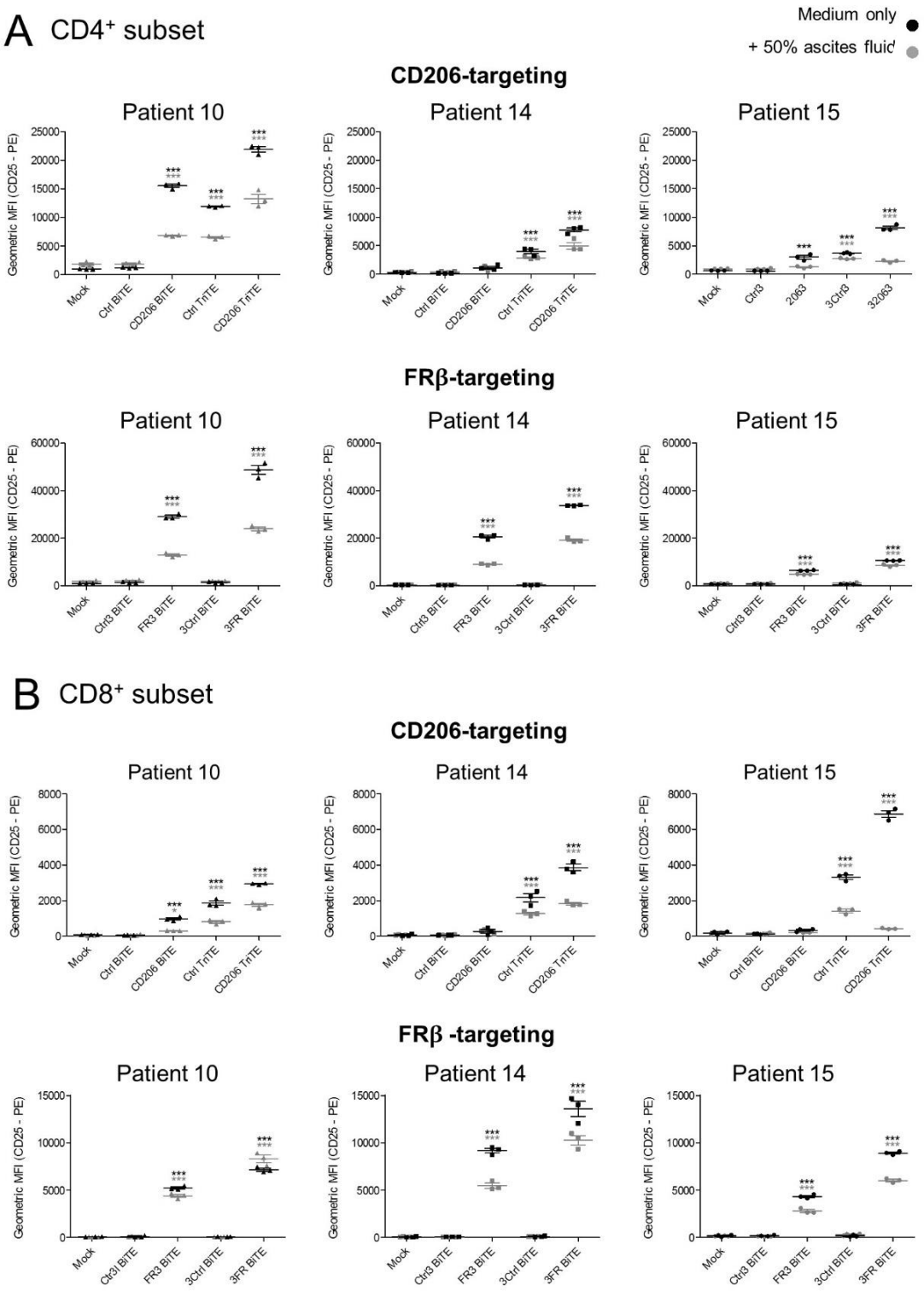

Figure 5.5. Geometric MFI values of individual patients. Total unpurified ascites cells from three different cancer patients (Patients 10, 14 and 15) were cultured for five days with 50 nM BiTEs/TriTEs in medium only or 50 % ascites fluid (v/v) from the same patient sample. Activation of endogenous $CD4^+$ and $CD8^+$ ascites T cells was assessed by flow cytometric measurement of CD25 expression after gating for CD4 **(A)** or CD8 **(B)** positivity. Data show the grand mean ± SD of three individual patient means (each calculated from biological triplicate). **(A, B)** Statistical significance was assessed by two-way ANOVA followed by Bonferroni post-hoc analysis, with each treatment comparing to the relevant "Mock" (*, $P < 0.05$; **, $P < 0.01$; ***, $P < 0.001$).

Supporting these findings, increased quantities of soluble IFN-γ were observed in the culture supernatants of all patient samples treated with the FRβ-targeting BiTEs, but not the CD206 BiTE (Figure 5.6). Indeed, in the presence of ascites fluid, the average levels of IFN-γ after treatment with the FR3 and 3FR BiTEs were 2147 pg/mL and 3761 pg/mL, respectively (Figure 5.6). By contrast, treatment with the CD206 TriTE triggered a significant rise (when compared to either untreated or Ctrl TriTE-treated samples) in soluble IFN-γ levels (to 1452 pg/mL) only when cells were cultured in medium alone (Figure 5.6). None of the relevant control T cell engagers elicited significant IFN-γ secretion (Figure 5.6).

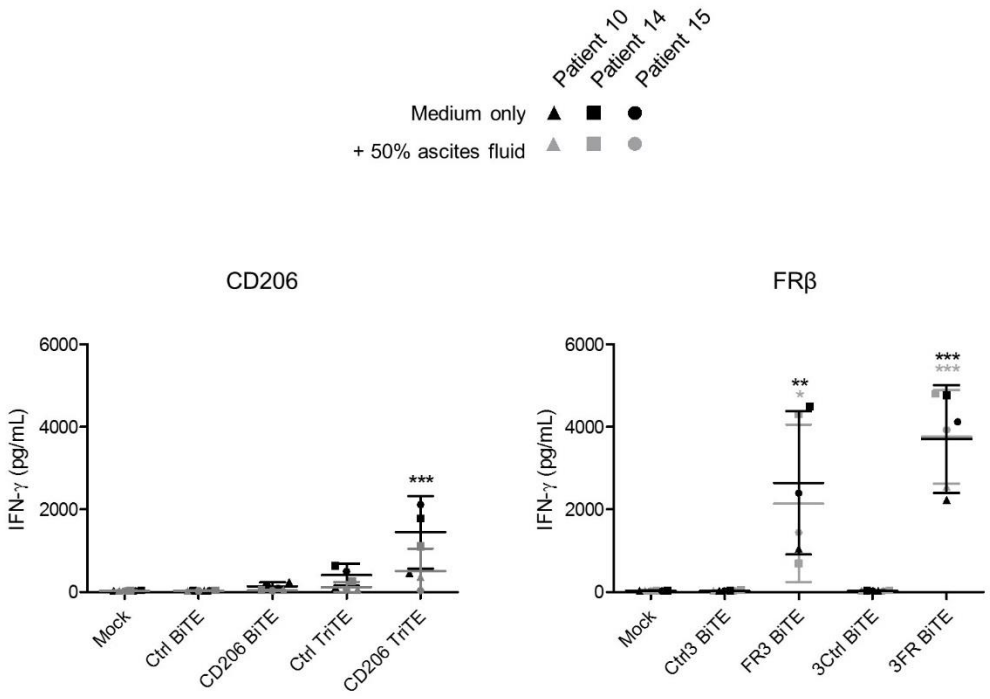

Figure 5.6. IFN-γ is detected in the cell supernatants of malignant ascites following treatment with macrophage-targeting T cell engagers. Total unpurified ascites cells from three different cancer patients (Patients 10, 14 and 15) were cultured for five days with 50 nM BiTEs/TriTEs in medium only or 50 % ascites fluid (v/v) from the same patient sample. IFN-γ in the culture supernatants was quantified by enzyme-linked immunosorbent assay. Data show the grand mean ± SD of three individual patient means (each calculated from biological triplicate). Statistical significance was assessed by two-way ANOVA followed by Bonferroni post-hoc analysis, with each treatment being compared to the relevant "Mock" condition (*, $P < 0.05$; **, $P < 0.01$; ***, $P < 0.001$).

5.3.4 The FRβ-targeting BiTEs trigger expansion of endogenous CD4+ and CD8+ ascites T cells

In addition to the expression of activation markers and secretion of cytokines, another important consequence of T cell activation (including by BiTEs) is the induction of T cell proliferation. To determine whether the TAM-targeting T cell engagers are capable of triggering endogenous ascites T cell proliferation in malignant ascites models, the three patient ascites samples were treated with the BiTEs/TriTEs for five days in the presence or absence of autologous ascites fluid (50% v/v). Cells were then harvested and processed for flow cytometry, as above. To facilitate determination of absolute cell counts, counting beads were added immediately prior to antibody staining.

As shown in Figure 5.7, the FRβ-targeting BiTEs triggered robust increases in the numbers of $CD4^+$ and $CD8^+$ T cell in all ascites samples tested. In the presence of ascites fluid, the average fold-increases in $CD4^+$ cell count were 16.5 and 22.3 for the FR3 and 3FR BiTEs, respectively, whilst the average fold-increases in $CD8^+$ cell count were 11.3 and 18.8 (Figure 5.7), respectively. No significant T cell activation or expansion was observed after treatment with the matched control BiTEs (Figure 5.7). Representative flow cytometric dot plots showing activation and expansion of $CD4^+$ and $CD8^+$ T cell populations after treatment with the 3FR BiTE are displayed in Figure 5.8. The finding of T cell expansion after FRβ-targeting BiTE treatment was further supported by the observation of increased numbers of small, round cells (indicating T cells), and cell clusters (indicating activated/proliferating T cells) by brightfield microscopy (Figure 5.9).

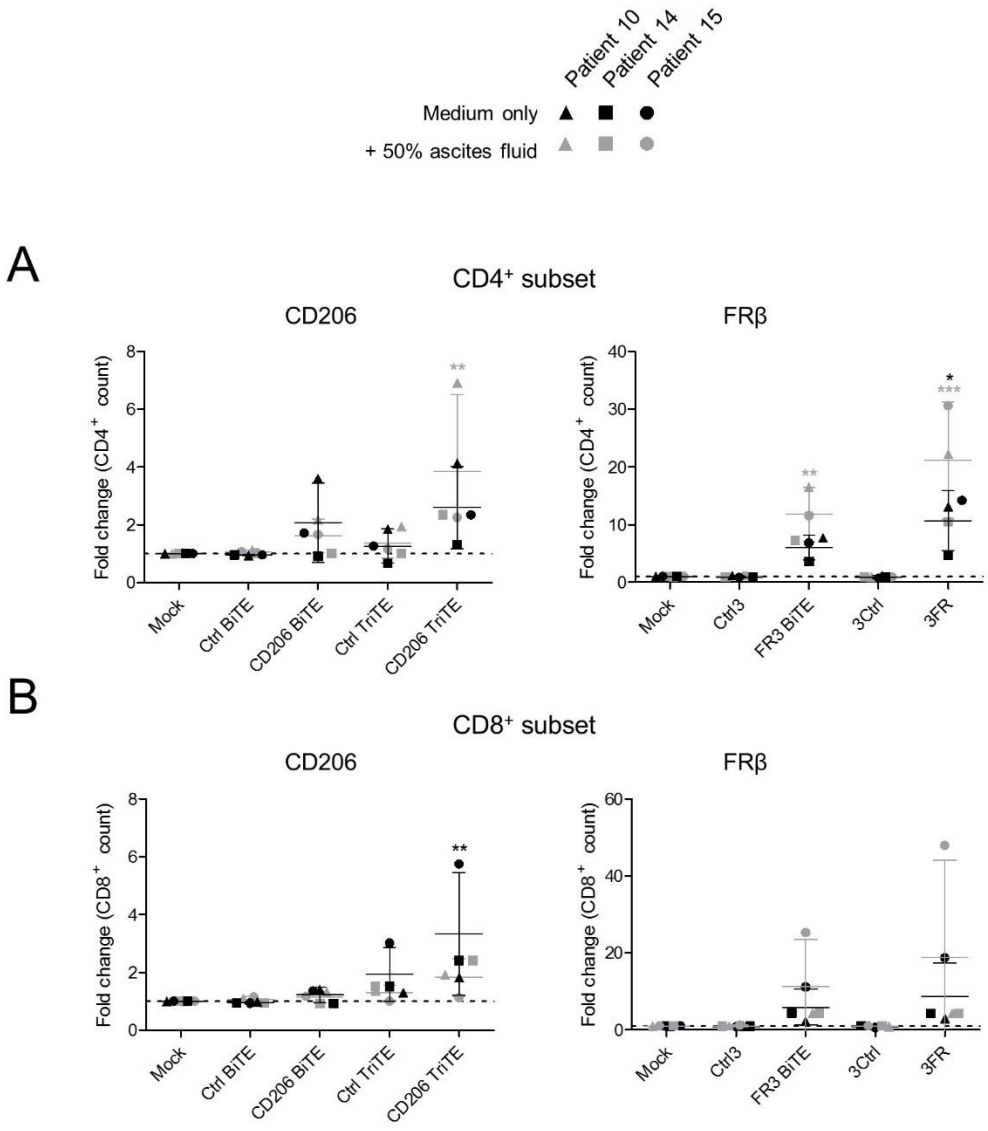

Figure 5.7. Treatment with the CD206-targeting TriTE and FRβ-targeting BiTEs triggers an increase endogenous ascites T cell numbers. Total unpurified ascites cells from three different cancer patients (Patients 10, 14 and 15) were cultured with 50 nM BiTEs/TriTEs in medium only or 50 % ascites fluid (v/v) from the same patient sample. Five days later, cells were harvested and processed for flow cytometry, staining with anti-CD4 and anti-CD8 antibodies, as well as a live/dead stain. Counting beads were added prior to antibody staining to determine absolute cell counts. Fold-changes in $CD4^+$ and $CD8^+$ cell counts were calculated relative to mock-treated samples, and are displayed in **(A)** and **(B)**, respectively. **(A, B)** Data show the grand mean ± SD of three individual patient means (each calculated from biological triplicate). Statistical significance was assessed by two-way ANOVA followed by Bonferroni post-hoc analysis, with each treatment being compared to the relevant "Mock" condition (*, $P < 0.05$; **, $P < 0.01$; ***, $P < 0.001$).

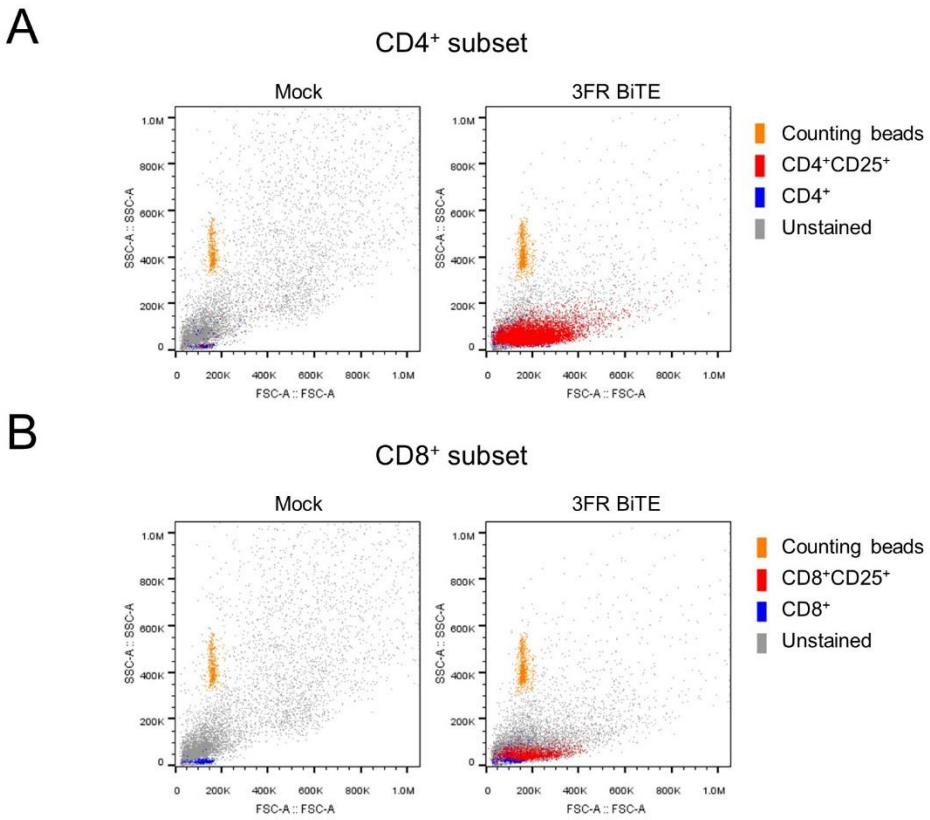

Figure 5.8. Representative flow cytometric dot plots showing activation and proliferation of endogenous ascites T cells induced by a FRβ-targeting BiTE. Whole ascites cells were treated with 50 nM BiTEs for five days, then stained with anti-CD4, anti-CD8 and anti-CD25 antibodies and analysed by flow cytometry. Counting beads (indicated in orange) were added prior to antibody staining to account for cell loss during flow cytometric processing, and thereby facilitate accurate determination of cell counts. Representative dot plots from one patient sample (Patient 10; cultured in the presence of autologous ascites fluid (50% v/v)) are displayed.

In line with its inability to trigger CD25 expression by ascites T cells, the CD206 BiTE did not elicit significant expansion of either $CD4^+$ or $CD8^+$ ascites cells populations (Figure 5.7). Expansion of $CD4^+$ and $CD8^+$ T cells was observed after treatment with the CD206 TriTE, however, albeit at far lower levels than that triggered by the FRβ-targeting BiTEs (3.8- and 1.8-fold for $CD4^+$ and $CD8^+$ T cell populations, respectively, in the presence of ascites fluid, Figure 5.7 and 5.9). No significant T cell expansion was induced by the control TriTE or nanobody-based control BiTE (Figure 5.7 and 5.9).

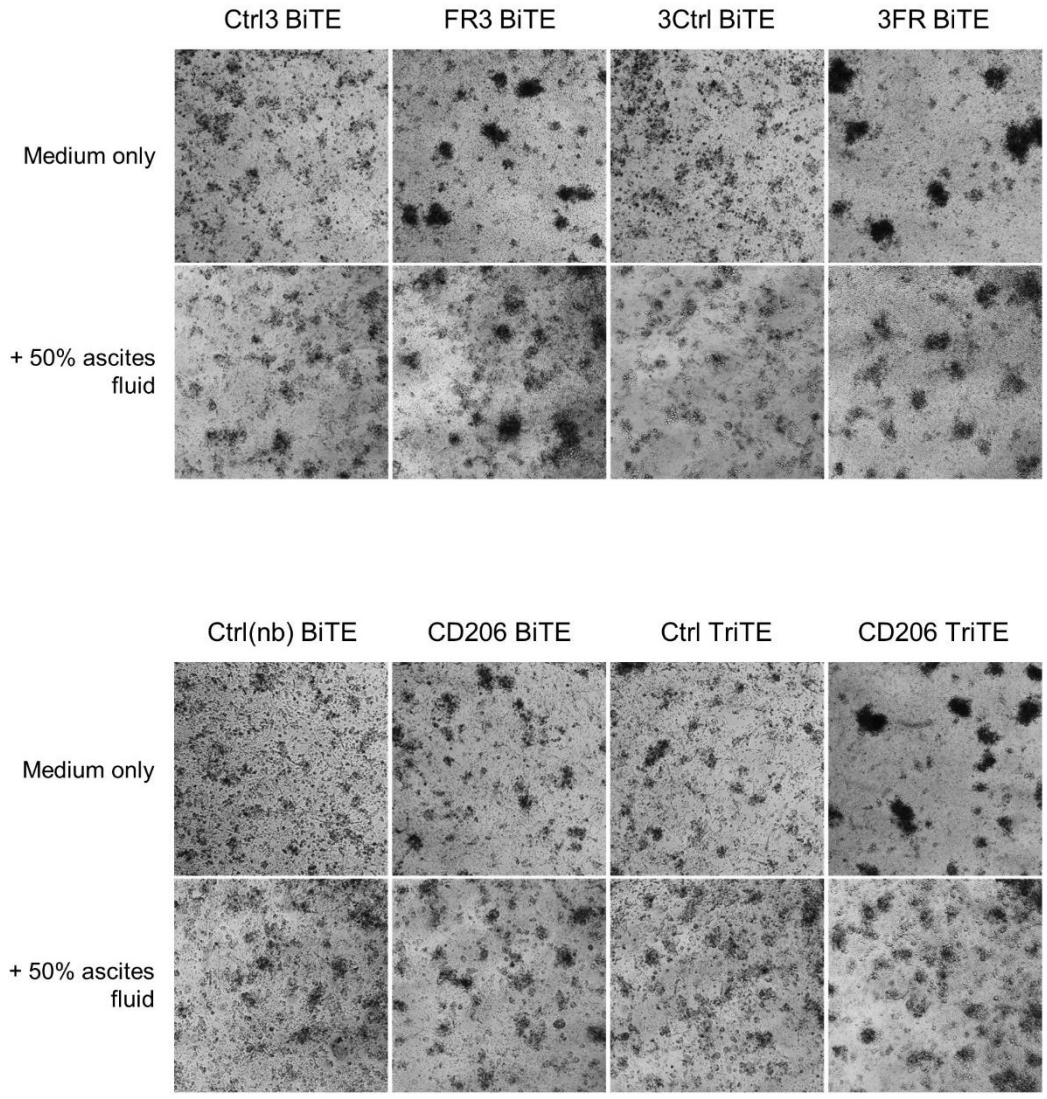

Figure 5.9. Representative brightfield microscopy images showing proliferation of endogenous ascites T cells after treatment with the CD206- and FRβ-targeting T cell engagers. Whole ascites cells were treated with 50 nM of the indicated BiTEs/TriTEs in the presence or absence of autologous ascites fluid. After five days, cells were imaged by brightfield microscopy with a Zeiss Axiovert 25 microscope. Representative images from one patient sample (Patient 10) are displayed.

Interestingly, despite exerting a suppressive effect on CD25 expression, the presence of ascites fluid appeared to enhance the proliferation of T cells, with fold-increases in $CD4^+$ and $CD8^+$ T cell numbers in the presence of ascites fluid roughly double that in its absence (e.g. after 3FR BiTE treatment, $CD4^+$ and $CD8^+$ T cell numbers increased 10.6- and 8.6-fold, respectively, in medium only, versus 21.1- and 18.8-fold in the presence of ascites fluid) (Figure 5.9).

We next sought to determine whether ascites T cell activation by the TAM-targeting T cell engagers would correspond with cytotoxic activity towards endogenous ascites macrophages. As above, the BiTEs/TriTEs were added to whole, unpurified malignant ascites cells from the three patient samples indicated, in the presence or absence of autologous ascites fluid (50% v/v). Five days later, cells were harvested and assessed by flow cytometry for macrophage killing.

As shown in Figure 5.10, T cell activation by the FRβ-targeting BiTEs lead to a marked reduction in the number of ascites macrophages. When cultured in medium alone, the % residual $CD11b^+CD64^+$ cells decreased to an average of 22.6% and 17.4% for the FR3 and 3FR BiTE treatments, respectively. Macrophage killing was decreased slightly in the presence of ascites fluid, giving an average % residual $CD11b^+CD64^+$ cells of 42.0% and 26.9% for the FR3 and 3FR BiTE treatments, respectively (Figure 5.10A). Representative flow cytometric dot plots showing depletion of $CD11b^+CD64^+$ cells after treatment with the 3FR BiTE are shown in Figure 5.10B.

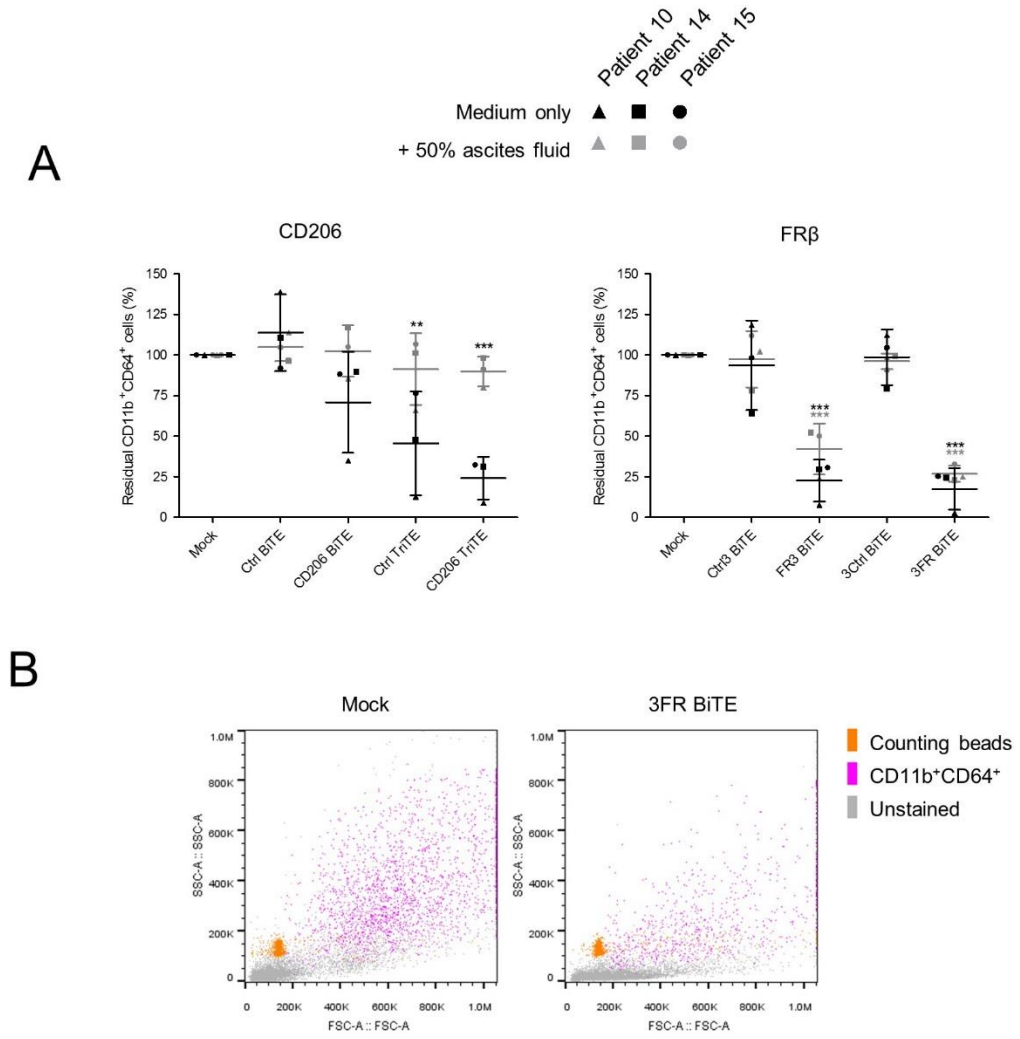

Figure 5.10. Macrophage-targeting T cell engagers trigger depletion of endogenous ascites macrophages. Whole ascites cells from three different patients (Patients 10, 14 and 15) were treated with the indicated BiTEs/TriTEs (50 nM) in the presence or absence of autologous ascites fluid, as specified. Five days later, cells were harvested and stained with anti-CD11b and –CD64 antibodies, as well as a live/dead stain. Counting beads were added prior to antibody staining to enable cell count determination. **(A)** % Live residual $CD11b^{+}CD64^{+}$ cells were calculated relative to "Mock"-treated samples. **(B)** Representative flow cytometry plots showing depletion of ascites macrophages (from Patient 10) after treatment with the 3FR-targeting BiTEs. **(A)** Data show the grand mean ± SD of three individual patient means (each calculated from biological triplicate). Statistical significance was assessed by two-way ANOVA followed by Bonferroni post-hoc analysis, with each treatment being compared to the relevant "Mock" condition (*, $P < 0.05$; **, $P < 0.01$; ***, $P < 0.001$).

CD206 TriTE treatment, on the other hand, induced killing of $CD11b^+CD64^+$ cells (to 24.2%) only when cells were incubated without ascites fluids (Figure 5.10A); furthermore, this activity was not entirely dependent on the target antigen, as similar effects were observed with the Ctrl TriTE (Figure 5.10A). The CD206 BiTE was unable to elicit significant killing of ascites macrophages either in the presence or absence of fluid when all three patient samples were considered collectively (Figure 5.10). Nevertheless, one patient sample ("Patient 10") appeared responsive to treatment, at least in the absence of ascites fluid (reduction in % residual $CD11b^+CD64^+$ to 35.0%). None of the relevant control BiTEs triggered a significant decrease in % residual $CD11b^+CD64^+$ cells for any patient sample tested (Figure 5.10A).

5.3.5 Residual malignant ascites macrophages are repolarised towards a more pro-inflammatory phenotype by the TAM-targeting T cell engagers

By targeting markers of M2-like macrophages and cancer-promoting TAMs, the T cell engagers generated in this study have been designed to deplete the most immunosuppressive TAMs. To determine whether this may be achieved in the malignant ascites model, we investigated the phenotypes of the $CD11b^+CD64^+$ cells remaining after TAM-targeting T cell engager treatment. Whole, unpurified ascites cells from the three selected patient samples were cultured with the BiTEs/TriTEs for five days in the presence or absence of autologous ascites fluid. Cells were then harvested and processed for flow cytometry, assessing the expression levels of M1-like macrophage markers CD64, CD80 and CD86.

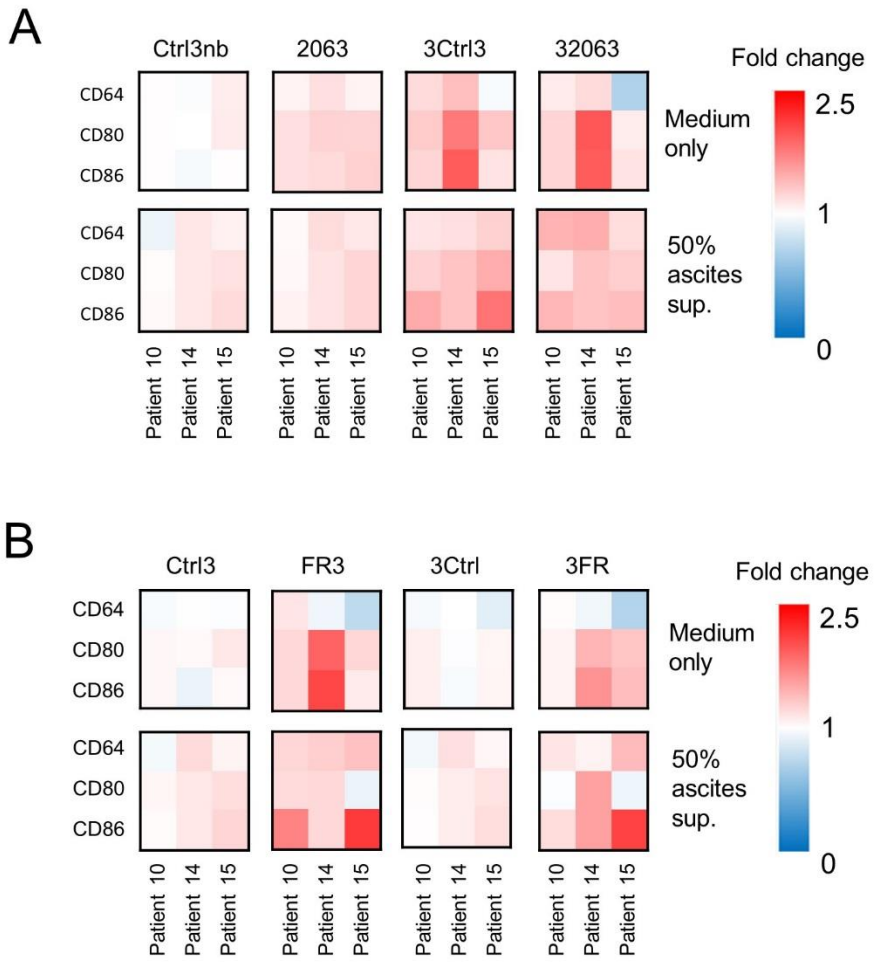

Figure 5.11. Macrophage-targeting T cell engagers induce repolarisation of residual ascites macrophages towards a more M1-like phenotype. Total unpurified ascites cells from three different patients were cultured for five days with 50 nM BiTEs/TriTEs in medium only or 50 % ascites fluid from the same patient sample. Cells were stained with anti-CD11b, anti-CD64, anti-CD80 and anti-CD86 antibodies, as well as a live/dead stain, then analysed by flow cytometry. Fold-changes in geometric MFI values of CD64, CD80 and CD86 on live CD11b$^+$CD64$^+$ ascites cells were calculated relative to "Mock"-treated samples for each patient sample. Fold-changes are displayed as a heat map.

Encouragingly, a shift towards a more pro-inflammatory macrophage phenotype was observed following treatment with the TAM-targeting T cell engagers (Figure 5.11). $CD11b^{+}CD64^{+}$ cells remaining after treatment with the FRβ-targeting BiTE exhibited particularly strong increases in CD86 expression (1.7- and 1.6-fold increases in geometric MFI values following FR3 and 3FR BiTE treatment, respectively), relative to untreated cells. The relevant control BiTEs had negligible effects on M1-like marker expression (Figure 5.11). A general increase in M1-like macrophage marker was also observed after treatment with the CD206 TriTE, although, in this case, the repolarising effects were non-specific, as the control TriTE exerted similar effects (Figure 5.11).

5.4 Chapter conclusions

1. The FRβ-targeting BiTEs induced robust activation of ascites-associated T cells, leading to killing of autologous ascites-associated macrophages.
2. The CD206-targeting TriTE, but not the parental BiTE, induced T cell-mediated killing of autologous ascites macrophages when cultured in medium only; however, this activity was diminished in the presence of autologous acellular ascites fluid.
3. The control TriTE induced a degree of non-specific T cell activation, although these effects were somewhat lessened in the presence of acellular ascites fluid.
4. Treatment with the FRβ-targeting BiTEs, as well as the CD206-targeting TriTE and the control TriTE, triggered repolarisation of remaining ascites-associated macrophages towards a more pro-inflammatory state.

5.5 Chapter discussion

In this chapter, we evaluated the activity of the TAM-targeting T cell engagers against three malignant ascites samples. These samples were determined to contain a high proportion of M2-like macrophages and exhausted T cells, suggestive of an immunosuppressed state (Figures 5.2 and 5.3). Despite this, the FRβ-targeting BiTEs were capable of inducing robust T cell activation and proliferation, IFN-γ production and killing of autologous ascites-associated macrophages in all samples tested, both in the presence and absence of acellular ascites fluid (Figures 5.4 to 5.10). Importantly, remaining ascites-associated macrophages exhibited a more pro-inflammatory, M1-like phenotype after FRβ BiTE treatment (Figure 5.11).

By contrast, the CD206-targeting BiTE was ineffective against all but one ascites sample, for which a minor level of T cell-mediated macrophage cytotoxicity was observed, and only in the absence of autologous ascites fluid (Figures 5.4 to 5.10). The CD206-targeting TriTE, meanwhile, induced T cell activation and redirected killing of ascites macrophages across all three samples tested; however, this activity was similarly diminished in the presence of autologous ascites fluid (Figures 5.4 to 5.10). Furthermore, the effects of the CD206 TriTE were not entirely antigen-dependent, as modest T cell activation was also induced by the matched control TriTE (Figures 5.4 to 5.10).

Thus, despite mediating robust killing of PBMC-derived MDMs cultured in the presence of acellular ascites fluid, the CD206 TriTE was ineffective against this more clinically-relevant model. As discussed in section 3.5, one possible reason for the inferior performance of the CD206-targeting T cell engagers is the large size of this target antigen, which may disfavour CD45 exclusion from the immunological synapse. Another explanation relates to target antigen density, with previous work describing a positive

correlation between antigen expression levels and BiTE potency (Hammond et al., 2007). In our PBMC model systems, we observed higher levels of CD206 on M2-polarised MDMs than FRβ (Figure 3.7). By contrast, levels of FRβ on ascites macrophages were higher than that of CD206 (Figures 3.1 and 5.2). Current understanding suggests that ascites macrophages are derived mainly from peritoneal (i.e. tissue-resident) macrophages, as opposed to infiltrating monocytes (Finkernagel et al., 2016). The differing activities of the CD206-targeting BiTEs/TriTEs against PBMC- and ascites-derived macrophages may therefore reflect differences in their ontogenies.

The increase in M1-like macrophage marker expression following FRβ-targeting BiTE treatment (Figure 5.11) was an encouraging finding, suggestive of either: i) a selective targeting of the most immunosuppressive TAMs with the highest expression levels of FRβ, sparing those with the most "M1 like" phenotype, or ii) incomplete macrophage cytotoxicity, with repolarisation of remaining cells due to BiTE-induced pro-inflammatory signals (such as IFN-γ), or a combination of both. Supporting a role for BiTE-induced pro-inflammatory signals, both the CD206 TriTE and its matched control also triggered an M1-like repolarisation of ascites-associated macrophages in the presence of autologous ascites fluid (Figure 5.11), despite their inability to mediate macrophage cytotoxicity in this setting. We hypothesise that the TriTEs induced a low-level of T cell activation which was sufficient to mediate macrophage repolarisation, but not killing.

Our findings are consistent with those of Freedman et al., who observed up-regulation of CD64 on ascites macrophages upon treatment of whole ascites with a CAF-targeting BiTE (Freedman et al., 2018). However, in contrast to our study, no increases in CD86 were induced by the CAF-targeting BiTE alone (Freedman et al., 2018). Although this discrepancy could stem from the small number of samples used in both studies, it may

also indicate a distinct effect of our approach, in which the BiTEs/TriTEs directly target macrophages, compared to theirs.

Altogether, we have demonstrated that the FRβ-targeting BiTEs, but not the CD206-targeting BiTEs/TriTEs, are capable of activating endogenous ascites T cells to kill autologous macrophages, despite the highly immunosuppressed nature of these samples. Most encouragingly, FRβ BiTE treatment resulted in ascites T cell proliferation, IFN-γ production and an upregulation of M1-like macrophage markers, suggestive of a repolarisation of the ascites microenvironment towards an immune-responsive state.

6 Generation of TAM-Targeting BiTE-Armed Oncolytic Adenoviruses for Localised Expression in Tumours

6.1 Introduction

Given the expression of CD206 and FRβ molecules on certain healthy tissues throughout the body (see section 3.1), tumour-restricted expression of the TAM-targeting T cell engagers will be essential for the safety of our approach. One promising strategy to achieve this involves the use of OVs "armed" with biologics that are expressed and secreted by infected cancer cells as the virus replicates. As a proof-of-concept, we next explored the possibility of encoding our T cell engagers within the genome of an oncolytic adenovirus, EnAd.

Identified through a process of bioselection on cancer cell lines, EnAd is a chimeric Ad11p/Ad3 adenovirus in Phase I/II clinical trials for various solid cancers. EnAd replicates selectively in cancer cells, triggering an immunogenic form of cell death termed "oncosis" (Dyer et al., 2017), and has demonstrated anti-tumour efficacy in xenograft models (Kuhn et al., 2008). Importantly, the capsid of EnAd is derived entirely from Ad11p, a group B adenovirus for which there is a low prevalence of neutralising antibodies among the general population (Vogels et al., 2003). Unlike most oncolytic viruses, EnAd exhibits high stability in whole human blood (Di et al., 2014), prompting its evaluation by intravenous delivery in clinical trials (Garcia-Carbonero et al., 2017; Machiels et al., 2019). In a Phase I Mechanism of Action study involving patients with various solid tumours, EnAd demonstrated convincing intratumoural replication following systemic delivery, which was accompanied by infiltration of $CD8^+$ T cells into tumours (Garcia-Carbonero et al.,

2017). EnAd is well-tolerated, with predictable and manageable influenza-like side effects (Garcia-Carbonero et al., 2017; Machiels et al., 2019).

Bearing deletions in the E3 and E4 regions, the genome of EnAd is 2470 bp shorter than Ad11p, indicating that its packaging capacity may exceed that of the parental virus. A versatile cloning system is available for DNA insertion into EnAd, whereby transgenes may be placed under the control of an exogenous promoter (e.g. CMV immediate-early) or an endogenous late viral promoter (adenovirus major late promoter, MLP, via a splice-acceptor (SA) site) (Marino et al., 2017). In the latter configuration, transgene expression is restricted to cells harbouring a productive virus infection, i.e. cancer cells. EnAd therefore offers an enticing opportunity for tumour-targeted expression of potent biologics following systemic delivery.

In light of the reported EnAd-mediated influx of $CD8^+$ T cells into tumours, this virus may be particularly valuable for the delivery of T cell therapies such as BiTEs (see section 1.6.7). EnAd-mediated expression of BiTEs has proven to be a powerful strategy at the pre-clinical level (Freedman et al., 2018; Freedman et al., 2017), with FAP BiTE-armed EnAd depleting CAFs and reversing tumour immune suppression, whilst maintaining its oncolytic activity (Freedman et al., 2018). However, a similar approach to target TAMs has yet to be explored.

In this chapter, we engineered EnAd to express the TAM-targeting T cell engagers. After performing quality control assays to assess their replicative and oncolytic properties, the BiTE/TriTE-armed EnAd viruses were evaluated against whole malignant ascites samples. Specifically, we assessed the abilities of BiTE/TriTE-armed EnAd to i) activate ascites T cells; ii) mediate depletion and/or repolarisation of ascites-associated macrophages and iii) kill cancer cells.

6.2 Chapter Aims

1. Engineer EnAd to express the TAM-targeting T cell engagers under the control of the endogenous major late viral promoter, or an exogenous CMV promoter
2. Generate and purify large-scale preparations of BiTE/TriTE-armed EnAd viruses
3. Assess the oncolytic/replicative properties of BiTE/TriTE-armed EnAd, as well as the production of BiTE/TriTE from virus-infected cells
4. Evaluate the activity of BiTE/TriTE-armed EnAd against whole ascites samples

6.3 Results

6.3.1 Cloning strategy to generate TAM-targeting T cell engager-armed oncolytic adenoviruses

The oncolytic adenovirus EnAd can be engineered to encode biologics that are expressed and secreted by infected tumour cells as the virus replicates, offering a multipronged and tumour-targeted therapeutic strategy (Freedman et al., 2018; Freedman et al., 2017; Marino et al., 2017). To explore the feasibility of this approach in the context of TAM-targeting T cell engagers, we inserted the CD206-targeting BiTE/TriTEs and FRβ-targeting BiTEs, as well as the matched control BiTEs/TriTEs, into SbfI-linearised EnAd viral backbone by Gibson assembly technology (cloning method as described in section 3.3.2). EnAd expressing the Ctrl3 BiTE was generated previously in our laboratory (Dr. Joshua Freedman, Seymour laboratory). TAM-targeting T cell engagers were placed downstream of the viral fibre gene, under the transcriptional control of either an exogenous promoter (CMV; EnAd-CMV-BiTE/TriTE), or the adenovirus major late promoter (MLP), via alternative splicing to an inserted splice acceptor (SA) site (EnAd-SA-BiTE/TriTE). In the former construct (EnAd-CMV-BiTE/TriTE), the expression and secretion of the BiTE/TriTEs should occur from all virus-infected cells following viral entry. By contrast, transgene expression from EnAd-SA-BiTE/TriTE constructs should be coupled to viral replication, thereby restricting its expression to cells supporting a productive virus infection. A schematic representation of BiTE/TriTE-armed EnAd is shown in Figure 6.1A. Successful transgene insertion was confirmed by diagnostic restriction digest (Figure 6.1B).

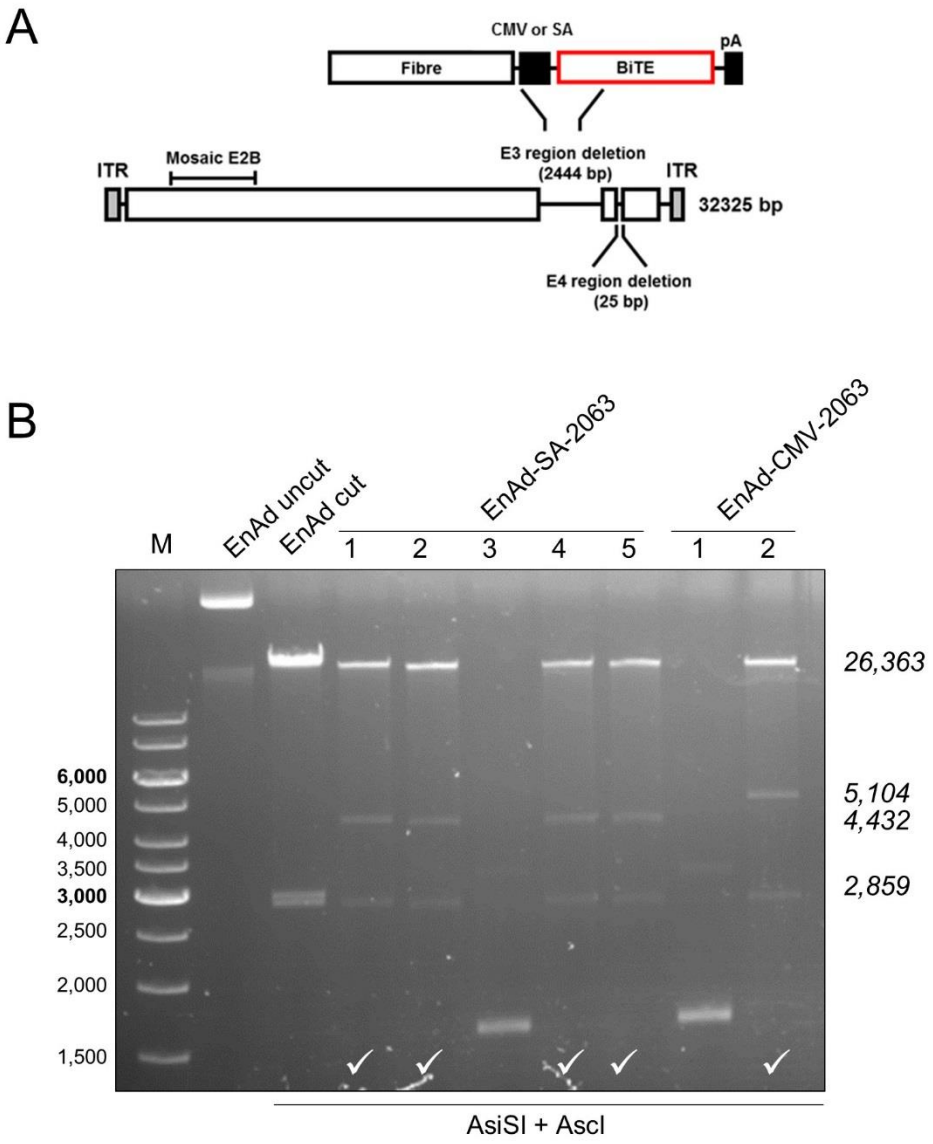

Figure 6.1. Engineering of BiTE-expressing EnAd (A) Schematic representation of EnAd engineered to express a BiTE downstream of a cytomegalovirus (CMV) promoter or splice acceptor (SA) site. pA, polyadenylation sequence; ITR, inverted terminal repeats. **(B)** BiTE transgene casettes were amplified by polymerase chain reaction and inserted into a linearised EnAd vector by Gibson assembly technology. An exemplary diagnostic restriction digest of DNA from single bacterial colonies transformed with BiTE-armed EnAd vectors is displayed. Expected DNA fragment sizes are noted in italics. Colonies with the predicted digestion pattern are indicated with a tick.

6.3.2 Robust BiTE/TriTE expression by engineered EnAd viruses is detectable only under the control of the CMV promoter

BiTE/TriTE-armed EnAd constructs were linearised with AscI prior to transfection into HEK293A cells, which were monitored closely for signs of cytopathic effect, indicating successful virus production (Figure 6.2A). Cells and supernatants were harvested upon observation of extensive CPE, and the supernatants probed by western blotting for the presence of BiTE/TriTEs. As shown in Figure 6.2B, EnAd-mediated CMV-driven BiTE/TriTE expression was robust, with His-tagged proteins of the predicted sizes detected in the supernatants of cells transfected with all the EnAd-CMV-BiTE/TriTE constructs, but not parental EnAd. On the other hand, MLP-driven BiTE/TriTE expression by engineered EnAd-SA-BiTE/TriTE constructs was very low or undetectable (Figure 6.2B), despite the observation of extensive CPE. For a proof-of-concept of our approach, we therefore proceeded with only the EnAd-CMV-BiTE/TriTE constructs.

6.3.3 Purification and amplification of EnAd-CMV-BiTE/TriTE constructs

The cell lysates and supernatants generated above represent "crude" virus preparations, possibly containing a mixture of transgene-armed and parental virus, as well as transfection reagents. We therefore sought to isolate single clones of the EnAd-CMV-BiTE/TriTE viruses (i.e. deriving from single virus particles) by plaque purification. In brief, HEK293A cells were infected with serially-diluted viruses, before being overlaid with 1% agarose. Single virus plaques (4-6 per construct) were isolated and expanded, with cells and supernatant subsequently harvested following the observation of extensive CPE (Figure 6.2A). As before, cell supernatants were probed by western blotting for successful expression and secretion of the BiTEs/TriTEs.

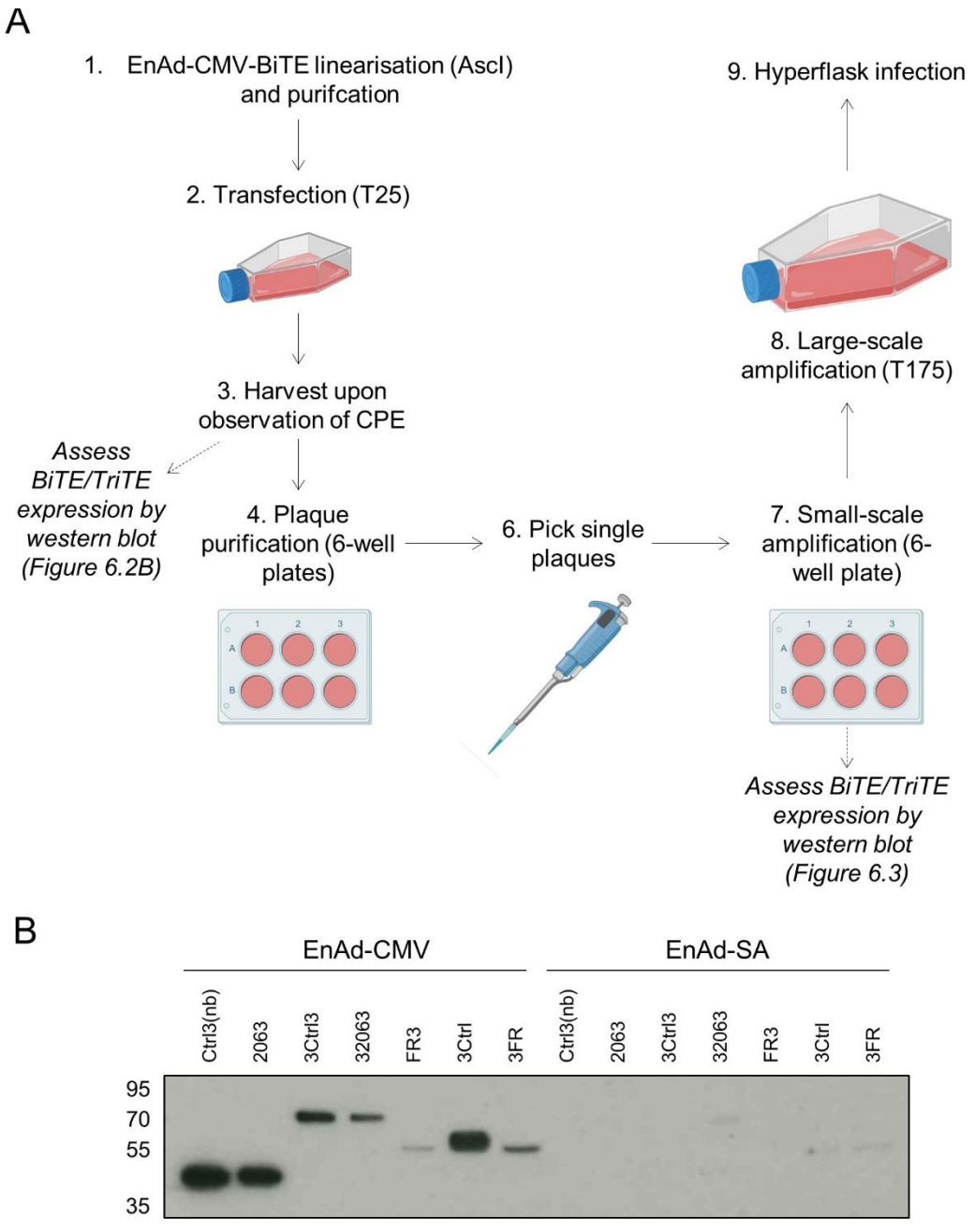

Figure 6.2. Generation and expansion of BiTE/TriTE-expressing EnAd viruses. (A) Overview of the strategy used to generate, isolate and expand the engineered EnAd viruses. Image created with BioRender. **(B)** Upon observation of CPE in T25 flasks after transfection with EnAd-BiTE/TrITE constructs, cells and supernatant were harvested. Before proceeding to plaque purification, BiTE/TriTE expression was assessed by western blotting analysis, using cell-free supernatants from the crude virus preparations. An anti-His primary antibody and a horseradish peroxidase-conjugated anti-mouse secondary antibody were utilised for BiTE/TriTE detection. CPE, cytopathic effect.

Robust expression of the TAM-targeting BiTEs and their matched controls was observed in the infected cell supernatants for every clone of EnAd-CMV-BiTE viruses tested (Figures 6.3A,B and E-G), which all yielded single bands of the predicted molecular weights. Virus clones selected for further amplification are indicated with a tick (Figures 6.3A,B and E-G).

By contrast, an unexpected pattern of bands was detected in the supernatants of cells infected with TriTE-expressing EnAd viruses (EnAd-CMV-32063 and EnAd-CMV-3Ctrl3; Figures 6.3C and D). Whilst His-tagged proteins of the predicted molecular weight for a TriTE (67 kDa) were present in the infected cell supernatants of most virus clones, they were co-expressed along with an unknown protein of low molecular weight (~30 kDa) (Figures 6.3C and D). Moreover, for several virus clones, only the unknown protein of low molecular weight was detectable (Figure 6.3C and D). For both EnAd-CMV-32063 and EnAd-CMV-3Ctrl3, two clones yielding the two expression patterns were selected for further analysis (indicated with asterisks, Figures 6.3C and D), as detailed in the next section.

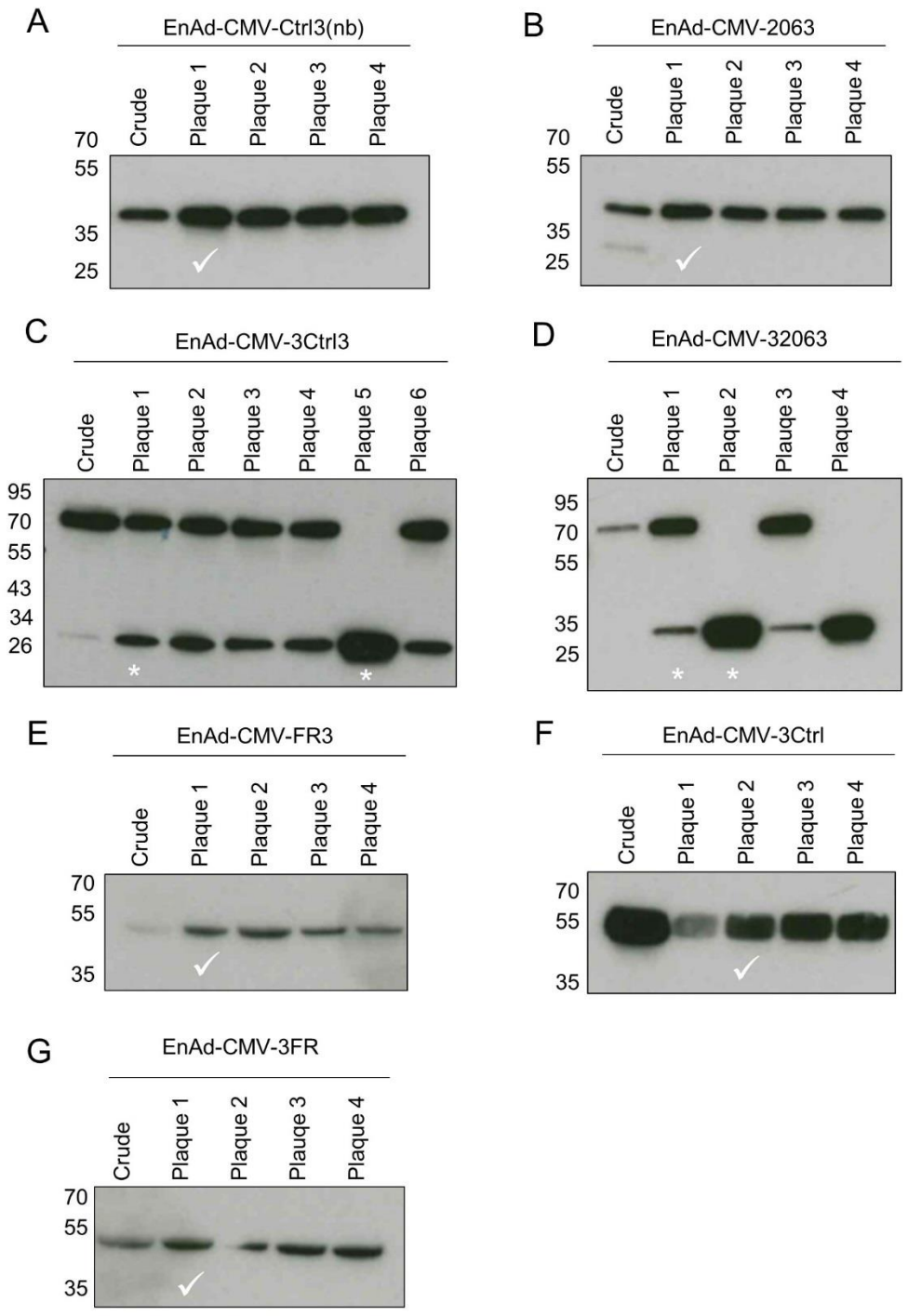

Figure 6.3. Selection of BiTE-expressing EnAd clones. (**A-G**) Plaque purification was performed on a monolayer of HEK293A cells using 10-fold serial dilutions of virus, which were removed after 4 h and replaced with an overlay of 1% agarose. Single virus clones were isolated and expanded. Upon observation of extensive cytopathic effect, infected cell supernatants were harvested and analysed by western blotting for BiTE expression using an anti-His primary antibody and horseradish peroxidase-conjugated anti-mouse secondary antibody. Virus clones selected for further expansion and purification are indicated with ticks. Virus clones selected for further plaque purification and study are indicated with asterisks.

6.3.4 EnAd-expressed TriTEs are functional, but are co-expressed along with a non-functional protein of low molecular weight

The unexpected pattern of protein expression by cells infected with EnAd-CMV-TriTEs prompted us to characterise these viruses in more detail before proceeding towards large-scale virus production.

We first asked whether supernatants from EnAd-CMV-TriTE-infected cells would function as expected when applied to co-cultures of MDMs and lymphocytes. DLD-1 colorectal adenocarcinoma cells were infected with the indicated EnAd-CMV-TriTE virus clones (diluted 1:100). Infected cell supernatants were harvested three days later and applied to co-cultures of CFSE-stained MDMs (IL-4 polarised to yield $CD206^{high}$ target cells) and autologous lymphocytes. After four days' co-culture, T cell activation and MDM killing was determined by flow cytometry and Celigo image cytometry, respectively. Infected cell supernatants containing only the low molecular weight protein (i.e. from cells infected with EnAd-CMV-3Ctrl3 "Clone 5" and EnAd-CMV-32063 "Clone 2") did not trigger appreciable T cell activation (as determined by CD25 expression) or MDM killing (Figure 6.4A and B). No detectable T cell activation or cytotoxicity towards MDMs was observed upon treatment of co-cultures with supernatant from cells infected with EnAd-CMV-3Ctrl3 "Clone 1", which yielded both the TriTE-sized and low molecular weight proteins (Figure 6.4A and B). Supernatant from cells infected with EnAd-CMV-32063 "Clone 1", which contained both the TriTE-sized and low molecular weight proteins, triggered T cell activation and MDM killing in a similar manner to co-cultures treated with free recombinant CD206 TriTEs (from transfected HEK293A cells) (Figure 6.4A and B). These data indicate that the EnAd-expressed TriTEs function as expected, and that their functionality is not compromised by the co-expression of the low molecular weight

protein. The low molecular weight protein alone does not appear to induce non-specific T cell activity of MDM killing.

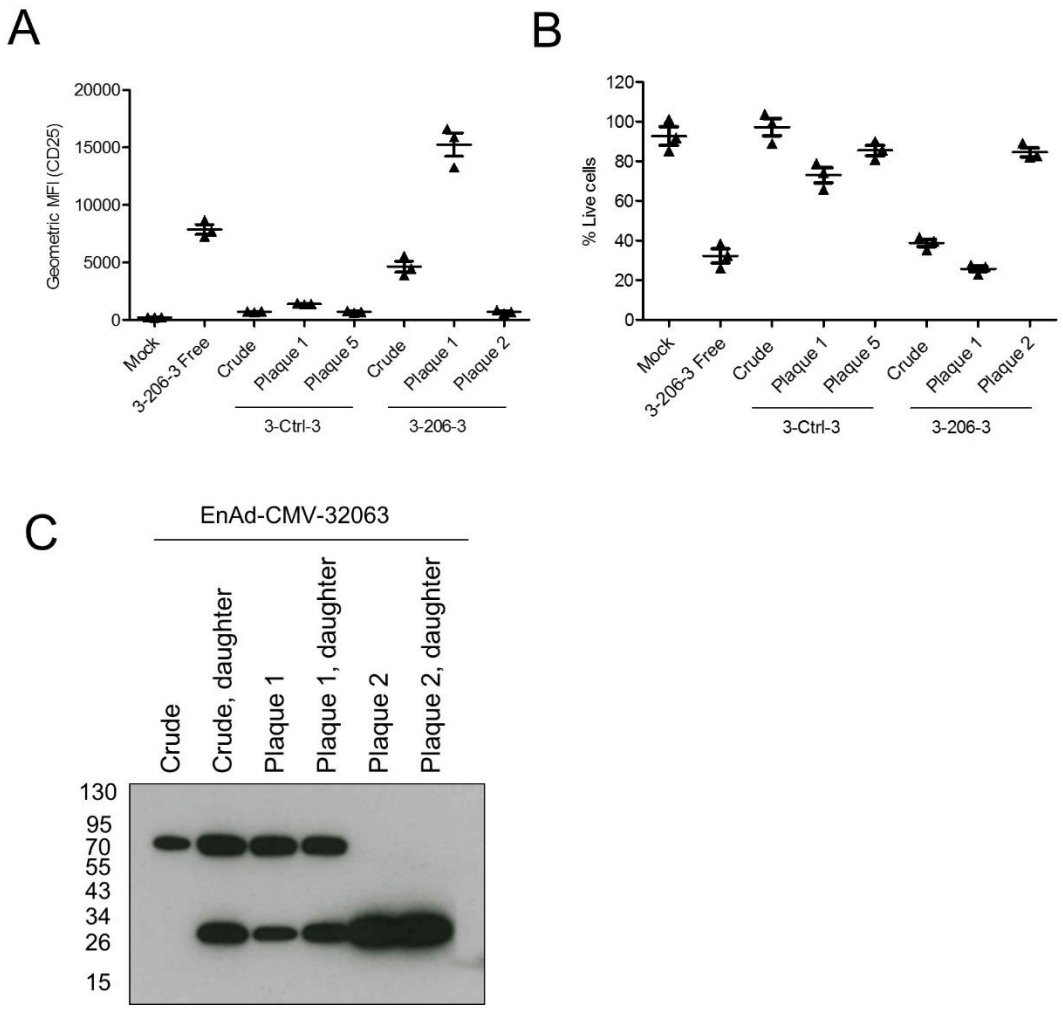

Figure 6.4. Virally-encoded TriTEs are functional, but are co-expressed along with a non-functional protein of low molecular weight. (A, B) Infected cell supernatants from plaque-purified, TriTE-expressing virus clones were applied to co-cultures of IL-4-polarised human MDMs and autologous lymphocytes. Free CD206 TriTE (50 nM) was included as a positive control. Co-cultures were incubated for four days. **(A)** T cell activation was determined by flow cytometric analysis of CD25 expression. **(B)** MDM killing was assessed by propidium iodide staining and Celigo image cytometry. **(C)** Plaque-purified CD206 TriTE-expressing EnAd clones were subjected to a further round of plaque purification on HEK293A cells, giving rise to "daughter" plaques. Supernatants from cells infected with the parental and daughter were subjected to western blotting analysis, using anti-His primary antibody and horseradish peroxidase-conjugated anti-mouse secondary antibody. **(A, B)** Data show mean ± SD of biological triplicates.

We next sought to determine whether a further round of plaque purification of the TriTE-expressing EnAd viruses would yield single clones of virus expressing only the functional TriTE. Supernatants from cells infected with EnAd-CMV-32063 "Clone 1" and "Clone 2" were serially-diluted, as previously, and applied to HEK293A cells, which were then overlaid with agarose (1% w/v). Single virus plaques were isolated and expanded, and the infected cell supernatants subsequently probed by western blotting for TriTE expression. As shown in Figure 6.4C, a further round of plaque purification failed to remove the low molecular weight protein, which in fact appeared to increase, suggesting that the TriTE was unstable.

6.3.5 Large-scale production and quantification of BiTE-armed EnAd viruses

In light of the issues surrounding the low molecular weight protein expressed by the EnAd-CMV-TriTE viruses, we proceeded to large-scale production of only the BiTE-armed EnAd viruses (CD206- and FRβ-targeting). In brief, large-scale virus infections were performed in hyperflasks, which were harvested upon observation of the first signs of CPE. Viruses were purified by double caesium chloride banding, as described in the Materials and Methods section.

Viral titres were determined by Picogreen assay and HPLC (Figure 6.5), yielding estimates of viral genomes (vg) and viral capsids per millilitre, respectively (Table 6.1).

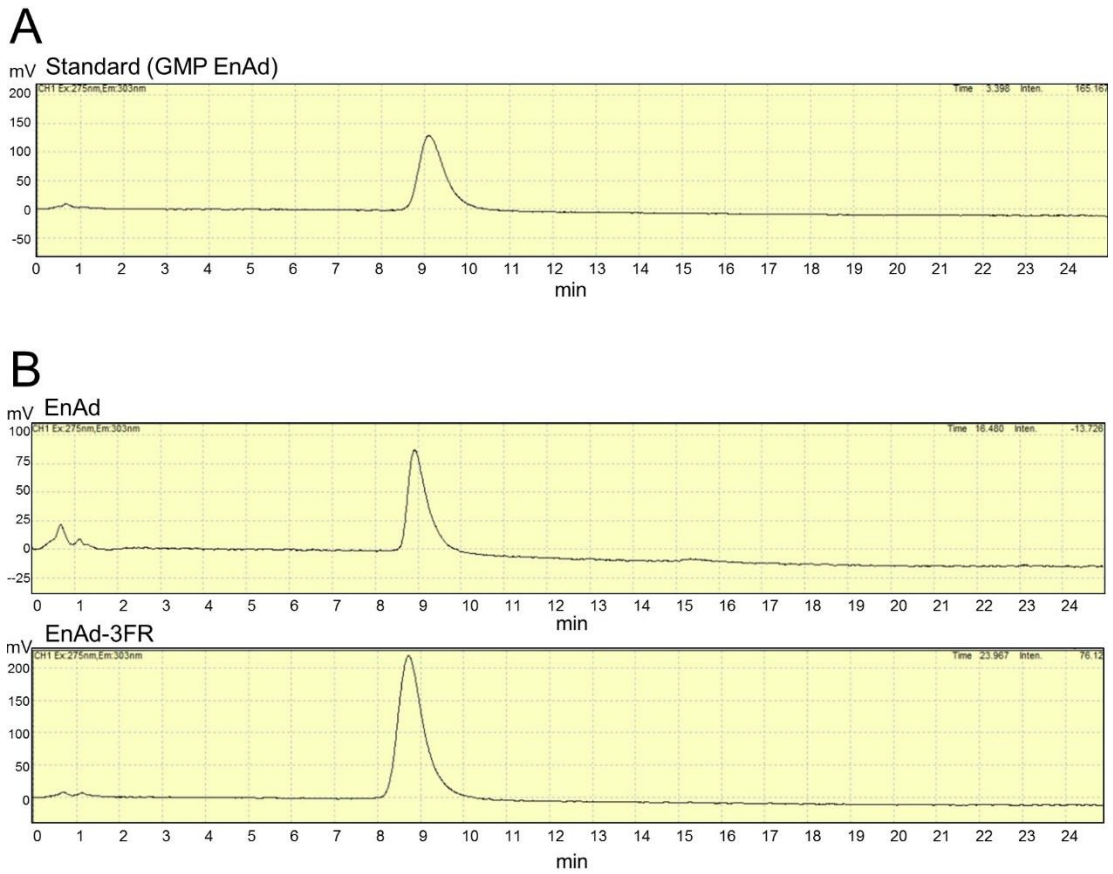

Figure 6.5. HPLC traces of purified virus stocks. (**A, B**) Anion exchange HPLC was employed to characterise and quantified all viruses, using a good manufacturing practice (GMP)-grade EnAd of known concentration to generate a standard curve. Samples were run using a robotic autosampler on a Shimadzu Prominence pre-fitted with a Resource Q (anion exchange) column. Representative traces are shown. This study was completed in collaboration with Dr. Brian Lyons (post-doctoral researcher, Seymour laboratory).

6.3.6 Virus genome replication and oncolytic activity is not impaired by addition of BiTE/TriTE transgenes

To compare the oncolytic properties of the engineered EnAd constructs with parental EnAd, we performed dose-response experiments of the purified viruses against DLD-1 cells. Cell viability was assessed five days post-infection by MTT assay. Importantly, the oncolytic activity of BiTE-expressing EnAd viruses was comparable to that of parental EnAd (Figure 6.6A).

	Picogreen	HPLC
	Viral genomes/mL	Viral particles/mL
EnAd	2.73×10^{11}	3.83×10^{11}
EnAd-Ctrl3(nb)	3.59×10^{11}	5.51×10^{11}
EnAd-2063	3.92×10^{11}	5.55×10^{11}
EnAd-Ctrl3(scFv)	5.42×10^{11}	8.02×10^{11}
EnAd-FR3	3.27×10^{11}	5.51×10^{11}
EnAd-3Ctrl	1.59×10^{11}	2.40×10^{11}
EnAd-3FR	9.25×10^{11}	1.75×10^{12}

Table 6.1. Quantification of purified viral stocks. Viral stocks were quantified by Picogreen and high performance liquid chromatography (HPLC), yielding estimates of viral genomes and viral particles per millilitre (mL), respectively.

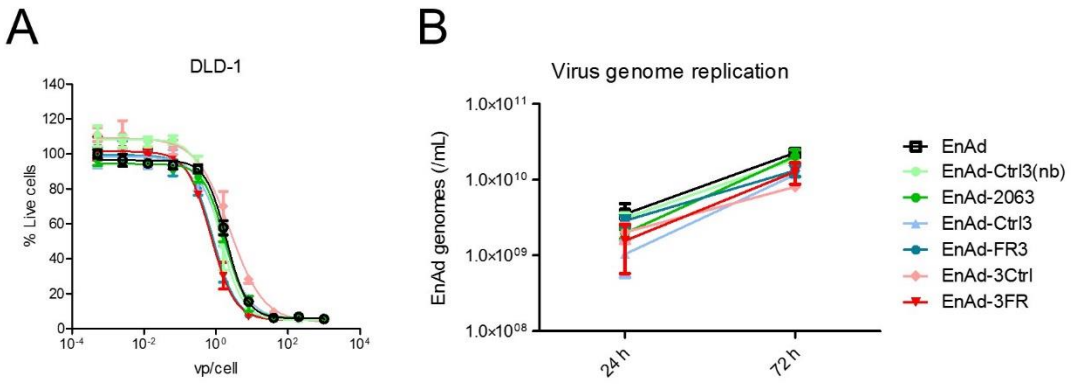

Figure 6.6. Viral genome replication and oncolytic activity of EnAd is not compromised by the insertion of BiTE-encoding transgenes. (A) DLD-1 cells were infected with increasing doses of the indicated viruses. Five days later, cell viability was assessed by MTT assay. % Live cells was calculated relative to uninfected cells. **(B)** DLD-1 cells were infected with parental or BiTE-expressing EnAd (100 vp/cell) and wells harvested 24 or 72 h later. Viral genomes were determined by quantitative polymerase chain reaction (qPCR), using primers recognising Ad11 viral hexon. **(A, B)** Data show mean ± SD of biological triplicates.

The replication kinetics of the recombinant viruses were then assessed. DLD-1 cells were infected with the recombinant or parental viruses at 100 vg/cell. At 24 h and 72 h post-infection, viral genomes were quantified by quantitative PCR. As shown in Figure 6.6B, the number of genomes of BiTE-armed EnAd constructs at each time-point were indistinguishable from that of parental EnAd, indicating that BiTE transgene insertion does not comprise their replication kinetics.

6.3.7 Supernatants from EnAd-CMV-BiTE-infected cells trigger T cell-mediated killing of autologous MDMs

As a first step to assess the functionality of EnAd-expressed BiTEs, infected cell supernatants were applied to co-cultures of MDMs and autologous lymphocytes. To generate BiTE-containing infected cell supernatants, DLD-1 cells were infected with BiTE-armed EnAd constructs at a dose of 100 vg/cell. Five days later, BiTE-containing infected cell supernatants were applied to co-cultures of lymphocytes and autologous MDMs, which were IL-4 polarised or M-CSF/IL-6-polarised, generating target cells with high levels of CD206 or FRβ, respectively. T cell activation and MDM killing were assessed four days later with flow cytometric analysis of CD25 expression and Celigo image cytometry, respectively. At both 1:100 and 1:1000 dilutions, supernatants from cells infected with EnAd expressing the CD206- and FRβ-targeting BiTEs triggered robust T cell activation in co-culture with the relevant target MDMs (Figure 6.7A). No significant T cell activation was detected after incubation with supernatants from cells infected with parental EnAd, EnAd-CMV-Ctrl3(nb) or EnAd-CMV-3Ctrl (Figure 6.7A). A modest rise in CD25 expression was observed following treatment with EnAd-CMV-Ctrl3 (Figure 6.7A), possibly due to stimulatory effects of cellular debris generated upon EnAd-mediated DLD-1 cell lysis.

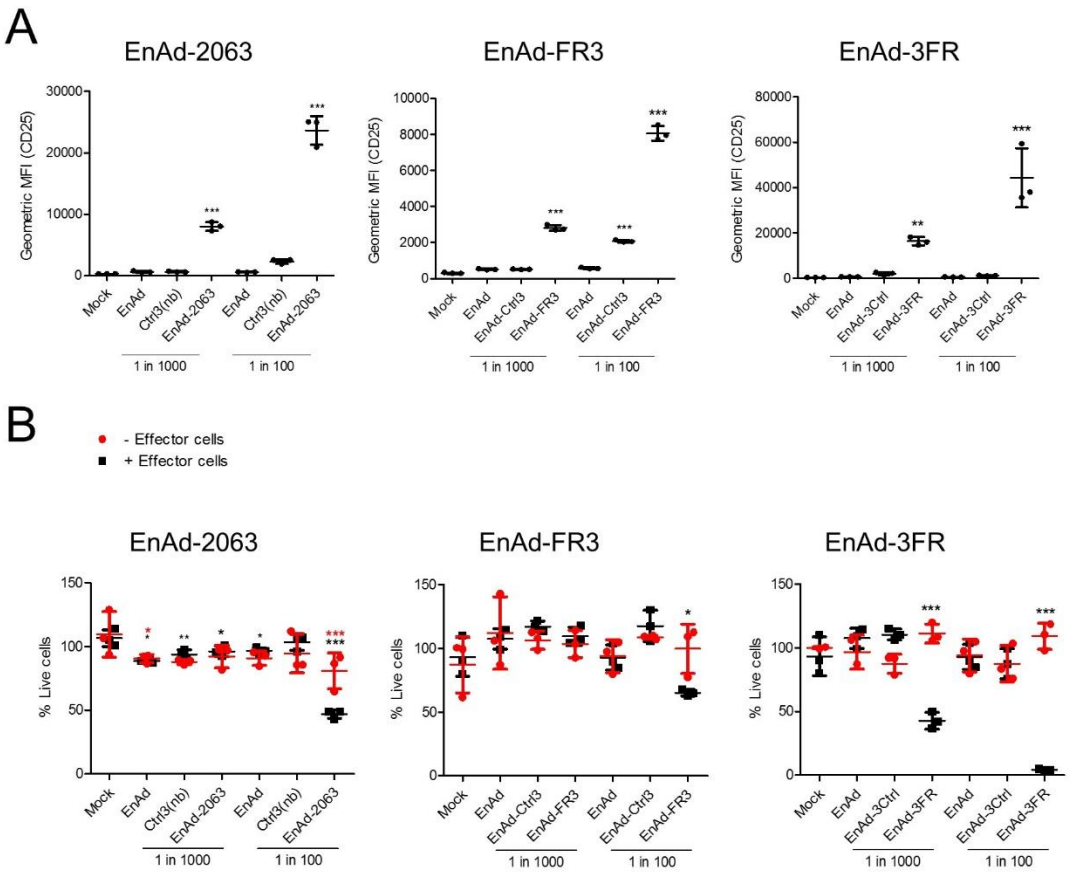

Figure 6.7. Supernatants from cells infected with BiTE-armed EnAd trigger T cell-mediated cytotoxicity of macrophages. **(A, B)** DLD-1 cells were infected with the indicated viruses at a dose of 100 viral genomes/cell. Three days later, supernatants were harvested and applied at the indicated dilutions to co-cultures of peripheral blood-derived T cells and CFSE-stained MDMs. Prior to co-culture, MDMs were polarised with IL-4 or M-CSF/IL-6 to generate CD206 or folate receptor β-high target cells, respectively, where appropriate. Co-cultures were incubated for a total of four days. **(A)** T cell activation was assessed by measuring CD25 expression with flow cytometry. **(B)** MDM killing was assessed with propidium iodide staining and Celigo image cytometry. **(A, B)** Data show mean ± SD of biological triplicates Statistical analysis was performed by one-way ANOVA followed by Dunnett's post-hoc analysis compared with "Mock"-treated cells **(A)**, or by two-way ANOVA with Bonferroni post-hoc tests comparing with the relevant "Mock" condition **(B)** (*, $P < 0.05$; **, $P < 0.01$; ***, $P < 0.001$).

T cell activation by EnAd-CMV-2063- and EnAd-CMV-FR3-infected cell supernatants (diluted 1:100) corresponded with a significant reduction in the % of live MDMs to around 50% (Figure 6.7B). The supernatants from cells infected with EnAd-CMV-3FR were more effective, reducing the % of live MDMs to 4.29% when diluted 1 in 100, and to 42.8% when diluted 1 in 1000 (Figure 6.7B). MDM killing by EnAd-CMV-BiTE-infected cell supernatants was dependent on the presence of T cells, with no appreciable cytotoxicity in their absence (Figure 6.7B). Moreover, no significant killing of MDMs was observed after treatment of the co-cultures with supernatants from parental EnAd or EnAd expressing the control BiTEs (Figure 6.7B).

6.3.8 BiTE-armed EnAd triggers the activation and expansion of endogenous T cells in human malignant ascites samples

We next explored the activity of the BiTE-armed EnAd viruses against whole malignant ascites. As before (see Chapter 5), ascites samples from three cancer patients (Patients 10, 14 and 15) were selected for assessment based on their high levels of CD11b$^+$ cells. Unpurified ascites cells were treated with BiTE-expressing or parental virus at a dose of 100 vg/cell in the presence or absence of autologous cell-free ascites fluid (50 % v/v). Five days later, cells were harvested and processed for flow cytometric analysis, staining with anti-CD4, -CD8 and –CD25 antibodies. Significant activation of the CD4$^+$ and CD8$^+$ cell subsets was observed for all three patient samples following treatment with EnAd-CMV-3FR (Figure 6.8A). Activation levels by EnAd-CMV-3FR were similar irrespective of the presence or absence of autologous ascites fluid, with an average % CD25 positivity in ascites fluid of 78.5% and 45.7% for CD4$^+$ and CD8$^+$ cells, respectively, and an average % CD25 positivity in medium only of 76.4% and 43.8%, respectively (Figure 6.8A). T cell activation by EnAd-CMV-FR3 was more modest, reaching significance only for the CD4$^+$

subset (average % CD25 positivity of 49.9% and 62.4% in the presence and absence of ascites fluid, respectively; Figure 6.8A). By contrast, EnAd expressing the CD206-targeting BiTE did not trigger significant T cell activation in any of the patient samples either in the presence or absence of autologous ascites fluid (Figure 6.8A). Neither parental nor control BiTE-expressing EnAd viruses elicited activation of $CD4^+$ or $CD8^+$ T cells (Figure 6.8A).

Numbers of $CD4^+$ and $CD8^+$ ascites cells after infection with the EnAd-CMV-BiTE viruses were assessed by flow cytometry, with counting beads employed to determine absolute cell counts. As shown in Figure 6.8B, there was a significant expansion of $CD4^+$ and $CD8^+$ cell subsets in ascites samples treated with EnAd-CMV-3FR. Fold-increases in $CD4^+$ count were 7.37 and 17.5 in the absence and presence of autologous ascites fluid, respectively. Expansion of the $CD8^+$ subset was less pronounced, averaging 4.96- and 7.28-fold in the absence and presence of autologous ascites fluid, respectively (Figure 6.8B). When considering all three patient samples collectively, EnAd-CMV-FR3 was unable to trigger significant expansion of either $CD4^+$ or $CD8^+$ cell subsets (Figure 6.8B). Nevertheless, the fold-increases in $CD4^+$ and $CD8^+$ cells in one ascites sample (from "Patient 14") after treatment with EnAd-CMV-FR3 were substantial (5.94- and 7.39-fold for $CD4^+$ cells, 4.94- and 4.88-fold for $CD8^+$ cells, in the absence or presence of ascites fluid, respectively). In line with its inability to induce T cell activation, EnAd-CMV-2063 did not induce expansion of either $CD4^+$ or $CD8^+$ cells (Figure 6.8B). No T cell expansion was observed in ascites samples infected with parental or control BiTE-expressing EnAd viruses (Figure 6.8B). These findings were confirmed by brightfield microscopy, which revealed cell clusters (indicating activated/proliferating T cells) in ascites cell samples treated with EnAd-CMV-3FR, but not the other recombinant viruses or parental EnAd (representative images in Figure 6.9).

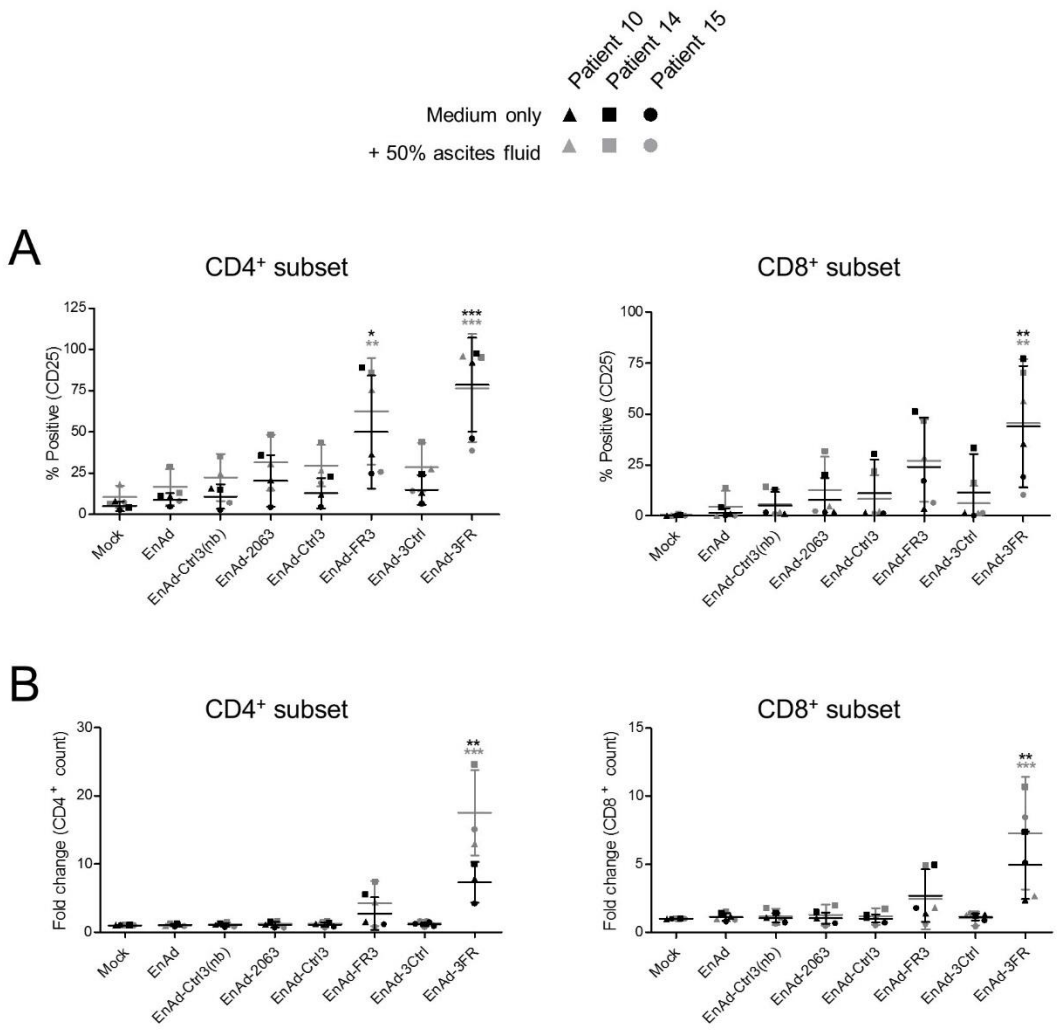

Figure 6.8. EnAd expressing FRβ-targeting BiTEs triggers activation and expansion of endogenous malignant ascites T cells. Total unpurified ascites cells from three different cancer patients were infected with 100 viral genomes/cell of parental or BiTE-expressing EnAd for five days in the presence or absence of autologous ascites fluid. **(A)** Activation of endogenous $CD4^+$ and $CD8^+$ ascites T cells was assessed by flow cytometric measurement of CD25 expression. **(B)** Numbers of $CD4^+$ and $CD8^+$ cells were determined through addition of counting beads to samples immediately prior to antibody staining. Fold-changes in $CD4^+$ and $CD8^+$ cell count were calculated relative to "Mock"-treated samples. **(A, B)** Data show the grand mean ± SD of three individual patient means (each calculated from biological triplicate). Statistical significance was assessed by two-way ANOVA followed by Bonferroni post-hoc analysis, with each treatment being compared to the relevant "Mock" condition (*, $P < 0.05$; **, $P < 0.01$; ***, $P < 0.001$).

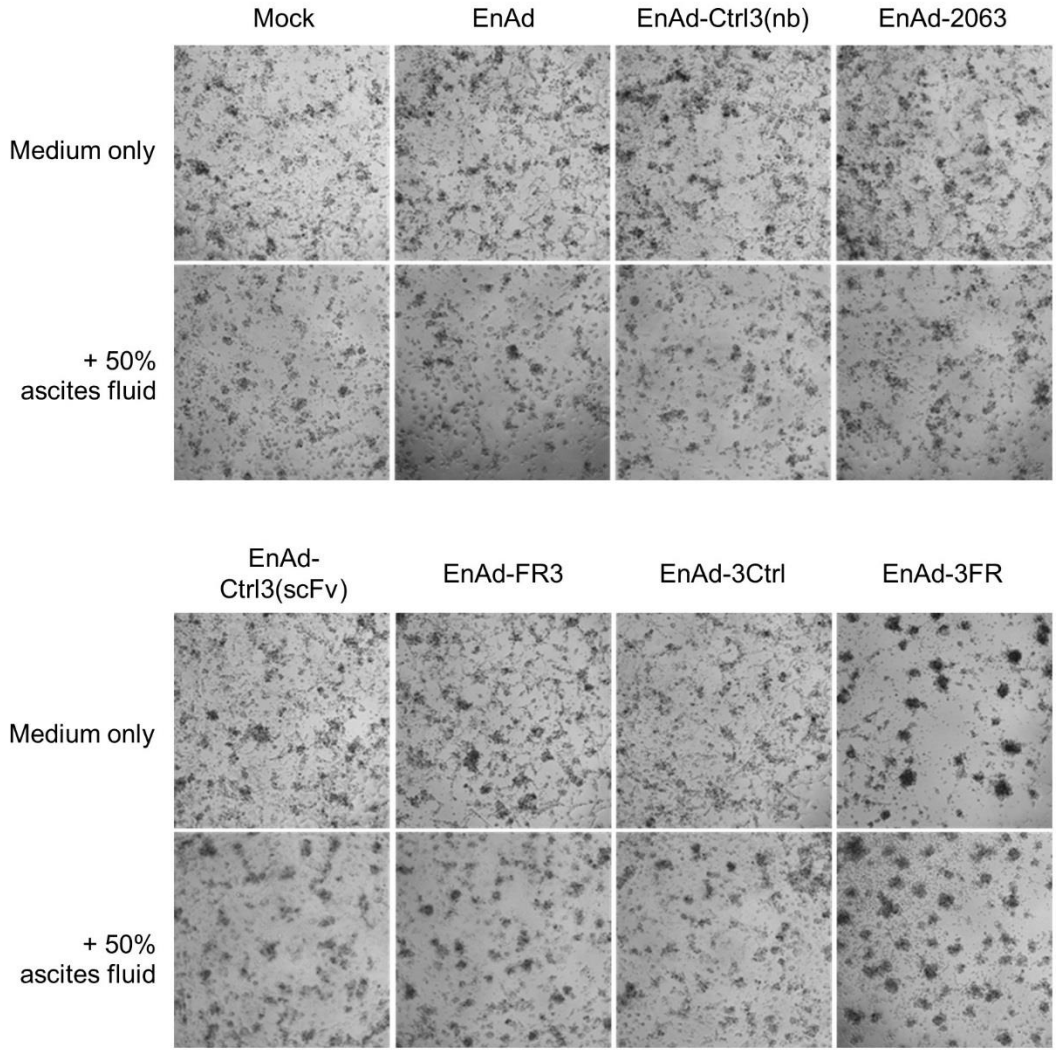

Figure 6.9. Brightfield microscopy images of malignant ascites cells treated with BiTE-expressing EnAd viruses. Total unpurified ascites cells from three different cancer patients were infected with 100 viral genomes/cell of parental or BiTE-expressing EnAd in the presence or absence of autologous ascites fluid. Five days later, cells were imaged by brightfield microscopy with a Zeiss Axiovert 25 microscope. Representative images from one patient sample (Patient 10) are displayed.

Quantities of soluble IFN-γ in the infected cell supernatants were then determined by ELISA. Treatment with EnAd-CMV-3FR induced high levels of IFN-γ secretion (averages of 2190 and 3080 pg/mL in the absence and presence of ascites fluid, respectively; Figure 6.10). In contrast, IFN-γ levels in the supernatants of ascites cells infected with EnAd-CMV-2063 and EnAd-CMV-FR3 were not significantly higher than the relevant mock-treated cell supernatants (Figure 6.10). Neither parental nor control BITE-expressing EnAd induced significant secretion of IFN-γ (Figure 6.10). Nevertheless, IFN-γ levels in the supernatants of ascites cells from one patient (Patient 14, square symbol in Figure 6.10) were elevated in all virus-treated cells, relative to mock-treated cells, suggesting that the virus alone exerted an immune-stimulatory effect.

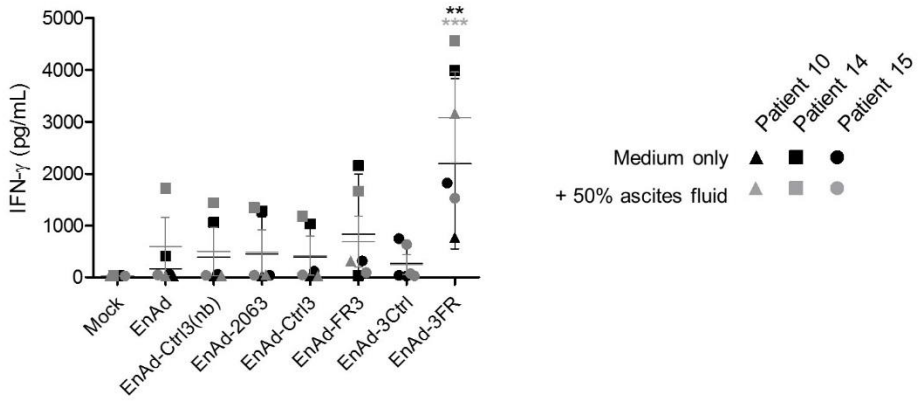

Figure 6.10. Treatment of malignant ascites samples with EnAd expressing FRβ-targeting BiTEs induces IFN-γ secretion. Total unpurified ascites cells from three different cancer patients were infected with 100 viral genomes/cell of parental or BiTE-expressing EnAd for five days in the presence or absence of autologous ascites fluid. Quantities of IFN-γ in the ascites cell supernatants were then determined by enzyme-linked immunosorbent assay. Data show the grand mean ± SD of three individual patient means (each calculated from biological triplicate). Statistical significance was assessed by two-way ANOVA followed by Bonferroni post-hoc analysis, with each treatment being compared to the relevant "Mock" condition (*, $P < 0.05$; **, $P < 0.01$; ***, $P < 0.001$).

Thus, consistent with its superior performance as a free BiTE, the 3FR BiTE outperformed the FR3 and CD206 BiTEs in terms of ability to trigger T cell activation, expansion and IFN-γ secretion when delivered from EnAd.

6.3.9 BiTE-armed EnAd viruses mediate a reduction in live ascites macrophages

The impact of EnAd-CMV-BiTE treatment upon ascites macrophage survival was then assessed. Ascites samples were treated with EnAd-CMV-BiTE or parental viruses at a dose of 100 vg/cell and incubated for five days with or without autologous ascites fluid (50% v/v), then harvested and analysed by flow cytometry. Treatment with EnAd-CMV-3FR triggered a significant decline in the number of ascites macrophages, with the average % residual $CD11b^{+}CD64^{+}$ cells across the three patient samples reducing to 23.1 and 39.8 % in the absence and presence of ascites supernatant, respectively (Figure 6.11). Consistent with their minor or non-significant activation of ascites T cells, EnAd-CMV-2063 and EnAd-CMV-FR3 did not trigger appreciable killing of ascites macrophages (Figure 6.11). Likewise, treatment of ascites with parental or control BiTE-armed EnAd did not lead to a significant reduction in the % residual ascites macrophages (Figure 6.11)

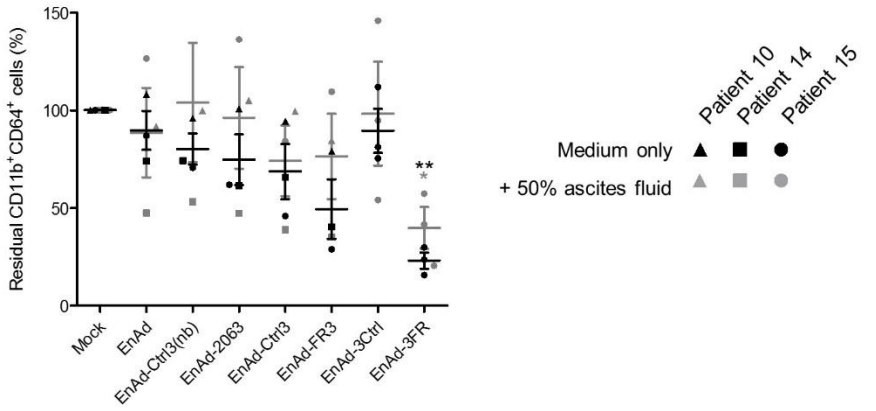

Figure 6.11. FRβ BiTE-expressing EnAd induces depletion of endogenous malignant ascites macrophages. Unpurified ascites cells from three different cancer patients were treated with parental and BiTE-expressing EnAd viruses at a dose of 100 viral genomes/cell, in the presence or absence of autologous ascites fluid (50% v/v). Five days later, cells were harvested and processed for flow cytometry, staining with anti-CD11b and anti-CD64 antibodies, as well as a live/dead stain. Counting beads were added prior to antibody staining to facilitate determination of absolute cell count. % Residual live $CD11b^+CD64^+$ cells were calculated relative to "Mock"-treated samples. Data show the grand mean ± SD of three individual patient means (each calculated from biological triplicate). Statistical significance was assessed by two-way ANOVA followed by Bonferroni post-hoc analysis, with each treatment being compared to the relevant "Mock" condition (*, $P < 0.05$; **, $P < 0.01$; ***, $P < 0.001$).

6.3.10 Residual ascites macrophages display increased M1-like marker expression following treatment with EnAd-CMV-BiTE viruses

To determine whether these treatments were capable of repolarising the residual $CD11b^+CD64^+$ ascites cells, we measured their expression of M1-like macrophage markers. As above, ascites cells were treated with the indicated viruses (at 100 vg/cell) in the presence or absence of autologous ascites fluid. Five days later, cells were harvested and processed for flow cytometry, staining with anti-CD11b, -CD64, -CD80 and –CD86 antibodies. For all three patient samples tested, addition of FR3, 3FR or 2063 BiTE-armed EnAd viruses, as well as parental EnAd and the relevant control BiTE-armed viruses, triggered a general increase in M1 marker expression above that of mock-treated cells

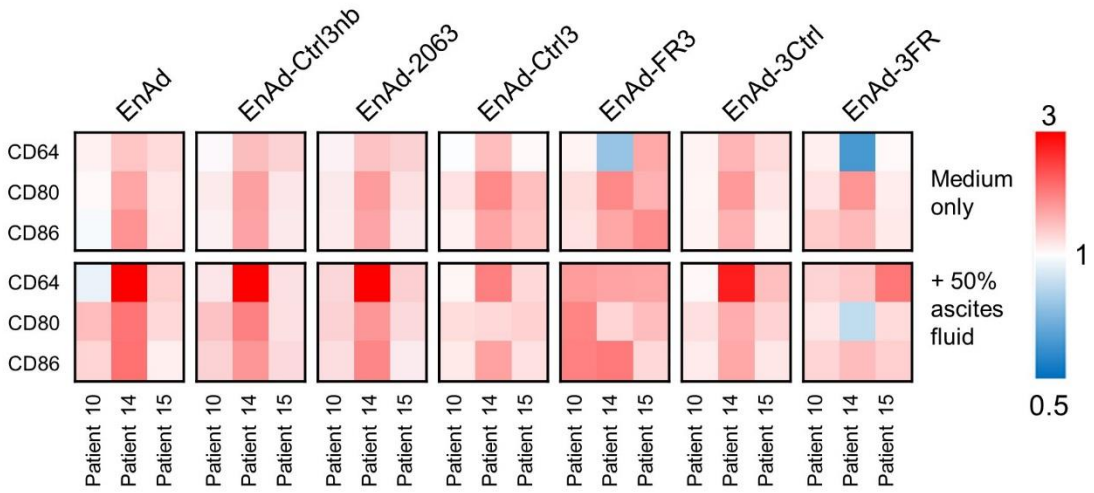

Figure 6.12. Parental and BiTE-expressing EnAd viruses induce repolarisation of endogenous malignant ascites macrophages towards a pro-inflammatory phenotype. Total ascites cells from three different cancer patients were infected with the indicated parental or BiTE-expressing EnAd viruses at 100 viral genomes/cell. After five days' incubation in the presence or absence of autologous ascites fluid, cells were processed for flow cytometric analysis, staining with anti-CD11b, anti-CD64, anti-CD80 and anti-CD86 antibodies, as well as a live/dead stain. Fold-changes in geometric mean fluorescence intensity values of CD64, CD80 and CD86 on live $CD11b^{+}CD64^{+}$ cells were calculated relative to "Mock"-treated samples, and displayed as a heat map.

(Figure 6.12). For two of three ascites patient samples (Patients 10 and 15), treatment with the FRβ BiTE-armed viruses (in one or both orientations) achieved significantly higher fold-increases in the expression of one or more M1 marker(s) than parental EnAd or the relevant control BiTE-armed viruses (Figure 6.13). Interestingly, despite its modest effects on T cell activation and inability to induce significant macrophage cytotoxicity, the FR3 BiTE-armed virus in some cases outperformed its 3FR BiTE-armed counterpart. For example, the expression levels of CD64, CD80 and CD86 were all significantly higher on $CD11b^{+}CD64^{+}$ cells from Patient 10 when treated with EnAd-CMV-FR3 than EnAd-CMV-3FR (in the presence of ascites fluid; Figure 6.13).

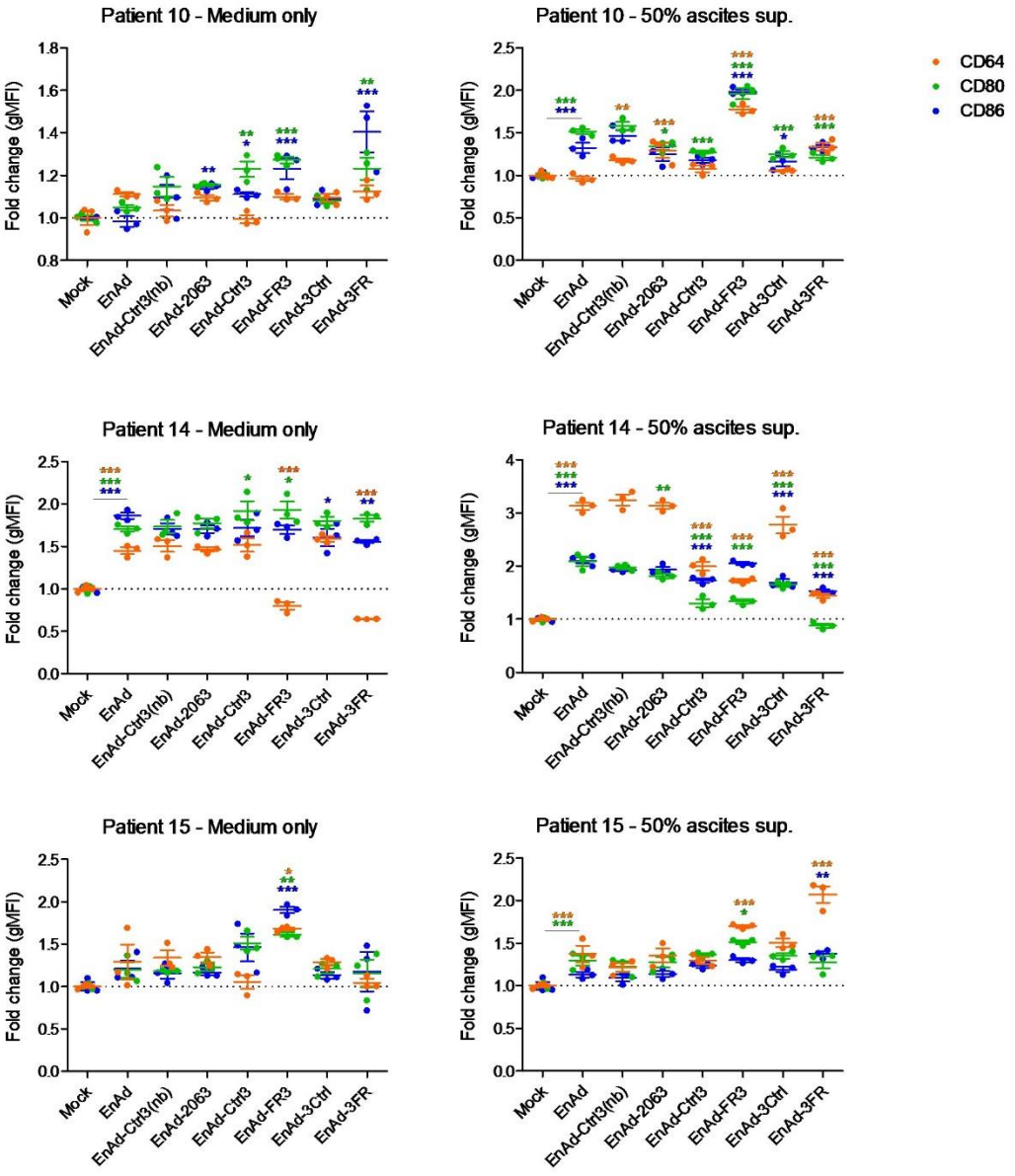

Figure 6.13. BiTE-expressing EnAd viruses induce greater repolarisation of ascites macrophage than parental EnAd in two of three cancer patient samples. Unpurified ascites cells from three different cancer patients were infected with the indicated parental or BiTE-expressing EnAd viruses at 100 viral genomes/cell. After five days' incubation in the presence or absence of autologous ascites fluid, cells were processed for flow cytometric analysis, staining with anti-CD11b, anti-CD64, anti-CD80 and anti-CD86 antibodies, as well as a live/dead stain. Fold-changes in geometric mean fluorescence intensity values of CD64, CD80 and CD86 on live $CD11b^{+}CD64^{+}$ cells were calculated relative to "Mock"-treated samples. Data show the grand mean ± SD of three individual patient means (each calculated from biological triplicate). Statistical significance was assessed by two-way ANOVA followed by Bonferroni post-hoc analysis, with each treatment being compared to parental "EnAd" or, in the case of EnAd, "Mock" (*, $P < 0.05$; **, $P < 0.01$; ***, $P < 0.001$).

Together, these data demonstrate the ability of FRβ BiTE-armed EnAd viruses to trigger activation and expansion of T cells in malignant ascites, leading to depletion of endogenous macrophages and up-regulation of pro-inflammatory markers on remaining macrophages.

6.3.11 BiTE-armed EnAd viruses co-target cancer cells and ascites macrophages

The BiTE-armed oncolytic adenoviruses generated in this study have been designed to mediate simultaneous killing of cancer cells and TAMs. However, previous work in our laboratory has demonstrated that, at a dose of 100 vg/cell, ascites-associated cancer cells display resistance to EnAd-mediated oncolysis (unpublished work by Dr. Joshua Freedman, Seymour laboratory). We therefore sought to establish a model system in which the ability of EnAd-CMV-BiTE viruses to co-target cancer cells and macrophages could be assessed.

Unpurified ascites cells from one cancer patient ("Patient 16") were seeded at a density of 200,000 cells/well in 96-well plates together with 5,000 DLD-1 colorectal cancer cells. Cells were treated with parental or BiTE-armed EnAd at 100 vg/cell and co-cultured in the presence or absence of ascites fluid (from "Patient 16"; 50% v/v). Five days post-infection, cells were harvested and processed for flow cytometry, staining with anti-CD11b, anti-CD64 and anti-EGFR antibodies, as well as a live/dead stain. All BiTE-armed EnAd viruses, as well as parental EnAd, triggered a significant depletion of $EGFR^+$ cells, reducing the % residual $EGFR^+$ cells to ~20% (Figure 6.14).

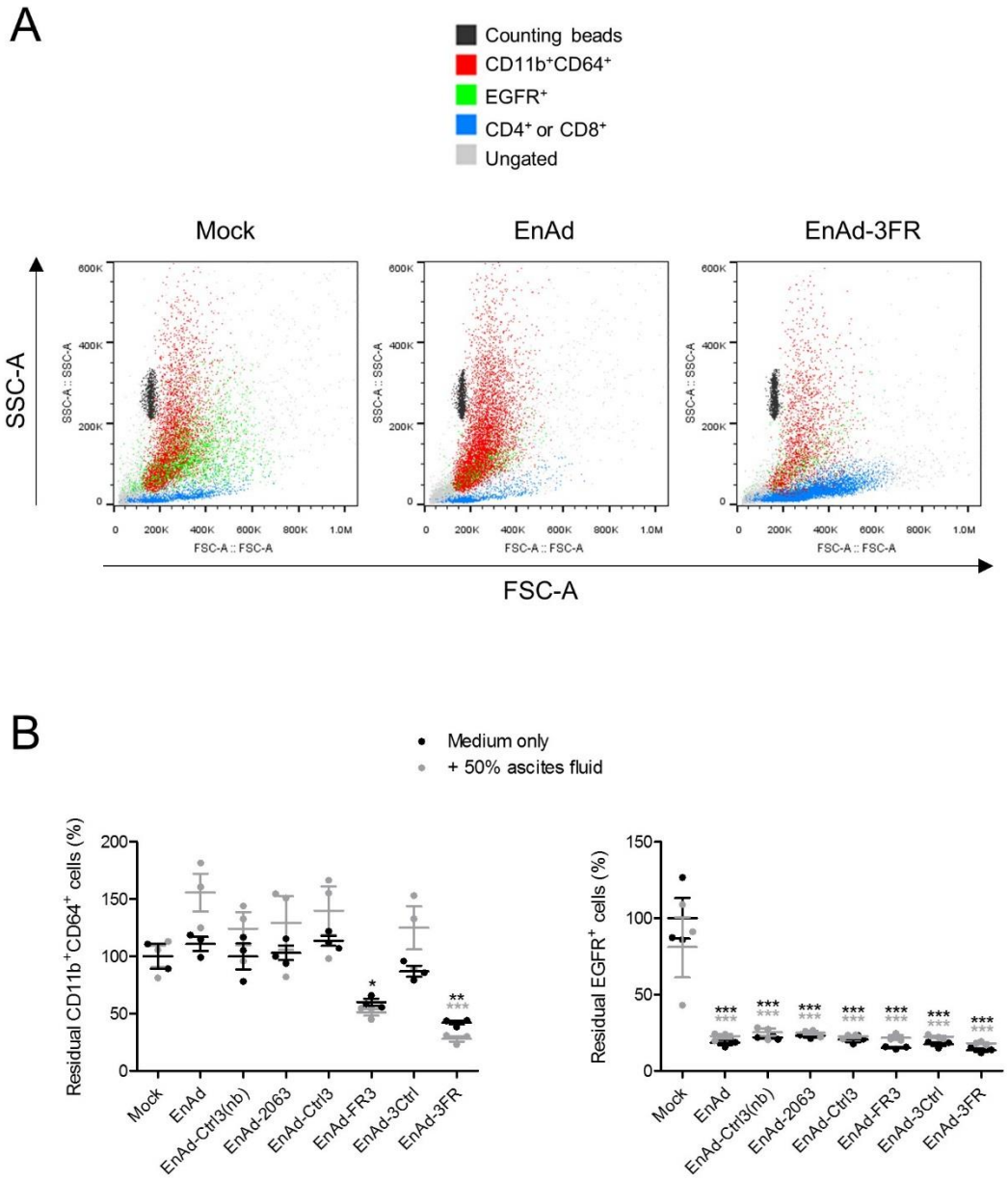

Figure 6.14. EnAd viruses armed with TAM-targeting BiTEs simultaneously deplete cancer cells and endogenous macrophages in a co-culture of whole ascites and DLD-1 tumour cells. (A, B) Whole ascites cells (200,000/well) were co-cultured with DLD-1 colorectal cancer cells (5,000/well) and treated with parental or BiTE-armed EnAd at 100 viral genomes/cell. After five days' co-culture in the presence or absence of autologous ascites fluid (50% v/v), cells were harvested and processed for flow cytometry, staining with anti-CD11b, -CD64 and –EGFR antibodies, as well as a live/dead stain. **(A)** Representative flow cytometric dot plots. **(B)** % Residual cells were calculated relative to "Mock"-treated samples. Data show the mean ± SD of biological triplicates. Statistical significance was assessed by two-way ANOVA followed by Bonferroni post-hoc analysis, with each treatment being compared to "Mock" (*, $P < 0.05$; **, $P < 0.01$; ***, $P < 0.001$).

As anticipated based on previous results, EnAd-CMV-3FR mediated a significant reduction in the numbers of residual $CD11b^+CD64^+$ cells both in medium only and in the presence of ascites fluid (to 38% and 28%, respectively), confirming the ability of this virus to co-target cancer cells and macrophages. In this model, macrophage depletion by EnAd-CMV-FR3 was also substantial, with % residual $CD11b^+CD64^+$ cells reducing to 59% and 51% in the absence and presence of ascites fluid, respectively (Figure 6.14). Together, these data establish the capacity of TAM-targeting BiTE-armed EnAd viruses to effectively co-target cancer cells and macrophages.

6.4 Chapter conclusions

1. The TAM-targeting T cell engagers were successfully expressed by engineered EnAd viruses when under the transcriptional control of an exogenous (CMV) promoter, but not the endogenous major late viral promoter (MLP).
2. A non-functional His-tagged protein of low molecular weight was co-expressed alongside the CD206 and control TriTEs.
3. BiTE/TriTE-armed EnAd viruses retained their oncolytic and replicative capacities.
4. In whole malignant ascites samples, EnAd viruses expressing the 3FR BiTE, but not the FR3 BiTE or CD206 BiTE, induced robust T cell-mediated killing of autologous ascites macrophages, with the remaining macrophages exhibiting a more pro-inflammatory phenotype.
5. 3FR BiTE-armed EnAd mediated simultaneous killing of cancer cells and ascites macrophages in co-cultures of DLD-1 and ascites cells.

6.5 Chapter discussion

Localising the expression of the TAM-targeting T cell engagers to the TME with "armed" OVs should enhance both their safety and efficacy. In this chapter, we engineered EnAd, an oncolytic adenovirus in early-phase clinical trials for solid cancers, to express the TAM-targeting BiTEs and TriTEs under the control of an exogenous (CMV) or endogenous (MLP) promoter. We demonstrated robust CMV-driven BiTE/TriTE expression by the engineered viruses (Figures 6.2 and 6.3), which retained their oncolytic and replicative capabilities (Figure 6.6). On the other hand, BiTE/TriTE expression driven by the viral MLP was undetectable (Figure 6.2). Moreover, although EnAd-expressed CD206 TriTE was functional, it was co-expressed alongside a non-functional fragment of low molecular weight (Figure 6.3 and 6.4).

We therefore proceeded to further evaluate only the EnAd-CMV-BiTE constructs. Using whole human malignant ascites, we demonstrated activation of endogenous T cells and killing of ascites macrophages following treatment with EnAd expressing the 3FR BiTE (and to a lesser extent the FR3 BiTE), but not the CD206 BiTE (Figure 6.7 to 6.11). These findings were consistent with the superior potency of the FRβ-targeting BiTEs against whole ascites samples observed in previous chapters. Interestingly, both parental and BiTE-armed EnAd viruses induced a general increase in pro-inflammatory markers on ascites macrophages (Figure 6.12), which was most pronounced (in 2/3 patient samples) with the FRβ BiTE-armed viruses (Figure 6.13). In co-cultures of whole ascites (from one patient) and DLD-1 cells, FRβ BiTE-armed EnAd mediated killing of both ascites macrophages and cancer cells, highlighting the multi-modal nature of this approach (Figure 6.14). Due to time constraints, we were unable to extend this final experimental model to other patient samples; this undoubtedly represents an area for future study.

The very low/undetectable levels of BiTE/TriTE expression when driven by the MLP was surprising given that the same strategy (with an identical splice acceptor sequence) has been used successfully by our laboratory and others (Freedman et al., 2018; Freedman et al., 2017; Marino et al., 2017). We speculate that our BiTE/TriTE sequences may contain specific, as-yet-unknown elements that interfere with the alternate splicing necessary for transgene expression by the MLP. Another issue that arose during this study was the appearance of non-functional His-tagged fragments of the TriTEs when expressed by EnAd (Figures 6.3 and 6.4). With a molecular weight equivalent to that of a single scFv (~30 kDa), these fragments most likely represent the products of recombination between the two DNA sequences encoding anti-CD3 scFv, which were identical. Indeed, most viruses (including adenoviruses (Robinson et al., 2013)) display a high propensity for homologous recombination as a means to enhance their genetic diversity. We anticipate that this problem will be overcome through alternations in the codon sequences of one of the anti-CD3 scFvs. Due to time constraints, we were unable to explore this hypothesis further.

Possible variability in the quantity and timing of BiTE production by virus infected cells makes direct comparisons between the efficacies of free- and virally-produced BiTE challenging. Nevertheless, it is interesting to note that the average fold-increase in M1 marker expression induced by the FRβ BiTE-armed viruses (1.70- and 1.38-fold for EnAd-FR3 and EnAd-3FR, respectively), was slightly higher than that of the free BiTEs (1.38 and 1.33 fold for FR3 and 3FR BiTEs, respectively), perhaps suggesting an additive or synergistic effect of EnAd and FRβ BiTE treatment on macrophage polarisation. Supporting this assertion is the previous finding by Freedman et al. that FAP BiTE armed virus, and not FAP BiTE or virus alone, triggered a significant increase in M1 marker CD86 (Freedman et

al., 2018), as well as the inherent immune stimulatory properties of EnAd (Dyer et al., 2017).

Together, this chapter provides a proof-of-concept for virally-mediated expression of the TAM-targeting BiTEs. The most promising (FRβ-targeting) BiTEs were successfully expressed by engineered EnAd without compromising its ability to replicate or kill cancer cells. FRβ BiTE-expressing EnAd triggered robust activation of ascites T cells, leading to a reduction in the number of ascites macrophages and a pro-inflammatory repolarisation of remaining macrophages. Thus, we have developed a powerful multi-mechanistic strategy which combines direct anti-cancer activity with a reduction in immunosuppressive TAMs.

7 Final Conclusions and Discussion

7.1 Overview of the Thesis

Immunosuppressive stromal cells represent critical obstacles to the success of solid tumour immunotherapy (Anderson et al., 2017). Key among these are TAMs, a diverse population of immune cells which promote angiogenesis, metastasis and immunosuppression (Mantovani et al., 2017). Most TAMs resemble M2-like macrophages, with tissue healing and/or immunoregulatory characteristics. Nevertheless, TAMs can also display features of M1-like macrophages (Reinartz et al., 2014), which carry out tumouricidal functions and promote Th1 immune responses (Mantovani et al., 2004). Consequently, the ratio of M2-to M1-like TAMs, and not total TAM numbers, is often an indicator of poor patient prognosis (Cui et al., 2013; Herwig et al., 2013; Lan et al., 2013; Le Page et al., 2012; Ma et al., 2010; Zhang et al., 2011; Zhang et al., 2014).

Selectively depleting cancer-supporting TAM subsets, whilst sparing those with anti-tumour potential, is a highly desirable goal (Yang et al., 2018). In this thesis, we have explored strategies to redirect T cell cytotoxicity towards cancer-promoting (M2-like) TAMs with engineered T cell engagers. Novel BiTEs targeting M2 macrophage markers CD206 and FRβ were generated and characterised initially in healthy PBMC-based models comprising macrophages and autologous T cells (Chapter 3). The CD206- and FRβ-targeting BiTEs triggered robust T cell-mediated cytotoxicity of M2- but not M1-polarised macrophages, demonstrating the feasibility of harnessing BiTEs to target cells with high but not low antigen levels. Crucially, this work was the first to demonstrate susceptibility of macrophages to BiTE-induced T cell-mediated killing of macrophages – a not entirely

expected finding given the reported privilege of macrophages from T cell-mediated cytotoxicity.

To increase the clinical relevance of the PBMC-based model, these experiments were repeated in the presence of acellular ascites fluid from patients with advanced metastatic cancer. Such fluids are abundant in immunomodulatory cytokines and serve to recapitulate features of the TME. In this more challenging model, the activity of the CD206- but not FRβ-targeting BiTE was greatly diminished. The next section of the thesis thus concerned the optimisation of CD206-targeting T cell engagers (Chapter 4) to improve their activity in challenging conditions.

Methods to improve the activity of immune cell engagers such as BiTEs are under intensive investigation (Husain and Ellerman, 2018). One such strategy involves the generation of multi-specific antibodies, with the aim of improving: i) tumour targeting (e.g. with two arms binding tumour cell target and/or ii) efficacy (e.g. binding two effector cell antigens. In Chapter 4, novel TriTEs were engineered, comprising the parental CD206 BiTE joined to an additional anti-CD3 or anti-CD28 domain. From this work, a bi-valent CD3-binding TriTE – the first of its kind - emerged as a promising candidate, capable of inducing T cell activation and killing of macrophages even in the presence of suppressive ascites fluids. The bi-valent anti-CD3 TriTE largely retained its selectivity for $CD206^{high}$ cells, though a degree of non-specific activation was observed. On the other hand, an anti-CD28-containing TriTE (as well as its matched control TriTE) elicited potent non-specific T cell activation, and further development of this construct was not explored.

As well as immunosuppressive soluble factors, malignant ascites typically contains a range of cancerous and non-cancerous cells which together form a tumour-like microenvironment (Ahmed and Stenvers, 2013). Whole, unsorted ascites samples

therefore offer a unique, fully human test system in which the efficacy of immunotherapies such as BiTEs can be explored. In Chapter 5, the activities of the CD206 BiTE/TriTE and FRβ-targeting BiTEs in whole ascites models were assessed. Though the CD206 TriTE (and not the CD206 BiTE) triggered endogenous T cell-mediated killing of ascites macrophages when cultured in medium alone, addition of autologous ascites abrogated its activity. Moreover, its effects were not entirely antigen-specific, as a reduction in macrophages (in medium only) was also observed upon treatment with the control TriTE. By contrast, the FRβ-targeting BiTEs, and not their matched controls, mediated powerful T cell activation and killing of ascites macrophages despite the immunosuppressed nature of these samples. Strikingly, remaining macrophages exhibited increased expression of M1-like macrophage markers, suggesting a shift in the ascites microenvironment towards a more inflammatory state.

The presence of CD206 and FRβ on some non-tumour tissues necessitates tumour-restricted delivery of the TAM-targeting BiTEs. A powerful strategy to localise biologic expression to the TMEs involves the use of "armed" oncolytic viruses, which mediate transgene expression by cancer cells as the virus replicates selectively within them. In the final results section (Chapter 6), an oncolytic adenovirus in early-phase clinical trials, EnAd, was engineered to express the TAM-targeting BiTEs/TriTEs under the control of an endogenous late viral promoter (MLP, linked to viral replication) or an exogenous promoter (CMV, constitutively active). Unexpectedly, BiTE/TriTE expression was detectable only in the supernatants of cells infected with CMV-driven viral constructs. Moreover, TriTEs were expressed alongside a non-functional protein of low molecular weight, suggesting recombination of the two anti-CD3 domains. Nevertheless, to provide a proof-of-concept for our approach, we proceeded to assess the activities of EnAd expressing the CD206 and FRβ BiTEs under the control of CMV.

CD206- and FRβ BiTE-armed EnAd viruses retained their oncolytic and replicative capacities whilst mediating robust BiTE expression and secretion from infected cancer cells. In whole ascites models, EnAd expressing the most promising BiTE candidate (3FR BiTE) triggered a robust T cell-mediated reduction in ascites macrophages, with remaining macrophages exhibiting a more M1-like phenotype. Moreover, in a co-culture of DLD-1 tumour cells and whole unsorted ascites cells, EnAd-CMV-3FR mediated concomitant killing of cancer cells and ascites macrophages, highlighting the multi-modal nature of this approach.

7.2 Final Discussion

Targeting cancer-promoting TAMs with BiTE-armed OVs represents a powerful strategy to reverse microenvironmental immunosuppression and simultaneously deplete cancer cells. This approach offers the potential for synergy through several mechanisms. Clinical experience with OVs including EnAd has revealed increased T cell infiltration of tumours following virus treatment (Boni et al., 2014; Garcia-Carbonero et al., 2017; Heinzerling et al., 2005; Kaufman et al., 2010; Mastrangelo et al., 1999; Sahin et al., 2012). A greater availability of intratumoural T cells may foreseeably enhance the efficacy of the BiTE by increasing the E:T ratio. On the other hand, BiTEs may at least temporarily redirect anti-viral T cells away from virus infected cells, facilitating greater viral spread (Scott et al., 2018). Of note, a similar strategy, in which EnAd is armed with a FAP-targeting BiTE and cytokines (NG-641), was recently approved for evaluation in a phase I trial involving patients with advanced epithelial tumours (NCT04053283), highlighting the feasibility of this approach.

The impact of TAM removal on OV therapy is difficult to predict (reviewed in (Denton et al., 2016)); however, several studies suggest an improvement in OV efficacy following TAM

depleting therapies. Treatment of glioma-bearing nude mice with cyclophosphamide, an immunomodulatory chemotherapeutic agent, enhanced the replication of an oncolytic adenovirus, as well as prolonging virus mediated transgene expression. This effect was associated with a marked reduction in intratumoural $CD68^+$ cells (Lamfers et al., 2006). In a more macrophage-targeted approach, clodronate liposomes (either delivered systemically to glioma-bearing mice or *ex vivo* in glioma slice models) increased the titres of an HSV-derived OV over five-fold (Fulci et al., 2007). Possible factors leading to improved OV titres after macrophage depletion include a reduction in macrophage-mediated phagocytosis of virally-infected cells, a phenomenon demonstrated in co-cultures of primary microglia and HSV-infected U87 glioma cells (Delwar et al., 2018). As expected, HSV entering microglia in this manner did not replicate (Delwar et al., 2018), highlighting the possibility for macrophages to act as "sinks" for OV particles. Depletion of macrophages with clodronate or trabectedin also improved the anti-tumour efficacy of an oncolytic HSV in Ewing's sarcoma xenograft models. In this case, the enhanced efficacy was attributed to a shift in the TME towards a more pro-inflammatory state (Denton et al., 2018).

An important consequence of this treatment strategy may be the activation and expansion of endogenous T cells within tumour deposits. Increasingly, it appears that such TILs can bear selectivity for tumour associated antigens (Lu et al., 2014; Poschke et al., 2016; Topalian et al., 1989). This raises the possibility that BiTE activated/expanded $CD8^+$ TILs will proceed to mediate cytotoxic activity via their own HLA-restricted specificity if concentrations of the BiTE fall sufficiently, perhaps diversifying the anti-cancer effect. Notably, BiTE-driven TIL expansion should occur in the context of OV-mediated immunogenic cell death and TAA release (Guo et al., 2014), increasing the possibility that the cancer-immunity cycle may be reinstated.

On the other hand, BiTE-mediated activation and expansion of different T cell subsets (i.e. other than cytotoxic $CD8^+$ cells) may have undesirable effects. For instance, although BiTEs have the potential to trigger cytolytic activity in Tregs, this will most likely be accompanied by stimulation of their suppressive functions. Indeed, *ex vivo* activation of patient-derived Tregs with blinatumomab (in the presence of $CD19^+$ target cells) triggered their production of IL-10, leading to inhibition of $CD8^+$ T cell proliferation and cytotoxic activity (Duell et al., 2017). In line with this, a high frequency of Tregs in the peripheral blood of patients with relapsed/refractory acute lymphoblastic leukaemia was associated with a low response rate to blinatumomab (Duell et al., 2017). The possible consequences of BiTE-mediated activation of different Th cell subsets (Th1, Th2, Th17) is also an important consideration, with the potential to promote antibody production but also tolerogenic responses. In an attempt to restrict activation to cytotoxic T cells, novel bispecific antibodies recognising CD8 and a TAA have been engineered; however, in the absence of stimulation via CD3 clustering, only pre-activated T cells were successfully redirected with this approach (Michalk et al., 2014). We speculate that a single-chain TriTE, similar in format to our own but comprising both anti-CD8 and anti-CD3 domains, may facilitate preferential activation of cytotoxic $CD8^+$ T cells.

As discussed in Chapter 3, the expression of CD206 and FRβ is not restricted solely to macrophages. Thus, although "on-target off-tumour" side effects of the CD206- and FRβ-targeting BiTEs can be avoided through OV-mediated localisation to the TME, it qis possible that other cells within the tumour will be targeted by these biologics. Most notably, a subset of monocyte-derived DCs has been found to express CD206 at high levels (Collin and Bigley, 2018). Monocyte-derived DCs are potent APCs and inducers of T cell responses, and therefore have the potential to promote anti-tumour immunity (Kuhn et al., 2015). On the other hand, mounting evidence suggests that these DCs are biased by

the TME towards a tolerogenic state in which they induce Tregs (Ramos et al., 2012). The possible consequences of their removal are therefore unclear, and may depend on tumour type/stage. Meanwhile, a subset of peripheral pro-inflammatory monocytes ($CD14^{high}CD16^{-}CCR2^{+}HLA\text{-}DR^{+}$) are positive for FRβ expression (Shen et al., 2014). Whilst their presence in solid tumours is yet to be explored, the reported recruitment of $FR\beta^{+}$ monocytes to sites of inflammation (Shen et al., 2014) suggests a relevance in cancer. Nevertheless, given that overall positivity for CD206 and FRβ, and not just CD206/FRβ positivity within the TAM population (Fan et al., 2019; Kurahara et al., 2012; Ren et al., 2017), is associated with poor patient prognosis, we anticipate that the dominant effect of $CD206^{+}/FR\beta^{+}$ cell removal will be a positive one.

Although beyond the scope of this work, it is important to note that a number of alternative markers of M2-like macrophages and TAMs are available for targeting with BiTEs. These include CD163 and macrophage receptor with collagenous structure (MARCO), both of which are associated with pro-tumour and immunosuppressive TAMs (Kridel et al., 2015; La Fleur et al., 2018). With a greater understanding of the roles of different macrophage subsets within the TME, our flexible strategy may be extended to the rational targeting of other macrophage sub-populations.

Additional areas for future investigation include the mechanism(s) by which the TAM-targeting T cell engagers may activate T cells. Target clustering and CD45 exclusion from the pseudo-immunological synapse has been described for other T cell-engaging bispecific antibodies (Li et al., 2017a; Offner et al., 2006), but whether these findings extend to the TAM-targeting BiTEs/TriTEs remains to be determined. Moreover, whilst this study focused on the downstream effects of T cell activation (CD25 upregulation, IFN-γ production, cytotoxicity), a thorough examination of proximal signalling events (e.g.

phosphorylation of zeta-chain-associated protein kinase 70 (ZAP-70) and linker for activation of T cells (LAT)) induced by the BiTEs/TriTEs could provide valuable insight into factors underlying their different potencies.

It is important to note that the TAM-targeting T cell engagers employed in this study were unpurified, with experiments conducted instead using crude BiTE/TriTE-containing supernatants from transfected HEK293A producer cells. Crucially, such supernatants may contain contaminating aggregated BiTE/TriTE species and/or cellular debris, potentially impacting upon our results. Moreover, BiTEs/TriTEs produced in this manner are less amenable to binding analysis, for instance with surface plasmon resonance, than purified samples, and thus the affinities of the TAM-targeting T cell engagers for their target antigens were not determined. To overcome these limitations, a two-step purification process comprising nickel column chromatography followed by size-exclusion chromatography was attempted during the course of this study; however, resultant yields were so low as to be undetectable by Western blotting analysis (results not shown). Larger-scale BiTE/TriTE production and/or optimisation of the purification methodology may be required in order to obtain sufficient quantities of purified sample for practical use.

Altogether, we foresee that our approach, combining T cell activation, immunosuppressive TAM removal and OV-mediated inflammation, carries the potential to switch immunologically "cold" solid tumours to "hot". Critically, such a conversion may prime tumours for subsequent immune checkpoint blockade. This phenomenon is well-exemplified by striking results from a Phase Ib trial of T-VEC and pembrolizumab, in which response to the combination therapy, unlike pembrolizumab monotherapy, was not associated with baseline $CD8^+$ T cell infiltration or IFN-γ expression (Ribas et al., 2017). Meanwhile, with pre-clinical data demonstrating improved efficacy of checkpoint

blockade upon macrophage depletion (Neubert et al., 2018; Peranzoni et al., 2018), a large number of clinical trials assessing ICIs in combination with anti-TAM agents are underway (NCT02452424, NCT02777710, NCT02880371, NCT02829723, NCT02323191, NCT02760797, NCT02713529, NCT025260170, NCT02807844, NCT02554812). Taken together, these results serve to highlight the great potential of immune conversion with TAM-targeting BiTE-armed OVs as a means to increase patient responsivity to immunotherapy.

7.3 Concluding Remarks

In this thesis, we have generated novel bi- and tri-valent T cell engagers capable of redirecting endogenous T cell cytotoxicity towards M2-like TAMs. We have engineered an oncolytic adenovirus, EnAd, to express the TAM-targeting T cell engagers without compromising its oncolytic activity, yielding a multi-pronged therapeutic modality to simultaneously target cancer cells and immunosuppressive TAMs. Altogether, we foresee that removal of cancer-promoting TAMs, combined with the immune-stimulatory effects of BiTEs and OVs, will provide a powerful therapeutic approach for removing barriers to anti-tumour immunity in patients with cancer.

Appendix I: Materials

Buffer	Application	Recipe
TAE buffer (50x)	Agarose gel electrophoresis	242 g Tris, 100 mL 0.5 M EDTA and 57.1 mL Glacial Acetic Acid in 1 L H2O
Running buffer (10x)	Western blotting	19.8 g Tris, 86.4 g glycine, 6 g SDS, deionised H2O to 1 L
Transfer buffer (10x)	Western blotting	30.29 g Tris, 144 g glycine, deionised H2O to 1 L
MACS buffer	Flow cytometry	0.5% BSA, 2 mM EDTA in PBS
1.32ρ Caesium Chloride	Adenovirus banding	192 g CsCl, 367.2 mL of distilled H2O, 40.8 mL of 0.5 M Tris-HCl (pH 7.9).
1.45ρ Caesium Chloride	Adenovirus banding	307.5g CsCl, 387 mL of distilled H2O, 43.5 mL of 0.5 M Tris-HCl (pH 7.9).
40% glycerol	Adenovirus banding	165 mL glycerol, 10 mL of 0.5M Tris-HCl (pH 7.9), 2.5 mL of 0.2 M EDTA (pH 8.0), made up to 500 mL using dH2O.
n-butanol	Adenovirus banding	20 mL of n-butanol is added to 20mls of distilled H2O; once the solution has settled, the top layer is water-saturated n-butanol
TE buffer	Picogreen assay	5 mL of 1 M Tris-HCl pH 8, 1 mL of 0.5 M EDTA (pH 8.0), made up to 500 mL using dH2O

BSA, bovine serum albumin; EDTA, ethylenediaminetetraacetic acid; PBS, phosphate buffered saline

Appendix II: DNA and amino acid sequences

Signal peptide (amino acid sequence)

MGWSCIILFLVATATGVHS

Signal peptide (DNA sequence)

ATGGGATGGAGCTGTATCATTCTGTTCTTGGTCGCTACCGCCACAGGAGTACACTCC

His tag (amino acid sequence)

HHHHHHHHHH

His tag (DNA sequence)

CATCACCATCACCATCACCACCATCACCAT

FR3 BiTE (amino acid sequence)

EVQLVQSGAEVKKPGASVKVSCKASGYTFTSYAMHWVRQAPGQRLEWMGWINAGNGNTKY
SQKFQGRVTITRDTSASTAYMELSSLRSEDTAVYYCARDISYGSFDYWGQGTLVTVSSGGGG
SGGGGSGGGGSSSELTQDPAVSVALGQTVRITCQGDSLRSNYANWYQQKPGQAPVLVIYGQ
NNRPSGIPDRFSGSSSGNTASLTITGAQAADEADYYCDSRVSTGNHVVFGGGTKLTVLGGGG
SDVQLVQSGAEVKKPGASVKVSCKASGYTFTRYTMHWVRQAPGQGLEWIGYINPSRGYTNYA
DSVKGRFTITTDKSTSTAYMELSSLRSEDTATYYCARYYDDHYCLDYWGQGTTVTVSSGEGTS
TGSGGSGGSGGADDIVLTQSPATLSLSPGERATLSCRASQSVSYMNWYQQKPGKAPKRWIYD
TSKVASGVPARFSGSGSGTDYSLTNSLEAEDAATYCQQWSSNPLTFGGGTKVEIK

FR3 BiTE (DNA sequence)

GAAGTACAACTCGTTCAGTCCGGTGCAGAGGTTAAAAAGCCCGGCGCGTCCGTGAAAGTA
TCTTGCAAAGCCTCCGGATATACTTTCACATCATATGCTATGCATTGGGTCCGGCAGGCTC
CCGGGCAACGCCTTGAGTGGATGGGGTGGATTAACGCAGGAAATGGAAACACAAAATACT
CACAAAAATTCCAGGGTAGGGTCACAATAACTCGAGATACCTCAGCGTCAACGGCCTACAT
GGAACTTTCCAGTCTCAGAAGTGAGGACACCGCGGTCTATTATTGTGCGAGGGACATATCA
TATGGCAGTTTCGATTATTGGGGGCAAGGGACACTCGTTACCGTTTCATCTGGGGGCGGT
GGATCCGGCGGTGGTGGAAGTGGAGGCGGTGGATCATCCTCAGAACTTACCCAGGACCC
AGCAGTGTCCGTTGCGTTGGGTCAAACCGTAAGGATAACCTGCCAGGGAGATAGCCTGAG
GTCTAACTATGCGAACTGGTATCAACAAAAACCAGGCCAGGCTCCCGTCCTGGTTATATAC
GGACAGAACAACCGGCCATCTGGCATTCCTGACCGATTCAGTGGCTCTTCTTCCGGAAAC
ACTGCGAGCCTCACAATCACTGGGGCGCAAGCTGCCGACGAAGCGGACTATTATTGCGAT
AGCCGCGTTTCCACTGGTAATCACGTGGTTTTTGGGGGCGGTACGAAACTGACCGTTCTC
GGCGGTGGTGGAAGCGATGTGCAACTCGTGCAGTCCGGTGCGGAAGTGAAAAAGCCGGG
CGCGAGCGTCAAAGTGTCATGCAAGGCGTCAGGATATACGTTTACTAGATACACTATGCAC
TGGGTGCGCCAGGCACCTGGTCAGGGCCTTGAATGGATCGGCTACATCAATCCGTCGAGA
GGCTACACTAATTACGCGGACTCAGTCAAAGGGCGCTTCACGATTACGACCGACAAGTCC
ACCTCGACTGCATACATGGAACTGTCCTCGCTGAGAAGCGAGGACACCGCTACTTACTACT
GCGCTAGATACTACGATGATCACTACTGCCTCGATTACTGGGGCCAGGGAACCACTGTCA
CGGTGTCATCGGGAGAGGGCACCTCAACCGGATCAGGGGGATCGGGAGGCTCGGGCGG
CGCAGACGACATCGTCCTGACCCAGTCGCCCGCCACCTTGTCGCTGTCCCCAGGAGAAAG
AGCGACCCTGTCATGCCGGGCGTCGCAAAGCGTGAGCTATATGAATTGGTATCAGCAGAA
GCCAGGAAAGGCGCCGAAGAGATGGATCTACGACACCTCCAAGGTCGCTTCAGGTGTCCC

GGCTAGATTCTCAGGATCGGGATCAGGAACGGACTACTCCCTGACCATCAATTCACTGGAA
GCAGAAGATGCGGCCACCTACTACTGTCAGCAGTGGTCCTCCAACCCGCTGACTTTCGGA
GGCGGAACTAAGGTCGAGATCAAG

3FR BiTE (amino acid sequence)

DVQLVQSGAEVKKPGASVKVSCKASGYTFTRYTMHWVRQAPGQGLEWIGYINPSRGYTNYAD
SVKGRFTITTDKSTSTAYMELSSLRSEDTATYYCARYYDDHYCLDYWGQGTTVTVSSGEGTST
GSGGSGGSGGADDIVLTQSPATLSLSPGERATLSCRASQSVSYMNWYQQKPGKAPKRWIYDT
SKVASGVPARFSGSGSGTDYSLTINSLEAEDAATYYCQQWSSNPLTFGGGTKVEIKGGGGSE
VQLVQSGAEVKKPGASVKVSCKASGYTFTSYAMHWVRQAPGQRLEWMGWINAGNGNTKYS
QKFQGRVTITRDTSASTAYMELSSLRSEDTAVYYCARDISYGSFDYWGQGTLVTVSSGGGGS
GGGGSGGGGSSSELTQDPAVSVALGQTVRITCQGDSLRSNYANWYQQKPGQAPVLVIYGQN
NRPSGIPDRFSGSSSGNTASLTITGAQAADEADYYCDSRVSTGNHVVFGGGTKLTVL

3FR BiTE (DNA sequence)

GATGTGCAACTCGTGCAGTCCGGTGCGGAAGTGAAAAAGCCGGGCGCGAGCGTCAAAGT
GTCATGCAAGGCGTCAGGATATACGTTTACTAGATACACTATGCACTGGGTGCGCCAGGC
ACCTGGTCAGGGCCTTGAATGGATCGGCTACATCAATCCGTCGAGAGGCTACACTAATTAC
GCGGACTCAGTCAAAGGGCGCTTCACGATTACGACCGACAAGTCCACCTCGACTGCATAC
ATGGAACTGTCCTCGCTGAGAAGCGAGGACACCGCTACTTACTACTGCGCTAGATACTAC
GATGATCACTACTGCCTCGATTACTGGGGCCAGGGAACCACTGTCACGGTGTCATCGGGA
GAGGGCACCTCAACCGGATCAGGGGGATCGGGAGGCTCGGGCGGCGCAGACGACATCG
TCCTGACCCAGTCGCCCGCCACCTTGTCGCTGTCCCCAGGAGAAAGAGCGACCCTGTCAT
GCCGGGCGTCGCAAAGCGTGAGCTATATGAATTGGTATCAGCAGAAGCCAGGAAAGGCG
CCGAAGAGATGGATCTACGACACCTCCAAGGTCGCTTCAGGTGTCCCGGCTAGATTCTCA
GGATCGGGATCAGGAACGGACTACTCCCTGACCATCAATTCACTGGAAGCAGAAGATGCG
GCCACCTACTACTGTCAGCAGTGGTCCTCCAACCCGCTGACTTTCGGAGGCGGAACTAAG
GTCGAGATCAAGGGCGGTGGTGGAAGCGAAGTACAACTCGTTCAGTCCGGTGCAGAGGTT
AAAAAGCCCGGCGCGTCCGTGAAAGTATCTTGCAAAGCCTCCGGATATACTTTCACATCAT
ATGCTATGCATTGGGTCCGGCAGGCTCCCGGGCAACGCCTTGAGTGGATGGGGTGGATTA
ACGCAGGAAATGGAAACACAAAATACTCACAAAAATTCCAGGGTAGGGTCACAATAACTCG
AGATACCTCAGCGTCAACGGCCTACATGGAACTTTCCAGTCTCAGAAGTGAGGACACCGC
GGTCTATTATTGTGCGAGGGACATATCATATGGCAGTTTCGATTATTGGGGGCAAGGGACA
CTCGTTACCGTTTCATCTGGGGGCGGTGGATCCGGCGGTGGTGGAAGTGGAGGCGGTGG
ATCATCCTCAGAACTTACCCAGGACCCAGCAGTGTCCGTTGCGTTGGGTCAAACCGTAAG
GATAACCTGCCAGGGAGATAGCCTGAGGTCTAACTATGCGAACTGGTATCAACAAAAACCA
GGCCAGGCTCCCGTCCTGGTTATATACGGACAGAACAACCGGCCATCTGGCATTCCTGAC
CGATTCAGTGGCTCTTCTTCCGGAAACACTGCGAGCCTCACAATCACTGGGGCGCAAGCT
GCCGACGAAGCGGACTATTATTGCGATAGCCGCGTTTCCACTGGTAATCACGTGGTTTTTG
GGGGCGGTACGAAACTGACCGTTCTC

3Ctrl BiTE (amino acid sequence)

DVQLVQSGAEVKKPGASVKVSCKASGYTFTRYTMHWVRQAPGQGLEWIGYINPSRGYTNYAD
SVKGRFTITTDKSTSTAYMELSSLRSEDTATYYCARYYDDHYCLDYWGQGTTVTVSSGEGTST
GSGGSGGSGGADDIVLTQSPATLSLSPGERATLSCRASQSVSYMNWYQQKPGKAPKRWIYDT
SKVASGVPARFSGSGSGTDYSLTINSLEAEDAATYYCQQWSSNPLTFGGGTKVEIKGGGGSEL
DIVMTQAPASLAVSLGQRATISCRASKSVSSSGYNYLHWYQQKPGQPPKLLIYLASNLESGVPA
RFSGSGSGTDFTLNIHPVEEEDAATYYCQHSREFPLTFGAGTKLEIKSSGGGGSGGGGGGSS
RSSLEVQLQQSGPELVKPGASVKISCKTSGYTFTGYTMHWVRQSHGKSLEWIGGINPKNGGII
YNQKFQGKATLTVDKSSSTASMELRSLTSDDSAVYYCARRVYDDYPYYYAMDYWGQGTSVTV
SSAKTTPPSVTS

3Ctrl BiTE (DNA sequence)

GACGTGCAGCTCGTCCAGTCGGGTGCCGAGGTGAAGAAGCCAGGAGCCTCCGTGAAGGT
CTCGTGCAAAGCCAGCGGCTACACTTTTACTAGGTACACTATGCACTGGGTGCGGCAAGC
GCCGGGACAAGGTCTGGAGTGGATCGGATACATCAATCCGTCGCGGGGATACACTAATTA
CGCGGACTCCGTCAAGGGACGGTTTACTATCACTACGGATAAGTCCACTAGCACCGCCTA
CATGGAACTGTCCTCGCTGCGGTCGGAAGACACTGCGACCTACTACTGCGCTAGATATTA
CGATGACCACTACTGCCTCGACTATTGGGGGCAGGGCACTACGGTCACCGTCTCGTCGGG
AGAAGGAACCTCAACTGGATCGGGCGGATCGGGAGGCTCCGGAGGAGCCGACGACATCG
TGCTTACCCAGTCGCCTGCGACCCTGTCCCTGTCCCCAGGAGAGAGAGCGACTCTTTCAT
GCAGGGCTTCCCAATCAGTCTCCTACATGAATTGGTATCAACAAAAACCCGGCAAGGCCCC
GAAACGCTGGATCTACGATACTTCAAAGGTGGCCAGCGGTGTGCCTGCCCGCTTCTCCGG
GTCGGGGTCCGGCACCGATTACTCGTTGACTATCAATAGCCTGGAGGCCGAGGACGCTGC
AACTTACTACTGCCAGCAGTGGTCCTCCAACCCTCTCACCTTCGGAGGCGGGACCAAGGT
GGAAATCAAAGGCGGCGGTGGAAGCGAACTGGACATCGTGATGACCCAGGCACCTGCAT
CACTGGCAGTGAGCCTGGGACAGAGAGCCACCATTTCATGCCGGGCCAGCAAGAGCGTG
TCGTCATCCGGATACAATTATCTGCACTGGTATCAGCAGAAACCAGGACAACCTCCAAAGC
TACTCATCTACCTGGCGTCGAACCTCGAATCGGGCGTCCCAGCTAGATTCTCAGGGAGCG
GTTCGGGAACCGATTTCACCCTGAACATCCACCCTGTGGAGGAGGAAGACGCGGCAACGT
ACTATTGCCAGCATTCCCGCGAGTTCCCTCTCACTTTCGGTGCGGGAACTAAGCTGGAGAT
CAAGTCCAGCGGCGGCGGAGGTAGCGGTGGAGGTGGCGGAGGAAGCTCCCGGTCGTCG
CTGGAGGTGCAGCTGCAACAATCCGGCCCGGAACTGGTCAAGCCAGGCGCATCCGTCAA
GATTTCATGCAAGACCTCGGGGTACACCTTCACCGGGTACACGATGCATTGGGTCAGGCA
GAGCCACGGCAAGTCCCTGGAATGGATCGGAGGAATCAACCCCAAAAACGGCGGCATCAT
CTACAACCAAAAGTTCCAGGGAAAAGCCACTCTGACCGTGGACAAGTCGTCGAGCACGGC
CAGCATGGAGCTGCGGTCCCTCACTTCCGACGACTCAGCCGTGTATTACTGCGCGAGACG
GGTCTACGATGACTACCCATACTACTACGCTATGGACTACTGGGGACAAGGAACCAGCGT
GACCGTCTCATCGGCGAAAACTACTCCGCCGTCGGTGACGTCG

CD206 BiTE (amino acid sequence)

QVQLQESGGGLVQPGGSLRLSCAASGFTLDYYAIGWFRQAPGKEREGISCISYKGGSTTYADS
VKGRFTISKDNAKNTAYLQMNNLKPEDTGIYYCAAGFVCYNYDYWGPGTQVTVSSGGGGSDV
QLVQSGAEVKKPGASVKVSCKASGYTFTRYTMHWVRQAPGQGLEWIGYINPSRGYTNYADSV
KGRFTITTDKSTSTAYMELSSLRSEDTATYYCARYYDDHYCLDYWGQGTTVTVSSGEGTSTGS
GGSGGSGGADDIVLTQSPATLSLSPGERATLSCRASQSVSYMNWYQQKPGKAPKRWIYDTSK
VASGVPARFSGSGSGTDYSLTINSLEAEDAATYYCQQWSSNPLTFGGGTKVEIK

CD206 BiTE (DNA sequence)

CAGGTGCAGCTTCAAGAAAGCGGGGGCGGGCTTGTCCAACCCGGAGGTTCACTTAGACTT
AGCTGTGCGGCCAGTGGCTTTACCCTCGACTATTACGCTATCGGGTGGTTTCGGCAGGCA
CCGGGGAAGGAGCGCGAGGGTATCTCATGCATATCTTATAAAGGCGGGTCCACCACGTAT
GCGGATTCCGTGAAGGGGCGATTCACTATCAGTAAGGATAATGCGAAAAACACTGCTTATC
TCCAGATGAACAACCTGAAGCCGGAGGACACGGGTATTTATTATTGTGCTGCTGGCTTCGT
CTGCTATAACTACGATTACTGGGGGCCAGGAACTCAAGTGACAGTCTCTAGCGGCGGTGG
TGGAAGCGATGTGCAACTCGTGCAGTCCGGTGCGGAAGTGAAAAAGCCGGGCGCGAGCG
TCAAAGTGTCATGCAAGGCGTCAGGATATACGTTTACTAGATACACTATGCACTGGGTGCG
CCAGGCACCTGGTCAGGGCCTTGAATGGATCGGCTACATCAATCCGTCGAGAGGCTACAC
TAATTACGCGGACTCAGTCAAAGGGCGCTTCACGATTACGACCGACAAGTCCACCTCGACT
GCATACATGGAACTGTCCTCGCTGAGAAGCGAGGACACCGCTACTTACTACTGCGCTAGA
TACTACGATGATCACTACTGCCTCGATTACTGGGGCCAGGGAACCACTGTCACGGTGTCAT
CGGGAGAGGGCACCTCAACCGGATCAGGGGGATCGGGAGGCTCGGGCGGCGCAGACGA
CATCGTCCTGACCCAGTCGCCCGCCACCTTGTCGCTGTCCCCAGGAGAAAGAGCGACCCT
GTCATGCCGGGCGTCGCAAAGCGTGAGCTATATGAATTGGTATCAGCAGAAGCCAGGAAA
GGCGCCGAAGAGATGGATCTACGACACCTCCAAGGTCGCTTCAGGTGTCCCGGCTAGATT
CTCAGGATCGGGATCAGGAACGGACTACTCCCTGACCATCAATTCACTGGAAGCAGAAGA
TGCGGCCACCTACTACTGTCAGCAGTGGTCCTCCAACCCGCTGACTTTCGGAGGCGGAAC
TAAGGTCGAGATCAAG

Ctrl(nb) BiTE (amino acid sequence)

EVQLVESGGGLVQAGGSLRLSCAASGRTLSSYRMGWFRQAPGKEREFISTISWNGRSTYYAD
SVKGRFIFSEDNAKNTVYLQMNSLKPEDTAVYYCAAALIGGYYSDVDAWSYWGPGTQVTVSS
GGGGSDVQLVQSGAEVKKPGASVKVSCKASGYTFTRYTMHWVRQAPGQGLEWIGYINPSRG
YTNYADSVKGRFTITTDKSTSTAYMELSSLRSEDTATYYCARYYDDHYCLDYWGQGTTVTVSS
GEGTSTGSGGSGGSGGADDIVLTQSPATLSLSPGERATLSCRASQSVSYMNWYQQKPGKAP
KRWIYDTSKVASGVPARFSGSGSGTDYSLTINSLEAEDAATYYCQQWSSNPLTFGGGTKVEIK

Ctrl(nb) BiTE (DNA sequence)

GAGGTCCAGTTGGTTGAGTCAGGGGGTGGCCTTGTTCAGGCTGGCGGGAGCCTCCGACT
GAGTTGCGCGGCCAGTGGTAGAACTCTGTCTAGTTATCGAATGGGGTGGTTTCGGCAAGC
GCCAGGGAAGGAACGAGAGTTTATCTCCACGATTAGTTGGAACGGGCGCTCTACCTATTAT
GCTGACTCCGTCAAGGGCCGCTTCATATTCAGTGAAGACAATGCAAAGAATACGGTCTATC
TGCAAATGAACAGTCTGAAACCAGAGGACACCGCTGTATACTATTGCGCTGCGGCACTTAT
TGGCGGGTATTATAGCGATGTCGATGCTTGGTCATATTGGGGTCCTGGTACCCAAGTCACT
GTGTCCTCAGGCGGTGGTGGAAGCGATGTGCAACTCGTGCAGTCCGGTGCGGAAGTGAA
AAAGCCGGGCGCGAGCGTCAAAGTGTCATGCAAGGCGTCAGGATATACGTTTACTAGATA
CACTATGCACTGGGTGCGCCAGGCACCTGGTCAGGGCCTTGAATGGATCGGCTACATCAA
TCCGTCGAGAGGCTACACTAATTACGCGGACTCAGTCAAAGGGCGCTTCACGATTACGAC
CGACAAGTCCACCTCGACTGCATACATGGAACTGTCCTCGCTGAGAAGCGAGGACACCGC
TACTTACTACTGCGCTAGATACTACGATGATCACTACTGCCTCGATTACTGGGGCCAGGGA
ACCACTGTCACGGTGTCATCGGGAGAGGGCACCTCAACCGGATCAGGGGGATCGGGAGG
CTCGGGCGGCGCAGACGACATCGTCCTGACCCAGTCGCCCGCCACCTTGTCGCTGTCCC
CAGGAGAAAGAGCGACCCTGTCATGCCGGGCGTCGCAAAGCGTGAGCTATATGAATTGGT
ATCAGCAGAAGCCAGGAAAGGCGCCGAAGAGATGGATCTACGACACCTCCAAGGTCGCTT
CAGGTGTCCCGGCTAGATTCTCAGGATCGGGATCAGGAACGGACTACTCCCTGACCATCA
ATTCACTGGAAGCAGAAGATGCGGCCACCTACTACTGTCAGCAGTGGTCCTCCAACCCGC
TGACTTTCGGAGGCGGAACTAAGGTCGAGATCAAG

20633 TriTE (amino acid sequence)

QVQLQESGGGLVQPGGSLRLSCAASGFTLDYYAIGWFRQAPGKEREGISCISYKGGSTTYADS
VKGRFTISKDNAKNTAYLQMNNLKPEDTGIYYCAAGFVCYNYDYWGPGTQVTVSSGGGGSDV
QLVQSGAEVKKPGASVKVSCKASGYTFTRYTMHWVRQAPGQGLEWIGYINPSRGYTNYADSV
KGRFTITTDKSTSTAYMELSSLRSEDTATYYCARYYDDHYCLDYWGQGTTVTVSSGEGTSTGS
GGSGGSGGADDIVLTQSPATLSLSPGERATLSCRASQSVSYMNWYQQKPGKAPKRWIYDTSK
VASGVPARFSGSGSGTDYSLTINSLEAEDAATYYCQQWSSNPLTFGGGTKVEIKGGGGSDVQ
LVQSGAEVKKPGASVKVSCKASGYTFTRYTMHWVRQAPGQGLEWIGYINPSRGYTNYADSVK
GRFTITTDKSTSTAYMELSSLRSEDTATYYCARYYDDHYCLDYWGQGTTVTVSSGEGTSTGSG
GSGGSGGADDIVLTQSPATLSLSPGERATLSCRASQSVSYMNWYQQKPGKAPKRWIYDTSKV
ASGVPARFSGSGSGTDYSLTINSLEAEDAATYYCQQWSSNPLTFGGGTKVEIK

20633 TriTE (DNA sequence)

CAGGTGCAGCTTCAAGAAAGCGGGGGCGGGCTTGTCCAACCCGGAGGTTCACTTAGACTT
AGCTGTGCGGCCAGTGGCTTTACCCTCGACTATTACGCTATCGGGTGGTTTCGGCAGGCA
CCGGGGAAGGAGCGCGAGGGTATCTCATGCATATCTTATAAAGGCGGGTCCACCACGTAT
GCGGATTCCGTGAAGGGGCGATTCACTATCAGTAAGGATAATGCGAAAAACACTGCTTATC
TCCAGATGAACAACCTGAAGCCGGAGGACACGGGTATTTATTATTGTGCTGCTGGCTTCGT
CTGCTATAACTACGATTACTGGGGGCCAGGAACTCAAGTGACAGTCTCTAGCGGCGGTGG
TGGAAGCGATGTGCAACTCGTGCAGTCCGGTGCGGAAGTGAAAAAGCCGGGCGCGAGCG
TCAAAGTGTCATGCAAGGCGTCAGGATATACGTTTACTAGATACACTATGCACTGGGTGCG
CCAGGCACCTGGTCAGGGCCTTGAATGGATCGGCTACATCAATCCGTCGAGAGGCTACAC
TAATTACGCGGACTCAGTCAAAGGGCGCTTCACGATTACGACCGACAAGTCCACCTCGACT

GCATACATGGAACTGTCCTCGCTGAGAAGCGAGGACACCGCTACTTACTACTGCGCTAGA
TACTACGATGATCACTACTGCCTCGATTACTGGGGCCAGGGAACCACTGTCACGGTGTCAT
CGGGAGAGGGCACCTCAACCGGATCAGGGGGATCGGGAGGCTCGGGCGGCGCAGACGA
CATCGTCCTGACCCAGTCGCCCGCCACCTTGTCGCTGTCCCCAGGAGAAAGAGCGACCCT
GTCATGCCGGGCGTCGCAAAGCGTGAGCTATATGAATTGGTATCAGCAGAAGCCAGGAAA
GGCGCCGAAGAGATGGATCTACGACACCTCCAAGGTCGCTTCAGGTGTCCCGGCTAGATT
CTCAGGATCGGGATCAGGAACGGACTACTCCCTGACCATCAATTCACTGGAAGCAGAAGA
TGCGGCCACCTACTACTGTCAGCAGTGGTCCTCCAACCCGCTGACTTTCGGAGGCGGAAC
TAAGGTCGAGATCAAGGGCGGTGGTGGAAGCGATGTGCAACTCGTGCAGTCCGGTGCGG
AAGTGAAAAAGCCGGGCGCGAGCGTCAAAGTGTCATGCAAGGCGTCAGGATATACGTTTA
CTAGATACACTATGCACTGGGTGCGCCAGGCACCTGGTCAGGGCCTTGAATGGATCGGCT
ACATCAATCCGTCGAGAGGCTACACTAATTACGCGGACTCAGTCAAAGGGCGCTTCACGAT
TACGACCGACAAGTCCACCTCGACTGCATACATGGAACTGTCCTCGCTGAGAAGCGAGGA
CACCGCTACTTACTACTGCGCTAGATACTACGATGATCACTACTGCCTCGATTACTGGGGC
CAGGGAACCACTGTCACGGTGTCATCGGGAGAGGGCACCTCAACCGGATCAGGGGGATC
GGGAGGCTCGGGCGGCGCAGACGACATCGTCCTGACCCAGTCGCCCGCCACCTTGTCGC
TGTCCCCAGGAGAAAGAGCGACCCTGTCATGCCGGGGTCGCAAAGCGTGAGCTATATGAA
TTGGTATCAGCAGAAGCCAGGAAAGGCGCCGAAGAGATGGATCTACGACACCTCCAAGGT
CGCTTCAGGTGTCCCGGCTAGATTCTCAGGATCGGGATCAGGAACGGACTACTCCCTGAC
CATCAATTCACTGGAAGCAGAAGATGCGGCCACCTACTACTGTCAGCAGTGGTCCTCCAAC
CCGCTGACTTTCGGAGGCGGAACTAAGGTCGAGATCAAG

32063 TriTE (amino acid sequence)

DVQLVQSGAEVKKPGASVKVSCKASGYTFTRYTMHWVRQAPGQGLEWIGYINPSRGYTNYAD
SVKGRFTITTDKSTSTAYMELSSLRSEDTATYYCARYYDDHYCLDYWGQGTTVTVSSGEGTST
GSGGSGGSGGADDIVLTQSPATLSLSPGERATLSCRASQSVSYMNWYQQKPGKAPKRWIYDT
SKVASGVPARFSGSGSGTDYSLTINSLEAEDAATYYCQQWSSNPLTFGGGTKVEIKGGGGSQ
VQLQESGGGLVQPGGSLRLSCAASGFTLDYYAIGWFRQAPGKEREGISCISYKGGSTTYADSV
KGRFTISKDNAKNTAYLQMNNLKPEDTGIYYCAAGFVCYNYDYWGPGTQVTVSSGGGGSDVQ
LVQSGAEVKKPGASVKVSCKASGYTFTRYTMHWVRQAPGQGLEWIGYINPSRGYTNYADSVK
GRFTITTDKSTSTAYMELSSLRSEDTATYYCARYYDDHYCLDYWGQGTTVTVSSGEGTSTGSG
GSGGSGGADDIVLTQSPATLSLSPGERATLSCRASQSVSYMNWYQQKPGKAPKRWIYDTSKV
ASGVPARFSGSGSGTDYSLTINSLEAEDAATYYCQQWSSNPLTFGGGTKVEIK

32063 TriTE (DNA sequence)

GATGTGCAACTCGTGCAGTCCGGTGCGGAAGTGAAAAAGCCGGGCGCGAGCGTCAAAGT
GTCATGCAAGGCGTCAGGATATACGTTTACTAGATACACTATGCACTGGGTGCGCCAGGC
ACCTGGTCAGGGCCTTGAATGGATCGGCTACATCAATCCGTCGAGAGGCTACACTAATTAC
GCGGACTCAGTCAAAGGGCGCTTCACGATTACGACCGACAAGTCCACCTCGACTGCATAC
ATGGAACTGTCCTCGCTGAGAAGCGAGGACACCGCTACTTACTACTGCGCTAGATACTAC
GATGATCACTACTGCCTCGATTACTGGGGCCAGGGAACCACTGTCACGGTGTCATCGGGA
GAGGGCACCTCAACCGGATCAGGGGGATCGGGAGGCTCGGGCGGCGCAGACGACATCG
TCCTGACCCAGTCGCCCGCCACCTTGTCGCTGTCCCCAGGAGAAAGAGCGACCCTGTCAT
GCCGGGCGTCGCAAAGCGTGAGCTATATGAATTGGTATCAGCAGAAGCCAGGAAAGGCG
CCGAAGAGATGGATCTACGACACCTCCAAGGTCGCTTCAGGTGTCCCGGCTAGATTCTCA
GGATCGGGATCAGGAACGGACTACTCCCTGACCATCAATTCACTGGAAGCAGAAGATGCG
GCCACCTACTACTGTCAGCAGTGGTCCTCCAACCCGCTGACTTTCGGAGGCGGAACTAAG
GTCGAGATCAAGGGCGGTGGTGGAAGCCAGGTGCAGCTTCAAGAAAGCGGGGGCGGGCT
TGTCCAACCCGGAGGTTCACTTAGACTTAGCTGTGCGGCCAGTGGCTTTACCCTCGACTAT
TACGCTATCGGGTGGTTTCGGCAGGCACCGGGGAAGGAGCGCGAGGGTATCTCATGCAT
ATCTTATAAAGGCGGGTCCACCACGTATGCGGATTCCGTGAAGGGGCGATTCACTATCAGT
AAGGATAATGCGAAAAACACTGCTTATCTCCAGATGAACAACCTGAAGCCGGAGGACACG
GGTATTTATTATTGTGCTGCTGGCTTCGTCTGCTATAACTACGATTACTGGGGGCCAGGAA
CTCAAGTGACAGTCTCTAGCGGCGGTGGTGGAAGCGATGTGCAACTCGTGCAGTCCGGTG
CGGAAGTGAAAAAGCCGGGCGCGAGCGTCAAAGTGTCATGCAAGGCGTCAGGATATACGT

TTACTAGATACACTATGCACTGGGTGCGCCAGGCACCTGGTCAGGGCCTTGAATGGATCG
GCTACATCAATCCGTCGAGAGGCTACACTAATTACGCGGACTCAGTCAAAGGGCGCTTCA
CGATTACGACCGACAAGTCCACCTCGACTGCATACATGGAACTGTCCTCGCTGAGAAGCG
AGGACACCGCTACTTACTACTGCGCTAGATACTACGATGATCACTACTGCCTCGATTACTG
GGGCCAGGGAACCACTGTCACGGTGTCATCGGGAGAGGGCACCTCAACCGGATCAGGGG
GATCGGGAGGCTCGGGCGGCGCAGACGACATCGTCCTGACCCAGTCGCCCGCCACCTTG
TCGCTGTCCCCAGGAGAAAGAGCGACCCTGTCATGCCGGGCGTCGCAAAGCGTGAGCTA
TATGAATTGGTATCAGCAGAAGCCAGGAAAGGCGCCGAAGAGATGGATCTACGACACCTC
CAAGGTCGCTTCAGGTGTCCCGGCTAGATTCTCAGGATCGGGATCAGGAACGGACTACTC
CCTGACCATCAATTCACTGGAAGCAGAAGATGCGGCCACCTACTACTGTCAGCAGTGGTC
CTCCAACCCGCTGACTTTCGGAGGCGGAACTAAGGTCGAGATCAAG

206328 TriTE (amino acid sequence)

QVQLQESGGGLVQPGGSLRLSCAASGFTLDYYAIGWFRQAPGKEREGISCISYKGGSTTYADS
VKGRFTISKDNAKNTAYLQMNNLKPEDTGIYYCAAGFVCYNYDYWGPGTQVTVSSGGGGSDV
QLVQSGAEVKKPGASVKVSCKASGYTFTRYTMHWVRQAPGQGLEWIGYINPSRGYTNYADSV
KGRFTITTDKSTSTAYMELSSLRSEDTATYYCARYYDDHYCLDYWGQGTTVTVSSGEGTSTGS
GGSGGSGGADDIVLTQSPATLSLSPGERATLSCRASQSVSYMNWYQQKPGKAPKRWIYDTSK
VASGVPARFSGSGSGTDYSLTINSLEAEDAATYYCQQWSSNPLTFGGGTKVEIKGGGGSDIEL
TQSPASLAVSLGQRATISCRASESVEYYVTSLMQWYQQKPGQPPKLLIFAASNVESGVPARFS
GSGSGTNFSLNIHPVDEDDVAMYFCQQSRKVPYTFGGGTKLEIKRGGGGSGGGGSGGGGSQ
VKLQQSGPGLVTPSQSLSITCTVSGFSLSDYGVHWVRQSPGQGLEWLGVIWAGGGTNYNSAL
MSRKSISKDNSKSQVFLKMNSLQADDTAVYYCARDKGYSYYYSMDYWGQGTTVTVSS

206328 TriTE (DNA sequence)

CAGGTGCAGCTTCAAGAAAGCGGGGGCGGGCTTGTCCAACCCGGAGGTTCACTTAGACTT
AGCTGTGCGGCCAGTGGCTTTACCCTCGACTATTACGCTATCGGGTGGTTTCGGCAGGCA
CCGGGGAAGGAGCGCGAGGGTATCTCATGCATATCTTATAAAGGCGGGTCCACCACGTAT
GCGGATTCCGTGAAGGGGCGATTCACTATCAGTAAGGATAATGCGAAAAACACTGCTTATC
TCCAGATGAACAACCTGAAGCCGGAGGACACGGGTATTTATTATTGTGCTGCTGGCTTCGT
CTGCTATAACTACGATTACTGGGGGCCAGGAACTCAAGTGACAGTCTCTAGCGGCGGTGG
TGGAAGCGATGTGCAACTCGTGCAGTCCGGTGCGGAAGTGAAAAAGCCGGGCGCGAGCG
TCAAAGTGTCATGCAAGGCGTCAGGATATACGTTTACTAGATACACTATGCACTGGGTGCG
CCAGGCACCTGGTCAGGGCCTTGAATGGATCGGCTACATCAATCCGTCGAGAGGCTACAC
TAATTACGCGGACTCAGTCAAAGGGCGCTTCACGATTACGACCGACAAGTCCACCTCGACT
GCATACATGGAACTGTCCTCGCTGAGAAGCGAGGACACCGCTACTTACTACTGCGCTAGA
TACTACGATGATCACTACTGCCTCGATTACTGGGGCCAGGGAACCACTGTCACGGTGTCAT
CGGGAGAGGGCACCTCAACCGGATCAGGGGGATCGGGAGGCTCGGGCGGCGCAGACGA
CATCGTCCTGACCCAGTCGCCCGCCACCTTGTCGCTGTCCCCAGGAGAAAGAGCGACCCT
GTCATGCCGGGCGTCGCAAAGCGTGAGCTATATGAATTGGTATCAGCAGAAGCCAGGAAA
GGCGCCGAAGAGATGGATCTACGACACCTCCAAGGTCGCTTCAGGTGTCCCGGCTAGATT
CTCAGGATCGGGATCAGGAACGGACTACTCCCTGACCATCAATTCACTGGAAGCAGAAGA
TGCGGCCACCTACTACTGTCAGCAGTGGTCCTCCAACCCGCTGACTTTCGGAGGCGGAAC
TAAGGTCGAGATCAAGGGCGGTGGTGGAAGCGACATCGAGCTCACTCAGTCTCCAGCTTC
TTTGGCTGTGTCTCTAGGGCAGAGAGCCACCATCTCCTGCAGAGCCAGTGAGAGTGTTGA
ATATTATGTCACAAGTTTAATGCAGTGGTACCAGCAGAAGCCAGGACAGCCACCCAAACTC
CTCATCTTTGCTGCATCCAACGTAGAATCTGGGGTCCCTGCCAGGTTTAGTGGCAGTGGGT
CTGGGACAAACTTCAGCCTCAACATCCATCCTGTGGACGAGGATGATGTTGCAATGTATTT
CTGTCAGCAAAGTAGGAAGGTTCCTTACACGTTCGGAGGGGGGACCAAGCTGGAAATAAA
ACGGGGAGGCGGCGGTTCTGGCGGTGGCGGATCAGGTGGCGGAGGCTCGCAGGTGAAA
CTGCAGCAGTCTGGACCTGGCCTGGTGACGCCCTCACAGAGCCTGTCCATCACTTGTACT
GTCTCTGGGTTTTCATTAAGCGACTATGGTGTTCACTGGGTTCGCCAGTCTCCAGGACAGG
GACTGGAGTGGCTGGGAGTAATATGGGCTGGTGGAGGCACGAATTATAATTCGGCTCTCA
TGTCCAGAAAGAGCATCAGCAAAGACAACTCCAAGAGCCAAGTTTTCTTAAAAATGAACAG

TCTGCAAGCTGATGACACAGCCGTGTATTACTGTGCCAGAGATAAGGGATACTCCTATTAC
TATTCTATGGACTACTGGGGCCAAGGGACCACGGTCACTGTCTCCTCG

282063 TriTE (amino acid sequence)

DIELTQSPASLAVSLGQRATISCRASESVEYYVTSLMQWYQQKPGQPPKLLIFAASNVESGVPA
RFSGSGSGTNFSLNIHPVDEDDVAMYFCQQSRKVPYTFGGGTKLEIKRGGGGSGGGGSGGG
GSQVKLQQSGPGLVTPSQSLSITCTVSGFSLSDYGVHWVRQSPGQGLEWLGVIWAGGGTNY
NSALMSRKSISKDNSKSQVFLKMNSLQADDTAVYYCARDKGYSYYYSMDYWGQGTTVTVSSG
GGGSQVQLQESGGGLVQPGGSLRLSCAASGFTLDYYAIGWFRQAPGKEREGISCISYKGGST
TYADSVKGRFTISKDNAKNTAYLQMNNLKPEDTGIYYCAAGFVCYNYDYWGPGTQVTVSSGG
GGSDVQLVQSGAEVKKPGASVKVSCKASGYTFTRYTMHWVRQAPGQGLEWIGYINPSRGYT
NYADSVKGRFTITTDKSTSTAYMELSSLRSEDTATYYCARYYDDHYCLDYWGQGTTVTVSSGE
GTSTGSGGSGGSGGADDIVLTQSPATLSLSPGERATLSCRASQSVSYMNWYQQKPGKAPKR
WIYDTSKVASGVPARFSGSGSGTDYSLTINSLEAEDAATYYCQQWSSNPLTFGGGTKVEIK

282063 TriTE (DNA sequence)

GACATCGAGCTCACTCAGTCTCCAGCTTCTTTGGCTGTGTCTCTAGGGCAGAGAGCCACC
ATCTCCTGCAGAGCCAGTGAGAGTGTTGAATATTATGTCACAAGTTTAATGCAGTGGTACC
AGCAGAAGCCAGGACAGCCACCCAAACTCCTCATCTTTGCTGCATCCAACGTAGAATCTGG
GGTCCCTGCCAGGTTTAGTGGCAGTGGGTCTGGGACAAACTTCAGCCTCAACATCCATCC
TGTGGACGAGGATGATGTTGCAATGTATTTCTGTCAGCAAAGTAGGAAGGTTCCTTACACG
TTCGGAGGGGGGACCAAGCTGGAAATAAAACGGGGAGGCGGCGGTTCTGGCGGTGGCG
GATCAGGTGGCGGAGGCTCGCAGGTGAAACTGCAGCAGTCTGGACCTGGCCTGGTGACG
CCCTCACAGAGCCTGTCCATCACTTGTACTGTCTCTGGGTTTTCATTAAGCGACTATGGTG
TTCACTGGGTTCGCCAGTCTCCAGGACAGGGACTGGAGTGGCTGGGAGTAATATGGGCTG
GTGGAGGCACGAATTATAATTCGGCTCTCATGTCCAGAAAGAGCATCAGCAAAGACAACTC
CAAGAGCCAAGTTTTCTTAAAAATGAACAGTCTGCAAGCTGATGACACAGCCGTGTATTACT
GTGCCAGAGATAAGGGATACTCCTATTACTATTCTATGGACTACTGGGGCCAAGGGACCAC
GGTCACTGTCTCCTCGGGCGGTGGTGGAAGCCAGGTGCAGCTTCAAGAAAGCGGGGGCG
GGCTTGTCCAACCCGGAGGTTCACTTAGACTTAGCTGTGCGGCCAGTGGCTTTACCCTCG
ACTATTACGCTATCGGGTGGTTTCGGCAGGCACCGGGGAAGGAGCGCGAGGGTATCTCAT
GCATATCTTATAAAGGCGGGTCCACCACGTATGCGGATTCCGTGAAGGGGCGATTCACTAT
CAGTAAGGATAATGCGAAAAACACTGCTTATCTCCAGATGAACAACCTGAAGCCGGAGGAC
ACGGGTATTTATTATTGTGCTGCTGGCTTCGTCTGCTATAACTACGATTACTGGGGGCCAG
GAACTCAAGTGACAGTCTCTAGCGGCGGTGGTGGAAGCGATGTGCAACTCGTGCAGTCCG
GTGCGGAAGTGAAAAAGCCGGGCGCGAGCGTCAAAGTGTCATGCAAGGCGTCAGGATAT
ACGTTTACTAGATACACTATGCACTGGGTGCGCCAGGCACCTGGTCAGGGCCTTGAATGG
ATCGGCTACATCAATCCGTCGAGAGGCTACACTAATTACGCGGACTCAGTCAAAGGGCGC
TTCACGATTACGACCGACAAGTCCACCTCGACTGCATACATGGAACTGTCCTCGCTGAGAA
GCGAGGACACCGCTACTTACTACTGCGCTAGATACTACGATGATCACTACTGCCTCGATTA
CTGGGGCCAGGGAACCACTGTCACGGTGTCATCGGGAGAGGGCACCTCAACCGGATCAG
GGGGATCGGGAGGCTCGGGCGGCGCAGACGACATCGTCCTGACCCAGTCGCCCGCCAC
CTTGTCGCTGTCCCCAGGAGAAAGAGCGACCCTGTCATGCCGGGCGTCGCAAAGCGTGA
GCTATATGAATTGGTATCAGCAGAAGCCAGGAAAGGCGCCGAAGAGATGGATCTACGACA
CCTCCAAGGTCGCTTCAGGTGTCCCGGCTAGATTCTCAGGATCGGGATCAGGAACGGACT
ACTCCCTGACCATCAATTCACTGGAAGCAGAAGATGCGGCCACCTACTACTGTCAGCAGTG
GTCCTCCAACCCGCTGACTTTCGGAGGCGGAACTAAGGTCGAGATCAAG

3Ctrl3 TriTE (amino acid sequence)

DIELTQSPASLAVSLGQRATISCRASESVEYYVTSLMQWYQQKPGQPPKLLIFAASNVESGVPA
RFSGSGSGTNFSLNIHPVDEDDVAMYFCQQSRKVPYTFGGGTKLEIKRGGGGSGGGGSGGG
GSQVKLQQSGPGLVTPSQSLSITCTVSGFSLSDYGVHWVRQSPGQGLEWLGVIWAGGGTNY
NSALMSRKSISKDNSKSQVFLKMNSLQADDTAVYYCARDKGYSYYYSMDYWGQGTTVTVSSG
GGGSEVQLVESGGGLVQAGGSLRLSCAASGRTLSSYRMGWFRQAPGKEREFISTISWNGRS

TYYADSVKGRFIFSEDNAKNTVYLQMNSLKPEDTAVYYCAAALIGGYYSDVDAWSYWGPGTQ
VTVSSGGGGSDVQLVQSGAEVKKPGASVKVSCKASGYTFTRYTMHWVRQAPGQGLEWIGYI
NPSRGYTNYADSVKGRFTITTDKSTSTAYMELSSLRSEDTATYYCARYYDDHYCLDYWGQGTT
VTVSSGEGTSTGSGGSGGSGGADDIVLTQSPATLSLSPGERATLSCRASQSVSYMNWYQQKP
GKAPKRWIYDTSKVASGVPARFSGSGSGTDYSLTINSLEAEDAATYYCQQWSSNPLTFGGGT
KVEIK

3Ctrl3 TriTE (DNA sequence)

GACATCGAGCTCACTCAGTCTCCAGCTTCTTTGGCTGTGTCTCTAGGGCAGAGAGCCACC
ATCTCCTGCAGAGCCAGTGAGAGTGTTGAATATTATGTCACAAGTTTAATGCAGTGGTACC
AGCAGAAGCCAGGACAGCCACCCAAACTCCTCATCTTTGCTGCATCCAACGTAGAATCTGG
GGTCCCTGCCAGGTTTAGTGGCAGTGGGTCTGGGACAAACTTCAGCCTCAACATCCATCC
TGTGGACGAGGATGATGTTGCAATGTATTTCTGTCAGCAAAGTAGGAAGGTTCCTTACACG
TTCGGAGGGGGGACCAAGCTGGAAATAAAACGGGGAGGCGGCGGTTCTGGCGGTGGCG
GATCAGGTGGCGGAGGCTCGCAGGTGAAACTGCAGCAGTCTGGACCTGGCCTGGTGACG
CCCTCACAGAGCCTGTCCATCACTTGTACTGTCTCTGGGTTTTCATTAAGCGACTATGGTG
TTCACTGGGTTCGCCAGTCTCCAGGACAGGGACTGGAGTGGCTGGGAGTAATATGGGCTG
GTGGAGGCACGAATTATAATTCGGCTCTCATGTCCAGAAAGAGCATCAGCAAAGACAACTC
CAAGAGCCAAGTTTTCTTAAAAATGAACAGTCTGCAAGCTGATGACACAGCCGTGTATTACT
GTGCCAGAGATAAGGGATACTCCTATTACTATTCTATGGACTACTGGGGCCAAGGGACCAC
GGTCACTGTCTCCTCGGGCGGTGGTGGAAGCGAGGTCCAGTTGGTTGAGTCAGGGGGTG
GCCTTGTTCAGGCTGGCGGGAGCCTCCGACTGAGTTGCGCGGCCAGTGGTAGAACTCTG
TCTAGTTATCGAATGGGGTGGTTTCGGCAAGCGCCAGGGAAGGAACGAGAGTTTATCTCC
ACGATTAGTTGGAACGGGCGCTCTACCTATTATGCTGACTCCGTCAAGGGCCGCTTCATAT
TCAGTGAAGACAATGCAAAGAATACGGTCTATCTGCAAATGAACAGTCTGAAACCAGAGGA
CACCGCTGTATACTATTGCGCTGCGGCACTTATTGGCGGGTATTATAGCGATGTCGATGCT
TGGTCATATTGGGGTCCTGGTACCCAAGTCACTGTGTCCTCAGGCGGTGGTGGAAGCGAT
GTGCAACTCGTGCAGTCCGGTGCGGAAGTGAAAAAGCCGGGCGCGAGCGTCAAAGTGTC
ATGCAAGGCGTCAGGATATACGTTTACTAGATACACTATGCACTGGGTGCGCCAGGCACCT
GGTCAGGGCCTTGAATGGATCGGCTACATCAATCCGTCGAGAGGCTACACTAATTACGCG
GACTCAGTCAAAGGGCGCTTCACGATTACGACCGACAAGTCCACCTCGACTGCATACATG
GAACTGTCCTCGCTGAGAAGCGAGGACACCGCTACTTACTACTGCGCTAGATACTACGAT
GATCACTACTGCCTCGATTACTGGGGCCAGGGAACCACTGTCACGGTGTCATCGGGAGAG
GGCACCTCAACCGGATCAGGGGGATCGGGAGGCTCGGGCGGCGCAGACGACATCGTCCT
GACCCAGTCGCCCGCCACCTTGTCGCTGTCCCCAGGAGAAAGAGCGACCCTGTCATGCC
GGGCGTCGCAAAGCGTGAGCTATATGAATTGGTATCAGCAGAAGCCAGGAAAGGCGCCGA
AGAGATGGATCTACGACACCTCCAAGGTCGCTTCAGGTGTCCCGGCTAGATTCTCAGGAT
CGGGATCAGGAACGGACTACTCCCTGACCATCAATTCACTGGAAGCAGAAGATGCGGCCA
CCTACTACTGTCAGCAGTGGTCCTCCAACCCGCTGACTTTCGGAGGCGGAACTAAGGTCG
AGATCAAG

28Ctrl3 TriTE (amino acid sequence)

DVQLVQSGAEVKKPGASVKVSCKASGYTFTRYTMHWVRQAPGQGLEWIGYINPSRGYTNYAD
SVKGRFTITTDKSTSTAYMELSSLRSEDTATYYCARYYDDHYCLDYWGQGTTVTVSSGEGTST
GSGGSGGSGGADDIVLTQSPATLSLSPGERATLSCRASQSVSYMNWYQQKPGKAPKRWIYDT
SKVASGVPARFSGSGSGTDYSLTINSLEAEDAATYYCQQWSSNPLTFGGGTKVEIKGGGGSE
VQLVESGGGLVQAGGSLRLSCAASGRTLSSYRMGWFRQAPGKEREFISTISWNGRSTYYADS
VKGRFIFSEDNAKNTVYLQMNSLKPEDTAVYYCAAALIGGYYSDVDAWSYWGPGTQVTVSSG
GGGSDVQLVQSGAEVKKPGASVKVSCKASGYTFTRYTMHWVRQAPGQGLEWIGYINPSRGY
TNYADSVKGRFTITTDKSTSTAYMELSSLRSEDTATYYCARYYDDHYCLDYWGQGTTVTVSSG
EGTSTGSGGSGGSGGADDIVLTQSPATLSLSPGERATLSCRASQSVSYMNWYQQKPGKAPK
RWIYDTSKVASGVPARFSGSGSGTDYSLTINSLEAEDAATYYCQQWSSNPLTFGGGTKVEIK

28Ctrl3 TriTE (DNA sequence)

GATGTGCAACTCGTGCAGTCCGGTGCGGAAGTGAAAAAGCCGGGCGCGAGCGTCAAAGT
GTCATGCAAGGCGTCAGGATATACGTTTACTAGATACACTATGCACTGGGTGCGCCAGGC
ACCTGGTCAGGGCCTTGAATGGATCGGCTACATCAATCCGTCGAGAGGCTACACTAATTAC
GCGGACTCAGTCAAAGGGCGCTTCACGATTACGACCGACAAGTCCACCTCGACTGCATAC
ATGGAACTGTCCTCGCTGAGAAGCGAGGACACCGCTACTTACTACTGCGCTAGATACTAC
GATGATCACTACTGCCTCGATTACTGGGGCCAGGGAACCACTGTCACGGTGTCATCGGGA
GAGGGCACCTCAACCGGATCAGGGGGATCGGGAGGCTCGGGCGGCGCAGACGACATCG
TCCTGACCCAGTCGCCCGCCACCTTGTCGCTGTCCCCAGGAGAAAGAGCGACCCTGTCAT
GCCGGGCGTCGCAAAGCGTGAGCTATATGAATTGGTATCAGCAGAAGCCAGGAAAGGCG
CCGAAGAGATGGATCTACGACACCTCCAAGGTCGCTTCAGGTGTCCCGGCTAGATTCTCA
GGATCGGGATCAGGAACGGACTACTCCCTGACCATCAATTCACTGGAAGCAGAAGATGCG
GCCACCTACTACTGTCAGCAGTGGTCCTCCAACCCGCTGACTTTCGGAGGCGGAACTAAG
GTCGAGATCAAGGGCGGTGGTGGAAGCGAGGTCCAGTTGGTTGAGTCAGGGGGTGGCCT
TGTTCAGGCTGGCGGGAGCCTCCGACTGAGTTGCGCGGCCAGTGGTAGAACTCTGTCTAG
TTATCGAATGGGGTGGTTTCGGCAAGCGCCAGGGAAGGAACGAGAGTTTATCTCCACGAT
TAGTTGGAACGGGCGCTCTACCTATTATGCTGACTCCGTCAAGGGCCGCTTCATATTCAGT
GAAGACAATGCAAAGAATACGGTCTATCTGCAAATGAACAGTCTGAAACCAGAGGACACCG
CTGTATACTATTGCGCTGCGGCACTTATTGGCGGGTATTATAGCGATGTCGATGCTTGGTC
ATATTGGGGTCCTGGTACCCAAGTCACTGTGTCCTCAGGCGGTGGTGGAAGCGATGTGCA
ACTCGTGCAGTCCGGTGCGGAAGTGAAAAAGCCGGGCGCGAGCGTCAAAGTGTCATGCA
AGGCGTCAGGATATACGTTTACTAGATACACTATGCACTGGGTGCGCCAGGCACCTGGTC
AGGGCCTTGAATGGATCGGCTACATCAATCCGTCGAGAGGCTACACTAATTACGCGGACT
CAGTCAAAGGGCGCTTCACGATTACGACCGACAAGTCCACCTCGACTGCATACATGGAAC
TGTCCTCGCTGAGAAGCGAGGACACCGCTACTTACTACTGCGCTAGATACTACGATGATCA
CTACTGCCTCGATTACTGGGGCCAGGGAACCACTGTCACGGTGTCATCGGGAGAGGGCA
CCTCAACCGGATCAGGGGGATCGGGAGGCTCGGGCGGCGCAGACGACATCGTCCTGACC
CAGTCGCCCGCCACCTTGTCGCTGTCCCCAGGAGAAAGAGCGACCCTGTCATGCCGGGC
GTCGCAAAGCGTGAGCTATATGAATTGGTATCAGCAGAAGCCAGGAAAGGCGCCGAAGAG
ATGGATCTACGACACCTCCAAGGTCGCTTCAGGTGTCCCGGCTAGATTCTCAGGATCGGG
ATCAGGAACGGACTACTCCCTGACCATCAATTCACTGGAAGCAGAAGATGCGGCCACCTA
CTACTGTCAGCAGTGGTCCTCCAACCCGCTGACTTTCGGAGGCGGAACTAAGGTCGAGAT
CAAG

Appendix III: References

Ahmed, N., and K.L. Stenvers. 2013. Getting to know ovarian cancer ascites: opportunities for targeted therapy-based translational research. *Front Oncol*. 3:256.

Anderson, K.G., I.M. Stromnes, and P.D. Greenberg. 2017. Obstacles Posed by the Tumor Microenvironment to T cell Activity: A Case for Synergistic Therapies. *Cancer Cell*. 31:311-325.

Arakaki, R., T. Yamasaki, T. Kanno, N. Shibasaki, H. Sakamoto, N. Utsunomiya, T. Sumiyoshi, S. Shibuya, T. Tsuruyama, E. Nakamura, O. Ogawa, and T. Kamba. 2016. CCL2 as a potential therapeutic target for clear cell renal cell carcinoma. *Cancer Med*. 5:2920-2933.

Aras, S., and M.R. Zaidi. 2017. TAMeless traitors: macrophages in cancer progression and metastasis. *Br J Cancer*. 117:1583-1591.

Arruebo, M., N. Vilaboa, B. Sáez-Gutierrez, J. Lambea, A. Tres, M. Valladares, and A. González-Fernández. 2011. Assessment of the evolution of cancer treatment therapies. *Cancers (Basel)*. 3:3279-3330.

Arwert, E.N., A.S. Harney, D. Entenberg, Y. Wang, E. Sahai, J.W. Pollard, and J.S. Condeelis. 2018. A Unidirectional Transition from Migratory to Perivascular Macrophage Is Required for Tumor Cell Intravasation. *Cell Rep*. 23:1239-1248.

Bacac, M., T. Fauti, J. Sam, S. Colombetti, T. Weinzierl, D. Ouaret, W. Bodmer, S. Lehmann, T. Hofer, R.J. Hosse, E. Moessner, O. Ast, P. Bruenker, S. Grau-Richards, T. Schaller, A. Seidl, C. Gerdes, M. Perro, V. Nicolini, N. Steinhoff, S. Dudal, S. Neumann, T. von Hirschheydt, C. Jaeger, J. Saro, V. Karanikas, C. Klein, and P. Umaña. 2016. A Novel Carcinoembryonic Antigen T-Cell Bispecific Antibody (CEA TCB) for the Treatment of Solid Tumors. *Clin Cancer Res*. 22:3286-3297.

Bajor, D.L., X. Xu, D.A. Torigian, R. Mick, L.R. Garcia, L.P. Richman, C. Desmarais, K.L. Nathanson, L.M. Schuchter, M. Kalos, and R.H. Vonderheide. 2014. Immune activation and a 9-year ongoing complete remission following CD40 antibody therapy and metastasectomy in a patient with metastatic melanoma. *Cancer Immunol Res*. 2:1051-1058.

Baldan, V., R. Griffiths, R.E. Hawkins, and D.E. Gilham. 2015. Efficient and reproducible generation of tumour-infiltrating lymphocytes for renal cell carcinoma. *Br J Cancer*. 112:1510-1518.

Bancroft, C.C., Z. Chen, G. Dong, J.B. Sunwoo, N. Yeh, C. Park, and C. Van Waes. 2001. Coexpression of proangiogenic factors IL-8 and VEGF by human head and neck squamous cell carcinoma involves coactivation by MEK-MAPK and IKK-NF-kappaB signal pathways. *Clin Cancer Res*. 7:435-442.

Barnett, G.C., C.M. West, A.M. Dunning, R.M. Elliott, C.E. Coles, P.D. Pharoah, and N.G. Burnet. 2009. Normal tissue reactions to radiotherapy: towards tailoring treatment dose by genotype. *Nat Rev Cancer*. 9:134-142.

Baroja, M.L., K. Lorre, F. Van Vaeck, and J.L. Ceuppens. 1989. The anti-T cell monoclonal antibody 9.3 (anti-CD28) provides a helper signal and bypasses the need for accessory cells in T cell activation with immobilized anti-CD3 and mitogens. *Cell Immunol*. 120:205-217.

Bauzon, M., and T. Hermiston. 2014. Armed therapeutic viruses - a disruptive therapy on the horizon of cancer immunotherapy. *Front Immunol*. 5:74.

Bazan-Peregrino, M., C.D. Arvanitis, B. Rifai, L.W. Seymour, and C.C. Coussios. 2012. Ultrasound-induced cavitation enhances the delivery and therapeutic efficacy of an oncolytic virus in an in vitro model. *J Control Release*. 157:235-242.

Beatty, G.L., E.G. Chiorean, M.P. Fishman, B. Saboury, U.R. Teitelbaum, W. Sun, R.D. Huhn, W. Song, D. Li, L.L. Sharp, D.A. Torigian, P.J. O'Dwyer, and R.H. Vonderheide. 2011. CD40 agonists alter tumor stroma and show efficacy against pancreatic carcinoma in mice and humans. *Science*. 331:1612-1616.

Beatty, G.L., D.A. Torigian, E.G. Chiorean, B. Saboury, A. Brothers, A. Alavi, A.B. Troxel, W. Sun, U.R. Teitelbaum, R.H. Vonderheide, and P.J. O'Dwyer. 2013. A phase I study of an agonist CD40 monoclonal antibody (CP-870,893) in combination with gemcitabine in patients with advanced pancreatic ductal adenocarcinoma. *Clin Cancer Res*. 19:6286-6295.

Beghein, E., and J. Gettemans. 2017. Nanobody Technology: A Versatile Toolkit for Microscopic Imaging, Protein-Protein Interaction Analysis, and Protein Function Exploration. *Front Immunol*. 8:771.

Ben-Avi, R., R. Farhi, A. Ben-Nun, M. Gorodner, E. Greenberg, G. Markel, J. Schachter, O. Itzhaki, and M.J. Besser. 2018. Establishment of adoptive cell therapy with tumor infiltrating lymphocytes for non-small cell lung cancer patients. *Cancer Immunol Immunother*. 67:1221-1230.

Benencia, F., M.C. Courrèges, J.R. Conejo-García, A. Mohamed-Hadley, L. Zhang, R.J. Buckanovich, R. Carroll, N. Fraser, and G. Coukos. 2005. HSV oncolytic therapy upregulates interferon-inducible chemokines and recruits immune effector cells in ovarian cancer. *Mol Ther*. 12:789-802.

Besser, M.J., R. Shapira-Frommer, A.J. Treves, D. Zippel, O. Itzhaki, L. Hershkovitz, D. Levy, A. Kubi, E. Hovav, N. Chermoshniuk, B. Shalmon, I. Hardan, R. Catane, G. Markel, S. Apter, A. Ben-Nun, I. Kuchuk, A. Shimoni, A. Nagler, and J. Schachter. 2010. Clinical responses in a phase II study using adoptive transfer of short-term cultured tumor infiltration lymphocytes in metastatic melanoma patients. *Clin Cancer Res*. 16:2646-2655.

Beyersdorf, N., T. Hanke, T. Kerkau, and T. Hünig. 2005. Superagonistic anti-CD28 antibodies: potent activators of regulatory T cells for the therapy of autoimmune diseases. *Ann Rheum Dis*. 64 Suppl 4:iv91-95.

Binnewies, M., E.W. Roberts, K. Kersten, V. Chan, D.F. Fearon, M. Merad, L.M. Coussens, D.I. Gabrilovich, S. Ostrand-Rosenberg, C.C. Hedrick, R.H. Vonderheide, M.J. Pittet, R.K. Jain, W. Zou, T.K. Howcroft, E.C. Woodhouse, R.A. Weinberg, and M.F. Krummel. 2018. Understanding the tumor immune microenvironment (TIME) for effective therapy. *Nat Med*. 24:541-550.

Biswas, S.K., L. Gangi, S. Paul, T. Schioppa, A. Saccani, M. Sironi, B. Bottazzi, A. Doni, B. Vincenzo, F. Pasqualini, L. Vago, M. Nebuloni, A. Mantovani, and A. Sica. 2006. A distinct and unique transcriptional program expressed by tumor-associated macrophages (defective NF-kappaB and enhanced IRF-3/STAT1 activation). *Blood*. 107:2112-2122.

Bluemel, C., S. Hausmann, P. Fluhr, M. Sriskandarajah, W.B. Stallcup, P.A. Baeuerle, and P. Kufer. 2010. Epitope distance to the target cell membrane and antigen size determine the potency of T cell-mediated lysis by BiTE antibodies specific for a large melanoma surface antigen. *Cancer Immunol Immunother*. 59:1197-1209.

Bonapace, L., M.M. Coissieux, J. Wyckoff, K.D. Mertz, Z. Varga, T. Junt, and M. Bentires-Alj. 2014. Cessation of CCL2 inhibition accelerates breast cancer metastasis by promoting angiogenesis. *Nature*. 515:130-133.

Boni, V., F.d.l. Portilla, A. Cubillo, M. Gill-Martin, E. Calvo, R. Salazar, C. Santos, A. Sanchez-Gastaldo, S. Prados, X. Sanjuan, J.M. Bozada, H. Duran, M. Jurado, C. Ellis, S. Alvis, J. Beadle, K. Fisher, C. Blanc, and R.G. Carbonero. 2014. A phase 1 mechanism of action study of intra-tumoural (IT) or intravenous (IV) administration of enadenotucirev, an

oncolytic Ad11/Ad3 chimeric group B adenovirus in colon cancer patients undergoing resection of primary tumour. *Ann Oncol*. 25 (suppl 4):iv368.

Bowman, R.L., F. Klemm, L. Akkari, S.M. Pyonteck, L. Sevenich, D.F. Quail, S. Dhara, K. Simpson, E.E. Gardner, C.A. Iacobuzio-Donahue, C.W. Brennan, V. Tabar, P.H. Gutin, and J.A. Joyce. 2016. Macrophage Ontogeny Underlies Differences in Tumor-Specific Education in Brain Malignancies. *Cell Rep*. 17:2445-2459.

Brentjens, R.J., M.L. Davila, I. Riviere, J. Park, X. Wang, L.G. Cowell, S. Bartido, J. Stefanski, C. Taylor, M. Olszewska, O. Borquez-Ojeda, J. Qu, T. Wasielewska, Q. He, Y. Bernal, I.V. Rijo, C. Hedvat, R. Kobos, K. Curran, P. Steinherz, J. Jurcic, T. Rosenblat, P. Maslak, M. Frattini, and M. Sadelain. 2013. CD19-targeted T cells rapidly induce molecular remissions in adults with chemotherapy-refractory acute lymphoblastic leukemia. *Sci Transl Med*. 5:177ra138.

Brinkmann, U., and R.E. Kontermann. 2017. The making of bispecific antibodies. *MAbs*. 9:182-212.

Brischwein, K., B. Schlereth, B. Guller, C. Steiger, A. Wolf, R. Lutterbuese, S. Offner, M. Locher, T. Urbig, T. Raum, P. Kleindienst, P. Wimberger, R. Kimmig, I. Fichtner, P. Kufer, R. Hofmeister, A.J. da Silva, and P.A. Baeuerle. 2006. MT110: a novel bispecific single-chain antibody construct with high efficacy in eradicating established tumors. *Mol Immunol*. 43:1129-1143.

Brunner, K.W., and C.W. Young. 1965. A METHYLHYDRAZINE DERIVATIVE IN HODGKIN'S DISEASE AND OTHER MALIGNANT NEOPLASMS. THERAPEUTIC AND TOXIC EFFECTS STUDIED IN 51 PATIENTS. *Ann Intern Med*. 63:69-86.

Butowski, N., H. Colman, J.F. De Groot, A.M. Omuro, L. Nayak, P.Y. Wen, T.F. Cloughesy, A. Marimuthu, S. Haidar, A. Perry, J. Huse, J. Phillips, B.L. West,

K.B. Nolop, H.H. Hsu, K.L. Ligon, A.M. Molinaro, and M. Prados. 2016. Orally administered colony stimulating factor 1 receptor inhibitor PLX3397 in recurrent glioblastoma: an Ivy Foundation Early Phase Clinical Trials Consortium phase II study. *Neuro Oncol*. 18:557-564.

Canli, Ö., A.M. Nicolas, J. Gupta, F. Finkelmeier, O. Goncharova, M. Pesic, T. Neumann, D. Horst, M. Löwer, U. Sahin, and F.R. Greten. 2017. Myeloid Cell-Derived Reactive Oxygen Species Induce Epithelial Mutagenesis. *Cancer Cell*. 32:869-883.e865.

Cannarile, M.A., M. Weisser, W. Jacob, A.M. Jegg, C.H. Ries, and D. Rüttinger. 2017. Colony-stimulating factor 1 receptor (CSF1R) inhibitors in cancer therapy. *J Immunother Cancer*. 5:53.

Carlisle, R.C., Y. Di, A.M. Cerny, A.F. Sonnen, R.B. Sim, N.K. Green, V. Subr, K. Ulbrich, R.J. Gilbert, K.D. Fisher, R.W. Finberg, and L.W. Seymour. 2009. Human erythrocytes bind and inactivate type 5 adenovirus by presenting Coxsackie virus-adenovirus receptor and complement receptor 1. *Blood*. 113:1909-1918.

Cassetta, L., and J.W. Pollard. 2018. Targeting macrophages: therapeutic approaches in cancer. *Nat Rev Drug Discov*. 17:887-904.

Cheever, M.A., and C.S. Higano. 2011. PROVENGE (Sipuleucel-T) in prostate cancer: the first FDA-approved therapeutic cancer vaccine. *Clin Cancer Res*. 17:3520-3526.

Chen, D.S., and I. Mellman. 2013. Oncology meets immunology: the cancer-immunity cycle. *Immunity*. 39:1-10.

Chen, L., and D.B. Flies. 2013. Molecular mechanisms of T cell co-stimulation and co-inhibition. *Nat Rev Immunol*. 13:227-242.

Chen, Z., X. Feng, C.J. Herting, V.A. Garcia, K. Nie, W.W. Pong, R. Rasmussen, B. Dwivedi, S. Seby, S.A. Wolf, D.H. Gutmann, and D. Hambardzumyan. 2017. Cellular and Molecular Identity of Tumor-Associated Macrophages in Glioblastoma. *Cancer Res*. 77:2266-2278.

Chesney, J., I. Puzanov, F. Collichio, P. Singh, M.M. Milhem, J. Glaspy, O. Hamid, M. Ross, P. Friedlander, C. Garbe, T.F. Logan, A. Hauschild, C. Lebbé, L. Chen, J.J. Kim, J. Gansert, R.H.I. Andtbacka, and H.L. Kaufman. 2018. Randomized, Open-Label Phase II Study Evaluating the Efficacy and Safety of Talimogene Laherparepvec in Combination With Ipilimumab Versus Ipilimumab Alone in Patients With Advanced, Unresectable Melanoma. *J Clin Oncol*. 36:1658-1667.

Choi, B.D., P.C. Gedeon, J.E. Herndon, G.E. Archer, E.A. Reap, L. Sanchez-Perez, D.A. Mitchell, D.D. Bigner, and J.H. Sampson. 2013a. Human regulatory T cells kill tumor cells through granzyme-dependent cytotoxicity upon retargeting with a bispecific antibody. *Cancer Immunol Res*. 1:163.

Choi, B.D., C.T. Kuan, M. Cai, G.E. Archer, D.A. Mitchell, P.C. Gedeon, L. Sanchez-Perez, I. Pastan, D.D. Bigner, and J.H. Sampson. 2013b. Systemic administration of a bispecific antibody targeting EGFRvIII successfully treats intracerebral glioma. *Proc Natl Acad Sci U S A*. 110:270-275.

Cieslewicz, M., J. Tang, J.L. Yu, H. Cao, M. Zavaljevski, K. Motoyama, A. Lieber, E.W. Raines, and S.H. Pun. 2013. Targeted delivery of proapoptotic peptides to tumor-associated macrophages improves survival. *Proc Natl Acad Sci U S A*. 110:15919-15924.

Clayton, K.L., D.R. Collins, J. Lengieza, M. Ghebremichael, F. Dotiwala, J. Lieberman, and B.D. Walker. 2018. Resistance of HIV-infected macrophages to CD8. *Nat Immunol*. 19:475-486.

Coates, A., S. Abraham, S.B. Kaye, T. Sowerbutts, C. Frewin, R.M. Fox, and M.H. Tattersall. 1983. On the receiving end--patient perception of the side-effects of cancer chemotherapy. *Eur J Cancer Clin Oncol*. 19:203-208.

Colegio, O.R., N.Q. Chu, A.L. Szabo, T. Chu, A.M. Rhebergen, V. Jairam, N. Cyrus, C.E. Brokowski, S.C. Eisenbarth, G.M. Phillips, G.W. Cline, A.J. Phillips, and R. Medzhitov. 2014. Functional polarization of tumour-associated macrophages by tumour-derived lactic acid. *Nature*. 513:559-563.

Collin, M., and V. Bigley. 2018. Human dendritic cell subsets: an update. *Immunology*. 154:3-20.

Cui, Y.L., H.K. Li, H.Y. Zhou, T. Zhang, and Q. Li. 2013. Correlations of tumor-associated macrophage subtypes with liver metastases of colorectal cancer. *Asian Pac J Cancer Prev*. 14:1003-1007.

Dao, T., D. Pankov, A. Scott, T. Korontsvit, V. Zakhaleva, Y. Xu, J. Xiang, S. Yan, M.D. de Morais Guerreiro, N. Veomett, L. Dubrovsky, M. Curcio, E. Doubrovina, V. Ponomarev, C. Liu, R.J. O'Reilly, and D.A. Scheinberg. 2015. Therapeutic bispecific T-cell engager antibody targeting the intracellular oncoprotein WT1. *Nat Biotechnol*. 33:1079-1086.

Darvin, P., S.M. Toor, V. Sasidharan Nair, and E. Elkord. 2018. Immune checkpoint inhibitors: recent progress and potential biomarkers. *Exp Mol Med*. 50:165.

Davis, S.J., and P.A. van der Merwe. 2006. The kinetic-segregation model: TCR triggering and beyond. *Nat Immunol*. 7:803-809.

de Sostoa, J., C.A. Fajardo, R. Moreno, M.D. Ramos, M. Farrera-Sal, and R. Alemany. 2019. Targeting the tumor stroma with an oncolytic adenovirus secreting a fibroblast activation protein-targeted bispecific T-cell engager. *J Immunother Cancer*. 7:19.

Decker, W.K., R.F. da Silva, M.H. Sanabria, L.S. Angelo, F. Guimarães, B.M. Burt, F. Kheradmand, and S. Paust. 2017. Cancer Immunotherapy: Historical Perspective of a Clinical Revolution and Emerging Preclinical Animal Models. *Front Immunol*. 8:829.

Delwar, Z.M., Y. Kuo, Y.H. Wen, P.S. Rennie, and W. Jia. 2018. Oncolytic Virotherapy Blockade by Microglia and Macrophages Requires STAT1/3. *Cancer Res*. 78:718-730.

DeNardo, D.G., D.J. Brennan, E. Rexhepaj, B. Ruffell, S.L. Shiao, S.F. Madden, W.M. Gallagher, N. Wadhwani, S.D. Keil, S.A. Junaid, H.S. Rugo, E.S. Hwang, K. Jirström, B.L. West, and L.M. Coussens. 2011. Leukocyte complexity predicts breast cancer survival and functionally regulates response to chemotherapy. *Cancer Discov*. 1:54-67.

Di, Y., L. Seymour, and K. Fisher. 2014. Activity of a group B oncolytic adenovirus (ColoAd1) in whole human blood. *Gene Ther*. 21:440-443.

Doak, G.R., K.L. Schwertfeger, and D.K. Wood. 2018. Distant Relations: Macrophage Functions in the Metastatic Niche. *Trends Cancer*. 4:445-459.

Dock, G. 1904. The influence of complicating diseases upon leukemia. *Am J Med Sci*. 127:563-592.

Dreier, T., G. Lorenczewski, C. Brandl, P. Hoffmann, U. Syring, F. Hanakam, P. Kufer, G. Riethmuller, R. Bargou, and P.A. Baeuerle. 2002. Extremely potent, rapid and costimulation-independent cytotoxic T-cell response against lymphoma cells catalyzed by a single-chain bispecific antibody. *Int J Cancer*. 100:690-697.

Druker, B.J., M. Talpaz, D.J. Resta, B. Peng, E. Buchdunger, J.M. Ford, N.B. Lydon, H. Kantarjian, R. Capdeville, S. Ohno-Jones, and C.L. Sawyers. 2001. Efficacy and safety of a specific inhibitor of the BCR-ABL tyrosine kinase in chronic myeloid leukemia. *N Engl J Med*. 344:1031-1037.

Dudley, M.E., C.A. Gross, M.M. Langhan, M.R. Garcia, R.M. Sherry, J.C. Yang, G.Q. Phan, U.S. Kammula, M.S. Hughes, D.E. Citrin, N.P. Restifo, J.R. Wunderlich, P.A. Prieto, J.J. Hong, R.C. Langan, D.A. Zlott, K.E. Morton, D.E. White, C.M. Laurencot, and S.A. Rosenberg. 2010. CD8+ enriched "young" tumor infiltrating lymphocytes can mediate regression of metastatic melanoma. *Clin Cancer Res*. 16:6122-6131.

Dudley, M.E., J.R. Wunderlich, J.C. Yang, R.M. Sherry, S.L. Topalian, N.P. Restifo, R.E. Royal, U. Kammula, D.E. White, S.A. Mavroukakis, L.J. Rogers, G.J. Gracia, S.A. Jones, D.P. Mangiameli, M.M. Pelletier, J. Gea-Banacloche, M.R. Robinson, D.M. Berman, A.C. Filie, A. Abati, and S.A. Rosenberg. 2005. Adoptive cell transfer therapy following non-myeloablative but lymphodepleting chemotherapy for the treatment of patients with refractory metastatic melanoma. *J Clin Oncol*. 23:2346-2357.

Dudley, M.E., J.C. Yang, R. Sherry, M.S. Hughes, R. Royal, U. Kammula, P.F. Robbins, J. Huang, D.E. Citrin, S.F. Leitman, J. Wunderlich, N.P. Restifo, A. Thomasian, S.G. Downey, F.O. Smith, J. Klapper, K. Morton, C. Laurencot, D.E. White, and S.A. Rosenberg. 2008. Adoptive cell therapy for patients with metastatic melanoma: evaluation of intensive myeloablative chemoradiation preparative regimens. *J Clin Oncol*. 26:5233-5239.

Duell, J., M. Dittrich, T. Bedke, T. Mueller, F. Eisele, A. Rosenwald, L. Rasche, E. Hartmann, T. Dandekar, H. Einsele, and M.S. Topp. 2017. Frequency of regulatory T cells determines the outcome of the T-cell-engaging antibody blinatumomab in patients with B-precursor ALL. *Leukemia*. 31:2181-2190.

Duluc, D., Y. Delneste, F. Tan, M.P. Moles, L. Grimaud, J. Lenoir, L. Preisser, I. Anegon, L. Catala, N. Ifrah, P. Descamps, E. Gamelin, H. Gascan, M. Hebbar, and P. Jeannin. 2007. Tumor-associated leukemia inhibitory factor and IL-6 skew monocyte differentiation into tumor-associated macrophage-like cells. *Blood*. 110:4319-4330.

Dunfield, L.D., T.G. Shepherd, and M.W. Nachtigal. 2002. Primary culture and mRNA analysis of human ovarian cells. *Biol Proced Online*. 4:55-61.

Dunn, G.P., A.T. Bruce, H. Ikeda, L.J. Old, and R.D. Schreiber. 2002. Cancer immunoediting: from immunosurveillance to tumor escape. *Nat Immunol*. 3:991-998.

Dyer, A., Y. Di, H. Calderon, S. Illingworth, G. Kueberuwa, A. Tedcastle, P. Jakeman, S.L. Chia, A. Brown, M.A. Silva, D. Barlow, J. Beadle, T. Hermiston, D.J. Ferguson, B. Champion, K.D. Fisher, and L.W. Seymour. 2017. Oncolytic Group B Adenovirus Enadenotucirev Mediates Non-apoptotic Cell Death with Membrane Disruption and Release of Inflammatory Mediators. *Mol Ther Oncolytics*. 4:18-30.

Ellerman, D. 2019. Bispecific T-cell engagers: Towards understanding variables influencing the in vitro potency and tumor selectivity and their modulation to enhance their efficacy and safety. *Methods*. 154:102-117.

Eshhar, Z., T. Waks, G. Gross, and D.G. Schindler. 1993. Specific activation and targeting of cytotoxic lymphocytes through chimeric single chains consisting of antibody-binding domains and the gamma or zeta subunits of the immunoglobulin and T-cell receptors. *Proc Natl Acad Sci U S A*. 90:720-724.

Etzerodt, A., K. Tsalkitzi, M. Maniecki, W. Damsky, M. Delfini, E. Baudoin, M. Moulin, M. Bosenberg, J.H. Graversen, N. Auphan-Anezin, S.K. Moestrup, and T. Lawrence. 2019. Specific targeting of CD163. *J Exp Med*.

Ezekowitz, R.A., K. Sastry, P. Bailly, and A. Warner. 1990. Molecular characterization of the human macrophage mannose receptor: demonstration of multiple carbohydrate recognition-like domains and phagocytosis of yeasts in Cos-1 cells. *J Exp Med*. 172:1785-1794.

Fajardo, C.A., S. Guedan, L.A. Rojas, R. Moreno, M. Arias-Badia, J. de Sostoa, C.H. June, and R. Alemany. 2017. Oncolytic Adenoviral Delivery of an EGFR-Targeting T-cell Engager Improves Antitumor Efficacy. *Cancer Res*. 77:2052-2063.

Fan, W., X. Yang, F. Huang, X. Tong, L. Zhu, and S. Wang. 2019. Identification of CD206 as a potential biomarker of cancer stem-like cells and therapeutic agent in liver cancer. *Oncol Lett*. 18:3218-3226.

Feig, C., J.O. Jones, M. Kraman, R.J. Wells, A. Deonarine, D.S. Chan, C.M. Connell, E.W. Roberts, Q. Zhao, O.L. Caballero, S.A. Teichmann, T. Janowitz, D.I. Jodrell, D.A. Tuveson, and D.T. Fearon. 2013. Targeting CXCL12 from FAP-expressing carcinoma-associated fibroblasts synergizes with anti-PD-L1 immunotherapy in pancreatic cancer. *Proc Natl Acad Sci U S A*. 110:20212-20217.

Feng, Q., W. Chang, Y. Mao, G. He, P. Zheng, W. Tang, Y. Wei, L. Ren, D. Zhu, M. Ji, Y. Tu, X. Qin, and J. Xu. 2019. Tumor-associated Macrophages as Prognostic and Predictive Biomarkers for Postoperative Adjuvant Chemotherapy in Patients with Stage II Colon Cancer. *Clin Cancer Res*. 25:3896-3907.

Fiedler, W.M., M. Wolf, M. Kebenko, Goebeler, Marie-Elisabeth, B. Ritter, A. Quaas, E. Vieser, Y. Hijazi, I. Patzak, M. Friedrich, P. Kufer, S. Frankel, R. Seggewiss-Bernhardt, and S. Kaubitzsch. 2012. A phase I study of

EpCAM/CD3-bispecific antibody (MT110) in patients with advanced solid tumors. *J Clin Oncol*. 30:Supplement abstr 2504.

Finkernagel, F., S. Reinartz, S. Lieber, T. Adhikary, A. Wortmann, N. Hoffmann, T. Bieringer, A. Nist, T. Stiewe, J.M. Jansen, U. Wagner, S. Müller-Brüsselbach, and R. Müller. 2016. The transcriptional signature of human ovarian carcinoma macrophages is associated with extracellular matrix reorganization. *Oncotarget*. 7:75339-75352.

Frankel, S.R., and P.A. Baeuerle. 2013. Targeting T cells to tumor cells using bispecific antibodies. *Curr Opin Chem Biol*. 17:385-392.

Franklin, R.A., W. Liao, A. Sarkar, M.V. Kim, M.R. Bivona, K. Liu, E.G. Pamer, and M.O. Li. 2014. The cellular and molecular origin of tumor-associated macrophages. *Science*. 344:921-925.

Fraser, G., C.A. Smith, K. Imrie, R. Meyer, and H.D.S.G.C.C.O.s.P.i.E.-B. Care. 2007. Alemtuzumab in chronic lymphocytic leukemia. *Curr Oncol*. 14:96-109.

Freedman, J.D., M.R. Duffy, J. Lei-Rossmann, A. Muntzer, E.M. Scott, J. Hagel, L. Campo, R.J. Bryant, C. Verrill, A. Lambert, P. Miller, B.R. Champion, L.W. Seymour, and K.D. Fisher. 2018. An Oncolytic Virus Expressing a T-cell Engager Simultaneously Targets Cancer and Immunosuppressive Stromal Cells. *Cancer Res*. 78:6852-6865.

Freedman, J.D., J. Hagel, E.M. Scott, I. Psallidas, A. Gupta, L. Spiers, P. Miller, N. Kanellakis, R. Ashfield, K.D. Fisher, M.R. Duffy, and L.W. Seymour. 2017. Oncolytic adenovirus expressing bispecific antibody targets T-cell cytotoxicity in cancer biopsies. *EMBO Mol Med*:e201707567.

Friedberg, J.W. 2005. Unique toxicities and resistance mechanisms associated with monoclonal antibody therapy. *Hematology Am Soc Hematol Educ Program*:329-334.

Friedrich, M., T. Raum, R. Lutterbuese, M. Voelkel, P. Deegen, D. Rau, R. Kischel, P. Hoffmann, C. Brandl, J. Schuhmacher, P. Mueller, R. Finnern, M. Fuergut, D. Zopf, J.W. Slootstra, P.A. Baeuerle, B. Rattel, and P. Kufer. 2012. Regression of human prostate cancer xenografts in mice by AMG 212/BAY2010112, a novel PSMA/CD3-Bispecific BiTE antibody cross-reactive with non-human primate antigens. *Mol Cancer Ther*. 11:2664-2673.

Fulci, G., N. Dmitrieva, D. Gianni, E.J. Fontana, X. Pan, Y. Lu, C.S. Kaufman, B. Kaur, S.E. Lawler, R.J. Lee, C.B. Marsh, D.J. Brat, N. van Rooijen, A.O. Stemmer-Rachamimov, A.S. Rachamimov, F.H. Hochberg, R. Weissleder, R.L. Martuza, and E.A. Chiocca. 2007. Depletion of peripheral macrophages and brain microglia increases brain tumor titers of oncolytic viruses. *Cancer Res*. 67:9398-9406.

Garcia-Carbonero, R., R. Salazar, I. Duran, I. Osman-Garcia, L. Paz-Ares, J.M. Bozada, V. Boni, C. Blanc, L. Seymour, J. Beadle, S. Alvis, B. Champion, E. Calvo, and K. Fisher. 2017. Phase 1 study of intravenous administration of the chimeric adenovirus enadenotucirev in patients undergoing primary tumor resection. *J Immunother Cancer*. 5:71.

Gazzaniga, S., A.I. Bravo, A. Guglielmotti, N. van Rooijen, F. Maschi, A. Vecchi, A. Mantovani, J. Mordoh, and R. Wainstok. 2007. Targeting tumor-associated

macrophages and inhibition of MCP-1 reduce angiogenesis and tumor growth in a human melanoma xenograft. *J Invest Dermatol*. 127:2031-2041.

Germano, G., R. Frapolli, C. Belgiovine, A. Anselmo, S. Pesce, M. Liguori, E. Erba, S. Uboldi, M. Zucchetti, F. Pasqualini, M. Nebuloni, N. van Rooijen, R. Mortarini, L. Beltrame, S. Marchini, I. Fuso Nerini, R. Sanfilippo, P.G. Casali, S. Pilotti, C.M. Galmarini, A. Anichini, A. Mantovani, M. D'Incalci, and P. Allavena. 2013. Role of macrophage targeting in the antitumor activity of trabectedin. *Cancer Cell*. 23:249-262.

Gibson, D.G., L. Young, R.Y. Chuang, J.C. Venter, C.A. Hutchison, and H.O. Smith. 2009. Enzymatic assembly of DNA molecules up to several hundred kilobases. *Nat Methods*. 6:343-345.

Gil-Martin, M., A. Cubillo, J.-P. Machiels, S. Rottie, F. Mardjuadi, K. Geboes, R. Salazar, C. Ellis, J.W. Beadle, K. Fisher, C. Blanc, and E. Calvo. 2014. A phase 1 study of enadenotucirev, an oncolytic Ad11/Ad3 chimeric group B adenovirus, administered intravenously – Analysis of dose expansion and repeat cycle cohorts in patients with metastatic colorectal cancer (mCRC). *Ann Oncol* 25 (suppl 4):iv367.

Ginhoux, F., J.L. Schultze, P.J. Murray, J. Ochando, and S.K. Biswas. 2016. New insights into the multidimensional concept of macrophage ontogeny, activation and function. *Nat Immunol*. 17:34-40.

Golan, T., D. Atias, I. Barshack, C. Avivi, R.S. Goldstein, and R. Berger. 2014. Ascites-derived pancreatic ductal adenocarcinoma primary cell cultures as a platform for personalised medicine. *Br J Cancer*. 110:2269-2276.

Gomez-Roca, C.A., A. Italiano, C. Le Tourneau, P.A. Cassier, M. Toulmonde, S.P. D'Angelo, M. Campone, K.L. Weber, D. Loirat, M.A. Cannarile, A.M. Jegg, C. Ries, R. Christen, G. Meneses-Lorente, W. Jacob, I. Klaman, C.H. Ooi, C. Watson, K. Wonde, B. Reis, F. Michielin, D. Rüttinger, J.P. Delord, and J.Y. Blay. 2019. Phase I Study of Emactuzumab Single Agent or in Combination with Paclitaxel in Patients with Advanced/Metastatic Solid Tumors Reveals Depletion of Immunosuppressive M2-like Macrophages. *Ann Oncol*.

Goodman, A.M., S. Kato, L. Bazhenova, S.P. Patel, G.M. Frampton, V. Miller, P.J. Stephens, G.A. Daniels, and R. Kurzrock. 2017. Tumor Mutational Burden as an Independent Predictor of Response to Immunotherapy in Diverse Cancers. *Mol Cancer Ther*. 16:2598-2608.

Griffioen, A.W., C.A. Damen, S. Martinotti, G.H. Blijham, and G. Groenewegen. 1996. Endothelial intercellular adhesion molecule-1 expression is suppressed in human malignancies: the role of angiogenic factors. *Cancer Res*. 56:1111-1117.

Guo, C., M.H. Manjili, J.R. Subjeck, D. Sarkar, P.B. Fisher, and X.Y. Wang. 2013. Therapeutic cancer vaccines: past, present, and future. *Adv Cancer Res*. 119:421-475.

Guo, Z.S., Z. Liu, and D.L. Bartlett. 2014. Oncolytic Immunotherapy: Dying the Right Way is a Key to Eliciting Potent Antitumor Immunity. *Front Oncol*. 4:74.

Haas, C., E. Krinner, K. Brischwein, P. Hoffmann, R. Lutterbüse, B. Schlereth, P. Kufer, and P.A. Baeuerle. 2009. Mode of cytotoxic action of T cell-engaging BiTE antibody MT110. *Immunobiology*. 214:441-453.

Hahne, M., D. Rimoldi, M. Schröter, P. Romero, M. Schreier, L.E. French, P. Schneider, T. Bornand, A. Fontana, D. Lienard, J. Cerottini, and J. Tschopp. 1996. Melanoma cell expression of Fas(Apo-1/CD95) ligand: implications for tumor immune escape. *Science*. 274:1363-1366.

Hall, M., H. Liu, M. Malafa, B. Centeno, P.J. Hodul, J. Pimiento, S. Pilon-Thomas, and A.A. Sarnaik. 2016. Expansion of tumor-infiltrating lymphocytes (TIL) from human pancreatic tumors. *J Immunother Cancer*. 4:61.

Hammond, S.A., R. Lutterbuese, S. Roff, P. Lutterbuese, B. Schlereth, E. Bruckheimer, M.S. Kinch, S. Coats, P.A. Baeuerle, P. Kufer, and P.A. Kiener. 2007. Selective targeting and potent control of tumor growth using an EphA2/CD3-Bispecific single-chain antibody construct. *Cancer Res*. 67:3927-3935.

Hanahan, D., and R.A. Weinberg. 2000. The hallmarks of cancer. *Cell*. 100:57-70.

Hanahan, D., and R.A. Weinberg. 2011. Hallmarks of cancer: the next generation. *Cell*. 144:646-674.

Harlin, H., Y. Meng, A.C. Peterson, Y. Zha, M. Tretiakova, C. Slingluff, M. McKee, and T.F. Gajewski. 2009. Chemokine expression in melanoma metastases associated with CD8+ T-cell recruitment. *Cancer Res*. 69:3077-3085.

Hattori, Y., J. Yamashita, C. Sakaida, K. Kawano, and E. Yonemochi. 2015. Evaluation of antitumor effect of zoledronic acid entrapped in folate-linked liposome for targeting to tumor-associated macrophages. *J Liposome Res*. 25:131-140.

Heinzerling, L., V. Künzi, P.A. Oberholzer, T. Kündig, H. Naim, and R. Dummer. 2005. Oncolytic measles virus in cutaneous T-cell lymphomas mounts antitumor immune responses in vivo and targets interferon-resistant tumor cells. *Blood*. 106:2287-2294.

Herrmann, I., P.A. Baeuerle, M. Friedrich, A. Murr, S. Filusch, D. Rüttinger, M.W. Majdoub, S. Sharma, P. Kufer, T. Raum, and M. Münz. 2010. Highly efficient elimination of colorectal tumor-initiating cells by an EpCAM/CD3-bispecific antibody engaging human T cells. *PLoS One*. 5:e13474.

Herwig, M.C., C. Bergstrom, J.R. Wells, T. Höller, and H.E. Grossniklaus. 2013. M2/M1 ratio of tumor associated macrophages and PPAR-gamma expression in uveal melanomas with class 1 and class 2 molecular profiles. *Exp Eye Res*. 107:52-58.

Hiraoka, K., M. Zenmyo, K. Watari, H. Iguchi, A. Fotovati, Y.N. Kimura, F. Hosoi, T. Shoda, K. Nagata, H. Osada, M. Ono, and M. Kuwano. 2008. Inhibition of bone and muscle metastases of lung cancer cells by a decrease in the number of monocytes/macrophages. *Cancer Sci*. 99:1595-1602.

Hodi, F.S., S.J. O'Day, D.F. McDermott, R.W. Weber, J.A. Sosman, J.B. Haanen, R. Gonzalez, C. Robert, D. Schadendorf, J.C. Hassel, W. Akerley, A.J. van den Eertwegh, J. Lutzky, P. Lorigan, J.M. Vaubel, G.P. Linette, D. Hogg, C.H. Ottensmeier, C. Lebbé, C. Peschel, I. Quirt, J.I. Clark, J.D. Wolchok, J.S.

Weber, J. Tian, M.J. Yellin, G.M. Nichol, A. Hoos, and W.J. Urba. 2010. Improved survival with ipilimumab in patients with metastatic melanoma. *N Engl J Med*. 363:711-723.

Hoffmann, P., R. Hofmeister, K. Brischwein, C. Brandl, S. Crommer, R. Bargou, C. Itin, N. Prang, and P.A. Baeuerle. 2005. Serial killing of tumor cells by cytotoxic T cells redirected with a CD19-/CD3-bispecific single-chain antibody construct. *Int J Cancer*. 115:98-104.

Hollingsworth, R.E., and K. Jansen. 2019. Turning the corner on therapeutic cancer vaccines. *NPJ Vaccines*. 4:7.

Hoster, H., R. Zanes, and E. Von Haam. 1949. Studies in Hodgkin's syndrome; the association of viral hepatitis and Hodgkin's disease; a preliminary report. *Cancer Res*. 9:473-480.

Huber, R., B. Meier, A. Otsuka, G. Fenini, T. Satoh, S. Gehrke, D. Widmer, M.P. Levesque, J. Mangana, K. Kerl, C. Gebhardt, H. Fujii, C. Nakashima, Y. Nonomura, K. Kabashima, R. Dummer, E. Contassot, and L.E. French. 2016. Tumour hypoxia promotes melanoma growth and metastasis via High Mobility Group Box-1 and M2-like macrophages. *Sci Rep*. 6:29914.

Hummel. Phase 1 study of pasotuxizumab (BAY 2010112), a PSMA-targeting Bispecific T cell Engager (BiTE) immunotherapy for metastatic castration-resistant prostate cancer (mCRPC).

Husain, B., and D. Ellerman. 2018. Expanding the Boundaries of Biotherapeutics with Bispecific Antibodies. *BioDrugs*. 32:441-464.

Iankov, I.D., B. Blechacz, C. Liu, J.D. Schmeckpeper, J.E. Tarara, M.J. Federspiel, N. Caplice, and S.J. Russell. 2007. Infected cell carriers: a new strategy for systemic delivery of oncolytic measles viruses in cancer virotherapy. *Mol Ther*. 15:114-122.

Idorn, M., M. Olsen, H.R. Halldórsdóttir, S.K. Skadborg, M. Pedersen, C. Høgdall, E. Høgdall, Ö. Met, and P. Thor Straten. 2018. Improved migration of tumor ascites lymphocytes to ovarian cancer microenvironment by CXCR2 transduction. *Oncoimmunology*. 7:e1412029.

Ito, D., K. Ogasawara, K. Iwabuchi, Y. Inuyama, and K. Onoé. 2000. Induction of CTL responses by simultaneous administration of liposomal peptide vaccine with anti-CD40 and anti-CTLA-4 mAb. *J Immunol*. 164:1230-1235.

Jen, E.Y., Q. Xu, A. Schetter, D. Przepiorka, Y.L. Shen, D. Roscoe, R. Sridhara, A. Deisseroth, R. Philip, A.T. Farrell, and R. Pazdur. 2019. FDA Approval: Blinatumomab for Patients with B-cell Precursor Acute Lymphoblastic Leukemia in Morphologic Remission with Minimal Residual Disease. *Clin Cancer Res*. 25:473-477.

John, L.B., L.J. Howland, J.K. Flynn, A.C. West, C. Devaud, C.P. Duong, T.J. Stewart, J.A. Westwood, Z.S. Guo, D.L. Bartlett, M.J. Smyth, M.H. Kershaw, and P.K. Darcy. 2012. Oncolytic virus and anti-4-1BB combination therapy elicits strong antitumor immunity against established cancer. *Cancer Res*. 72:1651-1660.

Jonker, D.J., C.J. O'Callaghan, C.S. Karapetis, J.R. Zalcberg, D. Tu, H.J. Au, S.R. Berry, M. Krahn, T. Price, R.J. Simes, N.C. Tebbutt, G. van Hazel, R.

Wierzbicki, C. Langer, and M.J. Moore. 2007. Cetuximab for the treatment of colorectal cancer. *N Engl J Med*. 357:2040-2048.

June, C.H., and M. Sadelain. 2018. Chimeric Antigen Receptor Therapy. *N Engl J Med*. 379:64-73.

Kalos, M., B.L. Levine, D.L. Porter, S. Katz, S.A. Grupp, A. Bagg, and C.H. June. 2011. T cells with chimeric antigen receptors have potent antitumor effects and can establish memory in patients with advanced leukemia. *Sci Transl Med*. 3:95ra73.

Kampan, N.C., M.T. Madondo, O.M. McNally, A.N. Stephens, M.A. Quinn, and M. Plebanski. 2017. Interleukin 6 Present in Inflammatory Ascites from Advanced Epithelial Ovarian Cancer Patients Promotes Tumor Necrosis Factor Receptor 2-Expressing Regulatory T Cells. *Front Immunol*. 8:1482.

Kantarjian, H., A. Stein, N. Gökbuget, A.K. Fielding, A.C. Schuh, J.M. Ribera, A. Wei, H. Dombret, R. Foà, R. Bassan, Ö. Arslan, M.A. Sanz, J. Bergeron, F. Demirkan, E. Lech-Maranda, A. Rambaldi, X. Thomas, H.A. Horst, M. Brüggemann, W. Klapper, B.L. Wood, A. Fleishman, D. Nagorsen, C. Holland, Z. Zimmerman, and M.S. Topp. 2017. Blinatumomab versus Chemotherapy for Advanced Acute Lymphoblastic Leukemia. *N Engl J Med*. 376:836-847.

Kantoff, P.W., C.S. Higano, N.D. Shore, E.R. Berger, E.J. Small, D.F. Penson, C.H. Redfern, A.C. Ferrari, R. Dreicer, R.B. Sims, Y. Xu, M.W. Frohlich, P.F. Schellhammer, and I.S. Investigators. 2010. Sipuleucel-T immunotherapy for castration-resistant prostate cancer. *N Engl J Med*. 363:411-422.

Kaufman, H.L., D.W. Kim, G. DeRaffele, J. Mitcham, R.S. Coffin, and S. Kim-Schulze. 2010. Local and distant immunity induced by intralesional vaccination with an oncolytic herpes virus encoding GM-CSF in patients with stage IIIc and IV melanoma. *Ann Surg Oncol*. 17:718-730.

Kebenko, M., M.E. Goebeler, M. Wolf, A. Hasenburg, R. Seggewiss-Bernhardt, B. Ritter, B. Rautenberg, D. Atanackovic, A. Kratzer, J.B. Rottman, M. Friedrich, E. Vieser, S. Elm, I. Patzak, D. Wessiepe, S. Stienen, and W. Fiedler. 2018. A multicenter phase 1 study of solitomab (MT110, AMG 110), a bispecific EpCAM/CD3 T-cell engager (BiTE®) antibody construct, in patients with refractory solid tumors. *Oncoimmunology*. 7:e1450710.

Kellner, C., J. Bruenke, J. Stieglmaier, M. Schwemmlein, M. Schwenkert, H. Singer, K. Mentz, M. Peipp, P. Lang, F. Oduncu, B. Stockmeyer, and G.H. Fey. 2008. A novel CD19-directed recombinant bispecific antibody derivative with enhanced immune effector functions for human leukemic cells. *J Immunother*. 31:871-884.

Kimiz-Gebologlu, I., S. Gulce-Iz, and C. Biray-Avci. 2018. Monoclonal antibodies in cancer immunotherapy. *Mol Biol Rep*. 45:2935-2940.

Kipriyanov, S.M., G. Moldenhauer, J. Schuhmacher, B. Cochlovius, C.W. Von der Lieth, E.R. Matys, and M. Little. 1999. Bispecific tandem diabody for tumor therapy with improved antigen binding and pharmacokinetics. *J Mol Biol*. 293:41-56.

Klinger, M., C. Brandl, G. Zugmaier, Y. Hijazi, R.C. Bargou, M.S. Topp, N. Gökbuget, S. Neumann, M. Goebeler, A. Viardot, M. Stelljes, M. Brüggemann, D. Hoelzer, E. Degenhard, D. Nagorsen, P.A. Baeuerle, A. Wolf, and P. Kufer. 2012. Immunopharmacologic response of patients with B-lineage acute lymphoblastic leukemia to continuous infusion of T cell-engaging CD19/CD3-bispecific BiTE antibody blinatumomab. *Blood*. 119:6226-6233.

Kochenderfer, J.N., W.H. Wilson, J.E. Janik, M.E. Dudley, M. Stetler-Stevenson, S.A. Feldman, I. Maric, M. Raffeld, D.A. Nathan, B.J. Lanier, R.A. Morgan, and S.A. Rosenberg. 2010. Eradication of B-lineage cells and regression of lymphoma in a patient treated with autologous T cells genetically engineered to recognize CD19. *Blood*. 116:4099-4102.

Koristka, S., M. Cartellieri, C. Arndt, A. Feldmann, K. Töpfer, I. Michalk, A. Temme, G. Ehninger, and M. Bachmann. 2014. Cytotoxic response of human regulatory T cells upon T-cell receptor-mediated activation: a matter of purity. *Blood Cancer J.* 4:e199.

Kowal, J., M. Kornete, and J.A. Joyce. 2019. Re-education of macrophages as a therapeutic strategy in cancer. *Immunotherapy*. 11:677-689.

Kridel, R., L. Xerri, B. Gelas-Dore, K. Tan, P. Feugier, A. Vawda, D. Canioni, P. Farinha, S. Boussetta, A.A. Moccia, P. Brice, E.A. Chavez, A.H. Kyle, D.W. Scott, A.D. Sanders, B. Fabiani, G.W. Slack, A.I. Minchinton, C. Haioun, J.M. Connors, L.H. Sehn, C. Steidl, R.D. Gascoyne, and G. Salles. 2015. The Prognostic Impact of CD163-Positive Macrophages in Follicular Lymphoma: A Study from the BC Cancer Agency and the Lymphoma Study Association. *Clin Cancer Res*. 21:3428-3435.

Kuhn, I., P. Harden, M. Bauzon, C. Chartier, J. Nye, S. Thorne, T. Reid, S. Ni, A. Lieber, K. Fisher, L. Seymour, G.M. Rubanyi, R.N. Harkins, and T.W. Hermiston. 2008. Directed evolution generates a novel oncolytic virus for the treatment of colon cancer. *PLoS One*. 3:e2409.

Kuhn, S., J. Yang, and F. Ronchese. 2015. Monocyte-Derived Dendritic Cells Are Essential for CD8(+) T Cell Activation and Antitumor Responses After Local Immunotherapy. *Front Immunol*. 6:584.

Kumar, V., L. Donthireddy, D. Marvel, T. Condamine, F. Wang, S. Lavilla-Alonso, A. Hashimoto, P. Vonteddu, R. Behera, M.A. Goins, C. Mulligan, B. Nam, N. Hockstein, F. Denstman, S. Shakamuri, D.W. Speicher, A.T. Weeraratna, T. Chao, R.H. Vonderheide, L.R. Languino, P. Ordentlich, Q. Liu, X. Xu, A. Lo, E. Puré, C. Zhang, A. Loboda, M.A. Sepulveda, L.A. Snyder, and D.I. Gabrilovich. 2017. Cancer-Associated Fibroblasts Neutralize the Anti-tumor Effect of CSF1 Receptor Blockade by Inducing PMN-MDSC Infiltration of Tumors. *Cancer Cell*. 32:654-668.e655.

Kurahara, H., S. Takao, T. Kuwahata, T. Nagai, Q. Ding, K. Maeda, H. Shinchi, Y. Mataki, K. Maemura, T. Matsuyama, and S. Natsugoe. 2012. Clinical significance of folate receptor β-expressing tumor-associated macrophages in pancreatic cancer. *Ann Surg Oncol*. 19:2264-2271.

Kurashige, M., M. Kohara, K. Ohshima, S. Tahara, Y. Hori, S. Nojima, N. Wada, J.I. Ikeda, K. Miyamura, M. Ito, and E. Morii. 2018. Origin of cancer-associated fibroblasts and tumor-associated macrophages in humans after sex-mismatched bone marrow transplantation. *Commun Biol*. 1:131.

La Fleur, L., V.F. Boura, A. Alexeyenko, A. Berglund, V. Pontén, J.S.M. Mattsson, D. Djureinovic, J. Persson, H. Brunnström, J. Isaksson, E. Brandén, H. Koyi, P. Micke, M.C.I. Karlsson, and J. Botling. 2018. Expression of scavenger receptor MARCO defines a targetable tumor-associated macrophage subset in non-small cell lung cancer. *Int J Cancer*.

Lahaye, T., B. Riehm, U. Berger, P. Paschka, M.C. Müller, S. Kreil, K. Merx, U. Schwindel, C. Schoch, R. Hehlmann, and A. Hochhaus. 2005. Response and resistance in 300 patients with BCR-ABL-positive leukemias treated with imatinib in a single center: a 4.5-year follow-up. *Cancer*. 103:1659-1669.

Lan, C., X. Huang, S. Lin, H. Huang, Q. Cai, T. Wan, J. Lu, and J. Liu. 2013. Expression of M2-polarized macrophages is associated with poor prognosis for advanced epithelial ovarian cancer. *Technol Cancer Res Treat*. 12:259-267.

Landskron, J., Ø. Helland, K.M. Torgersen, E.M. Aandahl, B.T. Gjertsen, L. Bjørge, and K. Taskén. 2015. Activated regulatory and memory T-cells accumulate in malignant ascites from ovarian carcinoma patients. *Cancer Immunol Immunother*. 64:337-347.

Laszlo, G.S., C.J. Gudgeon, K.H. Harrington, and R.B. Walter. 2015. T-cell ligands modulate the cytolytic activity of the CD33/CD3 BiTE antibody construct, AMG 330. *Blood Cancer J*. 5:e340.

Lauss, M., M. Donia, K. Harbst, R. Andersen, S. Mitra, F. Rosengren, M. Salim, J. Vallon-Christersson, T. Törngren, A. Kvist, M. Ringnér, I.M. Svane, and G. Jönsson. 2017. Mutational and putative neoantigen load predict clinical benefit of adoptive T cell therapy in melanoma. *Nat Commun*. 8:1738.

Le Gall, F., S.M. Kipriyanov, G. Moldenhauer, and M. Little. 1999. Di-, tri- and tetrameric single chain Fv antibody fragments against human CD19: effect of valency on cell binding. *FEBS Lett*. 453:164-168.

Le Gall, F., U. Reusch, M. Little, and S.M. Kipriyanov. 2004a. Effect of linker sequences between the antibody variable domains on the formation, stability and biological activity of a bispecific tandem diabody. *Protein Eng Des Sel*. 17:357-366.

Le Gall, F., U. Reusch, G. Moldenhauer, M. Little, and S.M. Kipriyanov. 2004b. Immunosuppressive properties of anti-CD3 single-chain Fv and diabody. *J Immunol Methods*. 285:111-127.

Le Page, C., A. Marineau, P.K. Bonza, K. Rahimi, L. Cyr, I. Labouba, J. Madore, N. Delvoye, A.M. Mes-Masson, D.M. Provencher, and J.F. Cailhier. 2012. BTN3A2 expression in epithelial ovarian cancer is associated with higher tumor infiltrating T cells and a better prognosis. *PLoS One*. 7:e38541.

Lee, C., S.S. Bae, H. Joo, and H. Bae. 2017a. Melittin suppresses tumor progression by regulating tumor-associated macrophages in a Lewis lung carcinoma mouse model. *Oncotarget*. 8:54951-54965.

Lee, C., H. Jeong, Y. Bae, K. Shin, S. Kang, H. Kim, J. Oh, and H. Bae. 2019a. Targeting of M2-like tumor-associated macrophages with a melittin-based pro-apoptotic peptide. *J Immunother Cancer*. 7:147.

Lee, H.J., Y.A. Kim, C.K. Sim, S.H. Heo, I.H. Song, H.S. Park, S.Y. Park, W.S. Bang, I.A. Park, M. Lee, J.H. Lee, Y.S. Cho, S. Chang, J. Jung, J. Kim, S.B. Lee, S.Y. Kim, M.S. Lee, and G. Gong. 2017b. Expansion of tumor-infiltrating lymphocytes and their potential for application as adoptive cell transfer therapy in human breast cancer. *Oncotarget*. 8:113345-113359.

Lee, H.T., S.H. Lee, and Y.S. Heo. 2019b. Molecular Interactions of Antibody Drugs Targeting PD-1, PD-L1, and CTLA-4 in Immuno-Oncology. *Molecules*. 24.

Leget, G.A., and M.S. Czuczman. 1998. Use of rituximab, the new FDA-approved antibody. *Curr Opin Oncol*. 10:548-551.

Leick, M.B., and M.V. Maus. 2019. CAR-T cells beyond CD19, UnCAR-Ted territory. *Am J Hematol*. 94:S34-S41.

Lewis, C.E., A.S. Harney, and J.W. Pollard. 2016. The Multifaceted Role of Perivascular Macrophages in Tumors. *Cancer Cell*. 30:365.

Lewis, J.S., R.J. Landers, J.C. Underwood, A.L. Harris, and C.E. Lewis. 2000. Expression of vascular endothelial growth factor by macrophages is up-regulated in poorly vascularized areas of breast carcinomas. *J Pathol*. 192:150-158.

Li, H., Y. Han, Q. Guo, M. Zhang, and X. Cao. 2009. Cancer-expanded myeloid-derived suppressor cells induce anergy of NK cells through membrane-bound TGF-beta 1. *J Immunol*. 182:240-249.

Li, J., N.J. Stagg, J. Johnston, M.J. Harris, S.A. Menzies, D. DiCara, V. Clark, M. Hristopoulos, R. Cook, D. Slaga, R. Nakamura, L. McCarty, S. Sukumaran, E. Luis, Z. Ye, T.D. Wu, T. Sumiyoshi, D. Danilenko, G.Y. Lee, K. Totpal, D. Ellerman, I. Hötzel, J.R. James, and T.T. Junttila. 2017a. Membrane-Proximal Epitope Facilitates Efficient T Cell Synapse Formation by Anti-FcRH5/CD3 and Is a Requirement for Myeloma Cell Killing. *Cancer Cell*. 31:383-395.

Li, M.C., R. Hertz, and D.M. Bergenstal. 1958. Therapy of choriocarcinoma and related trophoblastic tumors with folic acid and purine antagonists. *N Engl J Med*. 259:66-74.

Li, X., P. Wang, H. Li, X. Du, M. Liu, Q. Huang, Y. Wang, and S. Wang. 2017b. The Efficacy of Oncolytic Adenovirus Is Mediated by T-cell Responses against Virus and Tumor in Syrian Hamster Model. *Clin Cancer Res*. 23:239-249.

Lin, Y., J. Xu, and H. Lan. 2019. Tumor-associated macrophages in tumor metastasis: biological roles and clinical therapeutic applications. *J Hematol Oncol*. 12:76.

Lipson, E.J., and C.G. Drake. 2011. Ipilimumab: an anti-CTLA-4 antibody for metastatic melanoma. *Clin Cancer Res*. 17:6958-6962.

Lovo, E., M. Zhang, L. Wang, and P.G. Ashton-Rickardt. 2012. Serine protease inhibitor 6 is required to protect dendritic cells from the kiss of death. *J Immunol*. 188:1057-1063.

Lutterbuese, R., T. Raum, R. Kischel, P. Hoffmann, S. Mangold, B. Rattel, M. Friedrich, O. Thomas, G. Lorenczewski, D. Rau, E. Schaller, I. Herrmann, A. Wolf, T. Urbig, P.A. Baeuerle, and P. Kufer. 2010. T cell-engaging BiTE antibodies specific for EGFR potently eliminate KRAS- and BRAF-mutated colorectal cancer cells. *Proc Natl Acad Sci U S A*. 107:12605-12610.

Lv, S., Y. Wang, T. Sun, D. Wan, L. Sheng, W. Li, H. Zhu, Y. Li, and J. Lu. 2018. Overall Survival Benefit from Trastuzumab-Based Treatment in HER2-Positive Metastatic Breast Cancer: A Retrospective Analysis. *Oncol Res Treat*. 41:450-455.

Lynn, R.C., Y. Feng, K. Schutsky, M. Poussin, A. Kalota, D.S. Dimitrov, and D.J. Powell. 2016. High-affinity FRβ-specific CAR T cells eradicate AML and normal myeloid lineage without HSC toxicity. *Leukemia*. 30:1355-1364.

Ma, J., L. Liu, G. Che, N. Yu, F. Dai, and Z. You. 2010. The M1 form of tumor-associated macrophages in non-small cell lung cancer is positively associated with survival time. *BMC Cancer*. 10:112.

Machiels, J.P., R. Salazar, S. Rottey, I. Duran, L. Dirix, K. Geboes, C. Wilkinson-Blanc, G. Pover, S. Alvis, B. Champion, K. Fisher, H. McElwaine-Johnn, J. Beadle, and E. Calvo. 2019. A phase 1 dose escalation study of the oncolytic adenovirus enadenotucirev, administered intravenously to patients with epithelial solid tumors (EVOLVE). *J Immunother Cancer*. 7:20.

Mack, M., R. Gruber, S. Schmidt, G. Riethmüller, and P. Kufer. 1997. Biologic properties of a bispecific single-chain antibody directed against 17-1A (EpCAM) and CD3: tumor cell-dependent T cell stimulation and cytotoxic activity. *J Immunol*. 158:3965-3970.

Mantovani, A., F. Marchesi, A. Malesci, L. Laghi, and P. Allavena. 2017. Tumour-associated macrophages as treatment targets in oncology. *Nat Rev Clin Oncol*. 14:399-416.

Mantovani, A., A. Sica, S. Sozzani, P. Allavena, A. Vecchi, and M. Locati. 2004. The chemokine system in diverse forms of macrophage activation and polarization. *Trends Immunol*. 25:677-686.

Marino, N., S. Illingworth, P. Kodialbail, A. Patel, H. Calderon, R. Lear, K.D. Fisher, B.R. Champion, and A.C.N. Brown. 2017. Development of a versatile oncolytic virus platform for local intra-tumoural expression of therapeutic transgenes. *PLoS One*. 12:e0177810.

Martinez-Pomares, L., L.G. Hanitsch, R. Stillion, S. Keshav, and S. Gordon. 2005. Expression of mannose receptor and ligands for its cysteine-rich domain in venous sinuses of human spleen. *Lab Invest*. 85:1238-1249.

Massagué, J. 2008. TGFbeta in Cancer. *Cell*. 134:215-230.

Mastrangelo, M.J., H.C. Maguire, L.C. Eisenlohr, C.E. Laughlin, C.E. Monken, P.A. McCue, A.J. Kovatich, and E.C. Lattime. 1999. Intratumoral recombinant GM-CSF-encoding virus as gene therapy in patients with cutaneous melanoma. *Cancer Gene Ther*. 6:409-422.

Matherly, L.H., and D.I. Goldman. 2003. Membrane transport of folates. *Vitam Horm*. 66:403-456.

Matte, I., D. Lane, C. Laplante, C. Rancourt, and A. Piché. 2012. Profiling of cytokines in human epithelial ovarian cancer ascites. *Am J Cancer Res*. 2:566-580.

Mazor, R., M. Onda, and I. Pastan. 2016. Immunogenicity of therapeutic recombinant immunotoxins. *Immunol Rev*. 270:152-164.

McKee, T.D., P. Grandi, W. Mok, G. Alexandrakis, N. Insin, J.P. Zimmer, M.G. Bawendi, Y. Boucher, X.O. Breakefield, and R.K. Jain. 2006. Degradation of fibrillar collagen in a human melanoma xenograft improves the efficacy of an oncolytic herpes simplex virus vector. *Cancer Res*. 66:2509-2513.

Michalk, I., A. Feldmann, S. Koristka, C. Arndt, M. Cartellieri, A. Ehninger, G. Ehninger, and M.P. Bachmann. 2014. Characterization of a novel single-chain bispecific antibody for retargeting of T cells to tumor cells via the TCR co-receptor CD8. *PLoS One*. 9:e95517.

Mills, C.D., K. Kincaid, J.M. Alt, M.J. Heilman, and A.M. Hill. 2000. M-1/M-2 macrophages and the Th1/Th2 paradigm. *J Immunol*. 164:6166-6173.

Mitchem, J.B., D.J. Brennan, B.L. Knolhoff, B.A. Belt, Y. Zhu, D.E. Sanford, L. Belaygorod, D. Carpenter, L. Collins, D. Piwnica-Worms, S. Hewitt, G.M. Udupi, W.M. Gallagher, C. Wegner, B.L. West, A. Wang-Gillam, P. Goedegebuure, D.C. Linehan, and D.G. DeNardo. 2013. Targeting tumor-infiltrating macrophages decreases tumor-initiating cells, relieves immunosuppression, and improves chemotherapeutic responses. *Cancer Res*. 73:1128-1141.

Mittal, D., M.M. Gubin, R.D. Schreiber, and M.J. Smyth. 2014. New insights into cancer immunoediting and its three component phases--elimination, equilibrium and escape. *Curr Opin Immunol*. 27:16-25.

Moek, K. Phase 1 Study of AMG 211/MEDI-565 Administered as Continuous Intravenous Infusion (cIV) for Relapsed/Refractory Gastrointestinal (GI) Adenocarcinoma.

Mok, S., R.C. Koya, C. Tsui, J. Xu, L. Robert, L. Wu, T.G. Graeber, B.L. West, G. Bollag, and A. Ribas. 2014. Inhibition of CSF-1 receptor improves the antitumor efficacy of adoptive cell transfer immunotherapy. *Cancer Res*. 74:153-161.

Moore, R.J., D.M. Owens, G. Stamp, C. Arnott, F. Burke, N. East, H. Holdsworth, L. Turner, B. Rollins, M. Pasparakis, G. Kollias, and F. Balkwill. 1999. Mice deficient in tumor necrosis factor-alpha are resistant to skin carcinogenesis. *Nat Med*. 5:828-831.

Morgan, R.A., J.C. Yang, M. Kitano, M.E. Dudley, C.M. Laurencot, and S.A. Rosenberg. 2010. Case report of a serious adverse event following the administration of T cells transduced with a chimeric antigen receptor recognizing ERBB2. *Mol Ther*. 18:843-851.

Movahedi, K., D. Laoui, C. Gysemans, M. Baeten, G. Stangé, J. Van den Bossche, M. Mack, D. Pipeleers, P. In't Veld, P. De Baetselier, and J.A. Van Ginderachter. 2010. Different tumor microenvironments contain functionally distinct subsets of macrophages derived from Ly6C(high) monocytes. *Cancer Res*. 70:5728-5739.

Movahedi, K., S. Schoonooghe, D. Laoui, I. Houbracken, W. Waelput, K. Breckpot, L. Bouwens, T. Lahoutte, P. De Baetselier, G. Raes, N. Devoogdt, and J.A. Van Ginderachter. 2012. Nanobody-based targeting of the macrophage mannose receptor for effective in vivo imaging of tumor-associated macrophages. *Cancer Res*. 72:4165-4177.

Muralidharan, S., and P. Mandrekar. 2013. Cellular stress response and innate immune signaling: integrating pathways in host defense and inflammation. *J Leukoc Biol*. 94:1167-1184.

Murray, P.J., J.E. Allen, S.K. Biswas, E.A. Fisher, D.W. Gilroy, S. Goerdt, S. Gordon, J.A. Hamilton, L.B. Ivashkiv, T. Lawrence, M. Locati, A. Mantovani, F.O. Martinez, J.L. Mege, D.M. Mosser, G. Natoli, J.P. Saeij, J.L. Schultze, K.A. Shirey, A. Sica, J. Suttles, I. Udalova, J.A. van Ginderachter, S.N. Vogel, and T.A. Wynn. 2014. Macrophage activation and polarization: nomenclature and experimental guidelines. *Immunity*. 41:14-20.

Muthana, M., S. Rodrigues, Y.Y. Chen, A. Welford, R. Hughes, S. Tazzyman, M. Essand, F. Morrow, and C.E. Lewis. 2013. Macrophage delivery of an oncolytic virus abolishes tumor regrowth and metastasis after chemotherapy or irradiation. *Cancer Res*. 73:490-495.

Nagai, T., M. Tanaka, Y. Tsuneyoshi, B. Xu, S.A. Michie, K. Hasui, H. Hirano, K. Arita, and T. Matsuyama. 2009. Targeting tumor-associated macrophages in an experimental glioma model with a recombinant immunotoxin to folate receptor beta. *Cancer Immunol Immunother*. 58:1577-1586.

Neubert, N.J., M. Schmittnaegel, N. Bordry, S. Nassiri, N. Wald, C. Martignier, L. Tillé, K. Homicsko, W. Damsky, H. Maby-El Hajjami, I. Klaman, E. Danenberg, K. Ioannidou, L. Kandalaft, G. Coukos, S. Hoves, C.H. Ries, S.A. Fuertes Marraco, P.G. Foukas, M. De Palma, and D.E. Speiser. 2018. T cell-induced CSF1 promotes melanoma resistance to PD1 blockade. *Sci Transl Med*. 10.

Noel, M., E.M. O'Reilly, B.M. Wolpin, D.P. Ryan, A.J. Bullock, C.D. Britten, D.C. Linehan, B.A. Belt, E.C. Gamelin, B. Ganguly, D. Yin, T. Joh, I.A. Jacobs, C.T. Taylor, and M.A. Lowery. 2019. Phase 1b study of a small molecule antagonist of human chemokine (C-C motif) receptor 2 (PF-04136309) in combination with nab-paclitaxel/gemcitabine in first-line treatment of metastatic pancreatic ductal adenocarcinoma. *Invest New Drugs*.

Noy, R., and J.W. Pollard. 2014. Tumor-associated macrophages: from mechanisms to therapy. *Immunity*. 41:49-61.

Nywening, T.M., A. Wang-Gillam, D.E. Sanford, B.A. Belt, R.Z. Panni, B.M. Cusworth, A.T. Toriola, R.K. Nieman, L.A. Worley, M. Yano, K.J. Fowler, A.C. Lockhart, R. Suresh, B.R. Tan, K.H. Lim, R.C. Fields, S.M. Strasberg, W.G. Hawkins, D.G. DeNardo, S.P. Goedegebuure, and D.C. Linehan. 2016. Targeting tumour-associated macrophages with CCR2 inhibition in combination with FOLFIRINOX in patients with borderline resectable and locally advanced pancreatic cancer: a single-centre, open-label, dose-finding, non-randomised, phase 1b trial. *Lancet Oncol*. 17:651-662.

O'Shannessy, D.J., E.B. Somers, L.C. Wang, H. Wang, and R. Hsu. 2015. Expression of folate receptors alpha and beta in normal and cancerous gynecologic tissues: correlation of expression of the beta isoform with macrophage markers. *J Ovarian Res*. 8:29.

Offner, S., R. Hofmeister, A. Romaniuk, P. Kufer, and P.A. Baeuerle. 2006. Induction of regular cytolytic T cell synapses by bispecific single-chain antibody constructs on MHC class I-negative tumor cells. *Mol Immunol*. 43:763-771.

Ohno, S., H. Inagawa, D.K. Dhar, T. Fujii, S. Ueda, M. Tachibana, N. Suzuki, M. Inoue, G. Soma, and N. Nagasue. 2003. The degree of macrophage infiltration into the cancer cell nest is a significant predictor of survival in gastric cancer patients. *Anticancer Res*. 23:5015-5022.

Ohno, S., Y. Ohno, N. Suzuki, T. Kamei, K. Koike, H. Inagawa, C. Kohchi, G. Soma, and M. Inoue. 2004. Correlation of histological localization of tumor-associated macrophages with clinicopathological features in endometrial cancer. *Anticancer Res*. 24:3335-3342.

Ong, S.M., Y.C. Tan, O. Beretta, D. Jiang, W.H. Yeap, J.J. Tai, W.C. Wong, H. Yang, H. Schwarz, K.H. Lim, P.K. Koh, K.L. Ling, and S.C. Wong. 2012. Macrophages in human colorectal cancer are pro-inflammatory and prime T cells towards an anti-tumour type-1 inflammatory response. *Eur J Immunol*. 42:89-100.

Osada, T., D. Hsu, S. Hammond, A. Hobeika, G. Devi, T.M. Clay, H.K. Lyerly, and M.A. Morse. 2010. Metastatic colorectal cancer cells from patients previously treated with chemotherapy are sensitive to T-cell killing mediated by CEA/CD3-bispecific T-cell-engaging BiTE antibody. *Br J Cancer*. 102:124-133.

Patel, M.R., B.A. Jacobson, Y. Ji, J. Drees, S. Tang, K. Xiong, H. Wang, J.E. Prigge, A.S. Dash, A.K. Kratzke, E. Mesev, R. Etchison, M.J. Federspiel, S.J. Russell, and R.A. Kratzke. 2015. Vesicular stomatitis virus expressing interferon-β is oncolytic and promotes antitumor immune responses in a syngeneic murine model of non-small cell lung cancer. *Oncotarget*. 6:33165-33177.

Paulus, P., E.R. Stanley, R. Schäfer, D. Abraham, and S. Aharinejad. 2006. Colony-stimulating factor-1 antibody reverses chemoresistance in human MCF-7 breast cancer xenografts. *Cancer Res*. 66:4349-4356.

Peranzoni, E., J. Lemoine, L. Vimeux, V. Feuillet, S. Barrin, C. Kantari-Mimoun, N. Bercovici, M. Guérin, J. Biton, H. Ouakrim, F. Régnier, A. Lupo, M. Alifano, D. Damotte, and E. Donnadieu. 2018. Macrophages impede CD8 T cells from reaching tumor cells and limit the efficacy of anti-PD-1 treatment. *Proc Natl Acad Sci U S A*. 115:E4041-E4050.

Pienta, K.J., J.P. Machiels, D. Schrijvers, B. Alekseev, M. Shkolnik, S.J. Crabb, S. Li, S. Seetharam, T.A. Puchalski, C. Takimoto, Y. Elsayed, F. Dawkins, and J.S. de Bono. 2013. Phase 2 study of carlumab (CNTO 888), a human monoclonal antibody against CC-chemokine ligand 2 (CCL2), in metastatic castration-resistant prostate cancer. *Invest New Drugs*. 31:760-768.

Pinto, M.L., E. Rios, A.C. Silva, S.C. Neves, H.R. Caires, A.T. Pinto, C. Durães, F.A. Carvalho, A.P. Cardoso, N.C. Santos, C.C. Barrias, D.S. Nascimento, P. Pinto-do-Ó, M.A. Barbosa, F. Carneiro, and M.J. Oliveira. 2017. Decellularized human colorectal cancer matrices polarize macrophages towards an anti-inflammatory phenotype promoting cancer cell invasion via CCL18. *Biomaterials*. 124:211-224.

Pishvaian, M., M.A. Morse, J. McDevitt, J.D. Norton, S. Ren, G.J. Robbie, P.C. Ryan, S. Soukharev, H. Bao, and C.S. Denlinger. 2016. Phase 1 Dose Escalation Study of MEDI-565, a Bispecific T-Cell Engager that Targets Human Carcinoembryonic Antigen, in Patients With Advanced Gastrointestinal Adenocarcinomas. *Clin Colorectal Cancer*. 15:345-351.

Poh, A.R., and M. Ernst. 2018. Targeting Macrophages in Cancer: From Bench to Bedside. *Front Oncol*. 8:49.

Przepiorka, D., C.W. Ko, A. Deisseroth, C.L. Yancey, R. Candau-Chacon, H.J. Chiu, B.J. Gehrke, C. Gomez-Broughton, R.C. Kane, S. Kirshner, N. Mehrotra, T.K. Ricks, D. Schmiel, P. Song, P. Zhao, Q. Zhou, A.T. Farrell, and R. Pazdur. 2015. FDA Approval: Blinatumomab. *Clin Cancer Res*. 21:4035-4039.

Puig-Kröger, A., E. Sierra-Filardi, A. Domínguez-Soto, R. Samaniego, M.T. Corcuera, F. Gómez-Aguado, M. Ratnam, P. Sánchez-Mateos, and A.L. Corbí. 2009. Folate receptor beta is expressed by tumor-associated macrophages and constitutes a marker for M2 anti-inflammatory/regulatory macrophages. *Cancer Res*. 69:9395-9403.

Pulte, E.D., J. Vallejo, D. Przepiorka, L. Nie, A.T. Farrell, K.B. Goldberg, A.E. McKee, and R. Pazdur. 2018. FDA Supplemental Approval: Blinatumomab for Treatment of Relapsed and Refractory Precursor B-Cell Acute Lymphoblastic Leukemia. *Oncologist*. 23:1366-1371.

Qian, B.Z., J. Li, H. Zhang, T. Kitamura, J. Zhang, L.R. Campion, E.A. Kaiser, L.A. Snyder, and J.W. Pollard. 2011. CCL2 recruits inflammatory monocytes to facilitate breast-tumour metastasis. *Nature*. 475:222-225.

Quail, D.F., R.L. Bowman, L. Akkari, M.L. Quick, A.J. Schuhmacher, J.T. Huse, E.C. Holland, J.C. Sutton, and J.A. Joyce. 2016. The tumor microenvironment underlies acquired resistance to CSF-1R inhibition in gliomas. *Science*. 352:aad3018.

Rakhmilevich, A.L., K.L. Alderson, and P.M. Sondel. 2012. T-cell-independent antitumor effects of CD40 ligation. *Int Rev Immunol*. 31:267-278.

Ramos, R.N., L.S. Chin, A.P. Dos Santos, P.C. Bergami-Santos, F. Laginha, and J.A. Barbuto. 2012. Monocyte-derived dendritic cells from breast cancer patients are biased to induce CD4+CD25+Foxp3+ regulatory T cells. *J Leukoc Biol*. 92:673-682.

Rehman, H., A.W. Silk, M.P. Kane, and H.L. Kaufman. 2016. Into the clinic: Talimogene laherparepvec (T-VEC), a first-in-class intratumoral oncolytic viral therapy. *J Immunother Cancer*. 4:53.

Reinartz, S., T. Schumann, F. Finkernagel, A. Wortmann, J.M. Jansen, W. Meissner, M. Krause, A.M. Schwörer, U. Wagner, S. Müller-Brüsselbach, and R. Müller. 2014. Mixed-polarization phenotype of ascites-associated

macrophages in human ovarian carcinoma: correlation of CD163 expression, cytokine levels and early relapse. *Int J Cancer*. 134:32-42.

Ren, C.X., R.X. Leng, Y.G. Fan, H.F. Pan, B.Z. Li, C.H. Wu, Q. Wu, N.N. Wang, Q.R. Xiong, X.P. Geng, and D.Q. Ye. 2017. Intratumoral and peritumoral expression of CD68 and CD206 in hepatocellular carcinoma and their prognostic value. *Oncol Rep*. 38:886-898.

Renner, K., K. Singer, G.E. Koehl, E.K. Geissler, K. Peter, P.J. Siska, and M. Kreutz. 2017. Metabolic Hallmarks of Tumor and Immune Cells in the Tumor Microenvironment. *Front Immunol*. 8:248.

Reusch, U., J. Duell, K. Ellwanger, C. Herbrecht, S.H. Knackmuss, I. Fucek, M. Eser, F. McAleese, V. Molkenthin, F.L. Gall, M. Topp, M. Little, and E.A. Zhukovsky. 2015. A tetravalent bispecific TandAb (CD19/CD3), AFM11, efficiently recruits T cells for the potent lysis of CD19(+) tumor cells. *MAbs*. 7:584-604.

Reusch, U., K.H. Harrington, C.J. Gudgeon, I. Fucek, K. Ellwanger, M. Weichel, S.H. Knackmuss, E.A. Zhukovsky, J.A. Fox, L.A. Kunkel, J. Guenot, and R.B. Walter. 2016. Characterization of CD33/CD3 Tetravalent Bispecific Tandem Diabodies (TandAbs) for the Treatment of Acute Myeloid Leukemia. *Clin Cancer Res*. 22:5829-5838.

Ribas, A., R. Dummer, I. Puzanov, A. VanderWalde, R.H.I. Andtbacka, O. Michielin, A.J. Olszanski, J. Malvehy, J. Cebon, E. Fernandez, J.M. Kirkwood, T.F. Gajewski, L. Chen, K.S. Gorski, A.A. Anderson, S.J. Diede, M.E. Lassman, J. Gansert, F.S. Hodi, and G.V. Long. 2017. Oncolytic Virotherapy Promotes Intratumoral T Cell Infiltration and Improves Anti-PD-1 Immunotherapy. *Cell*. 170:1109-1119.e1110.

Ribas, A., P. Hersey, M.R. Middleton, H. Gogas, K.T. Flaherty, V.K. Sondak, and J.M. Kirkwood. 2012. New challenges in endpoints for drug development in advanced melanoma. *Clin Cancer Res*. 18:336-341.

Ries, C.H., M.A. Cannarile, S. Hoves, J. Benz, K. Wartha, V. Runza, F. Rey-Giraud, L.P. Pradel, F. Feuerhake, I. Klaman, T. Jones, U. Jucknischke, S. Scheiblich, K. Kaluza, I.H. Gorr, A. Walz, K. Abiraj, P.A. Cassier, A. Sica, C. Gomez-Roca, K.E. de Visser, A. Italiano, C. Le Tourneau, J.P. Delord, H. Levitsky, J.Y. Blay, and D. Rüttinger. 2014. Targeting tumor-associated macrophages with anti-CSF-1R antibody reveals a strategy for cancer therapy. *Cancer Cell*. 25:846-859.

Robert, C., J. Schachter, G.V. Long, A. Arance, J.J. Grob, L. Mortier, A. Daud, M.S. Carlino, C. McNeil, M. Lotem, J. Larkin, P. Lorigan, B. Neyns, C.U. Blank, O. Hamid, C. Mateus, R. Shapira-Frommer, M. Kosh, H. Zhou, N. Ibrahim, S. Ebbinghaus, A. Ribas, and K.-. investigators. 2015. Pembrolizumab versus Ipilimumab in Advanced Melanoma. *N Engl J Med*. 372:2521-2532.

Robinson, C.M., G. Singh, J.Y. Lee, S. Dehghan, J. Rajaiya, E.B. Liu, M.A. Yousuf, R.A. Betensky, M.S. Jones, D.W. Dyer, D. Seto, and J. Chodosh. 2013. Molecular evolution of human adenoviruses. *Sci Rep*. 3:1812.

Rodig, S.J., D. Gusenleitner, D.G. Jackson, E. Gjini, A. Giobbie-Hurder, C. Jin, H. Chang, S.B. Lovitch, C. Horak, J.S. Weber, J.L. Weirather, J.D. Wolchok,

M.A. Postow, A.C. Pavlick, J. Chesney, and F.S. Hodi. 2018. MHC proteins confer differential sensitivity to CTLA-4 and PD-1 blockade in untreated metastatic melanoma. *Sci Transl Med*. 10.

Rogers, T.L., and I. Holen. 2011. Tumour macrophages as potential targets of bisphosphonates. *J Transl Med*. 9:177.

Rohaan, M.W., J.H. van den Berg, P. Kvistborg, and J.B.A.G. Haanen. 2018. Adoptive transfer of tumor-infiltrating lymphocytes in melanoma: a viable treatment option. *J Immunother Cancer*. 6:102.

Rosenberg, S.A., J.C. Yang, R.M. Sherry, U.S. Kammula, M.S. Hughes, G.Q. Phan, D.E. Citrin, N.P. Restifo, P.F. Robbins, J.R. Wunderlich, K.E. Morton, C.M. Laurencot, S.M. Steinberg, D.E. White, and M.E. Dudley. 2011. Durable complete responses in heavily pretreated patients with metastatic melanoma using T-cell transfer immunotherapy. *Clin Cancer Res*. 17:4550-4557.

Roskopf, C.C., T.A. Braciak, N.C. Fenn, S. Kobold, G.H. Fey, K.P. Hopfner, and F.S. Oduncu. 2016. Dual-targeting triplebody 33-3-19 mediates selective lysis of biphenotypic CD19+ CD33+ leukemia cells. *Oncotarget*. 7:22579-22589.

Ross, S.L., M. Sherman, P.L. McElroy, J.A. Lofgren, G. Moody, P.A. Baeuerle, A. Coxon, and T. Arvedson. 2017. Bispecific T cell engager (BiTE®) antibody constructs can mediate bystander tumor cell killing. *PLoS One*. 12:e0183390.

Rødgaard-Hansen, S., A. Rafique, P.A. Christensen, M.B. Maniecki, T.D. Sandahl, E. Nexø, and H.J. Møller. 2014. A soluble form of the macrophage-related mannose receptor (MR/CD206) is present in human serum and elevated in critical illness. *Clin Chem Lab Med*. 52:453-461.

Sahin, T.T., H. Kasuya, N. Nomura, T. Shikano, K. Yamamura, T. Gewen, A. Kanzaki, T. Fujii, T. Sugae, T. Imai, S. Nomoto, S. Takeda, H. Sugimoto, T. Kikumori, Y. Kodera, Y. Nishiyama, and A. Nakao. 2012. Impact of novel oncolytic virus HF10 on cellular components of the tumor microenviroment in patients with recurrent breast cancer. *Cancer Gene Ther*. 19:229-237.

Salmon, H., K. Franciszkiewicz, D. Damotte, M.C. Dieu-Nosjean, P. Validire, A. Trautmann, F. Mami-Chouaib, and E. Donnadieu. 2012. Matrix architecture defines the preferential localization and migration of T cells into the stroma of human lung tumors. *J Clin Invest*. 122:899-910.

Sandhu, S.K., K. Papadopoulos, P.C. Fong, A. Patnaik, C. Messiou, D. Olmos, G. Wang, B.J. Tromp, T.A. Puchalski, F. Balkwill, B. Berns, S. Seetharam, J.S. de Bono, and A.W. Tolcher. 2013. A first-in-human, first-in-class, phase I study of carlumab (CNTO 888), a human monoclonal antibody against CC-chemokine ligand 2 in patients with solid tumors. *Cancer Chemother Pharmacol*. 71:1041-1050.

Sangisetty, S.L., and T.J. Miner. 2012. Malignant ascites: A review of prognostic factors, pathophysiology and therapeutic measures. *World J Gastrointest Surg*. 4:87-95.

Schachter, J., A. Ribas, G.V. Long, A. Arance, J.J. Grob, L. Mortier, A. Daud, M.S. Carlino, C. McNeil, M. Lotem, J. Larkin, P. Lorigan, B. Neyns, C. Blank, T.M. Petrella, O. Hamid, H. Zhou, S. Ebbinghaus, N. Ibrahim, and C. Robert.

2017. Pembrolizumab versus ipilimumab for advanced melanoma: final overall survival results of a multicentre, randomised, open-label phase 3 study (KEYNOTE-006). *Lancet*. 390:1853-1862.

Schadendorf, D., F.S. Hodi, C. Robert, J.S. Weber, K. Margolin, O. Hamid, D. Patt, T.T. Chen, D.M. Berman, and J.D. Wolchok. 2015. Pooled Analysis of Long-Term Survival Data From Phase II and Phase III Trials of Ipilimumab in Unresectable or Metastatic Melanoma. *J Clin Oncol*. 33:1889-1894.

Schubert, I., C. Kellner, C. Stein, M. Kügler, M. Schwenkert, D. Saul, B. Stockmeyer, C. Berens, F.S. Oduncu, A. Mackensen, and G.H. Fey. 2012. A recombinant triplebody with specificity for CD19 and HLA-DR mediates preferential binding to antigen double-positive cells by dual-targeting. *MAbs*. 4:45-56.

Schultze, J.L., A. Schmieder, and S. Goerdt. 2015. Macrophage activation in human diseases. *Semin Immunol*. 27:249-256.

Scott, E.M., M.R. Duffy, J.D. Freedman, K.D. Fisher, and L.W. Seymour. 2018. Solid Tumor Immunotherapy with T Cell Engager-Armed Oncolytic Viruses. *Macromol Biosci*. 18.

Sercombe, L., T. Veerati, F. Moheimani, S.Y. Wu, A.K. Sood, and S. Hua. 2015. Advances and Challenges of Liposome Assisted Drug Delivery. *Front Pharmacol*. 6:286.

Seymour, L.W., and K.D. Fisher. 2016. Oncolytic viruses: finally delivering. *Br J Cancer*. 114:357-361.

Shah, N.N., T. Maatman, P. Hari, and B. Johnson. 2019. Multi Targeted CAR-T Cell Therapies for B-Cell Malignancies. *Front Oncol*. 9:146.

Shapouri-Moghaddam, A., S. Mohammadian, H. Vazini, M. Taghadosi, S.A. Esmaeili, F. Mardani, B. Seifi, A. Mohammadi, J.T. Afshari, and A. Sahebkar. 2018. Macrophage plasticity, polarization, and function in health and disease. *J Cell Physiol*. 233:6425-6440.

Shen, J., A.R. Hilgenbrink, W. Xia, Y. Feng, D.S. Dimitrov, M.B. Lockwood, R.J. Amato, and P.S. Low. 2014. Folate receptor-β constitutes a marker for human proinflammatory monocytes. *J Leukoc Biol*. 96:563-570.

Shen, J., K.S. Putt, D.W. Visscher, L. Murphy, C. Cohen, S. Singhal, G. Sandusky, Y. Feng, D.S. Dimitrov, and P.S. Low. 2015. Assessment of folate receptor-β expression in human neoplastic tissues. *Oncotarget*. 6:14700-14709.

Shimura, S., G. Yang, S. Ebara, T.M. Wheeler, A. Frolov, and T.C. Thompson. 2000. Reduced infiltration of tumor-associated macrophages in human prostate cancer: association with cancer progression. *Cancer Res*. 60:5857-5861.

Shree, T., O.C. Olson, B.T. Elie, J.C. Kester, A.L. Garfall, K. Simpson, K.M. Bell-McGuinn, E.C. Zabor, E. Brogi, and J.A. Joyce. 2011. Macrophages and cathepsin proteases blunt chemotherapeutic response in breast cancer. *Genes Dev*. 25:2465-2479.

Shu, Q.H., Y.S. Ge, H.X. Ma, X.Q. Gao, J.J. Pan, D. Liu, G.L. Xu, J.L. Ma, and W.D. Jia. 2016. Prognostic value of polarized macrophages in patients with hepatocellular carcinoma after curative resection. *J Cell Mol Med*. 20:1024-1035.

Simpson-Abelson, M.R., J.L. Loyall, H.K. Lehman, J.L. Barnas, H. Minderman, K.L. O'Loughlin, P.K. Wallace, T.C. George, P. Peng, R.J. Kelleher, K. Odunsi, and R.B. Bankert. 2013. Human ovarian tumor ascites fluids rapidly and reversibly inhibit T cell receptor-induced NF-κB and NFAT signaling in tumor-associated T cells. *Cancer Immun*. 13:14.

Smith, R.R., R.J. Huebner, W.P. Rowe, W.E. Schatten, and L.B. Thomas. 1956. Studies on the use of viruses in the treatment of carcinoma of the cervix. *Cancer*. 9:1211-1218.

Song, Q., C.D. Zhang, and X.H. Wu. 2018. Therapeutic cancer vaccines: From initial findings to prospects. *Immunol Lett*. 196:11-21.

Southam, C.M., and A.E. Moore. 1952. Clinical studies of viruses as antineoplastic agents with particular reference to Egypt 101 virus. *Cancer*. 5:1025-1034.

Srivastava, M.K., P. Sinha, V.K. Clements, P. Rodriguez, and S. Ostrand-Rosenberg. 2010. Myeloid-derived suppressor cells inhibit T-cell activation by depleting cystine and cysteine. *Cancer Res*. 70:68-77.

Stone, J.D., D.H. Aggen, A. Schietinger, H. Schreiber, and D.M. Kranz. 2012. A sensitivity scale for targeting T cells with chimeric antigen receptors (CARs) and bispecific T-cell Engagers (BiTEs). *Oncoimmunology*. 1:863-873.

Suchard, S.J., P.M. Davis, S. Kansal, D.K. Stetsko, R. Brosius, J. Tamura, L. Schneeweis, J. Bryson, T. Salcedo, H. Wang, Z. Yang, C.A. Fleener, O. Ignatovich, C. Plummer, S. Grant, and S.G. Nadler. 2013. A monovalent anti-human CD28 domain antibody antagonist: preclinical efficacy and safety. *J Immunol*. 191:4599-4610.

Suntharalingam, G., M.R. Perry, S. Ward, S.J. Brett, A. Castello-Cortes, M.D. Brunner, and N. Panoskaltsis. 2006. Cytokine storm in a phase 1 trial of the anti-CD28 monoclonal antibody TGN1412. *N Engl J Med*. 355:1018-1028.

Tap, W.D., H. Gelderblom, E. Palmerini, J. Desai, S. Bauer, J.Y. Blay, T. Alcindor, K. Ganjoo, J. Martín-Broto, C.W. Ryan, D.M. Thomas, C. Peterfy, J.H. Healey, M. van de Sande, H.L. Gelhorn, D.E. Shuster, Q. Wang, A. Yver, H.H. Hsu, P.S. Lin, S. Tong-Starksen, S. Stacchiotti, A.J. Wagner, and E. investigators. 2019. Pexidartinib versus placebo for advanced tenosynovial giant cell tumour (ENLIVEN): a randomised phase 3 trial. *Lancet*.

Teng, K.Y., J. Han, X. Zhang, S.H. Hsu, S. He, N.A. Wani, J.M. Barajas, L.A. Snyder, W.L. Frankel, M.A. Caligiuri, S.T. Jacob, J. Yu, and K. Ghoshal. 2017. Blocking the CCL2-CCR2 Axis Using CCL2-Neutralizing Antibody Is an Effective Therapy for Hepatocellular Cancer in a Mouse Model. *Mol Cancer Ther*. 16:312-322.

Thorsson, V., D.L. Gibbs, S.D. Brown, D. Wolf, D.S. Bortone, T.H. Ou Yang, E. Porta-Pardo, G.F. Gao, C.L. Plaisier, J.A. Eddy, E. Ziv, A.C. Culhane, E.O. Paull, I.K.A. Sivakumar, A.J. Gentles, R. Malhotra, F. Farshidfar, A. Colaprico, J.S. Parker, L.E. Mose, N.S. Vo, J. Liu, Y. Liu, J. Rader, V. Dhankani, S.M. Reynolds, R. Bowlby, A. Califano, A.D. Cherniack, D. Anastassiou, D. Bedognetti, Y. Mokrab, A.M. Newman, A. Rao, K. Chen, A. Krasnitz, H. Hu, T.M. Malta, H. Noushmehr, C.S. Pedamallu, S. Bullman, A.I. Ojesina, A. Lamb, W. Zhou, H. Shen, T.K. Choueiri, J.N. Weinstein, J.

Guinney, J. Saltz, R.A. Holt, C.S. Rabkin, A.J. Lazar, J.S. Serody, E.G. Demicco, M.L. Disis, B.G. Vincent, I. Shmulevich, and C.G.A.R. Network. 2018. The Immune Landscape of Cancer. *Immunity*. 48:812-830.e814.

Thurber, G.M., S.C. Zajic, and K.D. Wittrup. 2007. Theoretic criteria for antibody penetration into solid tumors and micrometastases. *J Nucl Med*. 48:995-999.

Topalian, S.L., L.M. Muul, D. Solomon, and S.A. Rosenberg. 1987. Expansion of human tumor infiltrating lymphocytes for use in immunotherapy trials. *J Immunol Methods*. 102:127-141.

Topp, M.S., N. Gökbuget, G. Zugmaier, P. Klappers, M. Stelljes, S. Neumann, A. Viardot, R. Marks, H. Diedrich, C. Faul, A. Reichle, H.A. Horst, M. Brüggemann, D. Wessiepe, C. Holland, S. Alekar, N. Mergen, H. Einsele, D. Hoelzer, and R.C. Bargou. 2014. Phase II trial of the anti-CD19 bispecific T cell-engager blinatumomab shows hematologic and molecular remissions in patients with relapsed or refractory B-precursor acute lymphoblastic leukemia. *J Clin Oncol*. 32:4134-4140.

Topp, M.S., P. Kufer, N. Gökbuget, M. Goebeler, M. Klinger, S. Neumann, H.A. Horst, T. Raff, A. Viardot, M. Schmid, M. Stelljes, M. Schaich, E. Degenhard, R. Köhne-Volland, M. Brüggemann, O. Ottmann, H. Pfeifer, T. Burmeister, D. Nagorsen, M. Schmidt, R. Lutterbuese, C. Reinhardt, P.A. Baeuerle, M. Kneba, H. Einsele, G. Riethmüller, D. Hoelzer, G. Zugmaier, and R.C. Bargou. 2011. Targeted therapy with the T-cell-engaging antibody blinatumomab of chemotherapy-refractory minimal residual disease in B-lineage acute lymphoblastic leukemia patients results in high response rate and prolonged leukemia-free survival. *J Clin Oncol*. 29:2493-2498.

Tumeh, P.C., C.L. Harview, J.H. Yearley, I.P. Shintaku, E.J. Taylor, L. Robert, B. Chmielowski, M. Spasic, G. Henry, V. Ciobanu, A.N. West, M. Carmona, C. Kivork, E. Seja, G. Cherry, A.J. Gutierrez, T.R. Grogan, C. Mateus, G. Tomasic, J.A. Glaspy, R.O. Emerson, H. Robins, R.H. Pierce, D.A. Elashoff, C. Robert, and A. Ribas. 2014. PD-1 blockade induces responses by inhibiting adaptive immune resistance. *Nature*. 515:568-571.

Turtle, C.J., L.A. Hanafi, C. Berger, M. Hudecek, B. Pender, E. Robinson, R. Hawkins, C. Chaney, S. Cherian, X. Chen, L. Soma, B. Wood, D. Li, S. Heimfeld, S.R. Riddell, and D.G. Maloney. 2016. Immunotherapy of non-Hodgkin's lymphoma with a defined ratio of CD8+ and CD4+ CD19-specific chimeric antigen receptor-modified T cells. *Sci Transl Med*. 8:355ra116.

Tymoszuk, P., H. Evens, V. Marzola, K. Wachowicz, M.H. Wasmer, S. Datta, E. Müller-Holzner, H. Fiegl, G. Böck, N. van Rooijen, I. Theurl, and W. Doppler. 2014. In situ proliferation contributes to accumulation of tumor-associated macrophages in spontaneous mammary tumors. *Eur J Immunol*. 44:2247-2262.

Ueno, T., M. Toi, H. Saji, M. Muta, H. Bando, K. Kuroi, M. Koike, H. Inadera, and K. Matsushima. 2000. Significance of macrophage chemoattractant protein-1 in macrophage recruitment, angiogenesis, and survival in human breast cancer. *Clin Cancer Res*. 6:3282-3289.

Varol, C., and I. Sagi. 2018. Phagocyte-extracellular matrix crosstalk empowers tumor development and dissemination. *FEBS J*. 285:734-751.

Velasquez, M.P., C.L. Bonifant, and S. Gottschalk. 2018. Redirecting T cells to hematological malignancies with bispecific antibodies. *Blood*. 131:30-38.

Vogels, R., D. Zuijdgeest, R. van Rijnsoever, E. Hartkoorn, I. Damen, M.P. de Béthune, S. Kostense, G. Penders, N. Helmus, W. Koudstaal, M. Cecchini, A. Wetterwald, M. Sprangers, A. Lemckert, O. Ophorst, B. Koel, M. van Meerendonk, P. Quax, L. Panitti, J. Grimbergen, A. Bout, J. Goudsmit, and M. Havenga. 2003. Replication-deficient human adenovirus type 35 vectors for gene transfer and vaccination: efficient human cell infection and bypass of preexisting adenovirus immunity. *J Virol*. 77:8263-8271.

Vonderheide, R.H., J.M. Burg, R. Mick, J.A. Trosko, D. Li, M.N. Shaik, A.W. Tolcher, and O. Hamid. 2013. Phase I study of the CD40 agonist antibody CP-870,893 combined with carboplatin and paclitaxel in patients with advanced solid tumors. *Oncoimmunology*. 2:e23033.

Vonderheide, R.H., K.T. Flaherty, M. Khalil, M.S. Stumacher, D.L. Bajor, N.A. Hutnick, P. Sullivan, J.J. Mahany, M. Gallagher, A. Kramer, S.J. Green, P.J. O'Dwyer, K.L. Running, R.D. Huhn, and S.J. Antonia. 2007. Clinical activity and immune modulation in cancer patients treated with CP-870,893, a novel CD40 agonist monoclonal antibody. *J Clin Oncol*. 25:876-883.

Wang, W.Q., L. Liu, H.X. Xu, C.T. Wu, J.F. Xiang, J. Xu, C. Liu, J. Long, Q.X. Ni, and X.J. Yu. 2016. Infiltrating immune cells and gene mutations in pancreatic ductal adenocarcinoma. *Br J Surg*. 103:1189-1199.

Wang, X.B., B.F. Zhao, Q. Zhao, J.H. Piao, J. Liu, Q. Lin, and H.L. Huang. 2004. A new recombinant single chain trispecific antibody recruits T lymphocytes to kill CEA (carcinoma embryonic antigen) positive tumor cells in vitro efficiently. *J Biochem*. 135:555-565.

Webb, H.E., G. Wetherley-Mein, C.E. Smith, and D. McMahon. 1966. Leukaemia and neoplastic processes treated with Langat and Kyasanur Forest disease viruses: a clinical and laboratory study of 28 patients. *Br Med J*. 1:258-266.

Wong, R., C. Pepper, P. Brennan, D. Nagorsen, S. Man, and C. Fegan. 2013. Blinatumomab induces autologous T-cell killing of chronic lymphocytic leukemia cells. *Haematologica*. 98:1930-1938.

Wu, Z., and N.V. Cheung. 2018. T cell engaging bispecific antibody (T-BsAb): From technology to therapeutics. *Pharmacol Ther*. 182:161-175.

Xu, L., Y. Zhu, L. Chen, H. An, W. Zhang, G. Wang, Z. Lin, and J. Xu. 2014. Prognostic value of diametrically polarized tumor-associated macrophages in renal cell carcinoma. *Ann Surg Oncol*. 21:3142-3150.

Yan, D., J. Kowal, L. Akkari, A.J. Schuhmacher, J.T. Huse, B.L. West, and J.A. Joyce. 2017. Inhibition of colony stimulating factor-1 receptor abrogates microenvironment-mediated therapeutic resistance in gliomas. *Oncogene*. 36:6049-6058.

Yang, M., D. McKay, J.W. Pollard, and C.E. Lewis. 2018. Diverse Functions of Macrophages in Different Tumor Microenvironments. *Cancer Res*. 78:5492-5503.

Yang, T., F. Xu, D. Fang, and Y. Chen. 2015. Targeted Proteomics Enables Simultaneous Quantification of Folate Receptor Isoforms and Potential Isoform-based Diagnosis in Breast Cancer. *Sci Rep*. 5:16733.

Yu, F., X. Wang, Z.S. Guo, D.L. Bartlett, S.M. Gottschalk, and X.T. Song. 2014. T-cell engager-armed oncolytic vaccinia virus significantly enhances antitumor therapy. *Mol Ther*. 22:102-111.

Zamarin, D., R.B. Holmgaard, S.K. Subudhi, J.S. Park, M. Mansour, P. Palese, T. Merghoub, J.D. Wolchok, and J.P. Allison. 2014. Localized oncolytic virotherapy overcomes systemic tumor resistance to immune checkpoint blockade immunotherapy. *Sci Transl Med*. 6:226ra232.

Zarour, H.M. 2016. Reversing T-cell Dysfunction and Exhaustion in Cancer. *Clin Cancer Res*. 22:1856-1864.

Zeisberger, S.M., B. Odermatt, C. Marty, A.H. Zehnder-Fjällman, K. Ballmer-Hofer, and R.A. Schwendener. 2006. Clodronate-liposome-mediated depletion of tumour-associated macrophages: a new and highly effective antiangiogenic therapy approach. *Br J Cancer*. 95:272-281.

Zhang, B., G. Yao, Y. Zhang, J. Gao, B. Yang, and Z. Rao. 2011. M2-polarized tumor-associated macrophages are associated with poor prognoses resulting from accelerated lymphangiogenesis in lung adenocarcinoma. *Clinics (Sao Paulo)*. 66:1879-1886.

Zhang, M., Y. He, X. Sun, Q. Li, W. Wang, A. Zhao, and W. Di. 2014. A high M1/M2 ratio of tumor-associated macrophages is associated with extended survival in ovarian cancer patients. *J Ovarian Res*. 7:19.

Zhang, Q.W., L. Liu, C.Y. Gong, H.S. Shi, Y.H. Zeng, X.Z. Wang, Y.W. Zhao, and Y.Q. Wei. 2012. Prognostic significance of tumor-associated macrophages in solid tumor: a meta-analysis of the literature. *PLoS One*. 7:e50946.

Zhang, W., X.D. Zhu, H.C. Sun, Y.Q. Xiong, P.Y. Zhuang, H.X. Xu, L.Q. Kong, L. Wang, W.Z. Wu, and Z.Y. Tang. 2010. Depletion of tumor-associated macrophages enhances the effect of sorafenib in metastatic liver cancer models by antimetastatic and antiangiogenic effects. *Clin Cancer Res*. 16:3420-3430.

Zhang, Y., C. Fan, L. Zhang, and X. Ma. 2019. Glycosylation-dependent antitumor therapeutic monoclonal antibodies. *Prog Mol Biol Transl Sci*. 163:471-485.

Zhu, S., M. Niu, H. O'Mary, and Z. Cui. 2013. Targeting of tumor-associated macrophages made possible by PEG-sheddable, mannose-modified nanoparticles. *Mol Pharm*. 10:3525-3530.

Zhu, Y., J.M. Herndon, D.K. Sojka, K.W. Kim, B.L. Knolhoff, C. Zuo, D.R. Cullinan, J. Luo, A.R. Bearden, K.J. Lavine, W.M. Yokoyama, W.G. Hawkins, R.C. Fields, G.J. Randolph, and D.G. DeNardo. 2017. Tissue-Resident Macrophages in Pancreatic Ductal Adenocarcinoma Originate from Embryonic Hematopoiesis and Promote Tumor Progression. *Immunity*. 47:597.

Zhu, Y., B.L. Knolhoff, M.A. Meyer, T.M. Nywening, B.L. West, J. Luo, A. Wang-Gillam, S.P. Goedegebuure, D.C. Linehan, and D.G. DeNardo. 2014. CSF1/CSF1R blockade reprograms tumor-infiltrating macrophages and

improves response to T-cell checkpoint immunotherapy in pancreatic cancer models. *Cancer Res*. 74:5057-5069.